Hydrothermal Liquefaction of Black Liquor – Depolymerization of Lignin in Near-critical Water under the Influence of Salts

Zur Erlangung des akademischen Grades eines
DOKTORS DER INGENIEURWISSENSCHAFTEN (DR.-ING.)

von der KIT-Fakultät für Chemieingenieurwesen und Verfahrenstechnik des
Karlsruher Instituts für Technologie (KIT)
genehmigte

DISSERTATION

von
M.Sc. Maximilian Wörner
aus Bretten

Tag der mündlichen Prüfung: 29.07.2026

Erstgutachter: Prof. Dr. Nicolaus Dahmen

Zweitgutachterin: Prof. Dr. Andrea Kruse

Acknowledgements

First and foremost, I would like to express my sincere gratitude to my supervisor, Prof. Dr. Nicolaus Dahmen, for his outstanding support and guidance throughout the course of my doctoral studies. His continuous encouragement, scientific insight, and trust in my work have been invaluable. I am thankful for the freedom he provided to develop my own ideas, while always being available for discussion and direction when needed.

I am equally grateful to Dr. Ursel Hornung for her constant support and mentorship. She always had an open ear for my questions and challenges and was able to provide thoughtful advice at any time. Our scientific discussions and her constructive feedback significantly improved the quality of my work.

My sincere thanks also go to Prof. Dr. Andrea Kruse for kindly agreeing to serve as the second reviewer of this thesis. I highly appreciated her valuable feedback during the TAC meetings, which provided important impulses for my research activities.

I would like to acknowledge the BBW ForWerts Graduate Program Baden-Württemberg, in particular Prof. Dr. Thomas Rausch, Dr. Tanja Peskan-Berghoefer, and Hanni Truong, for giving me the opportunity to participate in this interdisciplinary program. Although I joined during its final two years, I greatly benefited from the diverse exchange of knowledge and the development of soft skills.

I am also deeply grateful to my collaborators in the Black Liquor to Fuels project, especially Dr. David Baudouin, Dr. Alexey Kourlov and Dr. Nicholas Islongo Canabarro from the Paul Scherrer Institute. Their support during my research stay, as well as their continuous scientific input, greatly enriched this work.

Furthermore, I would like to thank Prof. Dr. Alberto Wisniewski from the Universidade Federal de Sergipe for performing the HPLC-HRMS analyses of my samples. The insights gained from these analyses complemented my results in an excellent way.

I would also like to express my gratitude to all my colleagues and friends at the IKFT for the scientific exchange, the collaborative atmosphere, and the many enjoyable moments beyond work. It has been a pleasure working with all of you. In particular, I would like to thank Joscha, Henri, Ana, Frederico, Naiara, Carola, Bruno, Mariana, George, Julian, Marius and Eugen for their support and friendship throughout this journey. Also, a special thanks to Bruno who supported me with the kinetic modeling.

I am thankful to Birgit Rolli, Yannick Träutlein, Armin Lautenbach, Veronika Holderied, Jessica Heinrich, Thomas Zevaco, and Michael Zimmermann, who worked with my often challenging, odorous, and difficult samples and carried out essential analyses. The data generated by your efforts form a fundamental part of this thesis. I am especially grateful to Birgit, from whom I learned a lot about gas chromatography and general laboratory practice. I would also like to thank Thomas Tietz and Matthias Pagel for their technical support and for maintaining the micro-autoclaves. Without all of your help, the experimental work would have taken considerably longer.

I am also grateful to my students Alexandra, Elias, Lukas, Lea, and Manuel for their contributions and support in various aspects of this work.

Finally, my deepest and most heartfelt thanks go to my wife, Ann-Sophie, who has accompanied me throughout this entire journey and has always been a constant source of support and encouragement. I am equally thankful to my family for their support throughout the whole time. Without you, this achievement would not have been possible.

Preamble

This thesis is paper-based. Therefore, chapter 2, 3 and 4 of the presented content have already been published. As a result, some sections of the text are identical to the published work. Only minor changes such as the format or citation style have been made in these sections. The introduction and the chapter on material and methods of the publications have been significantly shortened to avoid repetition. A detailed introduction to the topic of this thesis has been provided in Chapter 1. All information on the publication can be found at the beginning of the respective chapter.

List of Publications

Peer-reviewed original publications included in this thesis

From Pulp to Aromatic Products – Reaction Pathways of Lignin Depolymerization; Maximilian Wörner, Alexandra Barsuhn, Thomas Zevaco, Ursel Hornung, and Nicolaus Dahmen; *Energy & Fuels*, 2024, 38 (7), 6020-6035; DOI: 10.1021/acs.energyfuels.3c04509

The Impact of Sulfur-Containing Inorganic Compounds during the Depolymerization of Lignin by Hydrothermal Liquefaction of Black Liquor; Maximilian Wörner, Lukas Werner, Ursel Hornung, Nicholas Islongo Canabarro, David Baudouin and Nicolaus Dahmen; *Energy & Fuels*, 2024, 38 (7), 6036-6047; DOI: 10.1021/acs.energyfuels.3c04737

From Pulp to Aromatic Products – Kinetic Modeling of Hydrothermal Lignin Depolymerization; Maximilian Wörner, Bruno Lacerda de Oliveira Campos, Ursel Hornung, and Nicolaus Dahmen; *Journal of Environmental Chemical Engineering,* 2026, 14 (3); 122311; https://doi.org/10.1016/j.jece.2026.122311

Peer-reviewed original publications not included in this thesis

Valorisation of the residual aqueous phase from hydrothermally liquefied black liquor by persulphate-based advanced oxidation; Lucía Pola, Sergio Collado, Maximilian Wörner, Ursel Hornung and Mario Díaz; *Chemosphere,* 2023, 339, 139737; DOI: https://doi.org/10.1016/j.chemosphere.2023.139737

Eutectic solvents for the valorisation of the aqueous phase from hydrothermally liquefied black liquor; Lucía Pola, Sergio Collado, Maximilian Wörner, Ursel Hornung and Mario Díaz; *Journal of Environmental Chemical Engineering,* 2023, 11 (5), 111040; DOI: https://doi.org/10.1016/j.jece.2023.111040

Development of strategies for continuous desalination of weak black liquor based on phase-behaviour analysis; Nicholas I. Canabarro; Darius J. Yeadon; Maximilian Wörner; Ursel Hornung; Frédéric Vogel; David Baudouin; *The Journal of Supercritical Fluids,* 2024, 209, 106230; DOI: https://doi.org/10.1016/j.supflu.2024.106230

Focus on hydrochars produced from hydrothermal liquefaction of beech wood, soda lignin and black liquor; Maximilian Wörner, Ursel Hornung, Selhan Karagöz, Thomas Zevaco, Nicolaus Dahmen; *Eur. J. Wood Prod.,* 2025, 83, 61; DOI: https://doi.org/10.1007/s00107-025-02214-2

Conference oral and poster presentations

Investigations on the influence of sulfur-containing salts on HTL of black liquor by using model mixtures; Maximilian Wörner, Lukas Werner, Ursel Hornung, Nicolaus Dahmen; *4th Doctoral Colloquium Bioenergy*, 2021, Eggenstein-Leopoldshafen, DE (presentation)

Hydrothermal liquefaction of black liquor; Maximilian Wörner, Ursel Hornung, Nicolaus Dahmen; 30th *European Biomass Conference and Exhibition (EUBCE),* 2022, Marseille (online) (presentation)

Behavior of the sulfur-containing salts during the hydrothermal liquefaction of black liquor; Maximilian Wörner, Lukas Werner, Ursel Hornung, Nicolaus Dahmen; *tcbiomass*, 2022, Denver, US (presentation)

Direct hydrothermal liquefaction of black liquor; Maximilian Wörner, Ursel Hornung, Nicolaus Dahmen; *DBFZ 7th HTP Fachforum*, 2022, Leipzig, DE (presentation)

Reaction pathways of monomers and oligomers during hydrothermal liquefaction of lignin; Maximilian Wörner, Ursel Hornung, Nicolaus Dahmen, *Pyroliq II conference*, 2023, Hernstein, AT (presentation and poster)

From pulp to aromatic products – Understanding the lignin depolymerization during hydrothermal liquefaction (HTL); Maximilian Wörner, Alexandra Barsuhn, Ursel Hornung, Nicolaus Dahmen; *31st EUBCE*, 2023, Bologna, IT (presentation)

Understanding the behavior of the oligomers during the hydrothermal liquefaction of black liquor; Maximilian Wörner, Ursel Hornung, Nicolaus Dahmen; *KNT Symposium*, 2023, Enschede, NL (presentation)

From Pulp to Aromatic Products – Description of a reaction mechanism for lignin depolymerization during hydrothermal liquefaction (HTL); Maximilian Wörner, Ursel Hornung, Nicolaus Dahmen; *32nd EUBCE*, 2024, Marseille, FR (poster)

From Pulp to Aromatic Products – Description of a reaction mechanism for lignin depolymerization during hydrothermal liquefaction; Maximilian Wörner, Ursel Hornung, Nicolaus Dahmen, *7th Doctoral Colloquium Bioenergy*, 2024, Leipzig, DE (presentation)

Abstract

As part of global efforts to reduce greenhouse gas emissions, it will be necessary to increasingly move away from fossil fuels and instead rely on renewable resources. This inevitably means that new sources of raw materials for important platform chemicals must also be found. The work presented here on the topic of “Hydrothermal liquefaction of black liquor” addresses this issue by investigating the conversion of lignin into aromatics under hydrothermal process conditions. Lignin is a promising raw material for the sustainable production of aromatics. In the pulp and paper industry, large quantities of lignin are dissolved in black liquor (BL) in the Kraft process. While many research projects on lignin utilization require prior separation of the lignin, the direct use of black liquor enables process integration without an additional extraction step. However, the complex matrix of BL, in particular the strongly basic and sulfur-containing salts, significantly influences the depolymerization of the lignin molecule, which makes it difficult to transfer the results from studies with extracted lignin. The aim of this work is therefore to systematically investigate hydrothermal liquefaction (HTL).

The experimental investigations were primarily carried out in batch micro autoclaves, but also in a continuous reactor. Temperatures between $250 - 400\,°C$, holding times of up to 30 minutes and pressures of approximately $200\,\mathrm{bar}$ were investigated. Black liquors from hardwood and softwood were examined comparatively, supplemented by model substances for the targeted analysis of individual reaction steps. The results show that direct HTL of black liquor leads to the formation of aromatic monomers, with catechol derivatives being the main products. The total yield of monomers was less than 5 wt% based on the biomass used, which is comparable to the yields of HTL of extracted lignin. The reaction temperature proved to be the dominant influencing factor, while the holding time played a minor role. The highest monomer yields were achieved at moderate temperatures of around $300 - 325\,°C$. At higher temperatures, the monomer yield decreased significantly, accompanied by increased solid formation.

To further understand the reaction mechanisms, oligomers were characterized using ^{13}C and ^{31}P NMR spectroscopy and size exclusion chromatography (SEC), in addition to monomers. It was found that the reactions observed in monomers, in particular demethoxylation, demethylation, and alkylation, also occur in oligomeric structures.

The intermediate 3-methoxycatechol plays a central role in the reaction network, especially in hardwood. As the temperature rises, repolymerization and condensation reactions increase, binding a large proportion of the carbon in solid, highly aromatic structures. The competition between depolymerization and repolymerization thus represents a significant limitation on monomer yield.

Based on the experimental results, a lumped reaction scheme was developed and a kinetic model was formulated and parameterized for the temperature range of 300 to $350\ °C$. The model describes the formation of key intermediate and final products with good agreement with the experimental data and consistently depicts both monomer formation and solid formation. A comparison of hardwood and softwood black liquor showed only minor differences in the overall yields, meaning that the model can be transferred with minor adjustments.

Another focus was on investigating the influence of the salts contained in the BL, in particular sodium sulfide (Na_2S). Experiments with model black liquor of varying HS^- concentrations showed that sulfide does not act solely as a catalyst, but is actively involved in organic reactions. Dimethyl sulfide (DMS) was identified as the dominant organic sulfur product, with a direct correlation between HS^- concentration and DMS yield. At the same time, increased sulfide concentrations accelerate depolymerization but also lead to increased secondary reactions. Compared to carbonates, hydroxides showed a slightly more favorable effect in terms of aromatic yield and reduction of solids formation.

Overall, the work provides an in-depth mechanistic and kinetic understanding of the hydrothermal liquefaction of black liquor. It shows that the direct use of BL for the formation of aromatic monomers is possible and yields results comparable to those obtained with extracted lignin, but identifies repolymerization, solid formation, and the formation of organosulfur compounds by HS^- ions in the feed as key challenges. The findings provide a robust foundation for further process optimization and the potential integration of HTL into the pulping industry for the sustainable production of aromatic platform chemicals.

Kurzzusammenfassung

Im Rahmen des globalen Bestrebens, die Treibhausgasemissionen zu reduzieren, wird es notwendig sein, immer mehr auf fossile Energieträger zu verzichten und stattdessen auf erneuerbare Ressourcen zurückzugreifen. Dies erfordert auch die Erschließung neuer Rohstoffquellen für wichtige Plattformchemikalien. Die vorliegende Arbeit zum Thema „Hydrothermale Verflüssigung von Schwarzlauge“ beschäftigt sich damit, in dem sie die stoffliche Nutzung von Lignin hin zu Aromaten unter hydrothermalen Prozessbedingungen untersucht. Lignin ist ein vielversprechender Rohstoff für die nachhaltige Herstellung von Aromaten. In der Zellstoff- und Papierindustrie fällt Lignin in großen Mengen gelöst in der Schwarzlauge (BL) im Kraft-Prozess an. Während viele Forschungsarbeiten zur Ligninverwertung eine vorherige Abtrennung des Lignins erfordern, ermöglicht die direkte Verwendung von Schwarzlauge eine Prozessintegration ohne zusätzlichen Isolationsschritt. Allerdings beeinflusst die komplexe Matrix der BL, insbesondere die stark basischen und schwefelhaltigen Salze, maßgeblich die Depolymerisierung des Ligninmoleküls, was die Übertragbarkeit der Ergebnisse aus Studien mit extrahiertem Lignin erschwert. Ziel der Arbeit ist es daher, die hydrothermale Verflüssigung (HTL) systematisch zu untersuchen.

Die experimentellen Untersuchungen wurden primär in Batch-Mikroautoklaven, aber auch in einem kontinuierlichen Reaktor durchgeführt. Dabei wurden Temperaturen zwischen $250 - 400\,°C$, Haltezeiten bis 30 Minuten und bei einem Druck von etwa $200\,\mathrm{bar}$ untersucht. Schwarzlaugen aus Laub- und Nadelholz wurden vergleichend untersucht, ergänzt durch Modellsubstanzen zur gezielten Analyse einzelner Reaktionsschritte. Die Ergebnisse zeigen, dass die direkte HTL von Schwarzlauge zur Bildung aromatischer Monomere führt, wobei Catechol-Derivate die Hauptprodukte darstellen. Die Gesamtausbeute an Monomeren lag unter 5 Gew.-% bezogen auf die eingesetzte Biomasse, was vergleichbar mit den Ausbeuten der HTL von extrahiertem Lignin ist. Die Reaktionstemperatur erwies sich als dominierender Einflussfaktor, während die Haltezeit eine untergeordnete Rolle spielte. Die höchsten Monomerausbeuten wurden bei moderaten Temperaturen von etwa $300 - 325\,°C$ erzielt. Bei höheren Temperaturen nahm die Monomerausbeute deutlich ab, begleitet von einer verstärkten Feststoffbildung.

Zur Aufklärung der Reaktionsmechanismen wurden neben den Monomeren auch Oligomere mittels ^{13}C- und ^{31}P NMR-Spektroskopie sowie Größenausschlusschromatographie (SEC) charakterisiert. Es zeigte sich, dass die an Monomeren beobachteten Reaktionen, insbesondere Demethoxylierung, Demethylierung und Alkylierung, auch an oligomeren Strukturen stattfinden. Das Intermediat 3-Methoxycatechol nimmt insbesondere bei Laubholz eine zentrale Rolle im Reaktionsnetzwerk ein. Mit steigender Temperatur treten verstärkt Repolymerisations- und Kondensationsreaktionen auf, wodurch ein erheblicher Anteil des Kohlenstoffs in festen, hoch aromatischen Strukturen gebunden wird. Die Konkurrenz zwischen Depolymerisation und Repolymerisation stellt somit eine wesentliche Limitierung der Monomerausbeute dar.

Auf Basis der experimentellen Ergebnisse wurde ein zusammengefasstes Reaktionsschema entwickelt und für den Temperaturbereich von $300 - 350\,°C$ ein kinetisches Modell formuliert und parametrisiert. Das Modell beschreibt die Bildung zentraler Zwischen- und Endprodukte mit guter Übereinstimmung zu den experimentellen Daten und bildet sowohl Monomerbildung als auch Feststoffentstehung konsistent ab. Der Vergleich von Laub- und Nadelholz-Schwarzlauge zeigte nur geringe Unterschiede in den Gesamtausbeuten, sodass das Modell mit geringfügigen Anpassungen übertragbar ist.

Ein weiterer Schwerpunkt lag auf der Untersuchung des Einflusses der in der BL enthaltenen Salze, insbesondere von Natriumsulfid (Na_2S). Experimente mit Modell-Schwarzlaugen unterschiedlicher HS^--Konzentrationen zeigten, dass Sulfid nicht ausschließlich katalytisch wirkt, sondern aktiv an organischen Reaktionen beteiligt ist. Dimethylsulfid (DMS) wurde als dominierendes organisches Schwefelprodukt identifiziert, wobei eine direkte Korrelation zwischen HS^--Konzentration und DMS-Ausbeute nachgewiesen wurde. Gleichzeitig beschleunigen erhöhte Sulfidkonzentrationen die Depolymerisation, führen jedoch auch zu verstärkten Sekundärreaktionen. Hydroxide zeigten im Vergleich zu Carbonaten eine leicht günstigere Wirkung hinsichtlich Aromatenausbeute und Reduktion der Feststoffbildung.

Insgesamt liefert die Arbeit ein vertieftes mechanistisches und kinetisches Verständnis der hydrothermalen Verflüssigung von Schwarzlauge. Sie zeigt, dass die direkte Nutzung von BL zur Bildung aromatischer Monomere möglich ist und vergleichbare

Ergebnisse wie mit extrahiertem Lignin liefert, identifiziert jedoch Repolymerisation und Feststoffbildung sowie die Bildung von Organoschwefelverbindungen durch HS^- Ionen im Feed als zentrale Herausforderungen. Die gewonnenen Erkenntnisse bilden eine fundierte Grundlage für die weitere Prozessoptimierung und die potenzielle Integration der HTL in die Zellstoffindustrie zur nachhaltigen Produktion aromatischer Plattformchemikalien.

Content

1 Introduction

1.1 Motivation

One of the greatest challenges facing humankind is mitigating climate change in order to minimize its threatening impact on the planet[1]. As a result, 195 countries agreed in the 2015 Paris Climate Agreement to keep global warming below 2 degrees Celsius in order to avoid exceeding possible irreversible tipping points[2]. The key objective is the reduction of CO_2 emissions, the most prominent of the greenhouse gases (GHG). However, the fact that global energy consumption continues to rise at the same time makes the challenges even more difficult[3]. In 2023, 619.63 EJ of primary energy was consumed, which is an increase of approx. 2 % compared to 2022[4]. Although the share of renewable energy increased slightly more than that of fossil fuels, the latter ones still cover approx. 81.4 % of global energy consumption[4]. In order to permanently reduce CO_2 emissions, the use of coal, oil and natural gas must inevitably be reduced. However, this will subsequently create shortages of by-products from fossil feedstocks. One prominent example is the class of aromatic compounds, which play a role in many different areas of our lives[5]. The most important ones are benzene, toluene and xylene, summarized under the acronym BTX, as they are produced in large quantities in the petroleum refining industry. The global (BTX) market was estimated at 128 MT in 2022[6]. Most of this is obtained as a by-product by catalytic cracking of the naphtha fraction or by steam cracking. If the use of crude oil to cover primary energy consumption is reduced, alternative production routes for aromatics must therefore be identified. Additionally, the feedstock should be based on renewable resources to achieve a positive impact on the GHG balance. Depending on the most promising feedstock and the process, which will be implemented in the future to replace the conventional refinery a shift from BTX to other aromatic compounds as basis chemicals may be inevitable.

1.2 Alternative process routes for aromatic compounds

For the production of aromatics on a largely CO_2-neutral basis, biomass can be used as a feedstock. Preferably, biomass should be utilized that does not compete to feed humans and animals at the same time[7]. One possible way of producing aromatic compounds is the methanol to aromatics (MtA) process via intermediate production of olefins. However, bio-based methanol must first be generated for this purpose[8,9]. Methanol synthesis from synthesis gas (CO/H_2) using a heterogeneous catalyst is the most common industrial route[10]. Biomass can, for example, be thermochemically converted to synthesis gas in a gasification process [11–13]. The optimal implementation of this process remains an active area of research and depends largely on the type of biomass and the desired purity of the product. In addition to the aforementioned reaction of CO and H_2 to methanol, this is also possible from CO_2. This has been investigated by Campos et al. in several studies ranging from micro-kinetics to a techno-economic assessment[14–16]. Bio-based aromatics could therefore be produced using the route from biomass via methanol.

Another approach to replace the BTX fraction from oil cracking is a Diels-Alder reaction of furan derivatives (furan, 2-methylfuran (MF), 2,5-dimethylfuran (DMF), furfural (FF), 5-hydroxymethylfurfural (HMF)) to aromatic hydrocarbons[17–19]. However, this also requires the production of furan derivatives based on the carbohydrate fraction of biomass[20]. Schade et al. carried out the direct catalytic conversion of sucrose to HMF and in a further step to 2,5-furandicarboxylic acid (FDCA)[21]. In general, furan compounds can be easily obtained from sugar. Therefore, biomass with a high sugar content is particularly suitable as a basis. In the work by Pfersich et al., sugar beet residues were therefore converted to HMF in a hydrothermal conversion[22]. It was shown that at moderate temperatures the sugar is first released in the form of glucose and fructose and then partially converted to HMF. It is therefore also possible to produce furan derivatives biobased and thus synthesize aromatics. However, a key limitation is that furan derivatives themselves already have great potential as platform chemicals. Thanks to the functional groups on the furan ring, various biopolymers can be produced which have the potential to replace polymers based on fossil raw materials[23–25].

In these two process routes presented for the production of bio-based aromatic compounds, several process steps are necessary to obtain the desired products. In

contrast, the process discussed in this work investigates how aromatic compounds can be produced thermochemically in one step from its precursors contained in lignin. For valorization of lignocellulosic biomass the above mentioned routes do not have to be in competition to each other. Due to the complexity of the feed and the large number of potentially viable products, it is necessary to combine suitable processes to achieve the most favourable outcome. The concept of biorefineries based on this approach is explained in more detail in the next chapter.

1.3 The biorefinery concept

Before discussing the direct thermochemical conversion of lignin in more detail, the concept of a biorefinery must be explained. The processes discussed above, as well as HTL of lignin as the main process investigated in this thesis, share a common limitation: they are unlikely to be economically viable as stand-alone processes. The biorefinery is a possible solution for producing chemicals or energy carriers as sustainably and economically as possible[26–30]. In a petrochemical refinery, crude oil as feedstock is divided into many product fractions through various thermochemical and catalytic processes and separation methods. The main focus is on the short and medium-chain fractions of gasoline, kerosene and diesel, while the highly viscous residues from vacuum distillation require further cracking or end up as bitumen in road asphalt or even solid petroleum coke, for example. In the case of biorefineries, a sustainable biomass-based feedstock serves as the primary input. Some of the process steps are identical or very similar to those in conventional refineries. Nevertheless, there are deviations, particularly in the treatment of water-rich process streams that usually occur when biomass is used. These can be, for instance, hydrothermal processes or aqueous phase reforming. Fermentation processes are also an option. Figure 1-1 provides an overview of typical processes that can be used in a biorefinery. There may be a defined target product for which the value chain is designed. In most cases, an isolated consideration of this main route is not competitive with conventional process routes based on fossil raw materials, as biomass is usually very heterogeneous in composition and often contains large quantities of water. However, different co- and by-products are produced during biorefining, each of which also has a potential value. The combination of all potential value streams can render the whole process economically viable.

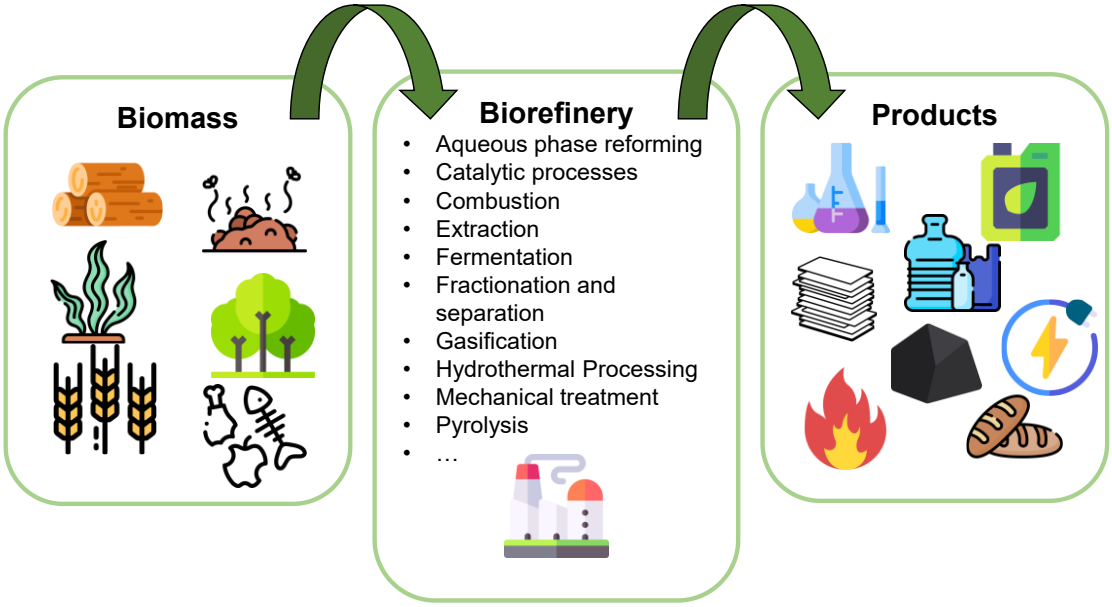

Figure 1-1: Typical processes for biomass conversion and valorization in a biorefinery concept; icons from Freepik, Flaticon[31]

An example of a biorefinery is the Äänekoski bioproduct mill in Äänekoski, Finland. It is a pulp mill based on softwoods and birch. The main product of the plant is pulp, with an annual production of approximately 1.3 million tons. In addition, there are various by-products that are obtained through various process steps. These make up 20 % of total sales[32]. These include, for instance, fiber products, biomethanol and bioenergy. The energy generated would theoretically be sufficient to supply more than two such biorefineries with enough electricity. Figure 1-2 shows an overview of the individual product streams. Other examples of wood-based biorefineries are Lenzing, Austria[33] and the biorefinery of UPM Biochemicals located in the chemical park Leuna in Germany, which is currently under construction[34]. Lignocellulosic biomass is particularly suitable for a biorefinery due to its different building blocks[35,36]. Lignin is suitable for both chemical and energy valorization. In addition to being used for paper production, cellulose can also be chemically modified or hydrolyzed into glucose for chemical conversions by catalytic reactions or fermentation processes. The same applies to hemicellulose.

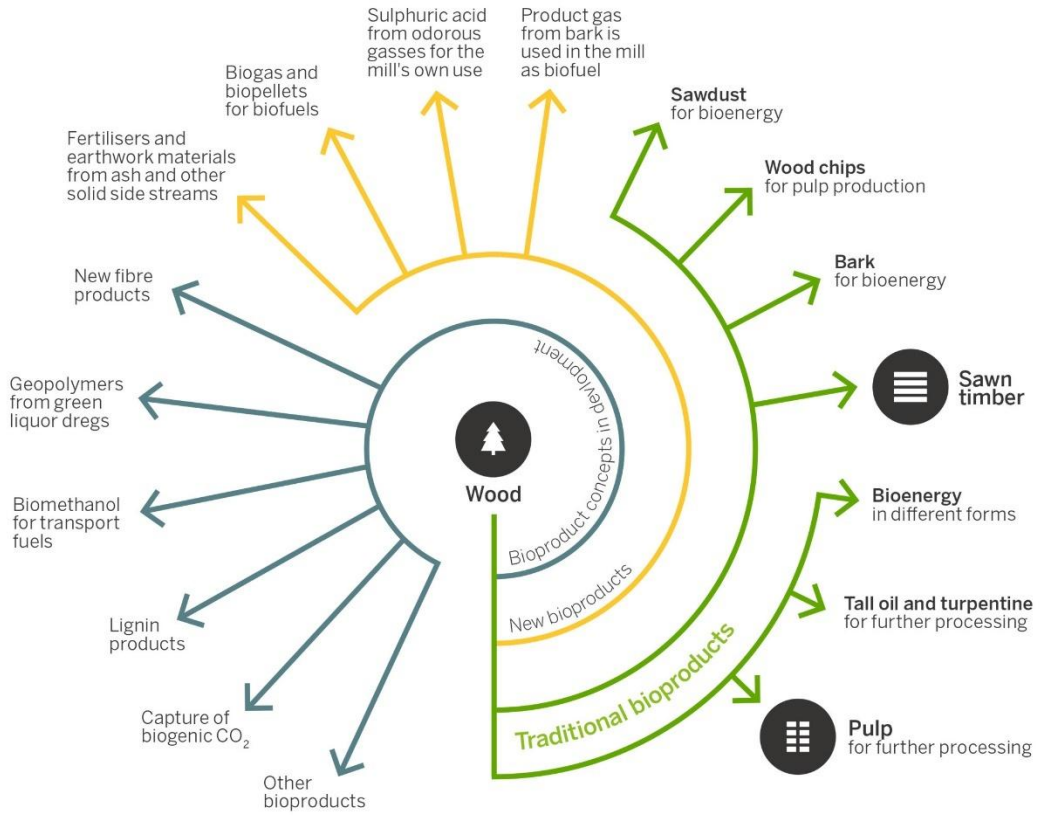

Figure 1-2: Overview of the different products from the Äänekoski bioproduct mill in Finland, all products are based on wood (lignocellulosic biomass), Copyright © Metsä Group [32]

1.4 Lignin – A biopolymer with high potential for chemical industry transformation

1.4.1 Origin and structure of the lignin molecule

The aforementioned biopolymer lignin offers great potential for the production of important chemicals or fuels. In nature, lignin always occurs together with cellulose and hemicellulose as part of lignocellulosic biomass[37]. Lignin is embedded in the cell walls of plant cells and provides structural strength[38,39]. Accordingly, the lignin content varies among different plant species, so trees have significantly more lignin, up to more than 30 %, than grasses. At the same time, it is the only molecule found in nature, apart from fossil resources, that has a high density of aromatic rings (see Figure 1-3). Therefore, lignin is interesting for the production of aromatics, as the structures are already present and no new aromatic structures need to be formed if direct conversion of lignin to aromatics is possible.

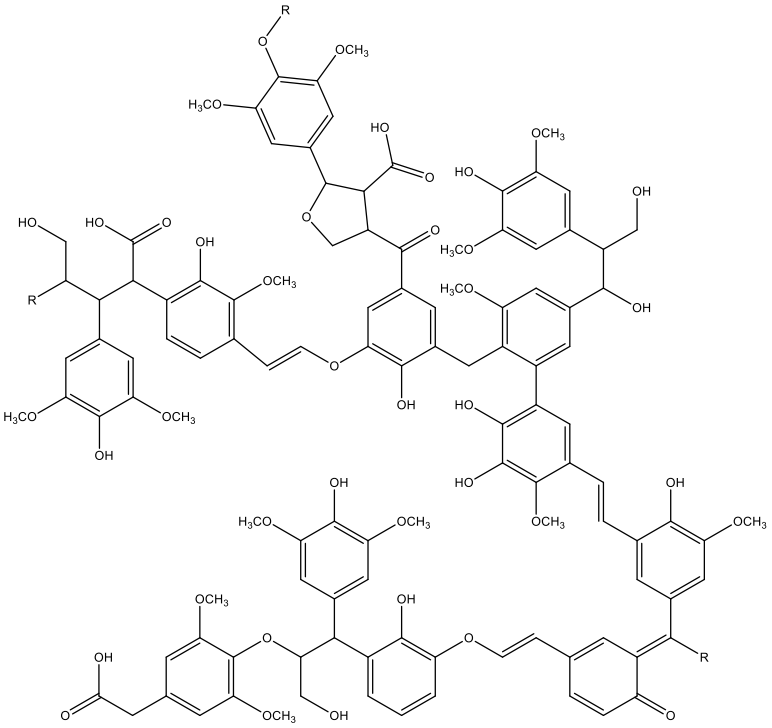

Figure 1-3: Possible chemical structure of a part of lignin; reproduced with permission from Lange et al.[40]; Copyright 2013 Elsevier.

The biopolymer is made up of three different phenylpropanoids: Coniferyl alcohol, sinapyl alcohol and p-coumaryl alcohol (see Figure 1-4). These three compounds are linked via various bonds, such as esters, ethers or C-C bonds, and form a highly branched macromolecule[41,42]. In nature, lignin is biosynthesized with the help of several enzymes[43]. Based on the three building blocks, the share of aromatic rings (C_6H_6) is around 40 – 50 % depending on the wood type.

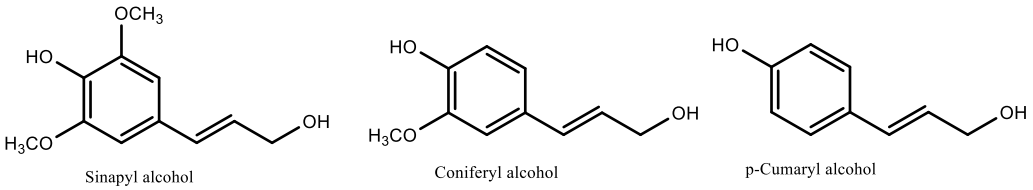

Figure 1-4: The three phenyl propanoid molecules which act as building blocks for the lignin macromolecule

The structural composition of lignin differs depending on the plant species. For the purposes of our work, the most important distinction is between softwood and hardwood. The first class includes the wood of pines or other conifers. Hardwood includes all deciduous trees, such as eucalyptus trees[44,45]. An important difference is, for example, the proportion of the three phenylpropanoids. Softwood is composed

almost exclusively of coniferyl alcohol (95 %), often referred to as the G type (guaiacyl group within the molecule). Hardwood, on the other hand, is mainly composed of sinapyl alcohol, also known as the S type (S for syringyl group). The S/G ratio is approximately 70:30. The share of p-coumaryl alcohol, also known as H type, only plays a subordinate role. The different proportions of the molecules used for the structure are reflected in the frequency of different bond types. Depending on the source and extraction or other separation method, the molecular weight of native lignin can range between 2000 and 50 000 $g \cdot mol^{-1}$ [46].

1.4.2 Different extraction methods and the main industrial source of lignin

As lignin is a by-product of various industrial forestry processes and does not contribute to the food-versus-fuel debate, it has long been the focus of research, especially as a feedstock for a possible biorefinery[36,47]. Despite the great research efforts and the great potential of lignin, only vanillin is currently produced as an aromatic product on an industrial scale from depolymerization processes[48].

Lignin is provided on the basis of various extraction options[42,49]. An alternative, but not yet commercially viable, approach is the Organosolv process, in which cellulose fibers are separated from the lignin under acidic conditions at elevated temperatures around 200 °C[50,51]. In this process, the lignin molecule is only slightly altered in structure. A major advantage is the production of sulfur-free lignin which is more suitable for downstream processing. The extraction of native, unmodified lignin from the lignocellulose is also possible, but rather complex for industrial implementation[52]. However, by far the biggest source of lignin is the production of pulp. The pulp and paper industry is a major producer of lignin, which is generated as a by-product. Approximately 50 million tons of lignin are produced annually in this sector[49]. The process used to separate cellulose fibers from wood materials is primarily the Kraft process, which is the most widely used method in pulp mills around the world. Figure 1-5 shows a simplified flow scheme of the conventional Kraft process. In this process, cellulose fibers are separated from other components of the wood, which are dissolved, together with the cooking chemicals, in an alkaline solution known as black liquor (BL).

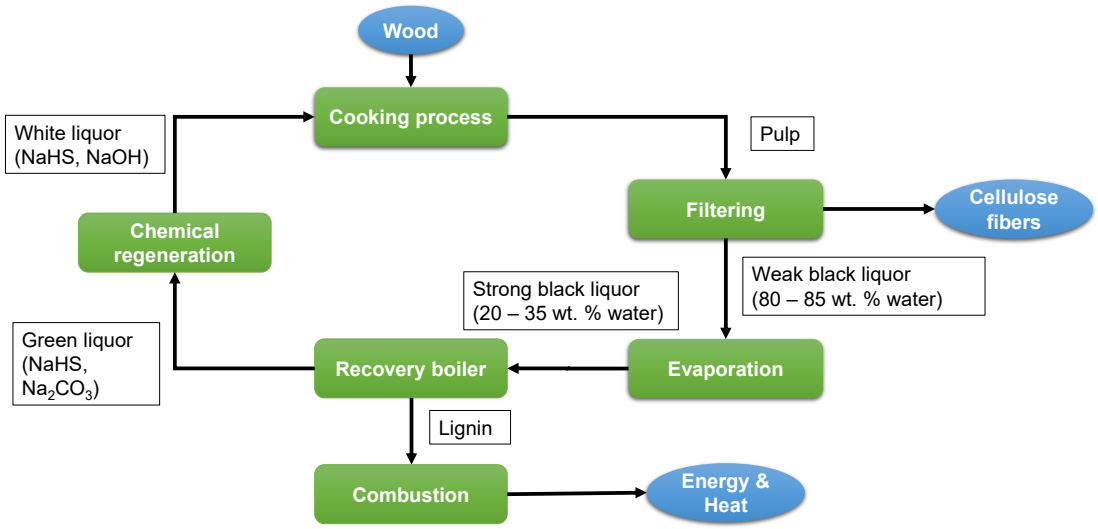

Figure 1-5: Simplified flow scheme of the conventional Kraft process

The lignin structure undergoes changes as specific bonds are broken. The resulting lignin is known as Kraft lignin, with bonds such as the aryl-alkyl ether bond (β-O-4 bond) being significantly reduced during the Kraft process[53,54]. This influences subsequent depolymerization reactions. Most of the lignin produced during the pulping process is burned to generate electricity and heat, as well as to recycle the pulping chemicals (white liquor) used in the process. Traditionally, the energy generated is used to cover the energy needs of the pulp mill. However, large modern pulp mills generate such a surplus of energy that it has to be sold on the market[55]. Additionally, a significant amount of energy is required to evaporate water and concentrate black liquor from 15 – 20 wt. % to 65 – 80 wt. %[56]. An alternative to burning lignin is to recover it for chemical use, converting it into higher-value products[57]. This could provide a greater economic benefit, if the production of platform chemicals could generate higher revenues and experience less price volatility than the sale of "green" electricity on the open market. However, lignin recovery and the further processing of black liquor require additional steps. The lignin must first be extracted from the black liquor and then dried to make it suitable for chemical processing. Due to its high content of aromatic rings, lignin appears particularly promising for producing aromatic compounds that can serve as platform chemicals or industrial substitutes. The recovery and further utilization of lignin thus represents a significant opportunity for the chemical industry.

1.5 State of the art of lignin depolymerization

The direct valorization of lignin to aromatics, which can be used as platform chemicals, has been investigated in many studies. Various C-C and C-O bonds in the lignin molecule are broken through catalytic or thermochemical depolymerization. Due to the lignin structure, aromatic monomers and oligomers are formed. The most important approaches are presented below. An overview is shown in Figure 1-6.

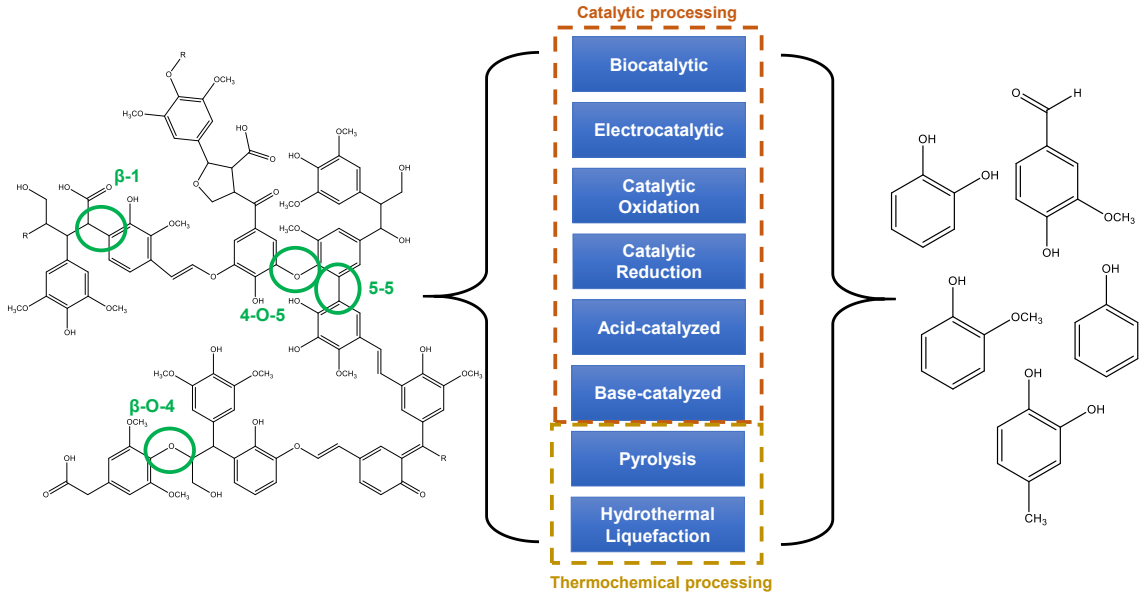

Figure 1-6: Overview of the described depolymerization processes for lignin depolymerization to aromatics; the most abundant and characteristic bonds in the lignin structure are highlighted in the green circles; molecule structure on the right is reproduced with permission from ref. Lange et al.[40]; Copyright 2013 Elsevier; the names of the aromatic compounds on the right side as well as others which will be part of the discussion in the thesis can be found in Figure 8-1 in the supplementary material

1.5.1 Catalytic Depolymerization

Biocatalytic depolymerization

One of the many ways to depolymerize lignin is a biocatalytic approach using enzymes[58]. Various fungal species or bacteria are known from nature that can decompose lignin using enzymes, e.g. the so-called laccases or peroxidases[59,60]. Jahn et al. were able to convert up to 9 % of the lignin into aromatic compounds using two different enzymes[61]. An important point here is the accessibility of the targeted bonds in the molecule for the enzyme. Catechol was one of the main products. In the study

by Rodriguez-Escribano et al. laccase enzymes were specifically adapted to the high pH > 10 of kraft lignin[62]. Depolymerization of the lignin molecules as well as demethylation could be demonstrated. Due to the additional component in the form of enzymes in the process, very careful regulation of the process parameters is necessary in order to achieve the best possible results. For this reason, the biotechnological depolymerization of lignin has not yet been developed beyond the laboratory scale.

Electro-catalyzed depolymerization

Another strategy for lignin decomposition that is being investigated in research is the application of electrochemical processes[63]. The advantages of these methods are, for example, the good integration of electricity generated from renewable sources and the milder reaction conditions compared to other types of process. Two of the most commonly used variants are electrooxidation and electroreduction. The catalysts used are usually the anode (heterogeneous catalyst) or the electrolyte (homogeneous catalyst). For example, Movil-Cabrera et al. used an anode consisting of a cobalt core coated with a partial layer of platinum. This allowed lignin to be oxidized to various platform chemicals such as phenol. In addition, it was observed that some products accumulated over time and were therefore stable, while others continued to react through subsequent reactions[64]. In a more complex system studied by Xie et al., the focus was on the electrolyte and mediators from transition metal complexes based on iron or manganese (electrolytic mediator system (EMS))[65]. These mediators serve as a link between the electrodes and the lignin by promoting electron transfer and should accelerate depolymerization. Di Marino et al. demonstrated that the use of deep eutectic solvents (DES) based on choline chloride as electrolyte results in a broader selection of materials for the electrodes[66]. Since DES are able to dissolve lignin even without a high pH value, metals, which would not be suitable under alkaline conditions, can be used as catalyst/electrode. In parallel, oxidative depolymerization was successful with vanillin and guaiacol as the most common products. By extending the system with methyl isobutyl ketone (MIBK) to an emulsion, it was even possible to extract the organic products directly in the system[67]. The results show that it is possible to depolymerize lignin with electrocatalysis, but also that the system between electrodes, electrolyte and lignin is very complex and must be harmonized. Therefore, a larger-scale technical implementation is not yet feasible.

In addition to the bio- and electrochemically catalyzed processes presented above, there are also several more conventional catalytic methods[68–70]. A distinction is made between metal catalyzed processes for hydrogenation[71,72] and oxidation[73,74] of the lignin molecule to break the intramolecular bonds, as well as acidic and basic catalysis[75,76].

Metal-catalyzed depolymerization – oxidation and reduction

The aim of oxidative depolymerization of lignin is to break the C-O and C-C bonds in the molecule by oxidation, e.g. to ketones, aldehydes or carboxyl groups[73]. Typically, oxidizing agents such as hydrogen peroxide or molecular oxygen are used[77,78]. Mild conditions of $T = 100 - 300\ °C$ at atmospheric or slightly higher pressure are preferred for catalysis. Ahmad et al. were even able to demonstrate depolymerization of the lignin molecule under ambient conditions[79]. However, the work did not use a metallic catalyst but nitric acid. Typical catalysts for oxidation are compounds containing transition metals such as copper, iron, manganese, zirconium or cobalt[69,80,81]. A prominent example is the Borregard process for the production of vanillin from Kraft lignin for which Cu(II) compounds are used[48,82,83]. Iron compounds such as $FeCl_3$ can also break C-O bonds such as the β-O-4 bond in lignin. Mottweiler et al. demonstrated this using model substances with β-O-4 bonds with the addition of peroxides[84]. In combination with the solvent dimethyl sulfoxide (DMSO), methyl radicals were formed, which accelerate the cleavage of the bonds. Typical aromatic compounds formed during oxidation are vanillin or syringaldehyde[85]. Due to the oxidative atmosphere, these are mostly aldehydes or acids. As many of the metal compounds are only effective in alkaline or basic atmospheres, research has shifted towards oxides. At best, these can also perform under neutral conditions in water. Hdidou et al. have produced CoFeO mixed oxides in the form of nanoparticles using an alginate gelation process. The performance of the catalysts in water at a pH 7 was evaluated, partly with the addition of methanol to reduce char formation. As expected, syringaldehyde and vanillin showed the highest selectivity among the aromatic compounds. The highest yields of aromatics were achieved at a reaction temperature of $T = 200\ °C$ and a 10 % oxygen atmosphere at $p = 100\ kPa$. A decrease in molecular weight and the associated breaking of various molecular bonds was verified using GPC analysis[86,87]. Other catalysts used for oxidative depolymerization include polyoxometalates[88,89] and perovskites[90–93].

In the reductive depolymerization of lignin, hydrogen plays an important role. The process usually takes place in a hydrogen atmosphere at a reaction temperature of $T = 250 - 400\,°C$ and a pressure $p = 30 - 200\,bar$[74]. The aim is to break the β-O-4 bond via a reduction in order to produce aromatics or alcohols. Due to the reductive environment, saturated hydrocarbons such as alkanes are also produced. Simultaneously, hydrodeoxygenation (HDO) takes place, which leads to a reduction in the oxygen content. As a result, biofuels are also conceivable as a product. Noble metals such as palladium, platinum or rhodium are usually used[94–96] , but cheaper alternatives such as the transition metals nickel, cobalt or iron can also be used[97,98]. Activated carbon, metal oxides or zeolites are usually used as support materials[94,99]. In addition to the use of H_2 as a hydrogen source, hydrogen donors can likewise be applied. Common hydrogen donors are, for example, short-chain alcohols such as methanol or ethanol or the corresponding aldehydes. These can be used as a pure medium or as a mixture with water as a solvent[94]. In their work, Paone et al. compared various C1-3 alcohols in inert and hydrogen-containing atmospheres to see how the typical C-O lignin bonds (β-O-4, 4-O-5) in model substances can be cleaved by hydrogenation and hydrogenolysis under these conditions[100]. The type of lignin also affects hydrogenolysis. Native lignin appears to have a higher affinity for cleavage by hydrogen compared to organosolv lignin and thus a higher yield of aromatics, possibly due to the greater abundance of β-O-4 bonds in the molecule[101]. Another interesting approach is the catalytic depolymerization of lignin in pure ethanol under supercritical conditions [102,103]. In an inert nitrogen atmosphere and temperatures between $T = 200 - 420\,°C$ as well as a CuMgAl oxide catalyst, the ethanol not only serves as a hydrogen donor but also ensures that repolymerization effects are prevented. In the studies, Huang et al. were able to obtain up to 67 wt. % monomers from the lignin used. It was also observed that condensation reactions were responsible for repolymerization at lower temperatures, while char formation was the decisive factor at higher temperatures. The range $T = 300 - 400\,°C$ proved to be the best for suppressing repolymerization due to alkylation of the aromatics by the supercritical ethanol. Another study by Xie et al. also shows that it is possible to form very specific products with catalytic depolymerization[104]. By adding ammonia (NH_3) to the hydrogen, a high yield of amines of up to 7.6 wt. % was achieved.

Acid- and base-catalyzed depolymerization

The acid-catalyzed depolymerization of lignin is based on various protonations induced by the acidic environment, e.g., of hydroxyl groups. Different mechanisms subsequently lead to the cleavage of the bond and stabilization of the resulting molecules[105,106]. Catalysis takes place at temperatures $T = 150 - 400\,°C$ and a pressure $p = 1 - 30\,\mathrm{bar}$. The solvent must be selected in such a way that the lignin is dissolved as completely as possible. Mixtures of water and an organic solvent or a solution of one or more organic solvents are usually used[107,108]. The reaction parameters play a role in the solubility. Ionic liquids can also be chosen, as they have special properties that make it possible to completely dissolve polyvalent molecules such as lignin[109]. Organic and mineral acids can be used as catalyst. Sturgeon et al. have shown, for example, using model substances that have the specific ß-O-4 bond in the molecular structure, that these bonds can be successfully broken using sulfuric acid as an acid catalyst[110]. Besides liquid acids, solid acids can also be applied. Various metal oxides or zeolites are used for this procedure[111,112]. In this manner, the typical aromatic compounds such as guaiacol, syringol and other phenol derivatives can be obtained from lignin.

Correspondingly, bases such as NaOH or KOH are used for base-catalyzed depolymerization[76,113]. In contrast to acid-catalyzed depolymerization, the reaction conditions are harsher. The temperature is usually around $T = 300\,°C$ and the corresponding pressure can exceed 200 bar, although this can already be referred to as hydrothermal liquefaction, in which the thermochemical properties are more important[114–116]. The main reaction promoted by base catalysis is the hydrolytic cleavage of the β-O-4 bond in the lignin molecule. Therefore, the typical aromatic compounds are also formed as products, partly in the form of an organic phase or dissolved in the aqueous phase, since phenolic aromatic compounds are preferably present as phenolate due to the alkalinity of the reaction medium[117,118]. Erdocia et al. have obtained 12 - 20 wt. % yield of oil from various organosolv lignins using NaOH-catalyzed depolymerization, which contains up to 30 wt. % aromatic compounds, with catechol as the dominant component[119]. As with the other processes, the type of lignin has a major influence on the composition of the products. In addition, the concentration of the base plays a role in the selectivity of the individual aromatics. Kim et al. showed that by increasing the NaOH concentration from 0 to 7 %, a shift in the main products

from syringol via guaiacol to catechols and phenols can be observed. The temperature increase from $T = 280\,°C - 320\,°C$ shows a similar effect[120]. As with acid-catalyzed depolymerization, solid catalysts can be used successfully. These include, for example, calcium oxide or sodium-based zeolites[121,122].

1.5.2 Thermochemical Depolymerization

Pyrolysis

All the processes described so far for the depolymerization of lignin are based mainly on catalytic effects. Pyrolysis, on the other hand, focuses on radical-induced cleavage reactions[123]. A difference is made between slow and fast pyrolysis, whereby only fast pyrolysis is relevant for the comparison with the HTL used in this work. The main differences are the heating rate, the reaction temperature and residence time before rapid cooling of the products, which ultimately leads to more solid (slow) or more liquid product (fast)[124]. Two important aspects for the pyrolysis process are the absence of atmospheric oxygen and the need for a dry feedstock, which limits the direct use of biomass without prior drying. Nevertheless, pyrolysis is probably the most advanced process from an industrial point of view for the production of bio-oil mainly for energetic use but also to obtain platform chemicals from biomass. Therefore, there are also some studies on aromatics production from lignin using pyrolysis. Shen et al. compared lignin from a maple tree with lignin of rice plants using a pyro-GC/MS in which pyrolysis took place at $T = 550 - 900\,°C$[125]. Phenolic as well as BTX compounds were detected in the pyrolysis product of all lignin types investigated. Further work with different types of lignin resulted in similar product compositions[126,127]. In the study of Patwardhan et al., the reduction of aromatic monomer yields due to repolymerization, which occurs in all depolymerization processes for lignin, is also discussed. It was shown that repolymerization reactions take place especially during condensation of the gases and vapors produced by the primary pyrolysis, which favors the formation of dimers and oligomers from monomers. This is presumably due to the fact that cooling causes the remaining free radicals to combine with various other compounds. Capping agents or co-processing of another feedstock are promising options for minimizing repolymerization activity. Fan et al. achieved a high selectivity of 82.6 % of mono-aromatics through the co-pyrolysis of lignin and waste cooking oil[128]. Further studies on the reaction mechanism with model substances suggest that the polar groups of the fatty acids act as a capping agent in combination with a zeolite catalyst. Even

without co-processing, the addition of catalysts can be used to shift the selectivity towards aromatic compounds, and the thermochemical cleavage reactions can be combined with the catalytic cleavage reactions. Several studies report successful testing of zeolites as catalysts during pyrolysis to obtain higher yields of aromatics[129,130]. In the work of Shen et al. the addition of zeolites resulted in BTX aromatics in particular being very prominent in the product phase compared to other aromatics such as phenols[131]. In comparison, the blank test delivered little to no BTX aromatics as products.

In principle, pyrolysis is well suited to converting dry biomass such as lignin largely into a bio-oil, which can be used for upgrading to fuel components or from which value-added chemicals can be extracted. However, efficient pyrolysis requires dry biomass. Biomass or waste streams such as municipal solid waste (MSW) and cattle manure, all of which are potentially suitable feedstocks for thermochemical conversion, always contain a certain amount of water[132]. In order to convert moist biomass or waste streams directly thermochemically, a hydrothermal process is an option. Doassans-Carrère et al. have compared fast pyrolysis with HTL[133]. The same feedstock, dried beech sawdust, was used for the comparison. Water was added for the HTL. Although pyrolysis achieves higher yields of the bio-oil fraction, on a water-free base the yields are closer together. Additionally, bio-oil based on pyrolysis consists of more oxygenated compounds. Pyrolysis also performed better for the aromatic monomers. Interestingly, however, the ^{1}H NMR analysis shows a higher proportion of hydrogen bound to aromatics in the HTL. This suggests that di- or oligomers have not yet been cleaved or formed by repolymerization. It can therefore be assumed that there is still potential for increasing aromatic yields in HTL.

1.5.3 Hydrothermal liquefaction of lignin

Prior to presenting some current studies on the hydrothermal liquefaction (HTL) of lignin, the HTL process itself will first be introduced in more detail, as this is the underlying process for this work. HTL falls into the category of hydrothermal processes. These are carried out in water at elevated temperatures and pressure. In contrast to pyrolysis, the presence of water is necessary, as it acts as reaction medium, catalyst, and reactant. Therefore, feedstocks with high moisture or feedstocks that are completely dissolved in water can beneficially be used directly in hydrothermal

processes. The parameters should be selected in such a way that the water does not evaporate at reaction temperature.

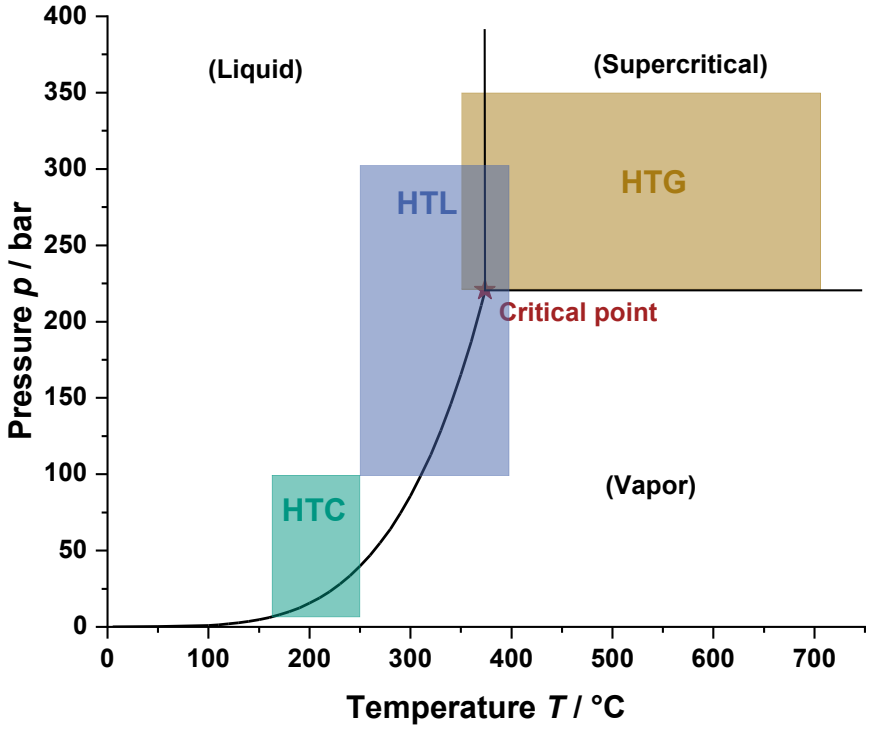

Figure 1-7: Vapor-pressure curve for water up to the critical point; HTC, HTL and HTG with their respective parameter range are included along the curve[134–138]

Figure 1-7 shows the vapor pressure curve of water up to the critical point ($T_c = 374$ °C, $p_c = 221$ bar) as well as the parameter range of three different types of hydrothermal processes. At temperatures of $T = 100 - 250$ °C and pressures of $p = 20 - 100$ bar, the process is referred to as hydrothermal carbonization (HTC). This method aims to produce a biochar from biomass or waste streams that has significantly better drying and heating properties, e.g. less oxygen content than in the feedstock[134,138]. In general, the process is very suitable for removing several inorganic substances and elements from a contaminated feedstock[139]. Close to or above the critical point of water is the area of hydrothermal gasification (HTG). As the name suggests, the aim is to produce a fuel gas. The main products are CH_4, CO_2 and H_2[140]. The parameter range for HTG without a catalyst is between $T = 550 - 700$ °C and $p = 250 - 350$ bar with H_2 as main product. By adding a catalyst, the process can also be carried out in the near-critical range to produce primarily CH_4 at low temperatures[141]. The range of hydrothermal liquefaction (HTL) relevant for this work lies between the two processes mentioned above at temperatures of $T = 250 - 400$ °C and pressures of $p = 150 - 300$ bar. In this

partially subcritical or supercritical range, the relevant product fraction is the liquid phase, referred to as bio-oil[136,137].

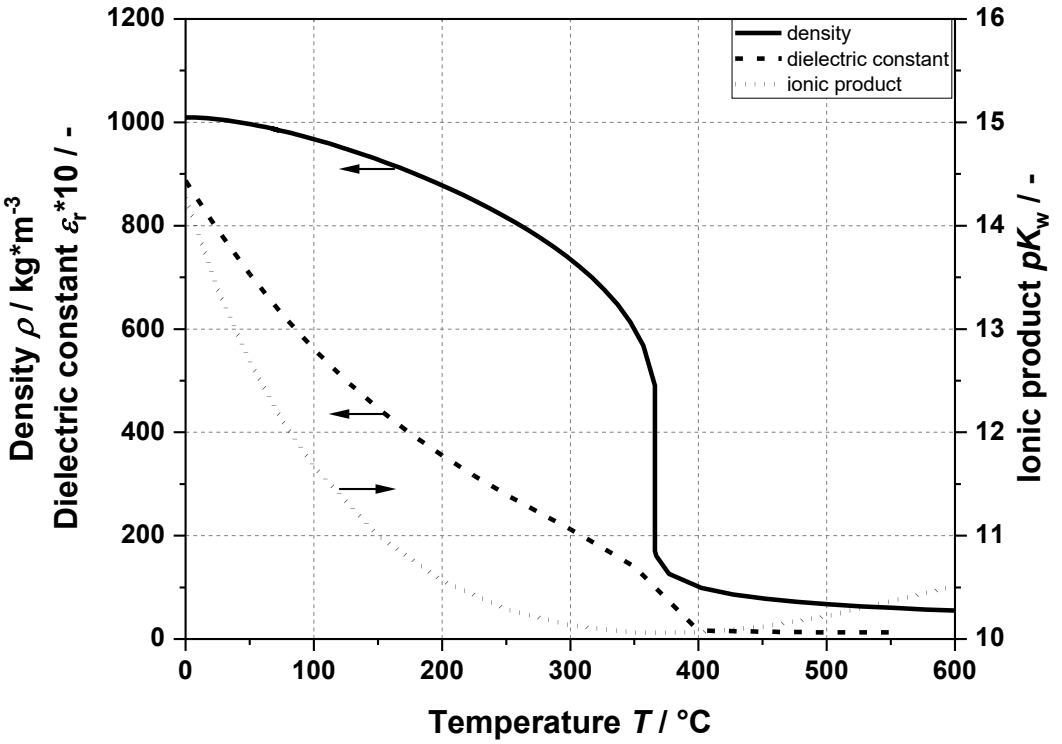

Figure 1-8: The change of density, the dielectric constant and the ionic product of water (negative logarithm) due to rising temperatures at pressure $p = 200\ \mathrm{bar}$[142–144]

Particularly in the near-critical range, the properties of the water change drastically. The resulting effects intensify and accelerate the depolymerization of the feedstock[145]. Figure 1-8 shows the density ρ, the dielectric constant ε_r and the ion product of water pK_w (negative logarithm) versus temperature at a pressure of $p = 200\ \mathrm{bar}$. It can be seen how the last two decrease steadily with increasing temperature and reach their minimum in the range between $T = 350 - 400\ °\mathrm{C}$. The density also falls to just above $T = 350\ °\mathrm{C}$, where a drastic drop can be seen. At this point, the liquid water changes its state into the gas phase. Since the dielectric constant is linked to the polarity of the solvent, this leads to water behaving like a nonpolar solvent under these near-critical conditions, capable of dissolving nonpolar organic substances occurring as intermediate or final products during the depolymerization of lignin. Water in this state acts more like acetone, for example (dielectric constant of $\varepsilon_r = 20.5$ at $T = 25\ °\mathrm{C}$). The decrease in density, in addition, is connected with a higher diffusivity as well as lower degree of hydrogen bonding and viscosity, which consequently leads to better transport properties of compounds in water[145]. Due to the higher ionic, the extent of

water self-dissociation is increased up to a 1000-fold higher concentration of H^+ and OH^- ions. Ultimately, a higher concentration of these ions accelerates acid- or base-catalyzed reactions during the HTL process[146,147].

Many scientific studies focus on understanding the depolymerization of lignin under typical hydrothermal liquefaction (HTL) conditions. This knowledge is essential to optimize product yields and better control reaction pathways as a prerequisite to process development. A common approach involves using technical lignin dissolved in an alkaline solution, typically with potassium or sodium salts such as hydroxides or carbonates (NaOH, KOH, Na_2CO_3, K_2CO_3), which also function as homogeneous catalysts. Belkheiri et al. investigated how varying the sodium-to-potassium ratio affects product yields across different phases, particularly phenolic compounds[148,149]. They found that increasing the sodium content led to a reduction in suspended solids within the light oil fraction, while solids increased in the heavy oil fraction. These differences were attributed to the solvents used in phase separation. Other properties, however, were largely unaffected by the Na/K ratio. As with other lignin depolymerization processes, the type and origin of lignin significantly influence the yield of aromatic monomers[150]. In addition to homogeneous catalysts, heterogeneous catalysts can also be employed. For instance, Breunig et al. used an iron–sulfur catalyst inspired by the Bergius process for coal hydrogenation[151]. Forchheim et al. explored the use of Raney nickel with lignin and model compounds under HTL conditions, which enhanced hydrodeoxygenation and increased phenol yields[152]. However, in both cases, catalyst recovery remains a major challenge. Solvent mixtures can also impact depolymerization. Cheng et al. demonstrated effective breakdown of lignin (initial molecular weight $M_w = 60{,}000\ \mathrm{g \cdot mol^{-1}}$) to $M_w = 1{,}010\ \mathrm{g \cdot mol^{-1}}$ using a 50:50 water/ethanol mixture[153]. A significant challenge in lignin depolymerization is repolymerization, which is driven by reactive intermediates formed during the process. To mitigate this, capping agents like phenol or boric acid have been proposed[148,154]. Due to the structural complexity of lignin, the resulting product spectrum consists of numerous chemical species, making it difficult to identify individual intermediates and final products. To address this, Wahyudiono et al. used model compounds such as catechol and guaiacol to produce phenol through HTL and determined kinetic parameters from these experiments[155–157]. Another approach to studying HTL kinetics involves minimizing experimental variability and using specialized reactors. Yong and Matsumura investigated lignin behavior under subcritical and supercritical water

conditions using a small-volume reactor[158,159]. This setup enabled rapid heating, which suppressed secondary reactions during heating and cooling. They examined very short reaction times (0–10 seconds), developed a kinetic model, and showed that lignin depolymerization follows a linear trend in the Arrhenius plot across both regimes. Despite progress in this field, many open questions remain. Continued research is needed to fully harness the potential of lignin valorization through HTL.

1.6 Direct HTL of black liquor and the „Black Liquor to Fuels" (BL2F) project

A common characteristic of all the studies discussed so far is that they are based on different types of extracted and solid lignin. However, this is counterproductive, especially with regard to HTL, as it takes away the advantage of the direct use of wet feedstock compared to processes such as pyrolysis. In chapter 1.5 it was mentioned that most of the lignin is produced as black liquor in pulp production. The lignin is dissolved in this liquor together with the cooking chemicals such as NaOH or Na_2S (see Table 1-1 for an example salt concentration in a BL).

Table 1-1: Mass fraction of inorganic salts in BL based on pine wood after Kraft process (dry-matter based)[160]

Na_2S	17 wt. %
Na_2SO_4	12 wt. %
$Na_2S_2O_3$	14 wt. %
Na_2SO_3	7 wt. %
NaOH	6 wt. %
Na_2CO_3	32 wt. %
Others	12 wt. %

Compared to the liquefaction of lignin starting with solid material, significantly fewer studies have investigated the direct utilization of black liquor in a liquefaction process. There are several possibilities for converting BL directly into promising products[161]. Jia et al. were able to extract some interesting compounds directly from the BL using acid precipitation with H_2SO_4 and subsequent fractionation with ethanol, as the lignin is already more depolymerized by the Kraft process[162]. Gasification to synthesis gas is another conceivable option, as the computer-aided process simulation by Domingos

et al. shows[163]. Due to the components and properties of the BL, it would make sense to utilize it directly in an HTL instead of first extracting and drying the lignin. At the same time, some of the alkali salts present in the BL are added anyway as a homogeneous catalyst or to improve the solubility of the lignin in water during HTL. There is still little research on the direct HTL of BL. A very detailed parameter study was carried out by Harisankar et al. but without using liquid BL. For their work, they first dried the BL to obtain a solid, which was then mixed with water[164]. The direct use of black liquor in the HTL was investigated by Orebom et al. at $T = 340 - 410\ °C$ and a residence time of $t = 10 - 120\ \mathrm{min}$. The evaluation of the experimental results focused primarily on the bio-oil and biochar yield[165]. In the work by Huet et al., BL was also introduced directly into the HTL reactor. The BL was previously produced by cooking wood chips. In contrast to the sulfur-containing BL from the Kraft process, however, soda digestion was used[166]. As a result, the feedstock is sulfur-free, which may influence the depolymerization of the lignin.

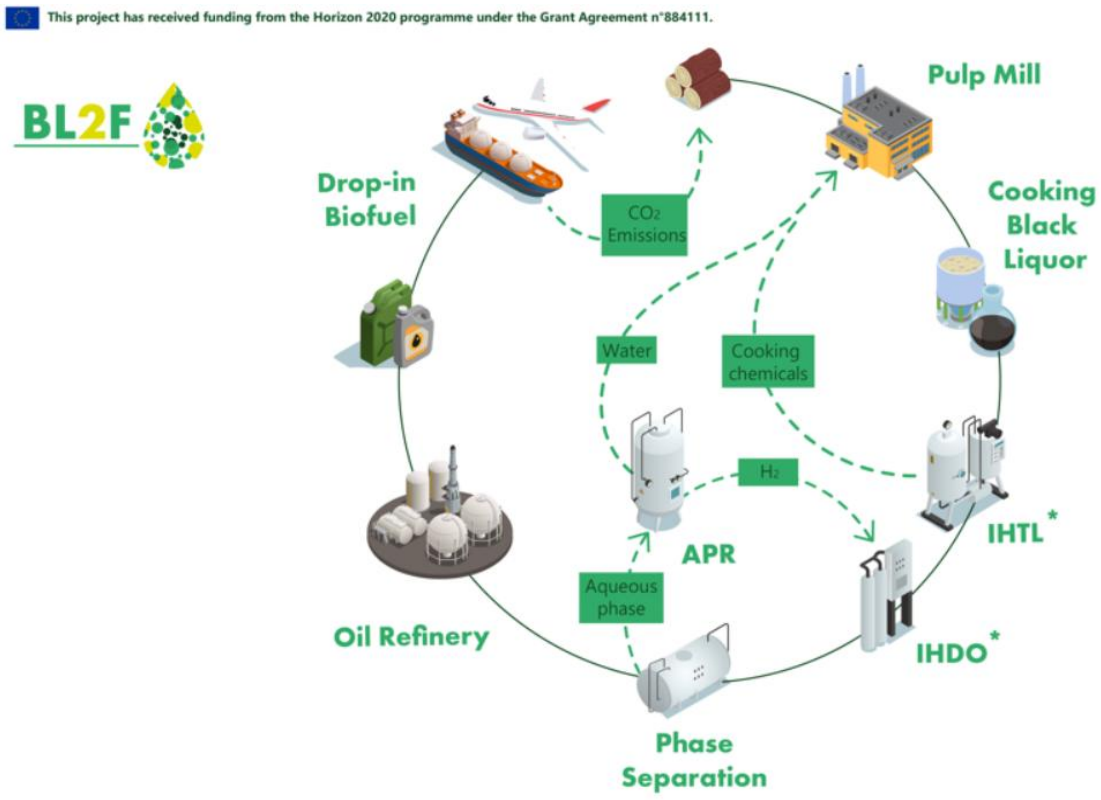

Figure 1-9: Graphic of recirculated product streams in the BL2F concept for an integrated HTL process into a pulp mill for direct lignin depolymerization; IHTL = Integrated hydrothermal liquefaction; IHDO = integrated hydrodeoxygenation[167]

Based on the economic and material potential for the direct use of black liquor and the research gaps, especially with regard to sulfur-containing BL and lignin polymerization, the EU Horizon 2020 project “Black Liquor to Fuels” (BL2F) was launched. The aim was to produce drop-in biofuels for marine or aviation applications from lignin using HTL. The black liquor was used directly in the HTL process. Based on the concept of biorefineries (see Chapter 1.3), HTL and hydrodeoxygenation (HDO) should be integrated directly into the pulp mill. In addition, all by-product streams, e.g. the aqueous phase in an aqueous phase reforming (APR) step, should be utilized (see Figure 1-9). The effect of the salts, especially Na_2S, on the HTL process and the depolymerization of the lignin as well as the recovery of the salts, which can then be recycled as cooking chemicals, were also important[168,169]. The flow scheme of a Kraft process with integrated HTL and recovery of the salts can be seen in Figure 1-10. Parts of this work also contributed to the project goals. The evaluation of the parameter and kinetic studies for the HTL of BL can be related to either bio-oil production or the production of aromatic compounds.

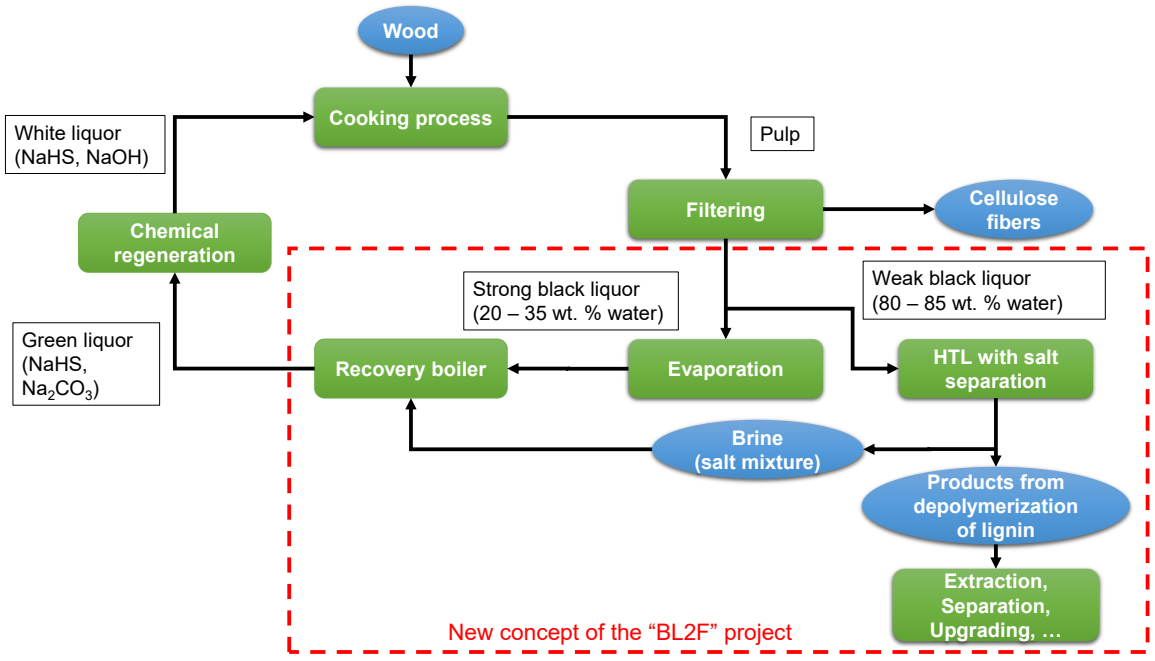

Figure 1-10: Simplified flow scheme of the upgraded Kraft process in the framework of the BL2F project. Additional HTL process with integrated salt separation resulting in salt-rich brine and a product phase

1.7 Research gaps and the resulting objectives of the work

In the previous chapters, the potential of the biopolymer lignin with regard to the production of aromatic compounds for the chemical industry was presented. The aromatic rings are already present in the molecule and do not have to be synthesized, e.g. using the MtA process. At the same time, when using lignin, the renewable raw material is used directly, whereas in the other cases a platform chemical (e.g. methanol) must first be synthesized from a bio-based raw material. On the other hand, the review of the current potential uses of lignin and the current state of research into various processes for the depolymerization of lignin made it clear that this has still not been sufficiently researched despite numerous studies. The various approaches to depolymerization all have different advantages and disadvantages, the limiting aspects of which have not yet been completely eliminated. In order to take the simplest and most direct route possible to the production of aromatic compounds based on biomass, the idea of using the black liquor from the pulp industry directly is therefore a promising approach. The implementation of biomass-based processes often fails due to the cost factor, which can be counteracted by a simple process chain without many intermediate steps. The integration of the material valorization of black liquor into a pulp mill also contributes to the concept of a biorefinery, which will play an important role in the future. However, the direct use of black liquor raises new questions that add to the existing research questions regarding lignin depolymerization to aromatics:

1. **Hydrothermal liquefaction using black liquor directly:**
    - How well can the black liquor be valorized in an HTL directly?
    - What are the best parameters for aromatic monomer production and which are the main products and their respective yields?
    - Is there a difference between the use of softwood and hardwood BL in terms of main products and yields or is the influence of the salt mixture more pronounced?
    - Are the main products and their yields comparable with HTL studies with solid lignin?
2. **Reaction pathways of lignin depolymerization in BL environment:**
    - What are the main reaction pathways for lignin depolymerization under the influence of the different salts in the BL?

- What do oligomeric structures look like and what are their molecular sizes?
- What are the reaction pathways of oligomers?
- Is there a difference between the behavior of softwood and hardwood BL under HTL conditions?

3. **The influence of the sulfide salts, mainly Na_2S, on the lignin depolymerization and the fate of sulfur**
    - Does the inorganic sulfur in the form of sulfur salts react with organic matter of the biomass, and if so, which and how many organo-sulfur compounds are formed?
    - In which product phases can sulfur-containing compounds be detected and which of them can be characterized?
    - How should the influence of other salts such as NaOH on the depolymerization of the lignin and the aromatic yields be rated in comparison to the influence of Na_2S?

The goal of this thesis is to deliver answers to the proposed questions by using experimental methods together with different analytical methods and kinetic modeling to provide a powerful tool, which will help in better understanding the process and the influence of different parameters as well as for future scale-up strategies. In the end, this work should give an idea the direct use of black liquor for lignin valorization in an HTL process is beneficial or not compared to extracted lignin. Chapter 2 describes an investigation of HTL of black liquor by extensive experimental parameter studies to understand the reaction pathways between the aromatic compounds and to develop a reaction scheme based on the results. Chapter 3 builds on these findings by developing and optimizing a kinetic model focusing on aromatic monomers. In Chapter 4 the influence of the sulfide concentration from Na_2S is studied. Main organo-sulfur compounds are identified and for one of them a reaction mechanism is proven by experimental runs with model black liquors. Chapter 5 briefly investigates the influence of other salts in the black liquor on the HTL process regarding the carbon mass balance and the aromatic monomer yields.

2 From Pulp to Aromatic Products – Reaction Pathways of Lignin Depolymerization

2.1 Abstract

This study investigated the depolymerization of lignin into aromatic monomer compounds under hydrothermal conditions. A reaction scheme highlighting secondary alkylation reactions as well as the molecular weight shift was developed based on the experimental data. Lignin is produced in large quantities in paper production and dissolved in what is known as black liquor (BL). To avoid lignin recovery as an additional process step, BL is used directly as feedstock in the hydrothermal liquefaction (HTL) in this work. We performed various batch experiments in micro autoclaves with BL and model substances at different reaction temperatures ($T_R = 250 - 400\,°C$) and a holding time of $t_R = 20\,min$, as well as continuous experiments ($T_R = 325 - 375\,°C$, $t_R = 20\,min$). We were able to show that different derivatives of catechols are the main products among the monomers in our process. With the help of the model substance experiments, we were able to work out three main reactions: demethoxylation, demethylation, and alkylation. This behavior could be observed in the case of BL from hardwood as well as from softwood. ^{31}P nuclear magnetic resonance (NMR) spectroscopy analysis has shown that these reactions take place on aromatic monomers as well as on larger aromatic oligomer structures. At higher temperatures, a large fraction of the carbon ends up in the solid product, while the yields of the monomers decrease sharply. ^{13}C NMR spectroscopy of the solid material shows that the monomers are probably incorporated into the solid phase by repolymerization. We were also able to see this effect using size exclusion chromatography analysis based on the relative molecular weight. From all of the analytical results of the products, a reaction scheme was developed that describes the reaction pathways of the lignin during HTL. Based on this, a reaction kinetic model can be developed in the next step.

2.2 Introduction

Because only a few studies have been published that investigated black liquor directly under hydrothermal conditions, one major goal of this work is to gain a more detailed understanding about the lignin depolymerization under these conditions. In particular, the cooking chemicals from the Kraft process make a straightforward comparison between HTL of BL and for example HTL of extracted Kraft lignin or other lignin types difficult because of their catalytic behavior.

Since BL can differ due to the wood type as well as from one supplier to the next[170], it was necessary to start with a parameter study utilizing BL and relevant model compounds as feedstock. The focus in this chapter is on the reaction temperature due to its dominant influence. Previous research has focused in most cases only on the monocyclic end products, for example Forchheim et al., who discussed the oligomers as a "black box" in the reaction scheme (see Figure 2-1)[171].

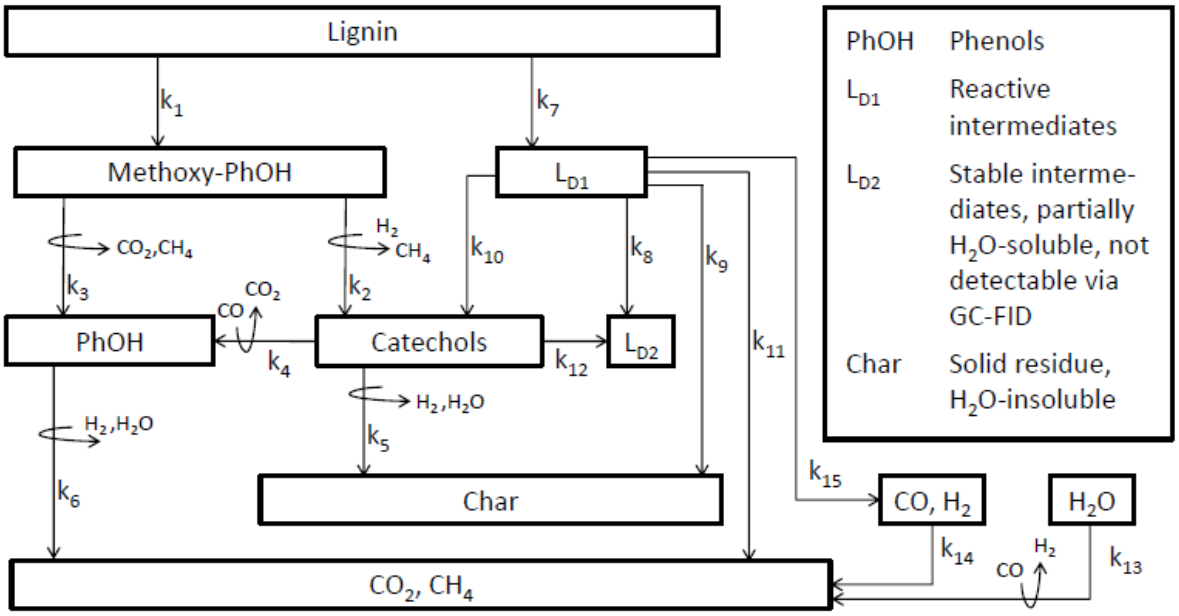

Figure 2-1: Reaction scheme of the HTL of spruce-lignin in subcritical water[171]

This work aims to provide a lumped reaction scheme that includes the behavior of oligomers and will be the basis of a kinetic model. To accomplish this, oligomeric products were investigated using advanced spectroscopic methods alongside the monomeric products to identify the similarities and differences between the smaller and larger molecules regarding the reaction pathways. For this purpose, we mainly

relied on 1D NMR analyses using ^{13}C and ^{31}P nuclei. In the field of spectroscopic characterization of lignocellulosic biomass, numerous publications are published using either plain 1D methods with mostly ^{1}H, ^{13}C, and ^{31}P after derivatization, or more complex 2D (^{13}C and ^{1}H)-correlated methods (e.g., HSQC: heteronuclear single quantum correlation). The majority of these methods are performed in solution using deuterated polar solvents (e.g., CD_3OD or DMSO-d_6) or they can also be performed on homogeneously ground solid-state samples (^{13}C MAS or CP/MAS: cross-polarization magic angle spinning)[172–179]. The most relevant papers were used as references to evaluate the NMR spectra obtained in the work. Together with size exclusion chromatography (SEC), this approach provided insight into the molecular size and functionalities of oligomers in order to setup a reaction mechanism for the depolymerization of lignin to aromatic compounds.

2.3 Materials and Methods

2.3.1 Feedstock

The BL was provided by the Figueira da Foz pulp mill in Portugal (the Navigator Company). The wood used for the Kraft process on site came from eucalyptus plantations based on the species *Eucalyptus globulus*. This wood species belongs to the hardwood category, which leads to an S/G ratio of approximately 70:30. The BL is a malodorous dark brown to black liquid. All constituents, such as lignin or cooking chemicals, are almost completely dissolved, resulting in a strong homogeneity. The relevant properties as well as the elemental composition of the BL are listed in Table 2-1 and Table 2-2. The yields in the results were calculated based on $w_{\mathrm{BL,\,burnable}}$. We assume that the burnable fraction is close to the organic fraction (see Cardoso et al. [170]). Differences between the burnable fraction and the real organic fraction arise due to the change in ash composition due to combustion. For comparison with BL based on softwood (spruce wood), three tests were carried out with softwood BL from Scandinavia. The properties were assumed to be equal to those of the other BL since the differences in dry matter content, pH, and density were only marginal.

Table 2-1: Properties of the BL used in the experiments; $w_{\mathrm{BL,\,burnable}}$ calculated from the loss on ignition corrected from the dry matter

dry matter w_{tr}	14.5 wt. %
ash content $w_{ash,\,815\,°C}$	6.1 wt. %
dry matter-based loss on ignition	57.9 wt. %
raw BL-based burnable matter $w_{BL,\,burnable}$	8.4 wt. %
density ρ_{BL}	1.0725 kg·L^{-1}
pH	>12.5

Table 2-2: Elemental composition of the dry mass of the BL and the extracted lignin; Analysis performed via elemental analysis (EA) and inductively coupled plasma-optical emission spectrometry (ICP-OES); oxygen calculated via difference, no other element was detected in relevant amounts

Element symbol	**Mass fraction dry mass BL / wt %**	**Mass fraction extracted lignin / wt. %**
C (EA)	34 ± 0.4	60.3 ± 0.1
H (EA)	3.4 ± 0.5	5.7 ± 0.1
N (EA)	<0.1	<0.1
S (EA)	4.7 ± 0.1	2.6 ± 0.1
O (diff.)	38.8	31
Na (ICP)	17.7 ± 0.9	0.4 ± 0.02
K (ICP)	1.3 ± 0.06	<1
Sum	100	100

Several tests were also carried out with different model substances for the sake of comparison. These are guaiacol, syringol, vanillin, and syringaldehyde (see Figure 2-2). In each case, 1 g of the substance was added to 15 mL of a salt solution corresponding to a real BL. The exact composition of this solution can be found in the Supporting Information in Table 8-1.

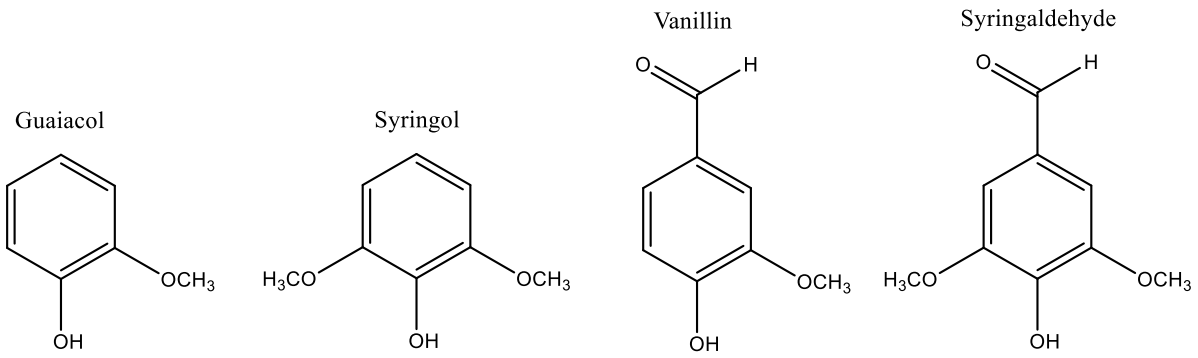

Figure 2-2: Monocyclic phenolic compounds used in experiments with model substances

2.3.2 Batch experiment setup and product separation

For the batch experiments, micro autoclaves were used, which were made of stainless steel 1.4571(316Ti) in the institute's mechanical workshop. Each of these autoclaves has a volume of $V_R = 25\ \mathrm{mL}$. Closing and opening of the reactors took place in a specially designed station (see Figure 8-2). The filling levels of BL had to be adjusted to the respective temperatures in order to avoid too large pressure fluctuations between the individual experiments. A pressure of 200 – 250 bar was specified as the target. The filling levels depend on the density of water at the respective temperatures and pressures [180] (volumes used can be found in Table 8-2).

To achieve a fast-heating rate, a fluidized sand bath (SBL 2, Techne, Stone, UK) was used. For ease of handling, it was decided to use a general heating time of $t_{pre} = 10\ \mathrm{min}$ for all experiments. Studies carried out previously with the same heating procedure showed that the desired reaction temperatures were reached within 10 min. After the heating time, the holding time t_R started at the corresponding reaction temperature T_R. This study investigated the reaction temperatures of $T_R = 250 - 400\ °C$ and holding times of $t_R = 5\ \mathrm{min}$ (model substances) and $t_R = 20\ \mathrm{min}$ (black liquor). As soon as the holding time t_R was reached, the autoclaves were cooled in a water bath in order to terminate all reactions taking place (quenching step). The gas was directed into a gas trap when the autoclaves were opened. Subsequently, the reactor was opened, and solids and liquids were separated by means of vacuum filtration. The filter used is made of nylon with a diameter of 47 mm and a pore size of 0.45 µm (Whatman, GE Healthcare, Buckinghamshire, UK). The accumulated solid was dried in an oven at 105 °C for at least 24 h. Liquid−liquid extraction (LLE) was performed to separate the organic phase from the aqueous phase. Two mL of the liquid phase had to be acidified with 6 M hydrochloric acid to a pH of 2 – 4. After filtration, 0.52 mL of ethyl acetate was

added to 1.3 mL of the filtrate, which served as the extractant. After shaking, the sample was allowed to rest in the vial for 1 h to allow for complete phase separation. For larger scale extraction, three samples from the same reaction conditions were poured together, and the amount of ethyl acetate used was increased to a 1:1 ratio with respect to the liquid product. Figure 2-3 shows the procedure for separating the products in a flowchart.

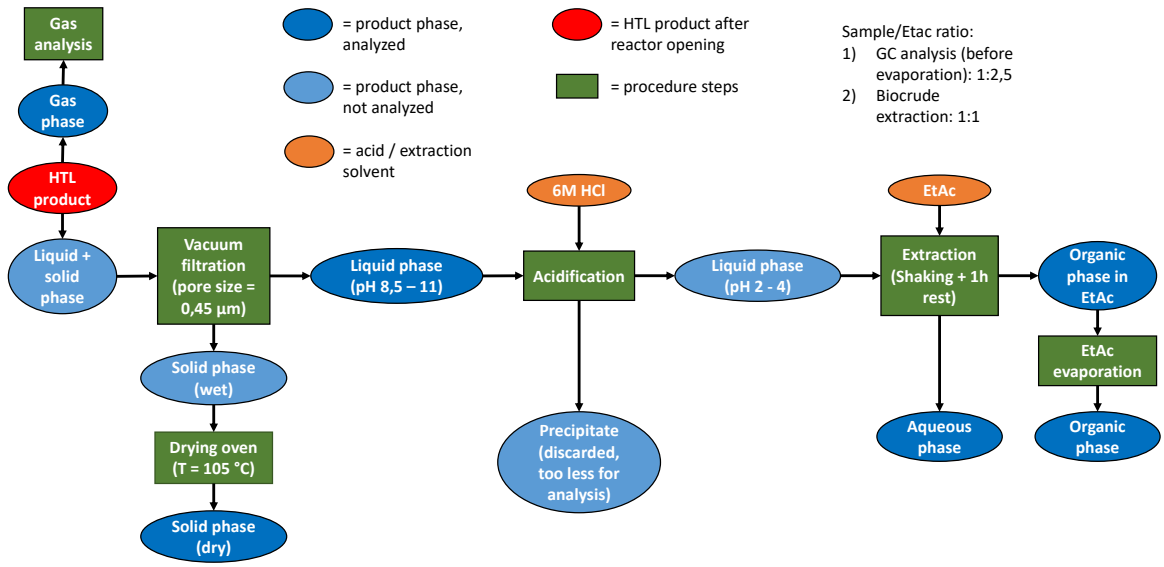

Figure 2-3: Procedure for HTL product sample separation and analysis with integrated legend; EtAc = ethyl acetate

2.3.3 Continuous experimental setup

The continuous HTL experiments were performed in a tube reactor (Figure 2-4). One feed stream with hot water ($T = 400\,°C$) and another with BL ($T = 100\,°C$) were combined in a preheated mixing head above the reactor in a 1:1 ratio. This ensured the desired reaction temperatures T_R. A three-headed diaphragm metering pump (ecoflow LDB1 diaphragm metering pump, LEWA, Leonberg, Germany) was used to supply the reactor with feedstock and process water. Heat was supplied to the reactor via three separate heating zones. After the outlet, the product stream ran into a phase separator. It was then possible to collect the products, liquid phase and solid. Three experiments were carried out at $T_R = 325, 350, \text{and } 375\,°C$ with a residence time $t_R = 20\,\text{min}$. The system was heated with a hot water stream beforehand. When the reaction temperature T_R was reached inside the reactor, the BL stream was added.

The overall feed rates were adjusted between 1.35 and 2 kg·h^{-1} depending on T_R. The plant ran for one h before we started the sampling process to make sure that the stationarity of the process was reached. Product preparation followed the same scheme as that for the batch experiments.

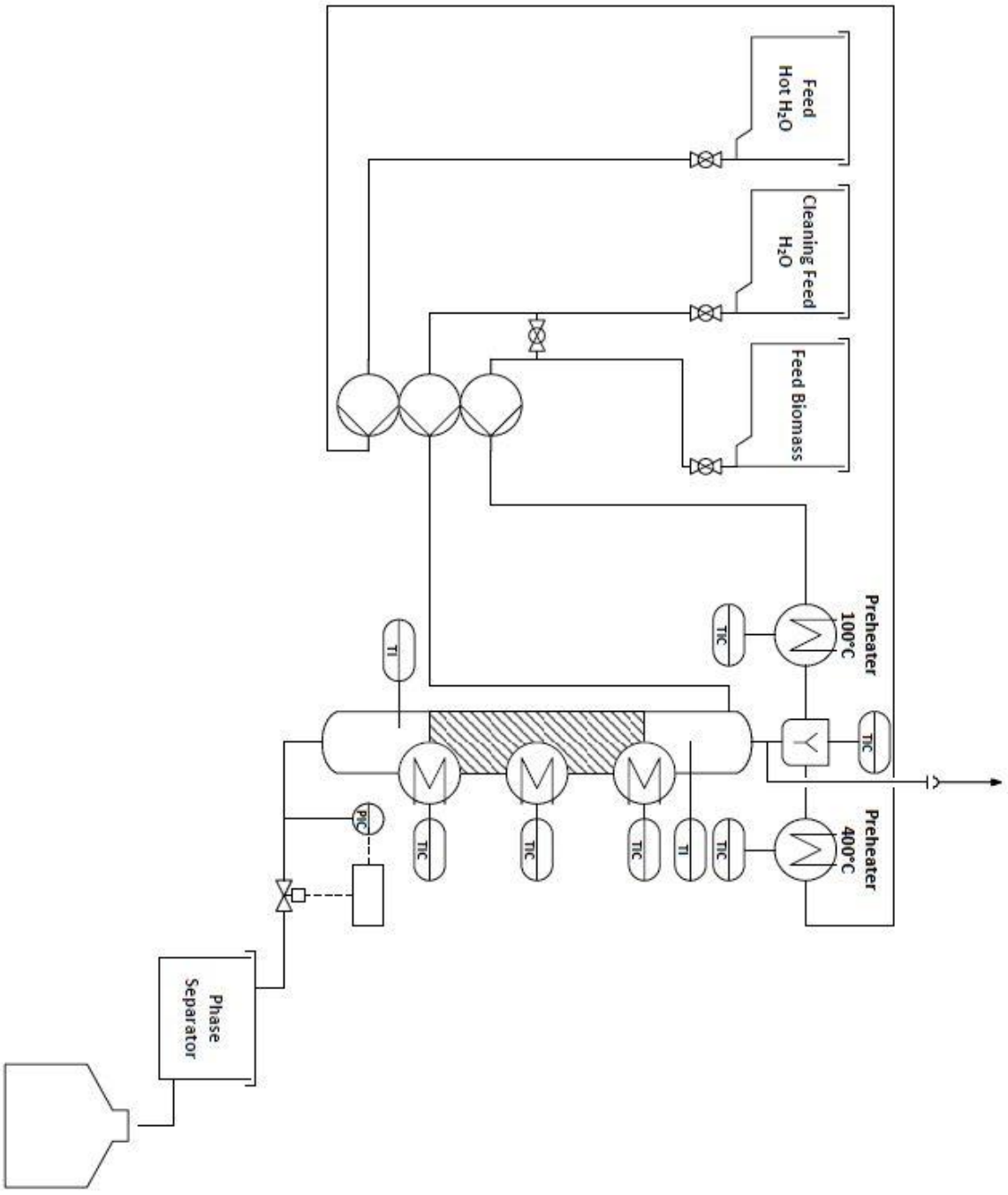

Figure 2-4: Process scheme of the continuous plant

2.3.4 Analytical procedure and assessment

Each intermediate or final product, colored orange in Figure 2-3, was analyzed with at least one analytical procedure. A sample of the gas phase collected in the gas trap after opening the micro autoclaves was injected with a gastight syringe into a gas chromatograph (GC 6890, Hewlett- Packard, now Agilent, Santa Clara, CA, USA; columns Hayesep Q, Molsieve 5A, Restek, Bellefonte, PA, USA). Using an FID (flame ionization detector) and a TCD (temperature conductivity detector), it was possible to detect and quantify various permanent gases and hydrocarbons (see **Table 8-4**). The samples were injected at 280 °C splitless mode, with 31.77 mL/min Helium as carrier gas flow. The temperature program in the oven started at 60 °C for 1 min and ramped up to 200 °C with a rate of 20 °C/min. The final temperature was hold for another 17 min. The quantified compounds were calibrated beforehand with a calibration gas mixture.The gas compounds that are detectable, as well as the calculation procedure for the carbon mass in the gas phase, are found in the Supporting Information. The dried solid was analyzed by EA (Vario EL Cube, Elementar Analysentechnik GmbH, Hanau, Germany). To complete the carbon mass balance, total organic and inorganic carbon concentrations (TOC and TIC) were determined in the total liquid product prior to extraction using a Dimatoc 2100 (Dimatec Analysentechnik GmbH, Essen, Germany). Together with the mass of the collected solid as well as the collected liquid, the C mass balance could be completed.

The organic phase in ethyl acetate after LLE was analyzed for aromatic monocyclic compounds using a GC−MS (GC 6890N and 5973 MSD (mass spectrometry detector), Agilent, Santa Clara, CA, USA) and a GC-FID (GC 7820A, Agilent, Santa Clara, CA, USA). In both systems, separations were carried out using an RTX-5 capillary column (30 m × 0.32 mm × 0.5 µm, Restek, Bellefonte, PA, USA). For GC–MS measurements, samples were injected at 280 °C in splitless mode. Helium was used as the carrier gas at a flow rate of 1.5 ml min^{-1}. The oven temperature program began at 35 °C with a 5 min hold, followed by heating to 240 °C at 8 °C min^{-1} and a final hold of 10 min. The mass spectrometer was operated in electron impact ionization mode at 70 eV, with the ion source maintained at 230 °C and the quadrupole at 150 °C. A solvent delay of 4.5 min was applied prior to data acquisition, after which spectra were recorded over a mass range of m/z 35–350 at a scan rate of 4.5 scans s^{-1}. For GC–FID analysis, samples were injected at 280 °C using a split ratio of 1:50. Helium served as the carrier

gas at a flow rate of 1.2 ml min⁻¹. The oven temperature was initially held at 50 °C for 2 min, then increased to 190 °C at 8 °C min⁻¹, followed by a second ramp to 230 °C at 20 °C min⁻¹ and a final hold of 5 min. All quantified compounds were calibrated beforehand with a five-point calibration covering the range of potential peak heights for each compound. By using the GC-FID and pentadecane as an internal standard (ISTD), we were able to quantify a selection of aromatic compounds. For this purpose, the ISTD was added to the ethyl acetate in a defined amount prior to extraction. Together with the distribution coefficients K_i of the individual components (see Table 8-5 in Supporting Information), this allowed us to calculate the concentration of species i in the total liquid phase ρ_i (see equation (2-1)). Factors a – c represent the total dilution of the original sample, the ratio between the sample volume and the volume of ethyl acetate, and the ISTD factor. $\rho_{\mathrm{i,\ raw}}$ represents the measured concentration in the sample. The yield in relation to the biomass in the BL feed Y_x was calculated using equation (2-2) with the obtained mass for liquid product $m_{\mathrm{liq,prod}}$, and the mass of feedstock m_{feed}.

$$\rho_\mathrm{i} = \frac{\rho_{\mathrm{i,raw}} * a * b * c}{K_\mathrm{i}} \tag{2-1}$$

$$Y_x = \frac{\frac{\rho_\mathrm{i}}{\rho_\mathrm{BL}} * m_{\mathrm{liq,prod}}}{\frac{w_{\mathrm{BL,burnable}}}{\rho_\mathrm{BL}} * m_{\mathrm{feed}}} \tag{2-2}$$

In addition, we quantified potential dimethylcatechols and trimethylcatechols over the areas of the peaks. The ratio of concentration to peak area of the other catechols (methylcatechols and catechols) was taken as a reference point for this. For experiments with model substances, the molar yields were determined. High-performance liquid chromatography (HPLC; Merck Hitachi Primaide, Hitachi, Tokyo, Japan; Aminex HPX87H, Bio-Rad, Feldkirchen, Germany) was used to determine acids and alcohols in the aqueous phase. After the evaporation of the ethyl acetate, the relative molecular weight of the biocrude obtained was first determined. We used SEC (LaChrom diode array detector DAD L- 2455, Merck, Darmstadt, Germany, with a Viscotek A2500 column, Malvern Panalytical, Malvern, UK).

In addition to standard analytical methods, various NMR spectra were recorded using adequate pulse sequences and probe heads. The solids were analyzed using 1D-^{13}C solid-state NMR. For the analysis of the liquid biocrude, we used 1D-^{31}P spectra after derivatization. The procedure for the ^{31}P NMR can be found in the paper published by

Korntner et al.[181] according to the following principle: the lignin hydroxy (OH) groups were quantified by ^{31}P NMR after derivatization of the lignin with a derivatization reagent. The dry lignin sample was dissolved in a mixture of pyridine, N,N-dimethylformamide, and deuterated chloroform ($CDCl_3$) in the presence of an ISTD and a relaxation reagent and then phosphorylated using a solution of derivatization reagent in a mixture of pyridine and $CDCl_3$. The NMR spectrum of the lignin and ISTD derivatives was then acquired using liquid NMR spectroscopy, and the OH groups were quantified by the relative integration of the corresponding signals for lignin and ISTD. These experiments were performed by BOKU University of Natural Resources and Life Sciences, Vienna. Single pulse ^{13}C MAS/CP-MAS NMR spectra were recorded under ambient conditions (1010 mbar, 20 °C) using a Jeol Spectrometer of the JNM-ECZR series, equipped with a 9.4 T Oxford cryo-magnet (resonance: ^{13}C @100.51621 MHz ^{1}H@ 399.90513 MHz). The solid-state spectra were recorded with a JEOL Automas solid-state probe head. More detailed information about the ^{13}C NMR can be found in SI chapter 8.2.5.

2.4 Results and Discussion

2.4.1 Batch HTL Experiments with BL

The first task was to determine which aromatic monomers achieved the highest yields. The GC−MS spectrum ($T_R = 350$ °C, $t_R = 20$ min; see Figure 2-5) shows typical degradation products from lignin. Interestingly, we found significantly more catechols (aromatic rings with two attached hydroxy groups) than phenol and other aromatic compounds with one hydroxy group (10 to 20 times higher yields). This does not coincide, for example, with the studies of Belkheiri et al.[149,182] in which the proportion of phenol in the organic phase is significantly higher. A study with more comparable results is that of Forchheim et al.[171]. The peaks between 12.5 and 15 min of retention time in the chromatogram represent the di- and trimethylcatechols. The problem here is that the underlying NIST database contains only multi-alkylated resorcinols and hydroquinones, isomers of catechol. However, since only catechol could be found in all samples, the detected compounds are more likely to be alkylated catechols. The mass spectra of the individual peaks clearly show alkyl fragmentation. For the possible dimethyl catechols, the main peaks are $\mathrm{m/z} = 123$ and $\mathrm{m/z} = 138$, for the possible trimethyl catechols, they are $\mathrm{m/z} = 137$ and $\mathrm{m/z} = 152$ (CH_3 fragment: $\mathrm{m/z} = 15$). It is

also possible that a small share of ethyl and propyl chains is involved, but for the sake of simplification, only methyl chains were considered. Since it was not possible to analyze these substances individually, a “semi-quantification” was based on the clearly determinable peaks of the catechol and the singly methylated catechols.

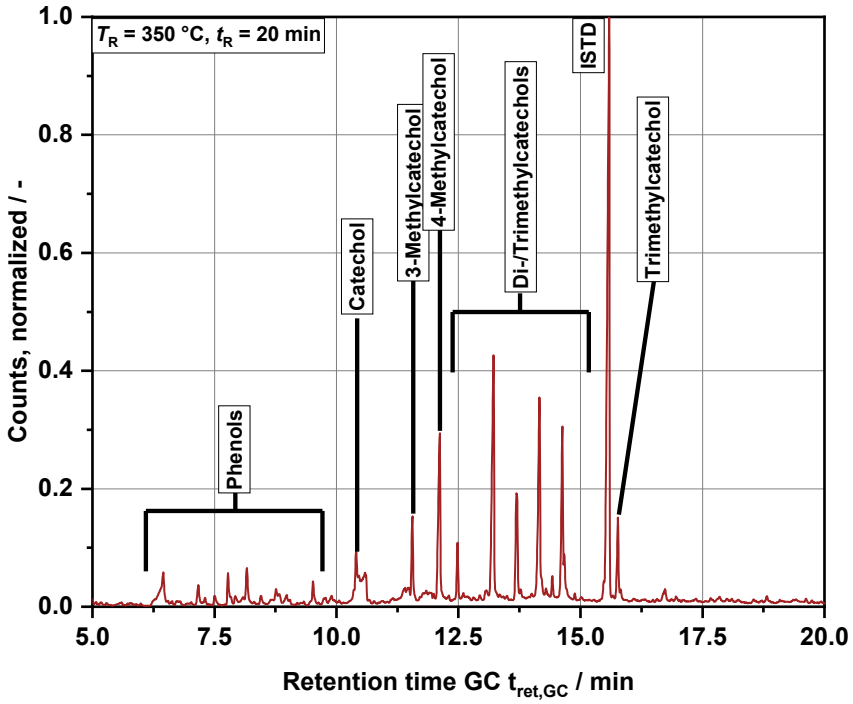

Figure 2-5: GC-MS spectrum of an extracted organic phase sample from the liquid product phase; major peaks are named; ISTD = pentadecane; the peaks put together in "phenols" include phenol, cresols and xylenols

Figure 2-6 shows the calculated yields of the various relevant phenolic monomers obtained in the range $T_R = 250 - 400\,°C$ at $t_R = 20\,min$ from the batch tests. Phenol itself, as well as cresols and xylenols, hardly plays a role and is not shown in the graph due to the very low measured yields. Basically, the aromatic monomers formed in the reaction can be divided into three sections on the basis of their different functionalities. The first to be generated are phenolic aromatics with at least one hydroxy (−OH) and one methoxy (−OCH_3) group. These include guaiacol and syringol, which can be derived from the two main building blocks, coniferyl and sinapyl alcohol. Interestingly, comparing the yields shows that the ratio of the two aromatics also matches the ratio of the building blocks in the lignin used. In addition, at lower reaction temperatures, 3 – methoxycatechol was quantified at higher concentrations up to a yield of 20 mg/g of biomass. As the reaction temperature T_R increases, the yields of these three substances decrease rapidly. From $T_R = 350\,°C$, none of these components could be

detected in the extracted organic liquid phase. Afterward, the yields of the various catechols increase sharply. Pure catechol with two hydroxy groups falls into the second category. The catechol yield reaches a maximum at $T_R = 300\,°C$ and then drops steadily at higher temperatures. Although 4 – methylcatechol behaves similarly, the decline in yield is slower. Therefore, this molecule, along with the other remaining aromatics shown in the graph, falls into the third range, that of alkylated catechols bearing at least one alkyl group in addition to the two hydroxy groups of the catechol. This group represents the final products of the aromatic monomers obtained from the depolymerization of lignin under hydrothermal conditions.

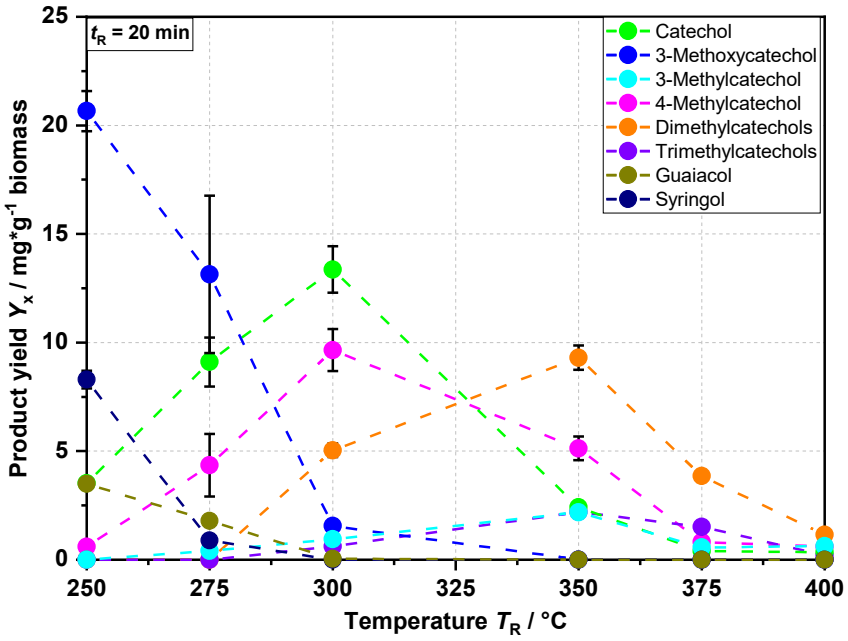

Figure 2-6: Product yields in mg per g biomass of the main aromatic monomer compounds at different reaction temperatures T_R; feedstock: BL

With further increasing reaction temperatures up to $T_R = 400\,°C$, the yields approach zero. In principle, it can be stated that the production of aromatics is possible from BL directly used as a feedstock in a HTL process without further precipitation of lignin. The lignin molecule is depolymerized as already described in other research papers[171,183] and forms various, mainly phenolic monomers. In our case, different derivatives of catechols are mainly formed. All catechols together lead to a maximum yield of around 30 mg/g of biomass at $300\,°C$. Since the yields are generally low, it is necessary to optimize this process for aromatic production. In order to accomplish this, it is first necessary to understand in more detail what happens to lignin under the prevailing conditions.

2.4.2 Batch HTL experiments with model substances

Since numerous products are formed from lignin that cannot be clearly assigned to one reaction pathway, we decided to simplify the feedstock and work with suitable model substances. We were primarily interested in guaiacol and syringol, which are parts of two basic building blocks of lignin. Figure 2-7 (guaiacol) and Figure 2-8 (syringol) show the yields of the aromatics obtained from the HTL of the model substances. If guaiacol is used, then a yield of 50 % catechol is possible. Much more interesting, however, is the aspect that in addition to catechol and the unreacted guaiacol, only methylated catechols occur as secondary products. While the yield of catechol decreases slightly at $T_R = 375\,°C$, their yields increase steadily with increasing reaction temperature. Neither syringol nor 3 – methoxycatechol could be detected, strongly suggesting that demethylation of the methoxy group takes place. Methane as a by-product in the gas phase is quantifiable. Increasing methane concentrations in the complex reaction mixture could subsequently lead to an increased production of methylated catechols. How the methylation of catechols actually proceeds is not clear. Possibly, different radicals, such as radical aromatics or methyl radicals, are formed under the prevailing conditions and can react with each other. Forchheim et al. worked out a simple consecutive reaction pathway via guaiacol under near-critical conditions and discussed a change in the reaction mechanism from hydrolysis at subcritical temperatures to radical-induced degradation at near-critical and supercritical temperatures[152,171]. Additionally, the activation energies were close to those for pyrolysis, in which mainly radical reactions take place.

Using syringol instead of guaiacol as a model substance provided further interesting insights. Overall, significantly more compounds were found by GC. While the main product remains catechol, the yield is about half that of guaiacol; 3 – methoxycatechol and guaiacol are also form, among others. This allows us to single out two reaction pathways occurring concurrently. On the one hand, the demethylation already mentioned takes place. While guaiacol produces catechol, syringol produces 3 – methoxycatechol from this reaction. This is indicated by the absence of 3 – methoxycatechol in the experiments with guaiacol. Further experiments with vanillin (based on guaiacol) and syringaldehyde (based on syringol) confirmed this hypothesis (see chapter 8.2.6). Only experiments with syringaldehyde were shown to produce 3 – methoxycatechol. The other parallel reaction is the single demethoxylation

of syringol, leading to guaiacol. Methanol is formed as a by-product, which has been detected in the liquid product. A second demethoxylation reaction to phenol is also conceivable but hardly plays a role due to the small amounts of phenol.

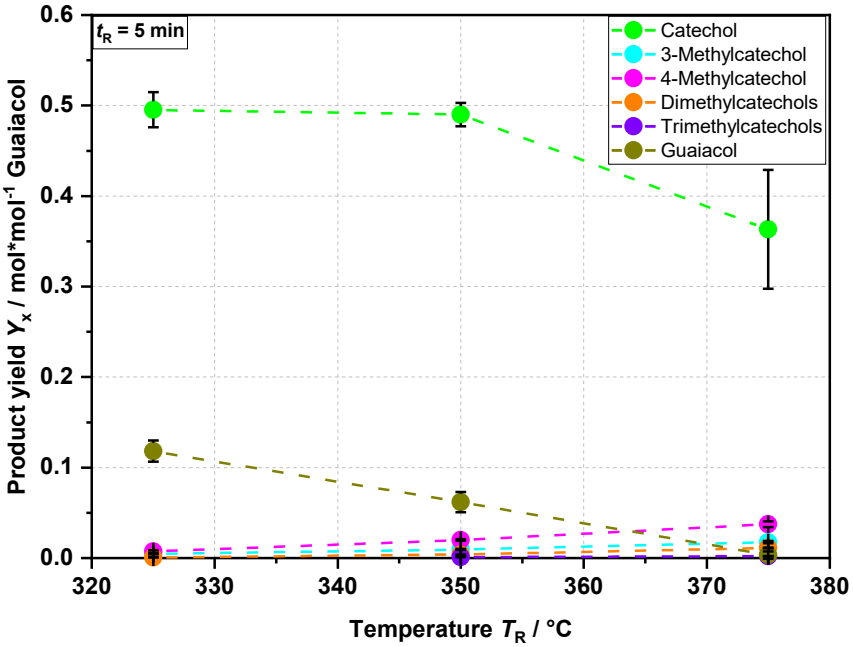

Figure 2-7: Product yields in mol per mol guaiacol of the main aromatic monomer compounds at different reaction temperatures T_R

According to the results, the first mechanism mentioned, demethylation, seems to proceed somewhat faster since the yield of 3 – methoxycatechol is higher. However, these reactions, demethylation and demethoxylation, might proceed in parallel on the same monomer. The significantly higher yield of catechol compared with all other possible molecules is a clear indication of this. In connection with the production of methylcatechols, transalkylation may also play an important role[184,185]. This is applicable to the pathway of guaiacol as well as to the pathway of syringol. In the work of Zhu et al., for the transalkylation of anisole in the context of a hydrodeoxygenation on acid sites of the catalyst, twice-methylated phenols (xylenol) are also given as products[186]. Thus, twice or three times methylated catechols based on syringol cannot be excluded. Further studies are needed to clearly define the predominant reaction pathway(s) and evaluate the complex interactions within the reaction network. For example, one approach would be to focus on the two byproducts generated via demethylation (CH_4) and demethoxylation (CH_3OH). However, this will not be straightforward with BL, since both methane and methanol can be formed from many other reactions occurring in parallel, e.g., from hemicellulose (compare Figure 2-11).

The results obtained from the experiments with the model substances can be transferred to the HTL experiments with BL and allow us to understand the observed product distribution better.

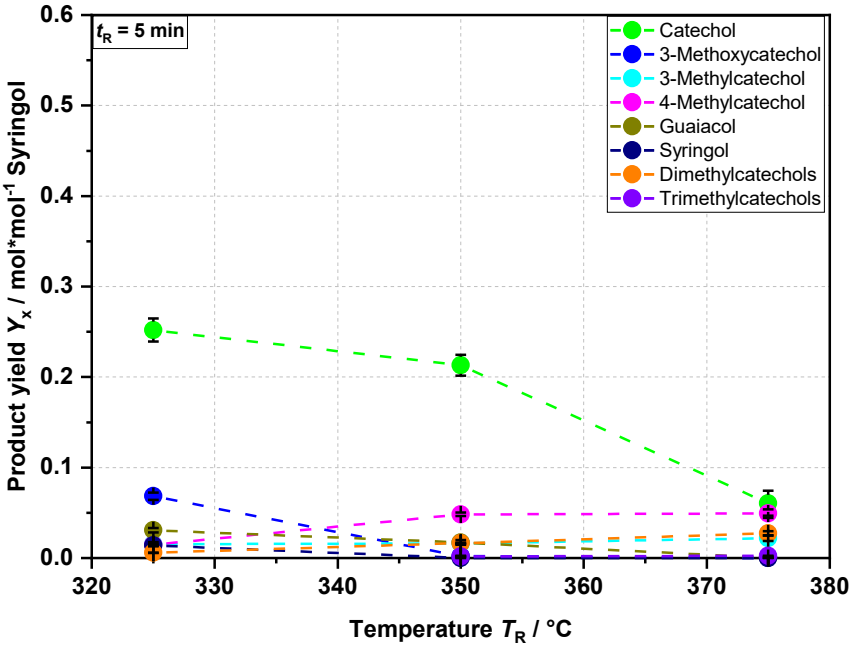

Figure 2-8: Product yields in mol per mol syringol of the main aromatic monomer compounds at different reaction temperatures T_R

2.4.3 Continuous HTL experiments with BL

Comparative tests were performed in a related continuous plant and confirmed the trends observed in batch tests. We were able to detect the same products in the extracted organic phase, catechol and its derivatives also being the main products (see Figure 2-9). The yields are slightly higher than those in the batch experiments. At $T_R = 375\,°C$ and a residence time of $t_R = 20\,\mathrm{min}$, well over 30 mg/g of biomass catechols could be observed. Interestingly, the dimethyl catechols play a much larger role. Moreover, the yields of all methylated catechols remained stable or increased in the temperature range studied. In contrast, at $T_R = 375\,°C$ in the batch experiment, the yields had already decreased significantly. However, a direct comparison at the same temperature and residence time is difficult since the heat transfer to the feedstock in the reactor is much better in the continuous plant than in the reactors operated batch-wise.

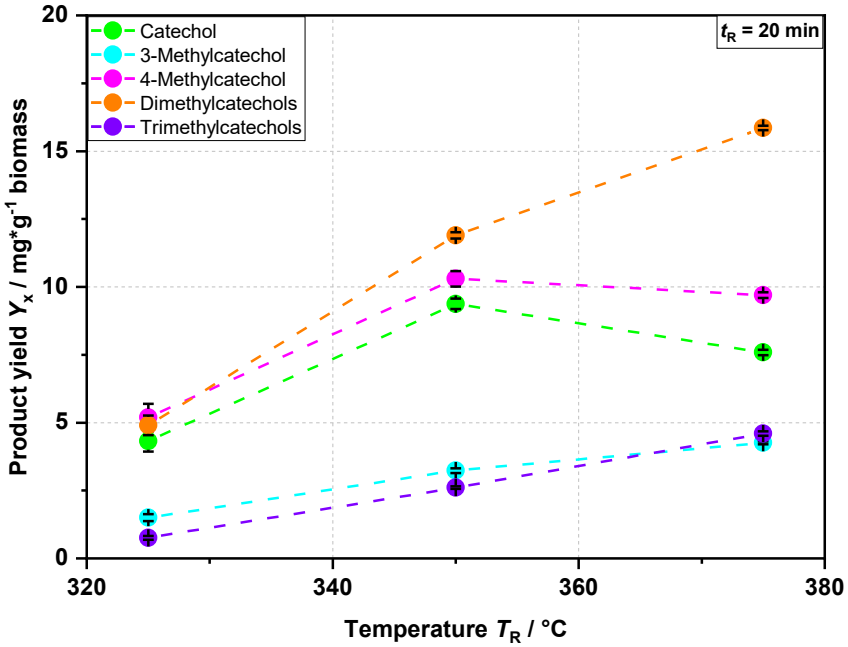

Figure 2-9: Products yields in mg per g biomass of the different catechol compounds at different reaction temperatures T_R; continuous experiments; feedstock: BL

During the batch experiments, the heat must first pass through the reactor wall to the center of the fluid, whereas in the continuous reactor, an additional heat carrier stream of hot water presumably heats small droplets of feedstock from all sides. The same applies to subsequent cooling. Therefore, it can be assumed that reactions in the continuous system can take place in a much more segregated manner with a far more limited number of side reactions than in the batch system. Thus, for example, repolymerization with solids may be limited, allowing the preferential formation of alkylated catechols. The methylation itself is not limited in the continuous process since it is a direct consecutive reaction and methyl radicals may not be diluted as much as in as in a batch system. In fact, it is even more pronounced than in the batch experiment results. Therefore, it is likely that a reaction scheme setup on the basis of the batch experiments also applies to the continuous process since we could observe the same ongoing reactions with both experimental designs.

2.4.4 Discussion of Carbon Mass Balance

With the results shown so far, a reaction network can be developed on the monomer side, specifically for the case studied here in this work. This fits well with other studies in the field. However, the low yields of monomeric compounds indicate that it is not sufficient to focus on only aromatic monomers. A first assumption would be that at a

high reaction temperature T_R, the regime of hydrothermal gasification is achieved, and therefore many organic compounds are in the gas phase[140]. However, considering the carbon mass balance for the batch experiments (Figure 2-10), it quickly becomes clear that this is not the case. The decrease in organic carbon in the liquid phase observed with increasing reaction temperature T_R (dark blue) is not reflected in an increase in the carbon share in the gas phase (red). In comparison, the carbon content in the solid product shows a significantly larger increase. At $T_R = 400\,°C$, this accounts for about half of the total carbon. At first glance, the observed phenomenon does not match the actual behavior of hydrothermal processes as hydrothermal carbonization is instead located in the lower reaction temperature range. However, monomers and oligomers can repolymerize rapidly due to the high density of functional groups present in the material[154,187]. Branched hydrocarbons and aromatics in particular seem to contribute to the production of high molecular weight substances such as coke, coal, or tar[188]. It is known from catalytic cracking, for example, that aromatics can quickly coke and thus deactivate the catalyst[189].

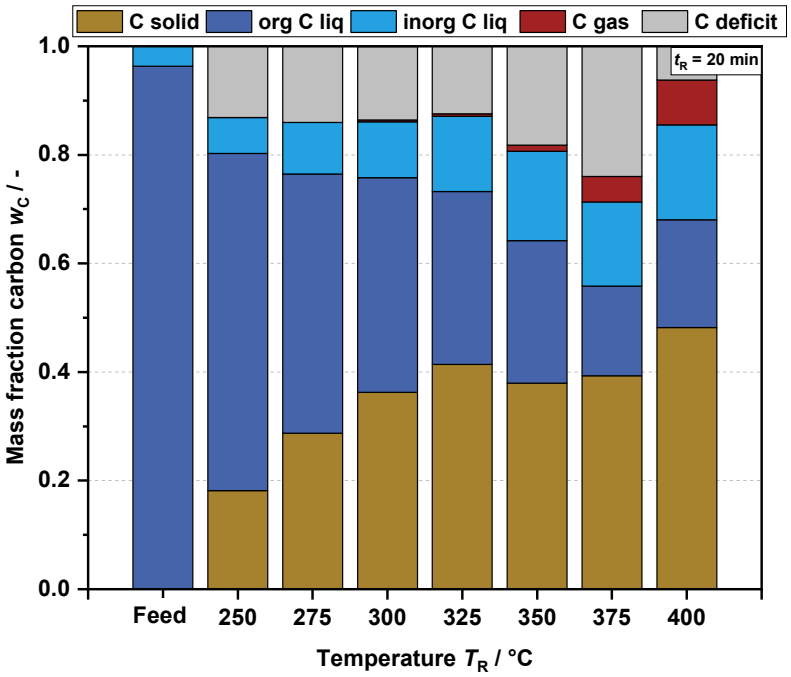

Figure 2-10: Carbon mass fractions at different reaction temperatures T_R and before processing (feed); brown: C mass fraction solid; green: organic C mass fraction liquid phase; blue: inorganic C mass fraction liquid phase; red: C mass fraction gas phase (calculated from the detected gas compounds); and gray: deficit of carbon

Ultimately, repolymerization side reaction effects lead to the fact that hardly any aromatic monomers are found in the liquid product phase at high temperatures. About 50 – 60 wt. % of the organic carbon in the liquid product phase (dark blue column section in the C balance) is detected via GC-FID and HPLC (see Figure 2-11) monomer analysis. This strongly suggests that almost half of the carbon present in liquid organic products after extraction is bound in aromatic oligomers or even larger molecules. Thus, in addition to the solid, this part must also be taken into account, since the organic liquid phase produced is the desired product of the process. The carbon deficit shown in the graph is most likely due to gaseous or volatile compounds that could not be detected by gas analysis. Another reason for the loss of carbon is residues in the reactor after opening.

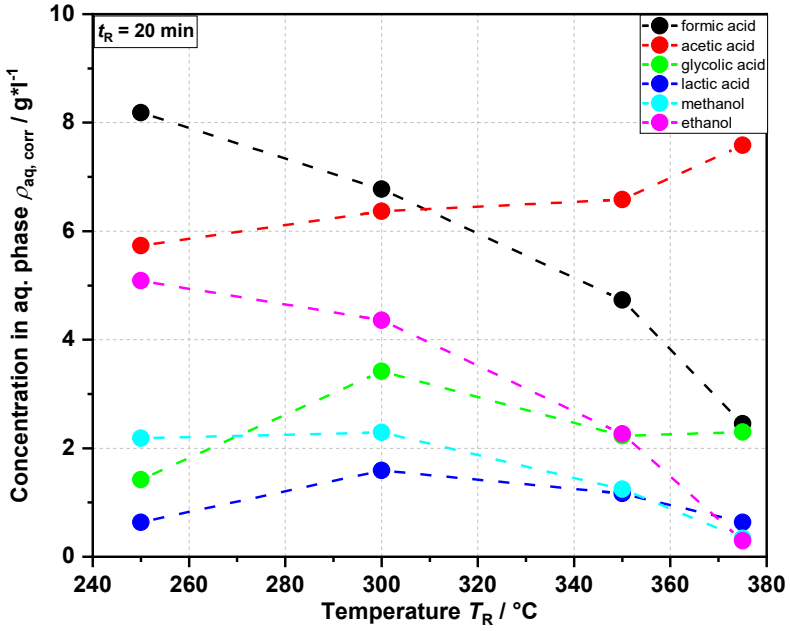

Figure 2-11: HPLC analysis of aqueous phase after extraction of the organic phase; ethyl acetate concentration (extract solvent) was subtracted to calculated correct mass concentrations

2.4.5 Comparison between softwood and hardwood BL as HTL feedstock

In addition to batch experiments with BL based on hardwood, we carried out experiments with BL based on softwood. In this way, we want to show that a reaction scheme based on the results shown so far is applicable for different types of BL as a feedstock. Figure 2-12 and Figure 2-13 show the yields of the aromatic monomers. In fact, the products hardly differ, either qualitatively or quantitatively. The only interesting differences are those that we also observed in the HTL of the model substances. The

3 – methoxycatechol, which we were able to detect in the experiments with syringol, is only present in the products of the HTL with the Hardwood BL. This makes sense since hardwood, as already mentioned, is composed of a significantly larger proportion of sinapyl alcohol, the molecule from which syringol is formed (around 70:30 S to G ratio). Softwood, on the other hand, consists almost exclusively of the building block coniferyl alcohol, the derivative of guaiacol (around 90 – 95 % G). Thus, the reaction pathway is only via the guaiacol, and 3 – methoxycatechol is not formed. Since the carbon mass balances (see Figure 2-14) are also very close to each other, it can be concluded that the wood type does not have a major effect on the HTL and its aromatic monomers as products. Instead, the salts probably have a much greater effect. It appears that in the softwood, the syringol is skipped in the sequence of reactions, but this ultimately has no visible effect on the yields of the different catechols. Therefore, it is probably possible to apply the reaction scheme to different BLs as long as the salt concentration does not deviate too much. The high loss of carbon shown in the mass balances is most likely a result of the issues mentioned above in the discussion about Figure 2-10. The statement about the negligible difference in the yields of the produced aromatics should not be affected by the carbon loss, since the experiments with softwood and hardwood BL share the same issue.

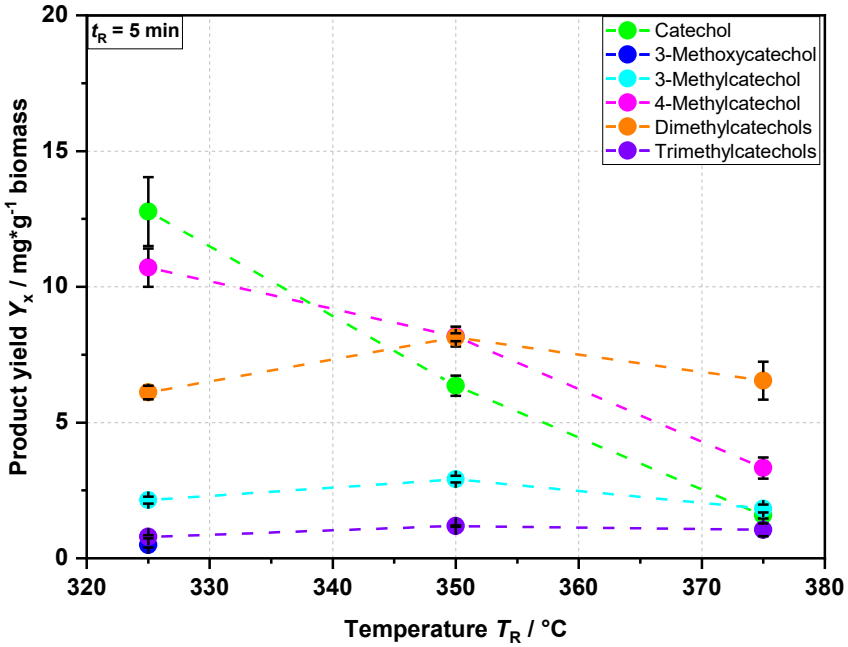

Figure 2-12: Product yields in mg per g biomass of the different catechol compounds at different reaction temperatures T_R; batch experiments; feedstock: hardwood BL

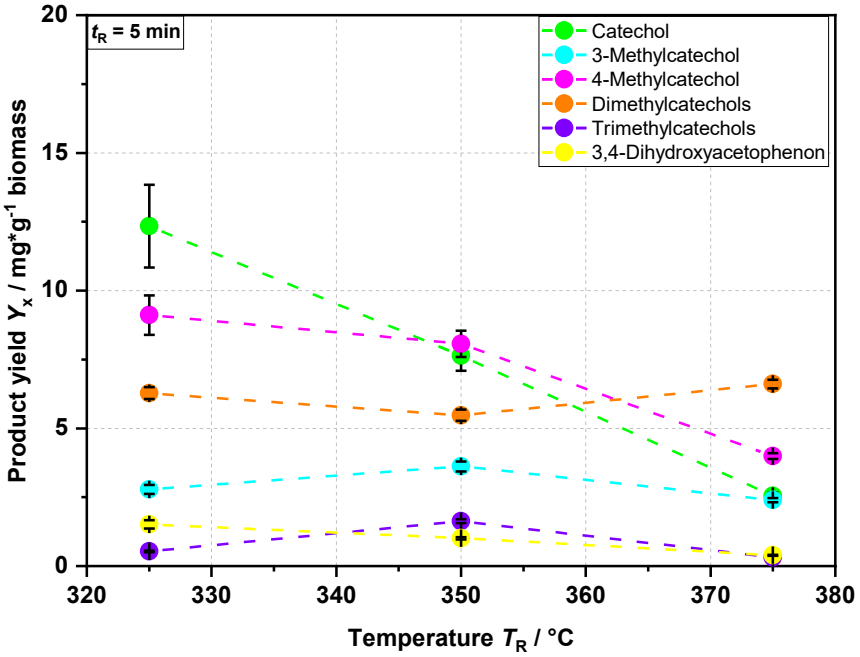

Figure 2-13: Product yields in mg per g biomass of the different catechol compounds at different reaction temperatures T_R; batch experiments; feedstock: softwood BL

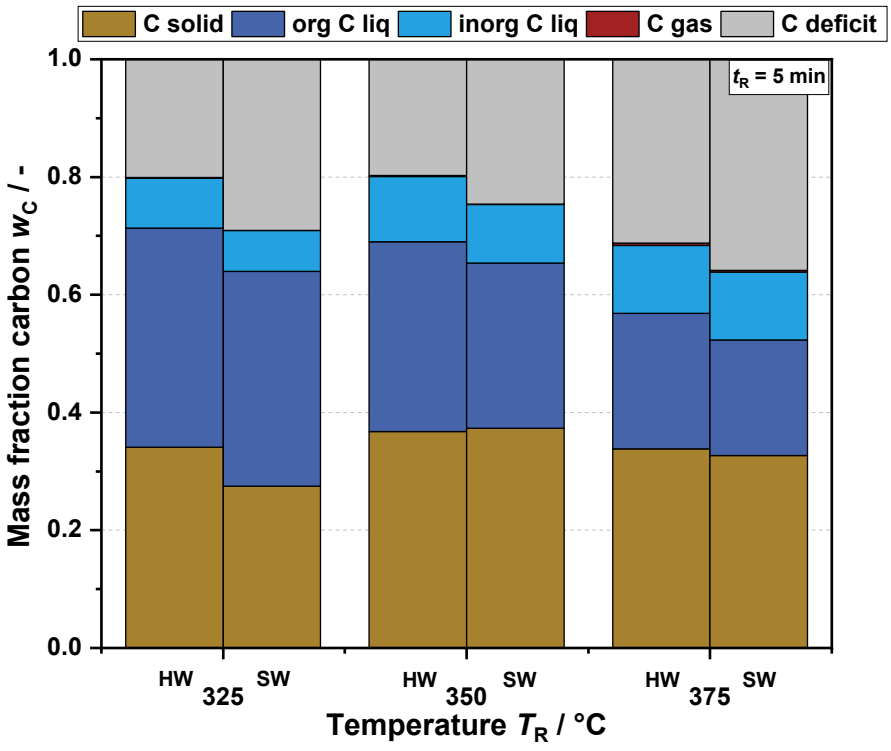

Figure 2-14: Carbon content in different product phases of batch experiments with hardwood-based (HW) BL and softwood-based (SW) BL at three different reaction temperatures TR

2.4.6 NMR analysis of liquid and solid product phase from HTL

In order to gather more information about the oligomers in the organic product, we searched for suitable parameters that could describe the evolution of these larger molecular structures. One possibility is the quantification of the hydroxy groups (−OH) present in lignin and its depolymerization products. Using a specific phospholysis derivatization technique followed by ^{31}P NMR analysis as described in the Materials and Methods section (chapter 2.3), it is possible to assign hydroxy groups quite precisely and, moreover, to quantify them to individual molecular groups depending on the observed chemical shifts. The high efficiency of the derivatization technique allows us to treat the extracted organic phase from the liquid product and assess all the hydroxy groups present in the complex reaction mixture. In Figure 2-15, the molality of the hydroxy groups is shown on the left Y-axis. We focused on guaiacyl-OH and syringyl-OH because they compare well with our quantified monomers. It is difficult to distinguish them from the catechols because the NMR signals partially overlap. Therefore, we assumed that the 3 – methoxycatechol signal is located close to the syringyl group and that the remaining catechols could be assigned to the guaiacyl group[190,191]. Due to the low mass of extracted biocrude, only four sample analyses and the feedstock analysis (extracted lignin) could be meaningfully evaluated. Nevertheless, the results of the ^{31}P NMR analysis are very interesting and fit well with the previous results. As expected, the lignin consists of a much larger fraction of syringyl groups since we are working with hardwood lignin[192]. As soon as the depolymerization of the lignin molecule starts, the molality of the hydroxy groups increases. This is due to the fact that β-O-4 bonds are preferably broken in the lignin structure, which presumably results in the formation of further hydroxy groups. From $T_R = 300\ °C$, hardly any syringyl-OH is present in the mixture, while significantly more guaiacyl-OH is produced. For comparison, the summed yields of the individual aromatics from GC-FID are plotted on the right Y-axis in the same Figure 2-15. The calculated amounts are related to the measured ^{31}P NMR regions, meaning that 3 – methoxycatechol is considered together with syringol as S-components and, similarly, the remaining catechols together with guaiacol as G-components. Only at $T_R = 250\ °C$ is the ratio of the yields of the S-components and the G-components significantly higher compared to the ratio of the molality of syringyl-OH and the guaiacyl-OH. This is possibly due to a “dual” role of 3- methoxycatechol: it is quite

possible that the second OH group present in the molecule produces a signal in the guaiacyl group range and its share is therefore in the guaiacyl-OH molality at the same time. Another reason may be oligomers, which are soluble enough to be detected using NMR but not volatile enough to be evaluated via GC. Nevertheless, the overall results are in good agreement, validating the chosen derivatization technique. Hence, it can be concluded that the reactions involving the hydroxy groups of the oligomers behave similarly. This again means that with increasing temperature, the hydroxy group is the predominant functional group on all aromatic structures within the biocrude. The behavior of the oligomeric organic structures in the liquid product phase is therefore clarified, and the same reaction scheme can be used for the monomers.

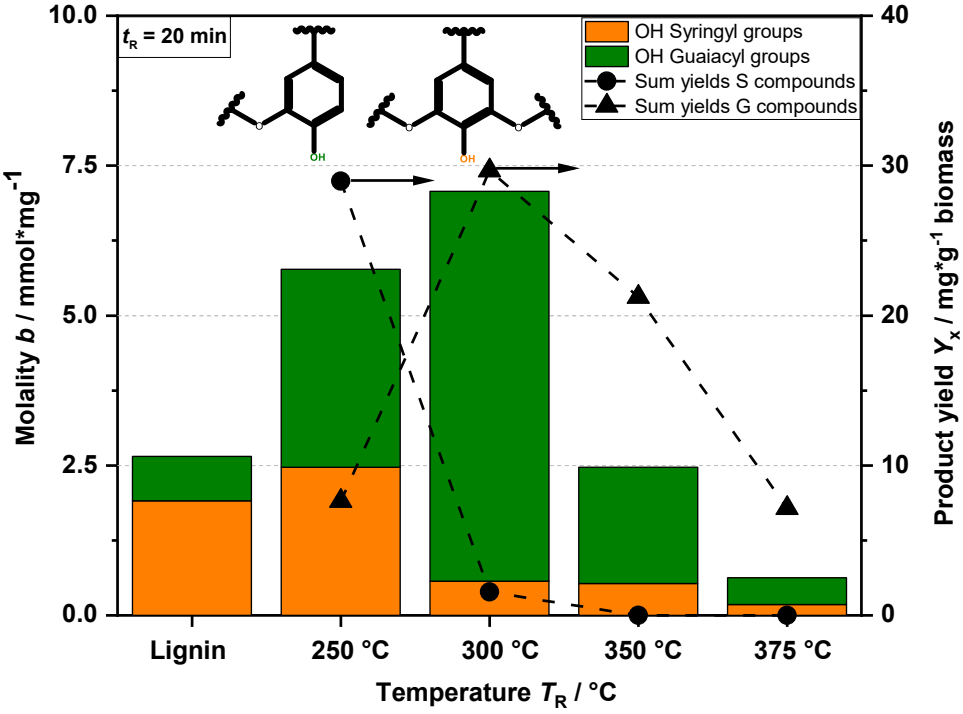

Figure 2-15: Molality of OH groups in syringyl groups and guaiacyl groups (see chemical structures in the figure) and the product yields of summed up S compounds and G compounds at different reaction temperatures T_R

Looking back at the carbon mass balance, it is noticeable that a large proportion of carbon ultimately ends up in the solid product. This is not desired but could not have been avoided with the parameters investigated. In order to understand what ultimately ends up in the solid, we analyzed three solid samples from three different batch tests ($T_R = 300\,°C,\ 350\,°C \text{ and } 400\,°C$) using ^{13}C solid-state NMR. The three NMR spectra produced can be seen in Figure 2-16. Two main signal regions are clearly visible. The

region in the low field (left in the spectra, 120 – 160 ppm) shows ^{13}C carbons present in aromatic compounds (aryl-C), and the region in the higher field (right-hand region group 25 – 50 ppm) shows carbon in alkyl compounds (alkyl-C). A region worthy of note can be found in the lower field, typical of carboxyl groups (carboxylic acids and derivatives like esters or amides: ranging from 170 to approximately 185 ppm) at $T_R = 300\ °C$. However, the signal at 180 ppm disappears at higher temperatures. The aromatic peak itself probably consists of an aryl-C−O-peak, which, however, is only visible clearly at $T_R = 300\ °C$, in addition to the pure aryl C-peak. The aryl-C−O bond fits to the phenolic structure of the lignin. At higher temperatures, the signal of this bond could be overshadowed by the aryl-C peak. An indication is the width of the peak, which looks like two signals merged together. The peak, which shows the aromatic bonds, could also be generated by C=C bonds. Since we were not able to observe carbon double bonds in any other analysis, we assume that the peak describes the aromatic carbon. In general, this signal indicates that the solid is preferably built up from aromatic building blocks. This is a consequence of using lignin as feedstock and its products. Likewise, it supports the assumption that the aromatics are a driver of repolymerization and preferentially remain in the solid product. Moreover, the ^{13}C solid-state NMR spectra fit very well with the observed yields of the monomers.

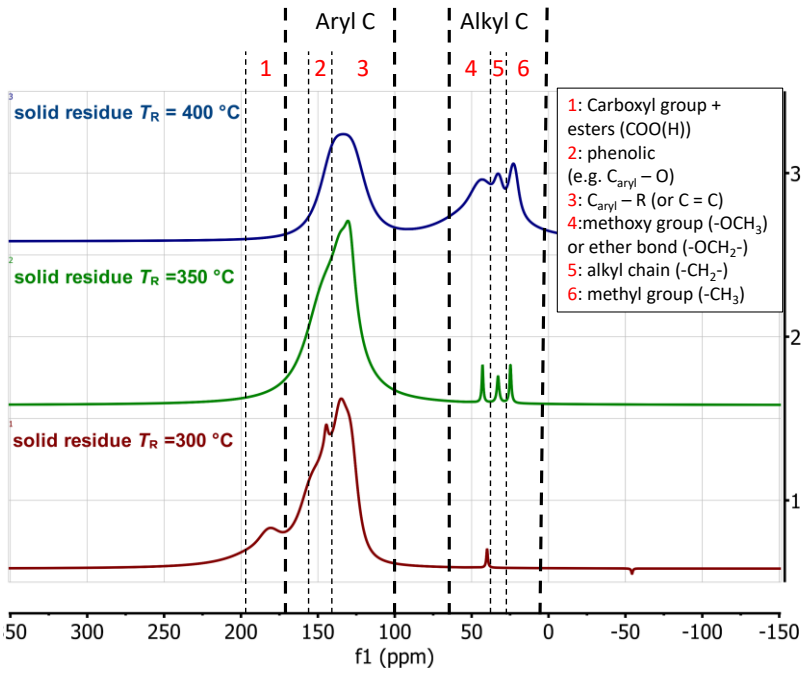

Figure 2-16: ^{13}C solid-state NMR spectra for the solid phase at three different reaction temperatures T_R

We observed that the yields of all aromatic monomers decreased with an increasing reaction temperature. We also saw that methoxy and hydroxy groups were preferentially present at lower reaction temperatures, and methyl groups were more prominent as the reaction temperature increased. The same pattern can be found in the NMR spectra for the solid product. At $T_R = 300\,°C$, the aromatic peak is clearly dominant. At a high reaction temperature of $T_R = 400\,°C$, the ratio of the aromatic peak to the alkyl peak is almost balanced. This strongly suggests that the monomers formed without a methyl group repolymerize first, and only later do the aromatics with an alkyl radical formed at higher reaction temperatures also appear. Another hypothesis is that reaction mechanisms similar to those for the monomers also apply to the solid, as already shown for the oligomers.

2.4.7 Investigation of the molecular mass of the biocrudes via SEC analysis

Another option to describe the depolymerization of lignin is to assess the molar mass of the molecules present in the extracted biocrude. The results of the SEC analysis are summarized in Figure 2-17, allowing for easy determination of the relative molecular mass M_{rel}. The UV signals of three biocrudes from batch experiments performed with different reaction temperatures T_{R} are plotted (together with the related calibration curve) versus the retention volume V_{ret}, the volume of eluent passed through the column. The column used was calibrated in the range of 246 to 20.700 g·mol^{-1}. The recorded eluent volumes are within the two dashed lines (minimum and maximum). This region delivers the most conclusive data. Only the lignin displays signals below the minimal limit, somehow impeding interpretation. It can be clearly observed how depolymerization progresses with increasing temperatures. The maximum peaks clearly shift to the right toward smaller molecular weights. New prominent peaks form at the three investigated reaction temperatures around 1000 and 1500 g·mol^{-1}. This would correspond to oligomers displaying 7 to 10 syringyl groups (see Figure 2-15). The beginning of repolymerization can also be observed. For instance, the peak around 1000 g·mol^{-1} is no longer present in the product obtained at $T_R = 350\,°C$. Instead, the 1500 and 4000 g·mol^{-1} peaks are much more pronounced. Monomers cannot theoretically be observed with the setup used, with the calibration range taken into consideration. However, the functional groups can interact with the column and lead to retention time shifts. Therefore, the measured molecular mass will be labeled as the relative molecular mass for the remainder of this paper.

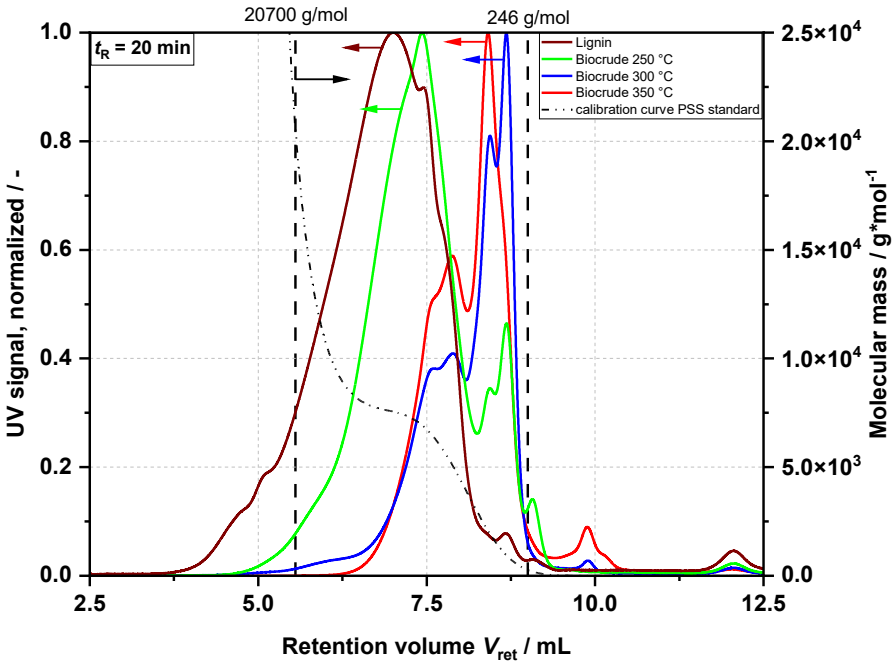

Figure 2-17: SEC analysis of different extracted biocrudes and lignin; left Y-axis: UV signal over retention time; right Y-axis: molecular mass over retention time; and calibration curve (dashed-dotted line) with the calibration minimum and maximum (vertical dashed lines at 20700 and 256 g·mol^{-1}

Finding a suitable setup for SEC analysis of lignin is difficult due to the dual polar and nonpolar character of the feed, without even first modifying the molecules, e.g., with acetylation. However, the idea was to gain direct information about the molecule sizes. Nevertheless, some trends can be detected by investigating depolymerization and repolymerization behavior. Figure 2-18 shows the weight-averaged relative molecular weight of various biocrudes. Up to $T_R = 300\ °C$, a significant decrease can be seen. Thereafter, interestingly, M_{rel} remains constant with an increasing reaction temperature T_R. It can be assumed that some kind of equilibrium is set between depolymerization and repolymerization. We assume that although the lignin molecule is cleaved into smaller molecules, the high temperatures used rapidly lead to partial repolymerization. One reason for the faster repolymerization reactions could be radical reactions, for example, which are known to occur more frequently at higher temperatures[152].

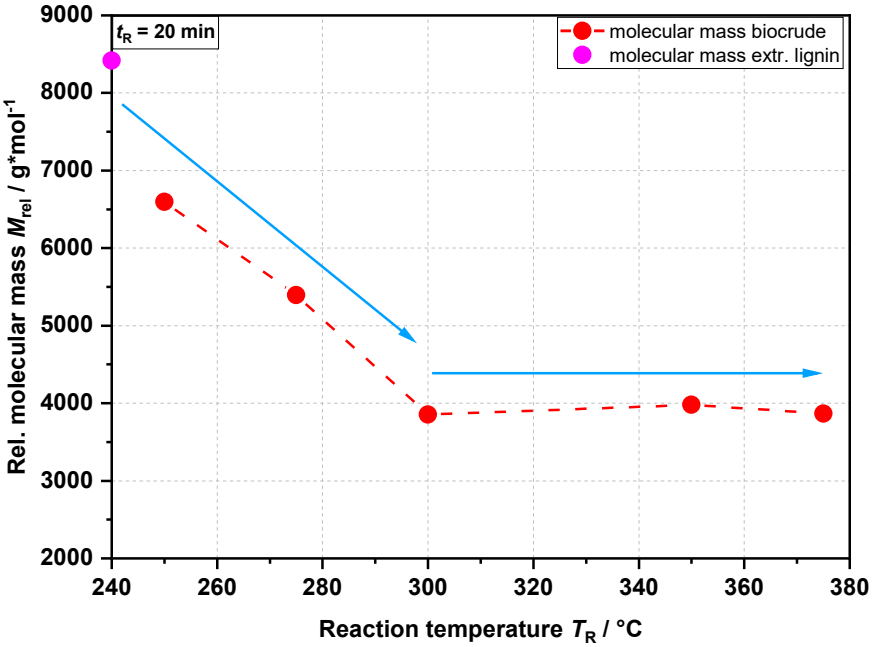

Figure 2-18: Relative molecular mass of extracted biocrudes at different reaction temperatures T_R (red) and the molecular mass of extracted lignin from BL (pink)

2.4.8 Development of a simplified reaction scheme

Based on the results gathered from the comprehensive analytics, a simplified reaction scheme can be tentatively proposed (Figure 2-19). Compared to the reaction scheme proposed by Forchheim et al.[171], the monomer products are somewhat different. In our work, the depolymerization of lignin by HTL under the influence of the cooking chemicals present in BL produces catechols as the main products. The reaction network includes three different reaction pathways, starting from syringol to catechol. They are shown together with the subsequent alkylation in parentheses. These reactions can happen on monomers, oligomers, and the lignin itself. The main reactions are demethylation (1) and demethoxylation (2). The by-products of the first of these reactions are methane and methyl radicals, whereas the latter leads to the formation of methanol. Detecting 3 – methoxycatechol in the product produced at $T_R = 250\,°C$ or $T_R = 275\,°C$, it can be assumed that demethylation proceeds preferentially in this temperature range. At higher temperatures, however, the difference hardly seems to exist since the yields of catechol and its derivatives clearly exceed those of the remaining oxygenated aromatics. Thus, in the range of $T_R = 300\,°C$ or higher, it can be assumed that both reactions can proceed simultaneously (3). In contrast, two similar reactions with the methoxy groups of the syringol are not the preferred reaction pathway. As confirmation, 1,2,3 – trihydroxybenzene (pyrogallol),

the product of a double demethylation of syringol, could be detected in the GC−MS spectrum, although the amount was too small for quantification. Similarly, phenol is produced, resulting from a double demethoxylation of the syringol. Phenol could be quantified, but the yields were much lower than those of catechols. Therefore, it appears that two different reactions starting from syringol are preferred.

After demethylation and demethoxylation, alkylation of catechol, mainly methylation (4), occurs more with increasing reaction temperature T_R. As already discussed, radical reactions with methyl radicals are probably responsible for this. The methyl radicals may be formed during demethylation, for example. Another possibility is transalkylation, in which a methylcatechol and a catechol molecule can be formed from a catechol and a guaiacol molecule, for example. The experimental data generated does not allow us to determine the extent to which the transalkylation reaction or the abovementioned radical reactions are ultimately decisive for the increase in methylated catechols. Using ^{31}P NMR analysis, we were able to show that the reactions of the monomers also proceed in a manner similar to that of the functional groups of the oligomers. It can be assumed that methylation also takes place within the oligomers. For the sake of simplification, it makes sense to apply the reaction pathways proposed for the monomers to the structurally related oligomers as well.

In addition to aromatics as the main components, many alcohols and acids are also formed on the monomer side. The formation of such acidic compounds can be explained not only by the cleavage of a wide variety of side groups, which occurs, for instance, in the demethoxylation mentioned above, but also from other components of the BL, such as hemicellulose. The organic acids and alcohols produced predominantly end up in the aqueous phase of the liquid product after extraction. In a technical approach, it would make sense to look for ways to utilize the aqueous phase. There is a lot of ongoing research into aqueous phase reforming, for example[193]. Another strategy is the recovery of phenolic compounds that did not transfer to the organic phase during extraction. A new methodology using hydrophobic eutectic solvents based on different mixtures of terpenes (menthol and thymol) and organic acids (octanoic acid, decanoic acid, and dodecanoic acid) was studied by Pola et al[194].

In the overall picture, the depolymerization of lignin under the conditions given in the research work results in three main phases. The gas phase is negligible regarding the carbon content but can be crucial for alkylation via the methane or methyl radicals.

Typical gas phase compounds are CO_2, H_2, and different small hydrocarbons. The two main product phases are the liquid and solid phases, which are closely linked. Presumably, small and larger oligomers or even monomers are separated from the lignin. Specific bonds break during this step, e.g., the remaining β-O-4 bonds. The same happens with the oligomeric structures in the following step, which ultimately produces more monomer compounds. It is possible that a certain portion of the lignin ends up directly in the solid due to precipitation and does not actively participate further in the depolymerization. It can likewise be assumed that as the reaction temperature T_R rises, the proportion of oligomers and monomers that react via repolymerization to form larger molecules that ultimately end up as solids increases sharply. Conversely, it is rather improbable that a material flow from the solid will return to the liquid phase. The different relative molecular weights can be used to show how the size ratios of the individual groups compare with each other. In the end, the solid does not differ much from the lignin itself, at about 8500 $g \cdot mol^{-1}$. In the case of the oligomers, there are various intermediates, as shown by the SEC analysis. The monomers have relative molecular weights in the range of 90 – 200 $g \cdot mol^{-1}$. A potential explanation for the intermediates could be the different activation energies of the bonds within the molecule.

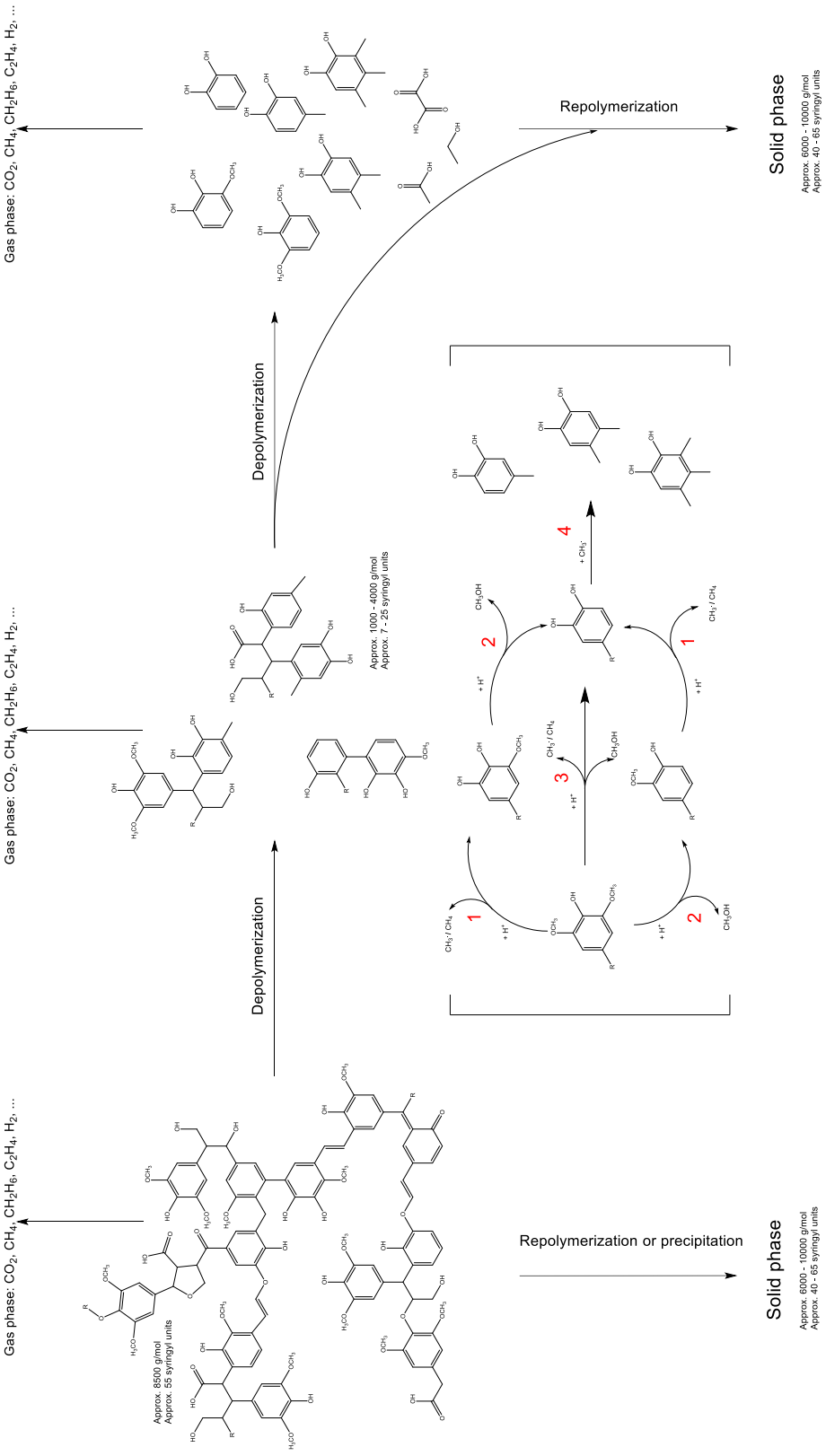

Figure 2-19: Reaction scheme of lignin depolymerization during HTL of BL based on the results of the experimental work; reaction mechanism in parentheses applies to all of the three groups (lignin, oligomers, and monomers); lignin structure on the right reproduced with permission from ref Lange et al.[40] Copyright 2013 Elsevier

2.5 Conclusions

In the present study, we were able to show that BL can be used directly in a HTL process for the production of aromatics. Derivatives of catechol were identified as the main products of depolymerization of the lignin dissolved in the BL, diverging from the results reported by numerous research groups that mentioned phenol as one of the main components. However, the yields produced remain low, in relation to the biomass used. Consequently, fruitful development of this process requires significant enhancement of the selectivity toward catechol and, on the other hand, better valorization of the main byproducts generated by the BL treatment. An important step in further developing the HTL is to better understand how depolymerization occurs. By calculating the yields of various monomers, three main reactions have become apparent. Starting from the lignin structure, it is demethylation and demethoxylation that lead to catechol. The catechol is then alkylated in the next step, probably by radical reactions or transalkylation catalyzed by the various salts present in the reaction mixtures. High temperatures (above $T_R = 350\ °C$) seem to accelerate repolymerization reactions, leading to a significant yield reduction. Regarding the lignin depolymerization, the behavior of the oligomers must also be thoroughly investigated. By carrying out NMR analyses, we were able to prove that the oligomers and their functional groups also participate in demethylation and demethoxylation reactions, which take place in a way similar to that observed with monomers. This greatly facilitates the establishment of the reaction scheme since the postulated reaction pathways can be adopted for the monomers in a lumped reaction scheme. The possibility of describing the depolymerization sufficiently on the basis of functional groups, such as the hydroxy groups, without a loss of relevant information is a great step forward. The first positive trends observed so far now have to be investigated in greater depth, for instance, with kinetic models and specific series of experiments. In addition, we used SEC analysis to determine a further parameter for describing the process. In doing so, we were able to illustrate once again how important it is to suppress repolymerization, as otherwise, no further progress can be seen in reducing the size of the molecules. This obviously leads to a high loss of valuable carbon in the solid phase. Lastly, we were able to show that in a direct HTL of BL, the cooking chemicals have a much greater influence than the wood species dissolved in the BL. The results between softwood and hardwood hardly differ. This clearly indicates that

the reaction scheme can be applied not only to one specific BL but also to other liquors as long as the composition of the cooking chemicals is somewhat similar.

3 From Pulp to Aromatic Products – Kinetic Modeling of Hydrothermal Lignin Depolymerization

3.1 Abstract

Lignin is a promising renewable feedstock for the production of aromatic platform chemicals due to its high content of aromatic structures linked by various chemical bonds. In the pulp industry, lignin occurs in large quantities dissolved in black liquor that provides a potential feedstock for depolymerization into interesting aromatic monomers. This work studied the lignin depolymerization process under hydrothermal conditions ($T_R = 300 - 350\ °C$, $t_R = 0 - 30\ min$, $p = 250\ bar$), using a black liquor based on eucalyptus wood as feedstock. The aim was to understand the main reaction pathways of the lignin depolymerization. Experiments were performed in batch micro autoclaves and the product phases were separated and characterized. The work focused on the principal aromatic monomers, mainly different forms of catechol. Based on the experimental results a reaction scheme was set up consisting of the aromatic monomers, lumped groups like oligomers, and gaseous compounds. A kinetic model was developed, parametrized, and trained, providing adequate results. The calculated kinetic parameters and the developed reaction scheme were compared with data from literature. In accordance with our model, the main pathway from lignin to methylated catechols is via 3-methoxycatechol and catechol. Finally, experimental results of hydrothermal liquefaction (HTL) with softwood black liquor were compared with the calculated yield curves and showed limited deviations. Hence, this implies that the model, with minor adjustments, can be used for the HTL of softwood black liquor as the dissolved salts presumably have a significantly greater influence than the type of wood.

3.2 Introduction

The investigations presented in the previous chapter show the potential of HTL of BL for the production of aromatics. We were able to show that catechol in particular is the main product among the aromatics, while methylated catechols are also strongly represented. At the same time, we found that the same reactions observed for monomers also occur in oligomers and that a large proportion of the carbon ends up in the solid phase under the conditions investigated. Overall, these results improved our understanding of the lignin depolymerization reaction network occurring during HTL of BL. In the next step, a kinetic model is developed based on the previous results. Kinetic modeling is a powerful tool for better understanding of the influence of process parameters in chemical processes and is useful for process scale-up and optimization. Forchheim et al. and Gasson et al. jointly developed a model for solvolysis with ethanol and HTL with water based on extracted lignin as feedstock[171,195]. In the work of Jayathilake et al. a numerical shrinking-core model was developed for lignocellulose under HTL conditions[196]. However, only hydrolysis reactions were considered. While this type of depolymerization reaction predominantly takes place in the lower temperature regime, radical reactions such as those that also take place during pyrolysis become dominant at higher temperatures. Yong and Matsumura were able to show this in their kinetic analysis using guaiacol as a model substance[158,159]. Overall, there are only a few models that describe the depolymerization of lignin. However, to the best of our knowledge, there is no model available in literature that was developed for HTL of BL. Therefore, in this chapter, a model based on the experimental data of the previous chapter is developed with a focus on aromatic compounds, particularly methylation, which is a dominant reaction pathway in the investigated temperature range. Such a model can be used as a basis for future works in this field and will be used for a possible scale-up of HTL processes.

3.3 Material and Methods

3.3.1 Experimental setup, product phase separation and analytical procedure

The experimental setup was the same as already described in chapter 2.3. The same black liquor as feedstock was used and the same filling, heating and opening process of the micro autoclaves was conducted. For the sake of useful datasets for the kinetic

model, new experiments at $T_R = 300\,°C$, $325\,°C$ and $350\,°C$ were performed. The heating time was varied between $t_R = 0 - 30\,min$. The heating curves were estimated based on heating experiments with water (see 8.3.1)

The following phase separation with the goal to achieve the best possible aromatic monomer analysis was carried out according to the scheme in Figure 2-3. The explanation can be found in chapter 2.3.2.

Afterwards the total organic and inorganic carbon (TOC and TIC) concentration were estimated. The gas phase was transferred by a gas tight syringe from the gas trap of the micro autoclave station to a GC-FID/TCD to get the carbon content in gas phase as well as the yields of interesting gaseous compounds. To complete the carbon mass balance an elemental analysis of the solid phase was performed. The yields of the aromatic monomers were quantified via the analysis of the organic liquid phase after the LLE with GC-FID. All the used analysis methods are already described in more detail in chapter 2.3.4.

3.4 Kinetic modeling

The reaction scheme from chapter 2.4.8 was used as a basis for the kinetic model. The reaction scheme was changed in some parts. A step-by-step methylation of the catechol was added and guaiacol and syringol were eliminated since the concentrations measured were too low and only detectable at temperatures below $T_R = 300\,°C$. The H^+ ion which is needed for demethoxylation was changed to water for sufficient stoichiometry. The model consists of $n = 13$ different components i and takes into account $j = 13$ reaction steps in its initial form. The model represents the depolymerization of lignin, even if it was not used directly, instead getting dissolved in the black liquor as feedstock. The mass of lignin was set at an equal level to the organic matter in the black liquor $w_{BL,burnable}$ for simplification, since the aim of the model is to describe the lignin depolymerization under the given conditions. The influence of hemicellulose or other organic molecules in the black liquor was not taken into account. The focus of the model is primarily on the reactions involving the aromatic compounds around the catechol. The reaction scheme from the previous work was adjusted at some points (see Figure 3-1). The intermediates syringol and guaiacol were not considered because their measured yields in the parameter range investigated were extremely low, making it possible to reduce the level of complexity. What remained

was the compound 3-methoxycatechol. This occurs in the previous study as a specific intermediate in hardwood sources and is formed directly from syringol. Since the BL used was also produced from hardwood, this route is the most relevant for catechol production. In addition, the intermediate oligomers (OL_int) were introduced, since it is unlikely that phenolic monomer compounds are formed directly from the lignin molecule. This model does not include the influence of changing water properties nor does it include the potential catalytic effects of the dissolved salts like carbonates, hydroxides and sulfides and produced organo-sulfur products like dimethyl sulfide (see chapter 4 and 5). The reaction pathways of lignin under hydrothermal conditions itself are not clear yet in relation to state-of-the-art standards. Accordingly, these need to be investigated prior to additional effects like the mentioned ones.

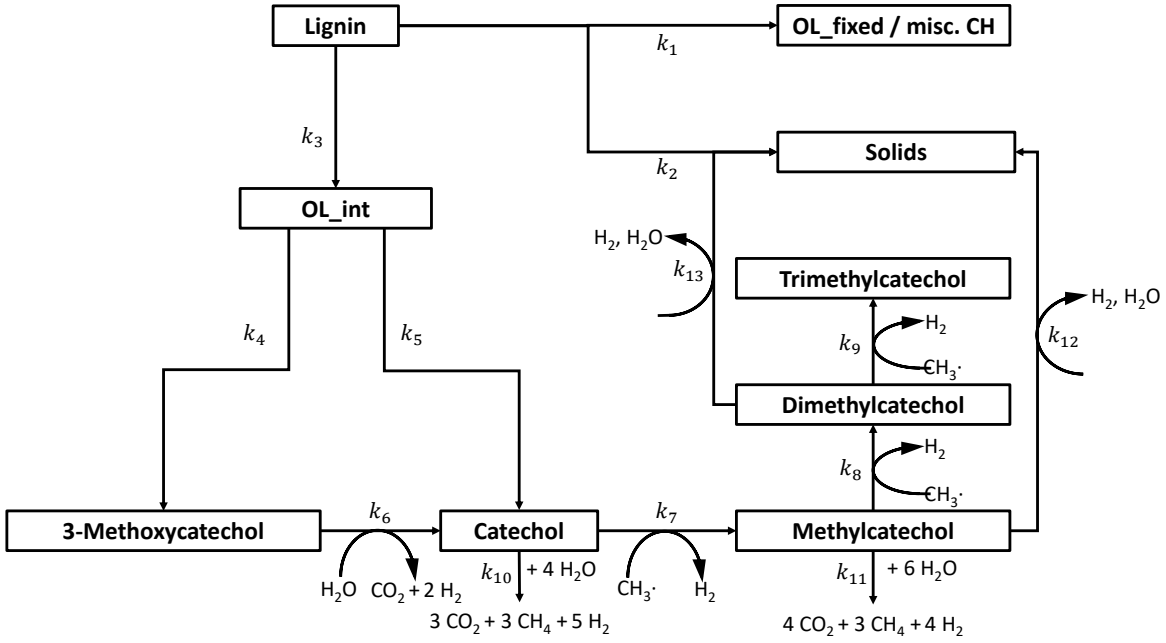

Figure 3-1: Reaction scheme for the developed kinetic model for lignin depolymerization under hydrothermal conditions with focus on the catechols based on chapter 2.4.8

The depolymerization and the reactions on the catechols are driven by hydrolysis and radical-induced reactions. Various studies served as the basis for the different reaction steps, from which hypotheses were derived for this work [156–159,197,198]. The reaction of 3-methoxycatechol to catechol (R6) is presumably dominated by radical-driven reactions (see Figure 3-2). The overall reaction is proposed in different pathways. In Fig.3-2a), methanol is released, especially at lower temperatures, but we were unable to quantify this. Therefore, consideration is given to the combined reactions of

methanol formation with methanol reforming to CO_2 and H_2 as a global side reaction (R10 and R11). Higher temperatures should elevate the methanol reforming anyway, which would support our assumption[199]. In Fig.3-2b), a direct radical split in the methoxy group is shown, which we consider to be one of the main pathways. Ionic reactions are also possible, for example a nucleophilic aromatic substitution which can transform the methoxy group into a hydroxy group, which is a common theory for guaiacol to catechol reactions[156]. The following hydrodeoxygenation or hydrolysis reactions can reduce the number of hydroxy groups attached to the ring. Since we could detect pyrogallol (3 hydroxy groups attached) and other aromatics with three oxygen-containing functional groups only in traces compared to 3-Methoxycatechol we assume that the radical reactions are dominant. Figure 3-3 illustrates the subsequent methylation of the catechol, probably by methyl radicals. Since radicals and their concentrations cannot be detected during the process, the intermediate oligomers (OL_int) are taken as methyl donors, as the methyl radicals can arise from all alkyl radicals on the molecules.

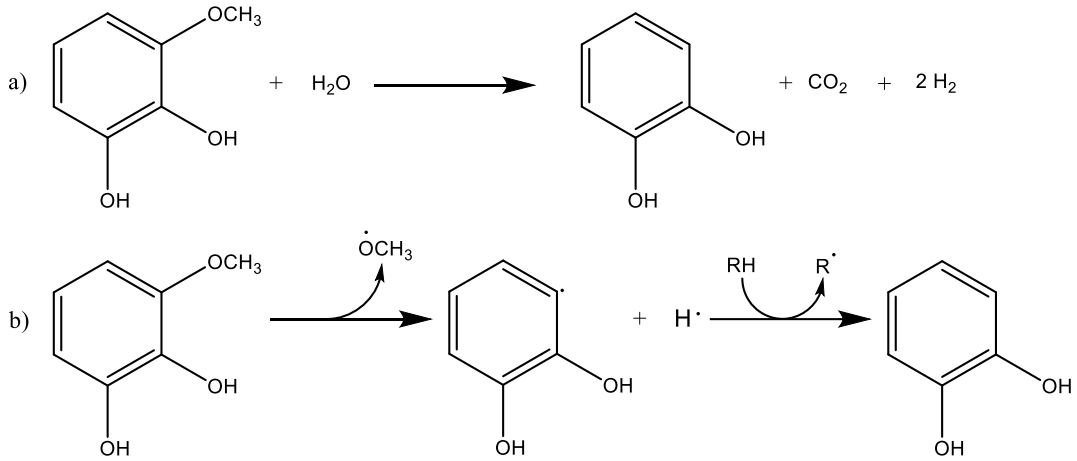

Figure 3-2: Overview of hypothetical reaction pathways for the step from 3-methoxycatechol to catechol based on observations and studies from Yong and Matsumura[158,159] and Wahyudiono et al.[155–157]. a) Reaction considered in the kinetic modeling, with direct conversion of methanol to carbon dioxide and hydrogen; b) Potential direct conversion of 3-methoxycatechol to catechol based on radical forming and interactions. The radical is converted to methanol afterwards, which is directly reformed as mentioned in description for a)

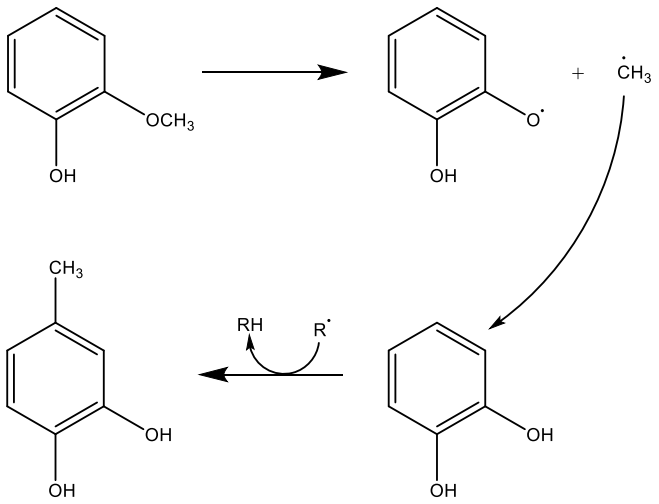

Figure 3-3: A possible source of methyl radicals from a methoxy group with the following radical driven methylation of a catechol molecule; This reaction step is implemented as R7 and adapted for R8 and R9.

The subsequent reaction steps are the repolymerization reactions of the molecules, represented in the model by the repolymerization of methylcatechols (R12) and dimethylcatechols (R13), as well as the complete degradation of catechols (R10) and methylcatechols (R11) to gas products, since the yield decrease of aromatics cannot be explained by repolymerization alone. Fixed oligomers (OL_fixed) and other hydrocarbons produced were summarized in a group and calculated using the difference of all yields starting from 100 %. SEC analysis in a previous study shows that there are some larger molecules which are not represented quantitatively in one of the used analysis methods. The same goes for other hydrocarbons in the aqueous phase like alcohols and acids (see chapter 2.4.4). These are represented with the OL_fixed lump in the model. We assume that H_2, CO_2, CH_4 are only present in the gas phase. The presence of other volatile compounds is negligible, as the carbon mass balance shows. In addition, this model focused primarily on the aromatic compounds in the liquid phase product. Water can be present in the liquid phase as well as in the gas phase. All other compounds are assumed to be present in the liquid phase. Therefore, all reactions were considered to take place only in the liquid phase. All reactions which a part of the kinetic model are listed in Table 3-1.

Table 3-1: Overview of all reactions in the kinetic model

Reaction N°	Reaction
(R1)	Lignin → Oligomers fixed (OL_fixed) /miscellaneous CH
(R2)	Lignin → Solids
(R3)	Lignin → Intermediate oligomers (OL_int)
(R4)	OL_int → 3-Methoxycatechol
(R5)	OL_int → Catechol
(R6)	3-Methoxycatechol + H_2O → Catechol + CO_2 + 2 H_2
(R7)	Catechol + CH_3· (from OL_int) → Methylcatechol + H_2
(R8)	Methylcatechol + CH_3· (from OL_int) → Dimethylcatechol + H_2
(R9)	Dimethylcatechol + CH_3· (from OL_int) → Trimethylcatechol + H_2
(R10)	Catechol + 4 H_2O → 3 CO_2 + 3 CH_4 + 5 H_2
(R11)	Methylcatechol + 6 H_2O → 4 CO_2 + 3 CH_4 + 4 H_2
(R12)	Methylcatechol → Solids + H_2 + H_2O
(R13)	Dimethylcatechol → Solids + H_2 + H_2O

The reaction rates (r_j) were calculated considering first order reaction in relation to the reactants (see Table 3-2). Here, k_j is the reaction constant of reaction j (h^{-1}) and ρ_i is the mass concentration of species i in the liquid ($kg \cdot m^{-3}$), calculated as follows:

$$\rho_i = \frac{m_{i,liq}}{V_L} \ [kg \cdot m^{-3}] \tag{3-1}$$

where $m_{i,liq}$ is the mass of component i in the liquid phase (kg) and V_L is the volume of the liquid set to 15 mL. We used mass concentration since we do not have absolute molar masses for lignin and oligomers.

Table 3-2: Reaction rate equations for all 13 reactions in the kinetic model

Reaction N°	Reaction rate equation
(R1)	$r_1 = k_1 \cdot \rho_1$
(R2)	$r_2 = k_2 \cdot \rho_1$
(R3)	$r_3 = k_3 \cdot \rho_1$
(R4)	$r_4 = k_4 \cdot \rho_2$
(R5)	$r_5 = k_5 \cdot \rho_2$
(R6)	$r_6 = k_6 \cdot \rho_3 \cdot \rho_{10}$
(R7)	$r_7 = k_7 \cdot \rho_4 \cdot \rho_2$
(R8)	$r_8 = k_8 \cdot \rho_5 \cdot \rho_2$
(R9)	$r_9 = k_9 \cdot \rho_6 \cdot \rho_2$
(R10)	$r_{10} = k_{10} \cdot \rho_4 \cdot \rho_{10}$
(R11)	$r_{11} = k_{11} \cdot \rho_5 \cdot \rho_{10}$
(R12)	$r_{12} = k_{12} \cdot \rho_5$
(R13)	$r_{13} = k_{13} \cdot \rho_6$

The reaction constants were calculated using a modified Arrhenius equation (see equation (3-2)): with $T_{\mathrm{ref}} = 325$ °C. Here, A_j (unitless) and $E_{A,j}$ (kJ·mol^{-1}) are the kinetic parameters and T_{R} is used in Kelvin. k_0 is a pre-exponential factor set to 1 h^{-1}.

$$k_j = k_0 \cdot exp\left(A_j - \frac{E_{A,j}}{R}\left(\frac{1}{T_R} - \frac{1}{T_{ref}}\right)\right) \ [h^{-1}] \tag{3-2}$$

Since all chemical reactions are assumed to occur exclusively in the liquid phase, which contains the overwhelming majority of the system mass and is dominated by water, the gas phase acts solely as a non-reactive pressure boundary. The gas phase consists only of water vapor and small amounts of non-condensable gases- Furthermore, its total amount of substance is negligible compared to that of the liquid phase. Consequently, gas-phase non-idealities do not influence reaction kinetics or

mass balances, and the ideal gas law provides a sufficient description of the gas phase. The total pressure in the gas phase was therefore specified by the vapor pressure of water p_{v,H_2O} which was calculated using the Antoine equation[200] (see equation (3-3)). Owing to the very high water content of the liquid phase, the activity of water remains close to unity, and the presence of non-volatile organic compounds has a negligible effect on the vapor pressure. Thus, the vapor pressure of pure water was used.

$$p_{v,H_2O} = 0{,}00133322 \cdot 10^{8{,}14019-\frac{1810{,}94}{T_R-28{,}665}}\ [bar] \tag{3-3}$$

The total amount of substance in the gas phase $n_{gas,tot}$ can be calculated using the ideal gas law (see equation (3-4)). The volume of the gas phase was calculated as follows with $V_G = V_R - V_L$, with reactor volume $V_R = 25\ mL$ and T_R is used in Kelvin:

$$n_{gas,tot} = \frac{V_G \cdot p_{vap}}{R \cdot T_R}\ [mol] \tag{3-4}$$

The proportion of gaseous water in the total amount of substance is calculated from the difference between the total amount of gases and the individual gas components with the exception of water (see equation (3-5))

$$n_{H_2O,gas} = n_{gas,tot} - \sum_{i=H_2,CH_4,CO_2} \frac{m_i}{M_i}\ [mol] \tag{3-5}$$

The amount of water in the liquid phase is then:

$$m_{H_2O,liq} = m_{H_2O,total} - n_{H_2O,gas} \cdot M_{H_2O} \tag{3-6}$$

In the next step the component mass balances in the autoclave are applied to set the differential equations for each compound:

$$\frac{dm_i}{dt} = V_L \cdot \sum_j SC_{i,j} \cdot r_j \tag{3-7}$$

Here, $SC_{i,j}$ is a stoichiometric factor in mass units. A total of 13 differential equations (see Table 3-3) are used in the model. The equations were integrated with the built-in function *ode45* from Matlab, with absolute tolerance set to 10^{-6} and relative tolerance set to 10^{-3}.

Table 3-3: Differential equation for each of the 13 reaction compounds that comprise the kinetic model

Compound number	Differential equation
1 (Lignin)	$\frac{dm_1}{dt} = V_L * (-(r_1 + r_2 + r_3))$
2 (OL_int)	$\frac{dm_2}{dt} = V_L * (r_3 - (r_4 + r_5) - 0.13r_7 - 0.11r_8 - 0.1r_9)$
3 (3-Methoxycatechol)	$\frac{dm_3}{dt} = V_L * (r_4 - 0.89r_6)$
4 (Catechol)	$\frac{dm_4}{dt} = V_L * (r_5 + 0.71r_6 - (0.87r_7 + 0{,}6r_{10}))$
5 (Methylcatechol)	$\frac{dm_5}{dt} = V_L * (0.98r_7 - (0.89r_8 + 0{,}54r_{11} + r_{12}))$
6 (Dimethylcatechol)	$\frac{dm_6}{dt} = V_L * (0.99r_8 - (0.9r_9 + r_{13}))$
7 (Trimethylcatechol)	$\frac{dm_7}{dt} = V_L * (0.99r_9)$
8 (Solids)	$\frac{dm_8}{dt} = V_L * (r_2 + 0.83r_{12} + 0.83r_{13})$
9 (OL_fixed/misc. CH)	$\frac{dm_9}{dt} = V_L * (r_1)$
10 (H_2O)	$\frac{dm_{10}}{dt} = V_L * (0.14(r_{12} + r_{13} - (0.11r_6 + 0.4 * r_{10} + 0.47 * r_{11}))$
11 (H_2)	$\frac{dm_{11}}{dt} = V_L * (0.01(r_6 + r_8 + r_9 + r_{10}) + 0.02r_7 + 0.03(r_{11} + r_{12} + r_{13}))$
12 (CH_4)	$\frac{dm_{12}}{dt} = V_L * (0.26r_{10} + 0.21r_{11})$
13 (CO_2)	$\frac{dm_{12}}{dt} = V_L * (0.28r_6 + 0.73r_{10} + 0.76r_{11})$

The kinetic parameters of each reaction A_j and $E_{A,j}$ were estimated by means of minimization of the sum of squared errors.Equation (3-8) shows the objective function $f(k)$ of which the minimum is determined numerically. q is the number of experiments l considered, $w_{i,l}$ is a specific weighting factor for each data point (see Table 8-7) and $m_{\mathrm{i,l,exp}}$ and. $m_{\mathrm{i,calc}}$ are the experimentally measured and calculated masses. Because

the focus of attention is on the aromatics, the weights in the objective function are heavier for these compounds

$$\min(f(k)) = \sum_{i=3}^{9}\sum_{l=1}^{q} w_{i,l}\left(\frac{m_{\mathrm{i,exp}} - m_{\mathrm{i,calc}}(k)}{m_{\mathrm{i,exp}}}\right)^2 \tag{3-8}$$

Not all components were considered in the optimization function. Lignin was fully converted, the intermediate oligomers could not be measured, nor could water (the concentration variation of which is also minimal). Furthermore, the focus of the model were the aromatics and not the gas products. Therefore, only components 3 to 9 were considered in the optimization function. The described model was implemented in MATLAB 2024A (version 24.1.0). The objective function was optimized using the nonlinear least-squares solver *lsqnonlin*, which has proven to be fast and robust for the problem described. Table 6 shows the limits of the parameters $\boldsymbol{A_j}$ and $\boldsymbol{E_{A,j}}$ The threshold for experimental values was set to 0.1 wt. % of the total biomass.

Table 3-4: Boundaries for $\mathbf{ln}(\boldsymbol{A_j})$ and $\boldsymbol{E_{A,j}}$ and threshold for experimental data used for the optimization

	Lower bound	**Upper bound**
$\boldsymbol{A_j}$	-20	10
$\boldsymbol{E_{A,j}}$	0 kJ/mol	1000 kJ/mol

To optimize and to evaluate the robustness the model, a cross validation (CV) was applied, more precisely a 5-fold CV[201]. Cross-validation is commonly used in the field of kinetics[202,203]. In this case, 15 of the 17 experimentally determined points were randomly assigned to 5 different groups, each with 3 points. The optimization process was performed five times, each one omitting the points of one of the groups. To avoid large fluctuations for 3-methoxycatechol, Point 1 ($T_{\mathrm{R}} = 300$ °C, $t_{\mathrm{R}} = 0$ min) and point 6 ($T_{\mathrm{R}} = 325$ °C, $t_{\mathrm{R}} = 0$ min) were always included in the training database. For each kinetic parameter $\theta_j \in \{A_j, E_{A,j}\}$, the sample standard deviation across all five validation groups was computed:

$$s_j = \sqrt{\frac{1}{k-1}\sum_{i=1}^{k}(\theta_{j,i} - \overline{\theta_j})^2} \tag{3-9}$$

$k = 5$ is the number of groups and $\overline{\theta_j}$ is the mean parameter value. The confidence interval (CI) for each parameter $\theta_{j,i}$ was calculated based on the standard deviation of the estimates obtained from the five cross-validation groups, assuming a Student's t-distribution with four degrees of freedom. The general form of the two-sided confidence interval is given by equation (3-10)) where α is the significance level, which is set to 0.05 in this study. $t_{\alpha/2,k-1}$ is the critical value from Student's t-distribution with $k-1$ degrees of freedom.

$$CI_{(1-\alpha)}(\theta_j) = s_j * \frac{t_{\alpha/2,k-1}}{\sqrt{k}} \tag{3-10}$$

The best performing parameter set, the one with the lowest objective function value $\min(f(k))$ was selected. If the absolute parameter value was smaller than the calculated CI, it was considered as statistically insignificant and it was removed from the model. This procedure was repeated iteratively, each time reoptimizing the reduced model, until all remaining parameters were statistically relevant.

Three different statistical error calculations were conducted to evaluate the validity of the model. In addition to the R^2 value, the mean absolute error (MAE) and the root mean square error (RMSE) were also calculated (equation (3-11), (3-12)and (3-13)) with n as the sample size.

$$R^2 = 1 - \frac{\sum(Y_{i,exp} - Y_{i,calc})^2}{\sum(Y_{i,exp} - \overline{Y_{i,exp}})^2} \tag{3-11}$$

$$MAE = \frac{1}{n}\sum_{i=1}^{n}\left|Y_{i,exp} - Y_{i,calc}\right| \tag{3-12}$$

$$RMSE = \sqrt{\frac{1}{n}\sum_{i=1}^{n}(Y_{i,exp} - Y_{i,calc})^2} \tag{3-13}$$

3.5 Results and Discussion

3.5.1 Carbon mass balance of the performed experiments

The carbon mass balances of the various HTL experiments (see Figure 3-4) confirm the observations and conclusions drawn in the previous chapter 2.4.4. The influence of temperature T_R clearly outweighs the influence of the holding time t_R, as can be seen, for example, from the decrease in the organic carbon content in the liquid phase from 30 to over 40 wt. % at $T_R = 300\,°C$ and $T_R = 325\,°C$ to below 20 wt. % at $T_R = 350\,°C$. Even if the reaction is stopped directly after the heating time, the value at $T_R = 350\,°C$ for the organic carbon is just under 30 wt. %. The carbon content in the solid is also higher at the highest temperature in almost all cases than at the others, regardless of the holding time t_R, which indicates an increased repolymerization rate. The decisive factor here is the high density of functional groups on the oligomers and monomers[154]. At the same time, aromatics are likewise a source of char and tar formation, especially at higher temperatures[188]. In addition, typical pyrolysis reactions, such as radical-induced reactions, further contribute to increased char formation[189]. This may be one reason why more carbon ends up in the solid, especially at higher temperatures.

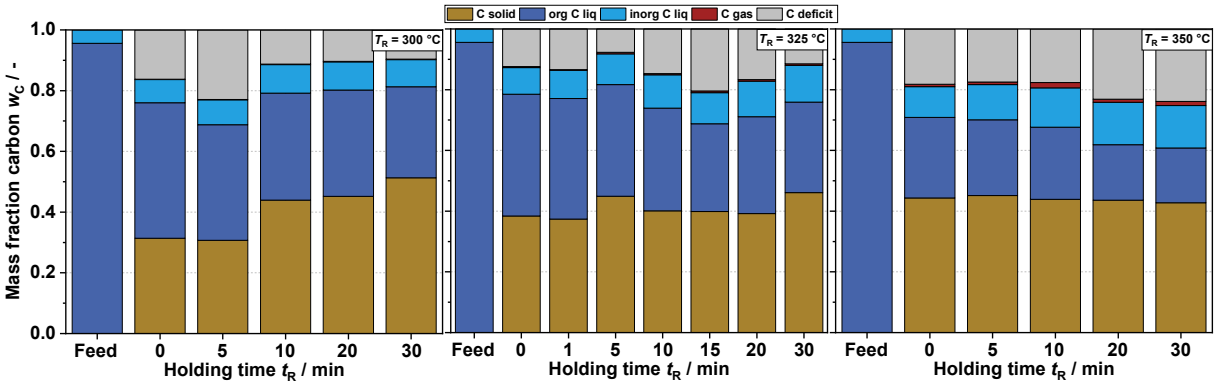

Figure 3-4: Carbon mass fractions at different reaction temperatures T_R and different holding times t_R and before processing (feed); brown: C mass fraction solid; green: organic C mass fraction liquid phase; blue: inorganic C mass fraction liquid phase; red: C mass fraction gas phase (calculated from the detected gas compounds); and gray: deficit of carbon.

The experiments at $T_R = 300\,°C$ and holding times from $t_R = 10\,\mathrm{min}$ are an exception here. While the carbon content in the solid is largely constant at the other reaction temperatures investigated, a clear increase can be seen here. The lower reaction rate

of repolymerization could be one reason for this observation. The gases hardly play a role with regard to the distribution of carbon. This applies both to permanent gases, where only CO_2 and no CO was detected, and to hydrocarbons. Among the latter, CH_4 is the most frequently produced gas. For this reason, too, it was decided to focus the model mainly on the aromatics and to allow the gases to occur only as by-products.

3.5.2 Experimental estimated yields of the aromatic monomer compounds

The most interesting part of the carbon mass balance for this study is the dark blue section, which represents the organic carbon. Approx. 5 – 30 wt. % of the carbon in this section can be traced back to aromatic monomers. GC-FID and GC-MS were used to identify and quantify these compounds. Based on the previous work, we know that the primary monomers are catechols. While we mainly focused on the influence of temperature, in this study we also looked at the influence of holding time. Figure 3-5 shows the yields of various aromatic monomers at $T_R = 300\ °C$, $325\ °C$ and $350\ °C$ and holding times of $t_R = 0 - 30\ min$. The highest yield of a single substance, in this case 22.0 mg catechol per g biomass, was achieved at $T_R = 325\ °C$ and a holding time of $t_R = 1\ min$. In principle, it can be stated that the yields are highest at $T_R = 325\ °C$ compared to the other two investigated temperatures. While at $T_R = 300\ °C$ intermediates with methoxy groups such as syringol or 3-methoxycatechol are still present, at $T_R = 350\ °C$ repolymerization or decomposition, e.g. by hydrolysis, is more pronounced. The second point can be confirmed by the fact that the methylated catechols in particular have not yet passed through a maximum at the two lower temperatures at $t_R = 30\ min$ or that largely stable yields can be observed over several of the holding times investigated. Overall, the results fit well with the reaction scheme in Figure 3-1. The intermediates such as 3-methoxycatechol are clearly visible and, in contrast to the other catechols, they decrease rapidly even at a low reaction temperature of $T_R = 300\ °C$. This indicates the instability of the methoxy group under the given conditions. As in the postulated reaction mechanisms in Figure 3-2, this can occur either by hydrolysis or by the formation of radicals, which then contribute to the formation of the methyl catechols further down the line. The low yields of syringol and guaiacol with 2 mg per g biomass or less and only detectable at $T_R = 300\ °C$ support the decision of not considering these two substances in their own right in this model. A more detailed discussion about the monomer yields compared to state-of-the-art research on this topic can be found in our chapter 2.

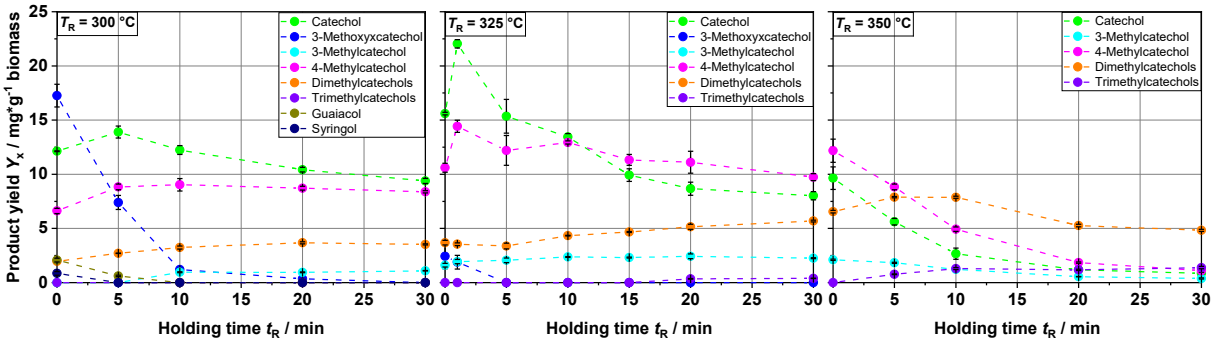

Figure 3-5: Product yields in mg per g biomass of the different aromatic monomers with focus on compounds with methoxy groups and hydroxy groups. The experimental results at different holding times t_R at three different reaction temperatures $T_R = 300$ °C, 325 °C and 350 °C (from left to right) are shown. The analysis was done by GC-FID.

3.5.3 Evaluation of the kinetic model

In Figure 3-6, Figure 3-7 and Figure 3-8, show the yield curves of the individual components based on the developed kinetic model. In addition, the measured yields including error bars are also shown. Four graphs are shown for each of the three reaction temperatures. All components involved in the reaction components are plotted with the exception of water. Table 3-5 lists the calculated errors (R^2, MAE and RMSE) for the aromatic monomers. Due to the assumption that the original kraft lignin is no longer present in the black liquor after heating starts, its degradation is very rapid over all three temperatures and does not show any major differences. Consequently, there are also hardly any visible differences for the solid and the fixed oligomers and other hydrocarbons, as these are formed primarily from the lignin. The intermediate OL_int is visible at all three temperatures, although the reaction times are slightly shorter with increasing T_R, as can be seen from the slightly faster decrease in yield. The very stable values for fixed oligomers and solids after the heating time fit well with the carbon mass balances. Only at $T_R = 300$ °C is the increase in the solid phase in the carbon mass balance not visible in the calculated data from the kinetic model for solids and fixed oligomers.

The main focus of the work is on the aromatic monomers. Together with the results of the simulation for the gaseous compounds, a good overview of the depolymerization of lignin under hydrothermal conditions is obtained. The gas components H_2, CH_4, and CO_2 are clearly overdetermined at $T_R = 300$ °C and 325 °C, but at $T_R = 350$ °C the simulated values for H_2 and CO_2 correlate well with the experimental results. The

significantly higher yields of the two components at lower temperatures can be explained by methanol reforming in supercritical water, which is accelerated at higher temperatures[199]. Methanol reforming is already integrated in the model directly from $T_R = 300$ °C, as the model did not take account of as a theoretical product of 3-methoxycatechol to catechol, due to the points already mentioned. The values for methane are clearly too high. This is a product of the gasification reactions of catechol and methylcatechol. Studies on the gasification of catechol under hydrothermal conditions by Kruse et al. at 700 °C and 400 bar have shown that virtually no methane is produced at very low catechol concentrations[204]. This may also apply to milder conditions, such as those used for hydrothermal liquefaction. However, since we assume a methane source and given that the combination of methyl and hydrogen radicals to methane cannot be represented due to a lack of data, methane is present as a product of the gasification of the monomers. In addition, due account needs to be taken of the fact that it is difficult to detect and quantify all of these gases due to the very small quantities of gas formed.

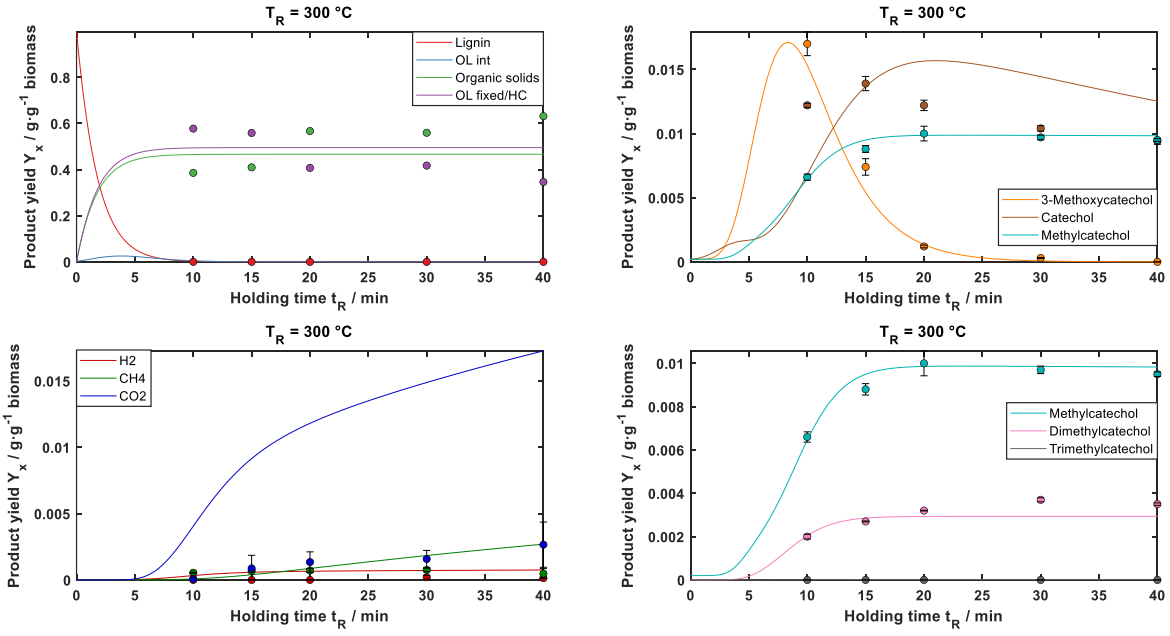

Figure 3-6: Comparison between calculated kinetic model fits (lines) and the experimental results (dots) for the batch experiments at reaction temperature $T_R = 300$ °C and holding times $t_R = 0 - 30$ min. No experimental values for OL_int. The heating phase from $t_R = 0 - 10$ min is included; top left: oligomeric structures; top right: main aromatic monomers; bottom left: gaseous compounds; bottom right: methylated catechols

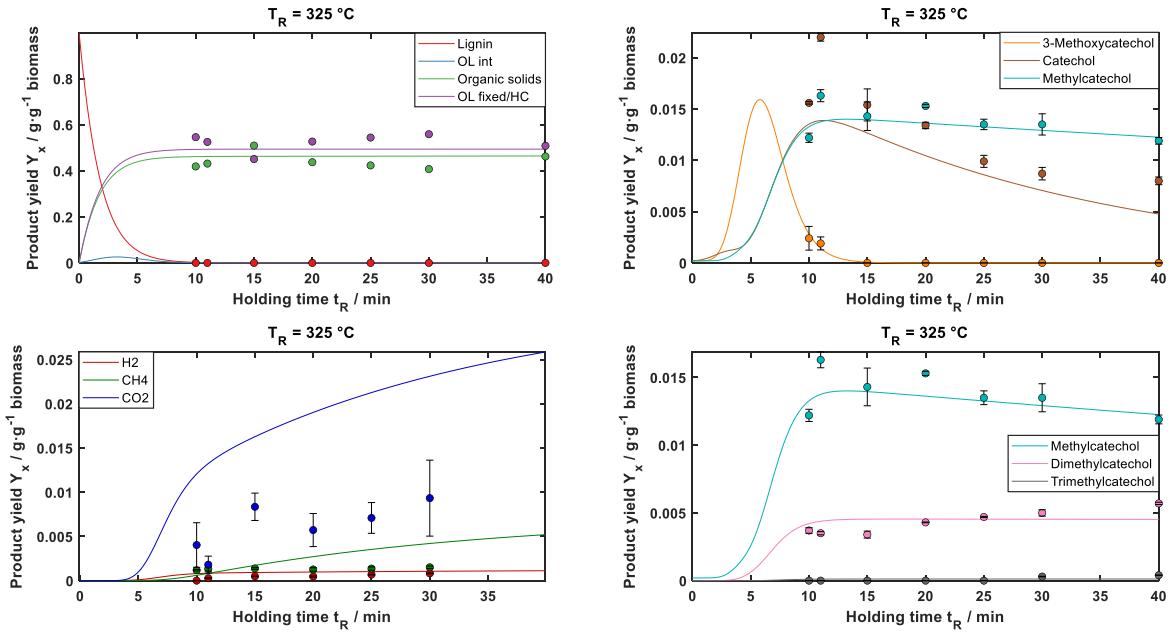

Figure 3-7: Comparison between calculated kinetic model fits (lines) and the experimental results (dots) for the batch experiments at reaction temperature $T_R = 325$ °C and holding times $t_R = 0 - 30$ min. No experimental values for OL_int. The heating phase from $t_R = 0 - 10$ min is included; top left: oligomeric structures; top right: main aromatic monomers; bottom left: gaseous compounds; bottom right: methylated catechols

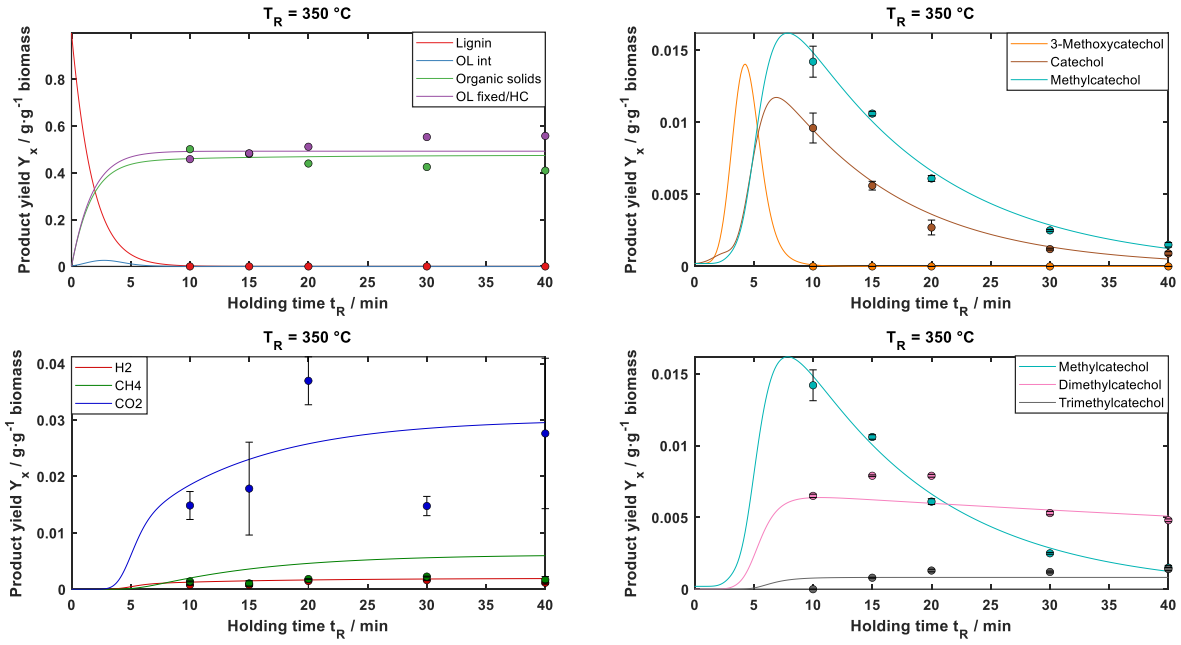

Figure 3-8: Comparison between calculated kinetic model fits (lines) and the experimental results (dots) for the batch experiments at reaction temperature $T_R = 350$ °C and holding times $t_R = 0 - 30$ min. No experimental values for OL_int. The heating phase from $t_R = 0 - 10$ min is included; top left: oligomeric structures; top right: main aromatic monomers; bottom left: gaseous compounds; bottom right: methylated catechols

At all three different temperatures, it is evident that many decisive reactions already take place during the heating time. This is particularly clear with 3-methoxycatechol, which shows a significant maximum within 10 minutes at all three reaction temperatures. The decisive factor here are the high experimental values at $T_R = 300$ °C. Due to the high syringyl group content in the black liquor used, this is the logical consequence, as the methoxy groups are already split off at lower temperatures or are converted to hydroxyl groups. In a study on pyrolysis reactions by Pan et al. with catalysts, the decomposition of syringol to phenolic compounds was investigated at higher temperatures (above 300 °C) with the result that radical reactions typical of pyrolysis in particular take place[198]. In addition, other studies on demethoxylation with different catalysts already show syringol decomposition at below 300 °C[185,205,206]. Due to the special properties of water, we assume that in our case both are possible at temperatures below or around 300 °C and for this reason the intermediates guaiacol and syringol are already almost completely degraded after the heating phase and 3-methoxycatechol as a prominent intermediate of syringol degradation also reaches its maximum. The coefficient of determination for 3-methoxycatechol is $R^2 > 0.9$ for $T_R = 300$ °C and $T_R = 325$ °C. In contrast, the developed model overestimated and underestimated catechol at these two temperatures. Nevertheless, the model is satisfactory as the curves match the experimental values. Although the R^2 value for $T_R = 325$ °C is 0.3 and even negative at $T_R = 300$ °C, the absolute (MAE) and weighted error (RMSE) is not too high between 0.032 and 0.038 g/g biomass. One major issue with the R^2 value is the high fluctuation for extremely low values for example di and trimethylcatechol yields. Since R^2 actually represents the deviations of the model compared to the deviations that a simple average value would yield, when experimental values are always near each other and have low values, it follows that small deviations can lead to very bad R^2 values, The same thing occurs when the curve estimated by the model has the right shape but does not pass through the data points like the catechol at $T_R = 300$ °C and 325 °C. Therefore, we decided to use MAE and RMSE values as well, which are measurements of absolute error. These show that our model is not too far removed from the experimental data.

Table 3-5: Error estimations for the simulated aromatic monomer compound yields at different reaction temperatures T_R

	300 °C			325 °C			350 °C		
	R^2	MAE / g*g^{-1}	RMSE/ g*g^{-1}	R^2	MAE/ g*g^{-1}	RMSE/ g*g^{-1}	R^2	MAE/ g*g^{-1}	RMSE/ g*g^{-1}
3-Methoxycatechol	0.97	0.0008	0.0011	0.94	0.0001	0.0002	n.a.	n.a.	n.a.
Catechol	-4.5	0.0033	0.0037	0.30	0.0032	0.0038	0.98	0.0004	0.0005
Methylcatechol	0.92	0.0003	0.0003	0.28	0.001	0.0012	0.99	0.0005	0.0005
Dimethylcatechol	0.4	0.0004	0.0005	0.09	0.0007	0.0008	0.24	0.0008	0.0011
Trimethylcatechol	n.a.	n.a.	n.a.	0.02	0.0001	0.0002	0.02	0.0004	0.0005

Kinetic modeling shows that the additional route via OL_int to catechol is probably not sufficient to reach the peaks of the experimental values at $t_R = 0 - 5\ \mathrm{min}$. Due to the fact that the experiments only produced very low values for guaiacol (see Figure 3-5), it would be conceivable to improve the model by conducting experiments at lower temperatures, such as in chapter 2.4.1 where temperatures go down to $T_R = 250\ °C$. Based on this type of data, the reaction pathway assumed by Schuler et al. could possibly be represented[183,207]. On the other hand, however, it must be considered that the near-critical range is already further away at a reaction temperature of $T_R = 250\ °C$ and ionic reactions probably dominate. This raises the question of whether it makes sense to lower the temperature range to this extent for a model to describe the depolymerization of lignin under near-critical conditions. A more appropriate approach than lowering the temperature would be to investigate the yields occurring during the heating phase. However, these experiments need to be designed for the phase transition and the near-critical range in order to avoid as far as possible any fluctuations caused by these transitions. At $T_R = 350\ °C$, when the radical-induced reactions in particular are dominant, for instance the methylation of the catechol, the model provides a particularly good result with an R^2 = 0.98 and extremely low errors. The same also applies to the various methylcatechols as secondary products. This shows clearly that the strength of the model lies in these primarily radical reaction steps. The single methylated catechols in particular are very accurately represented by the kinetic model (R^2 = 0.28 – 0.99, MAE, RMSE ≤ 0.0012 g/g biomass). The calculated values for the di- and trimethylcatechols are also within the range of the experimental values.

Although the R^2 values are extremely low in some cases, due account must be taken here of the fact that fluctuations at these low yields, especially for trimethylcatechol, have a large influence on the R^2 value. In contrast, the MAE and RMSE values are significantly better. An important point that still needs to be discussed here is the repolymerization of the multiple methylated catechols. In the initial model, repolymerization of dimethylcatechols is present, but not for trimethylcatechols. This decision was based on the temperature range studied up to $T_R = 350\ °C$. We know from other experiments that the yields of all aromatic monomers decrease sharply at higher temperatures, but this step is not relevant for the model in the temperature interval studied, as the cross validation will also show later.

The parity plots in Figure 3-9 confirm the impression that the model accounts very well for methylation in particular. Furthermore, it seems to be a reasonable approach to combine 3-methylcatechol and 4-methylcatechol into one group. The results are satisfactory and at the same time this makes the model less complex. In addition to the successful integration of the methylation, the second new finding, the kinetic model also represents the degradation of syringyl groups to catechol via 3-methoxycatechol very effectively. The major deficiency is catechol at $T_R = 300\ °C$ and $325\ °C$, which is illustrated clearly by the parity plots. The scattering over -20 % and + 20 % deviation from the experimental values is clearly evident. The model can still be optimized in this area. Overall, it can be stated that the model satisfactorily represents the various aromatic monomers that are formed during the depolymerization of lignin in BL under the given conditions in batch experiments. Due to the similar product distribution in initial continuous experiments (see chapter 2.4.3) the model is well suited for making initial predictions as to how a continuous experimental plant tailored to specific products should be designed.

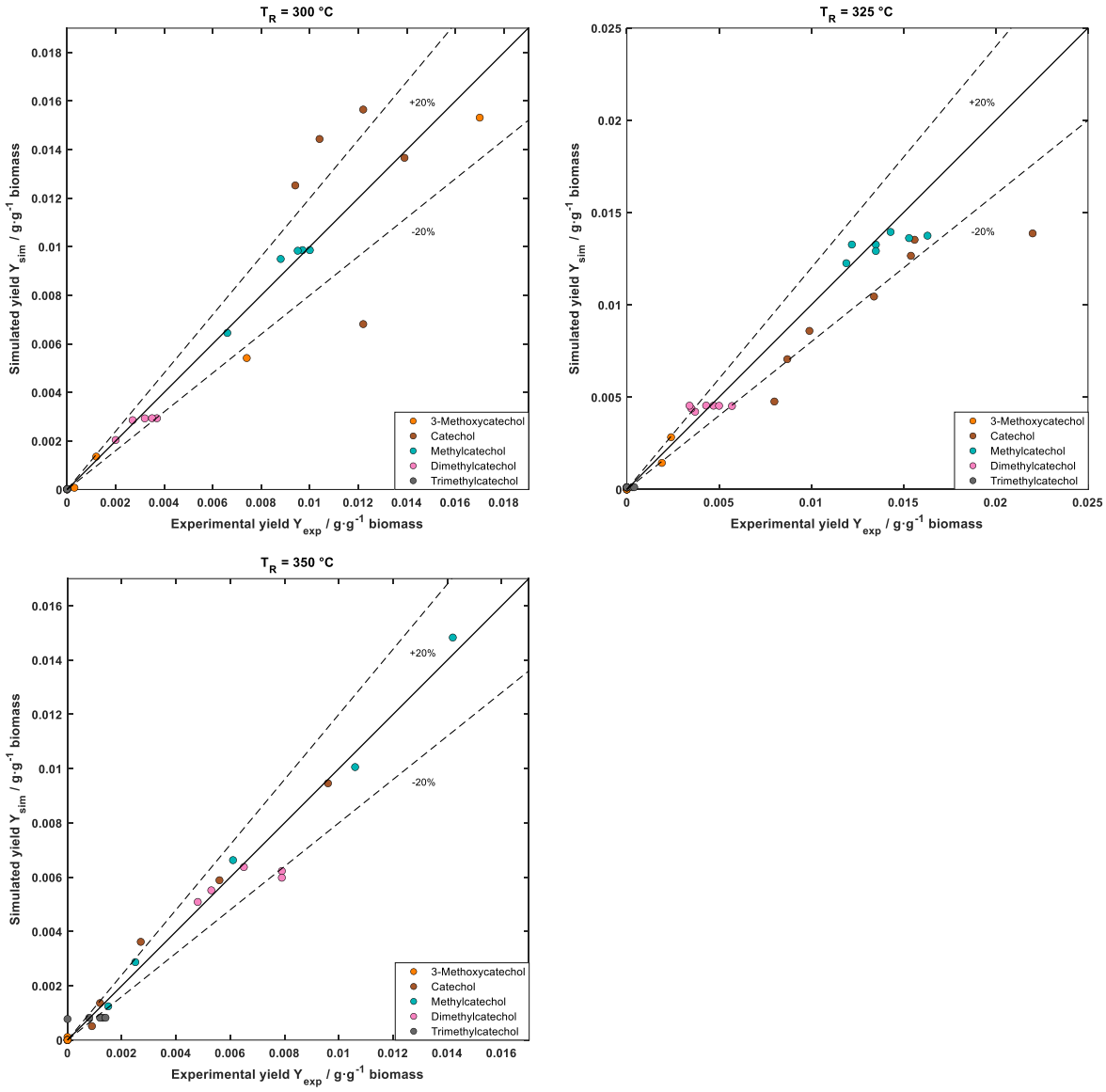

Figure 3-9: Simulation vs experimental results at reaction temperature $T_R = 300$ °C, 325 °C and 350 °C

3.5.4 Results of the 5-fold cross validation

The 5-fold CV can be used to identify statistically irrelevant parameters and reaction paths in line with the kinetic parameters and the model can be optimized if necessary. Figure 3-10 shows the optimized reaction scheme. The gray dashed lines and reactions show those that were removed from the model using the CV. For a deeper analysis of the model, an interpretation of the calculated kinetic parameters and the rate constants for each of the three reaction temperatures is provided (see Table 3-6: Activation energies $E_{A,j}$, Arrhenius factor A_j and the respective rate coefficients k_j for each reaction temperature for the 10 reactions of the developed model after cross

validation. The kinetic parameters for all 13 reactions in the original reaction network before applying CV can be found in the Supporting Information in Table 8-11. Additionally, the positive or negative change in the estimated errors compared to the errors from the non-validated model can be found in Table 8-12. Looking at the parameter table, it can be seen that the reaction constants for the first two reactions are 0 kJ/mol and therefore have no influence on the model, regardless of the temperature. The same applies to R5 with an $E_{A,5} = 0.01\ \mathrm{kJ/mol}$. In this case, even the entire reaction pathway from OL_int to catechol is not statistically relevant, as the model is almost exclusively about 3-methoxycatechol. Accordingly, this can be removed completely. Interestingly, the catechol peak at $t_R = 1\ \mathrm{min}$ and $T_R = 325\ °C$ cannot be achieved with this reaction pathway, something which was originally deemed to be feasible. Instead, this pathway has little to no effect on the model. In contrast to R5, the other two removed reaction steps R11 and R13 have exceedingly high activation energies. However, both reactions play scarcely no role in the investigated temperature range. Possibly both would become more relevant at a higher reaction temperature.

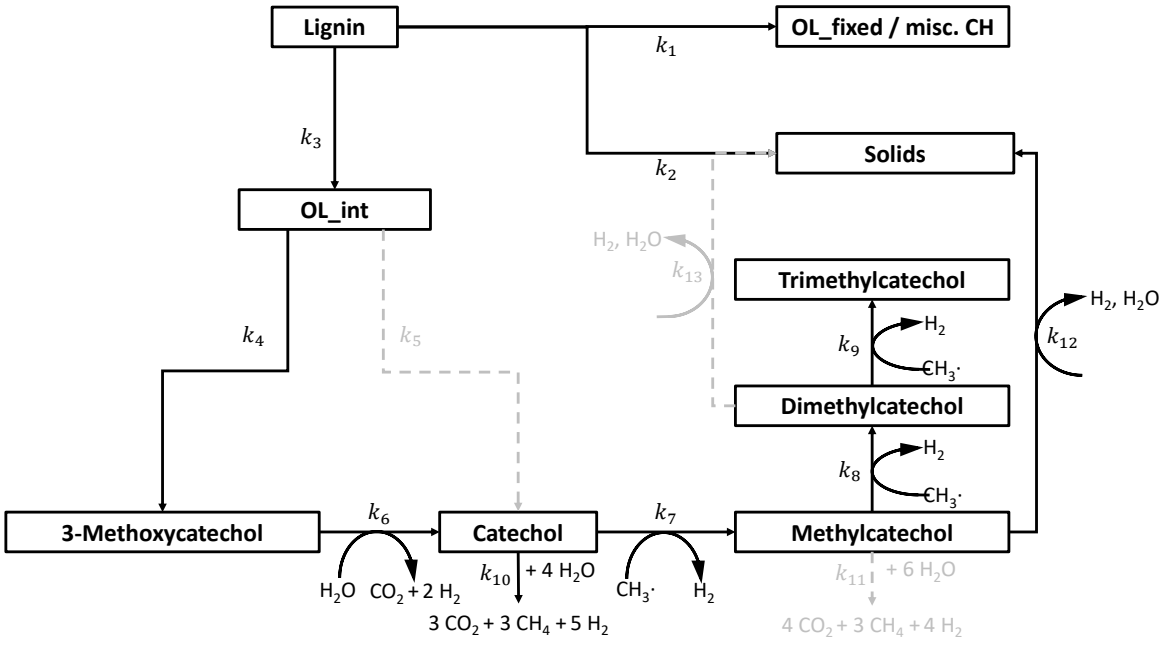

Figure 3-10: Updated reaction scheme after 5-fold cross validation. The light gray reaction paths were classified by CV as not relevant for the kinetic model.

However, since the yield of aromatic compounds decreases drastically with increasing reaction temperature, both reactions can be removed to optimize the model. In the

case of R11, it is likely that the gas production via catechol decomposition in R10 is already sufficient and therefore the decomposition of methylcatechol is neglected in the model. Overall, the performance of the model has become even better and faster without having too great an impact on the results. These results can be found in chapter 8.3.4

The depolymerization of the lignin (R3), as well as the direct conversion to the fractions of fixed oligomers and solids (R1 & R2), which do not contribute further to the formation of aromatic monomers, exhibit very low activation energies $E_{A,\,j.}$ This suggests that under the given conditions the activation energy for depolymerization has scarcely no role to play and proceeds independently of it. In accordance with the model, it is also the case that a large proportion of biomass is removed from the reaction network directly at the beginning, presumably already in the heating phase, remaining in the solid or the fixed oligomers. Noticeable are the high-rate constants of the reactions over 3-methoxycatechol to methylcatechol (R4, R6, R7) with $k_j > 1\ \mathrm{min}^{-1}$, especially at $T_R = 350\ °C$. In the case of R4 and R6, this can be explained by the very high peak of 3-methoxycatechol and the subsequent rapid decrease over a few minutes. Accordingly, the experimentally recorded values also cause the reaction constants to increase. For R7, catechol to methylcatechol, on the other hand, the already high yield of methylcatechol shortly after the heating phase probably plays a role. There may also be another reaction pathway to methylcatechol that was not revealed by the experiments conducted. Interestingly, the assumed effect due to repolymerization via the aromatic compounds is extremely low (R12 & R13). This is shown by the high activation energies together with the low-rate constants up to the order of $10^{-6}\ \mathrm{min}^{-1}$. The kinetic parameters for all 13 reactions in the original reaction network before applying CV can be found in Table 8-11. The kinetic model here definitely favors the formation of solids via the direct path from the lignin. However, this evaluation needs to take account of the small proportion of the total mass accounted for by the compounds on which the work is focusing. Repolymerization will almost certainly have a major influence, especially with regard to higher temperatures. Repolymerization is also conceivable within reactions R1 and R2. The same applies to the decomposition of methylcatechols into gases (R11, see Table 8-11). In contrast, the decomposition of catechol into gases is more relevant (R10).

Table 3-6: Activation energies $E_{A,j}$, Arrhenius factor A_j and the respective rate coefficients k_j for each reaction temperature for the 10 reactions of the developed model after cross validation

Reaction N°	$E_{A,j}$ / kJ*mol^{-1}	A_j / -	k (300 °C) / min^{-1}	k (325 °C) / min^{-1}	k (350 °C) / min^{-1}
1	0	4.38 ± 0.13	$1.33 \cdot 10^{0}$	$1.33 \cdot 10^{0}$	$1.33 \cdot 10^{0}$
2	0	4.30 ± 0.15	$1.23 \cdot 10^{0}$	$1.23 \cdot 10^{0}$	$1.23 \cdot 10^{0}$
3	15.54 ± 2.81	4.02 ± 0.41	$8.10 \cdot 10^{-1}$	$9.28 \cdot 10^{-1}$	$1{,}05 \cdot 10^{0}$
4	33.12 ± 8.96	3.42 ± 0.22	$3.81 \cdot 10^{-1}$	$5.10 \cdot 10^{-1}$	$6.66 \cdot 10^{-1}$
6	125.29 ± 10.38	4.11 ± 0.03	$3.38 \cdot 10^{-1}$	$1.01 \cdot 10^{0}$	$2.79 \cdot 10^{0}$
7	14.85 ± 17.35	3.84 ± 0.41	$6.78 \cdot 10^{-1}$	$7.72 \cdot 10^{-1}$	$8.71 \cdot 10^{-1}$
8	13.65 ± 16.67	2.44 ± 0.31	$1.70 \cdot 10^{-1}$	$1.91 \cdot 10^{-1}$	$2.14 \cdot 10^{-1}$
9	234.95 ± 42.09	0.69 ± 0.54	$4.21 \cdot 10^{-3}$	$3.34 \cdot 10^{-2}$	$2.24 \cdot 10^{-1}$
10	121.46 ± 13.82	1.30 ± 0.06	$2.11 \cdot 10^{-2}$	$6.12 \cdot 10^{-2}$	$1.63 \cdot 10^{-1}$
12	344.60 ± 45.69	-1.17 ± 0.34	$2.51 \cdot 10^{-4}$	$5.15 \cdot 10^{-3}$	$8.30 \cdot 10^{-2}$

3.5.5 Comparison with kinetic studies from literature

For validation of the model, studies on the depolymerization of lignin under HTL conditions, which have also developed a kinetic model, are used. In their two studies, Wahyudiono et al. investigated the kinetic parameters of the conversion of model substances under hydrothermal conditions. The study on catechol[157] as carried out at higher temperatures between $T_R = 370 - 420\ °C$ at a pressure of 300 bar. The rate constant k for the catechol conversion is in the order of $10^{-4} - 10^{-3}$. This is significantly smaller compared to the calculated values of this work for reaction R7 and R10. The activation energy of $50.72\ \mathrm{kJ/mol}$, on the other hand, is much closer to this study, comparable to $E_{A,7}$ of $56.24\ \mathrm{kJ/mol}$. The comparison with the parameters for the conversion of guaiacol in the second study[156] reaches a similar conclusion, despite the fact that temperatures in the subcritical range are also investigated here ($T_R = 210 - 400\ °C$). However, in this case as well, the kinetic parameters do only approach those from this study for the reactions R4 – R6, which are closest to a conversion of methoxypehnols, at high temperatures in the supercritical range. A major difference here is that a pressure of 8 MPa was used in the low temperature range. Furthermore, this process does not include salts or other catalytically active

substances that can accelerate or favor the reactions to certain products. Yong and Matsumura have determined higher rate constants in their work on the depolymerization of lignin under subcritical and supercritical conditions in water[159]. The values for lignin decomposition to guaiacol are between $6.42\ \mathrm{min^{-1}}$ ($T_R = 300\ °C$) and $12.18\ \mathrm{min^{-1}}$ ($T_R = 370\ °C$). Comparable to this are R3 and R4, which describe the lignin decomposition to 3-methoxycatechol. In particular, R4 with a rate constant of $k_4 = 1.09\ \mathrm{min^{-1}}$ at $T_R = 350\ °C$ is close to the values from the study. In their work, they also included the lumped group TOC in their reaction network, which describes the other organic products in the liquid phase. The comparison with R1 is therefore useful, as the other organic products based on the biomass are also included here. The rate constants of $6.35 \cdot 10^{-1}\ \mathrm{min^{-1}}$ to $1.09\ \mathrm{min^{-1}}$ ($300 - 370\ °C$) enclose the rate constant calculated for our case, which is independent of the activation energy. However, due to the special design of their experimental apparatus for these kinetic measurements, an exceedingly small continuous flow reactor with 0.5 – 10 s residence time, mass and heat transfer effects can occur to different degrees compared to the batch operation used in this study. A study comparable to this one in terms of experimental design is that of Forchheim et al.[171]. In this study, a formal kinetic model with pseudo-first order was also developed on the basis of batch experiments on lignin depolymerization under hydrothermal conditions. However, the resulting rate constants are lower than in this study, e.g. the reaction of lignin to methoxyphenols to catechol. A consistent finding is the negligible repolymerization from the monomers to solids in accordance with the models compared to the reaction from lignin directly or via oligomers to solids. Interestingly, the calculated and experimental yields for catechol remain largely constant in their work, which is definitely not valid in the case of this study. The reasons for the larger differences despite the similar setup could be related to the feedstock, which is enzymatically produced lignin and not kraft lignin. The literature hardly contains any work that deals with the methylation of catechol in kinetic models for lignin depolymerization. The conversion of a hydroxyl group to a methyl group and the resulting cresols are discussed more frequently. This is also imaginable for a hypothetical pathway from syringol to pyrogallol (benzene ring with three hydroxy groups) and a subsequent conversion to methylcatechols, but would not be applicable to the results described here. As already mentioned, the multiple methylated catechols strongly indicate radical reactions. One work in which at least the reaction of catechol to methylcatechol is integrated in a kinetic model is that of Schuler[208]. For $T_R = 300\ °C$

the reaction constant is $k = 3.54 \cdot 10^{-3}\ \mathrm{min}^{-1}$, and at $T_R = 350\ °C$ k $= 2.63 \cdot 10^{-2}\ \mathrm{min}^{-1}$. Thus, the values are clearly below those from the model developed here for R6. Even the rate constants for R7 and R8 are significantly higher. The heating period, which is not in a sand bath but in a GC oven, i.e., heat transfer via air, may have played a role in the differences. Overall, it can be stated that the results provided by the developed kinetic model correlate well with the literature data. The difficulty in comparison is mainly due to the different experimental setups as well as the different lignin types. In terms of the results, this study tends to be more in line with the very fast, often continuously operated reactors with a low flow rate, such as those of Yong et al. or Abad-Fernandez et al. who also achieved similarly high or even higher values for lignin polymerization to monomers and used a reactor with an ultra-fast heating time[159,209,210].

3.5.6 Adaption of the kinetic model for softwood black liquor

In the last part of this work, a comparison is made with data from tests with softwood. In chapter 2.4.5, it was shown that the yields of aromatics obtained from the depolymerization of lignin when using black liquor directly differed only slightly when using BL based on softwood or hardwood. The major difference between the two is that 3-methoxycatechol does not occur as an intermediate in softwood experiments, as it can only be formed via syringyl groups. Therefore, it is reasonable to assume that a kinetic model based on the use of hardwood BL also provides suitable values for softwood BL. Accordingly, the route via 3-methoxycatechol was removed from the model developed in this work. As before, the kinetic parameters were calculated based on the results of the experiments with hardwood BL. Figure 3-11 shows the simulated yield curves for $T_R = 350\ °C$ and compares them with the experimentally determined yields for HTL experiments with softwood BL at $T_R = 350\ °C$ and three different holding times $t_R = 1, 5$ and $10\ \mathrm{min}$. In fact, the points are well within the trend of the curves, despite the presence of some deviations. Overall, this is a promising result, showing as it does that the yields based on softwood depolymerization can also be represented with only minor changes to the existing kinetic model. Possible improvements could be the introduction of guaiacol as a single component, as this is by far the most important intermediate for catechol formation in the depolymerization of softwood lignin. However, further experiments with softwood BL need to be conducted for this purpose. Finally, it is shown again that the depolymerization is less influenced by the type of

wood, but rather by the other components in the black liquor, whereby the various salts should be emphasized in particular.

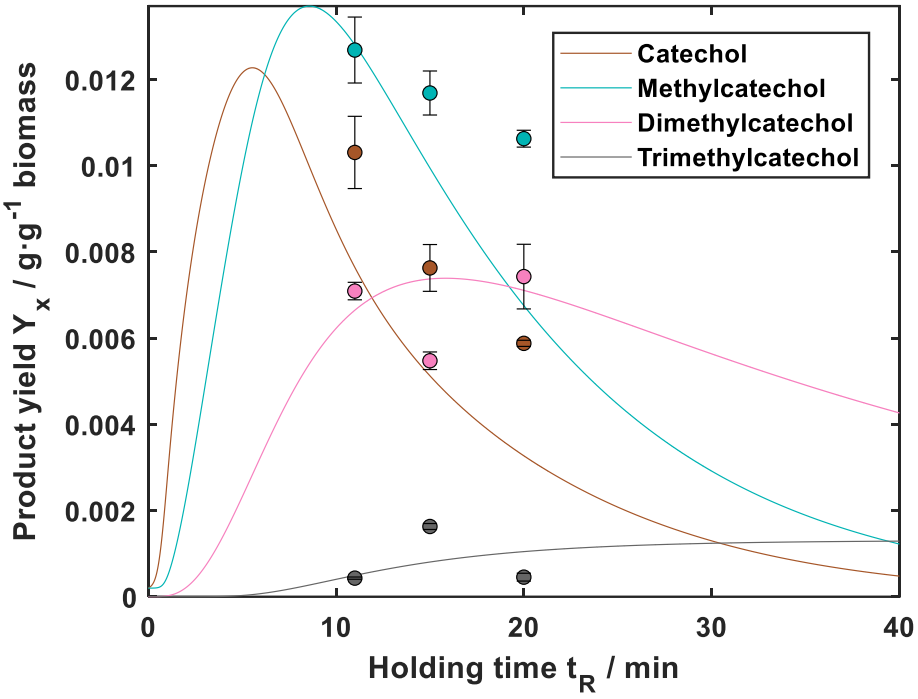

Figure 3-11: Simulated yields based on the developed kinetic model without the 3-Methoxycatechol pathway (R4, R6) (lines) in comparison with experimental results of HTL with softwood BL. More information about these experiments can be found in chapter 2.4.5.

3.6 Conclusion

The kinetic model developed in this study gives adequate simulations of the depolymerization of lignin under HTL conditions. A unique aspect here is the direct use of black liquor in which the lignin is dissolved. As a result, in addition to the effect of the catalytic effect of the water under the given conditions, the high concentration of salts such as sodium sulfide also influences depolymerization. The model describes the initial degradation of the lignin molecule to monomers, in the case of this work preferably catechols. The primary reaction pathway via 3-methoxycatechol, which has not yet been described in this way, was included in the model. In addition, the focus was on the subsequent methylation of catechol, probably due to radical reactions, as these are the main products among the aromatic monomers alongside catechol. Both experimental observations were successfully incorporated into the kinetic model. With the help of cross validation, it was afterwards possible to reduce the reaction scheme and the number of kinetic parameters, improving parameter identifiability without losing relevant information. The comparison with literature proved to be difficult, as although there are studies on lignin depolymerization in hydrothermal conditions, certain parameters are different. Nevertheless, similarities can be found in literature. The studies with extremely fast heating rates in particular show similar high-rate constants to those in this study, which are presumably due to the high salt concentration and the use of Kraft lignin. In addition, the literature also shows that the monomers and their formation only represent a small part of the entire reactions and products. The majority takes place in the oligomers and in the solid fraction. Although repolymerizations also take place between monomers, these contribute only slightly to the overall production of the solid. Finally, it was shown that the developed model may also provide useful results for the depolymerization of softwood lignin when black liquor is used directly in the HTL. For this purpose, only the path via 3-methoxycatechol had to be removed. This shows that it is primarily the salts in the black liquor that influence depolymerization. In summary, a promising kinetic model based on experimental data was developed in this work, which contains new proposed reaction pathways and whose range of application can possibly be extended.

4 The Impact of Sulfur-Containing Inorganic Compounds during the Depolymerization of Lignin by Hydrothermal Liquefaction of Black Liquor

4.1 Abstract

Lignin is a promising resource for the sustainable production of platform chemicals and biofuels. The paper industry produces large quantities of lignin every year, mostly dissolved in a black liquor. With the help of hydrothermal liquefaction, black liquor can be used directly as a feedstock to depolymerize the lignin to desired products. However, because various cooking chemicals (e.g., NaHS, NaOH) used in the Kraft process, dominant in the paper industry, are also dissolved in the black liquor, it is necessary to study in detail their influence on the process as well as their fate. In this work, the focus was on the fate of sulfur and the influence of sulfide (HS^-). For this purpose, hydrothermal liquefaction experiment ($T_R = 250 - 400\,°C$) were carried out with black liquor and self-prepared model black liquor with different sulfide concentrations (0 – 3 $g \cdot L^{-1}$ HS^-) in batch reactors ($V_R = 25\,mL$), and the products were analyzed to understand the chemical pathways involving sulfur. It was found that the inorganic sulfur compounds react with organic matter to produce organic sulfur compounds. Dimethyl sulfide is the most abundant of these products. The HS^- concentration correlates with the amount of dimethyl sulfide produced. Because methanethiol has also been qualitatively detected, the reaction mechanism of Karnofski et al. for the formation of dimethyl sulfide in the Kraft process also applies to the hydrothermal liquefaction of black liquor. Increased sulfide concentration in the feed leads to an accelerated depolymerization of lignin. In contrast, the yields of some aromatic monomers decrease slightly, possibly as a result of repolymerization reactions also occurring more quickly.

4.2 Introduction

In the previous chapters it was already mentioned that salts, especially the alkali metal salts like sodium and potassium hydroxide, are used as a homogeneous catalyst in the HTL of lignocellulosic biomass[149,211]. The salts used or formed in the Kraft process and dissolved in BL are mostly similar to those tested as catalysts[160]. Most of them are sodium salts, of which carbonate has the highest proportion. However, the second most common one in the cited study of Niemelä et al. is sodium sulfide. Other sulfur-containing salts like sulfate or thiosulfate are also common. The question arises how these various cooking chemicals in the BL behave in a direct liquefaction process. This issue has not yet been addressed in studies about HTL of lignin. It should be noted that the pulp industry strives to recycle these salts. In an integrated HTL of the BL, as studied in the BL2F project, this recycling process must therefore also be implemented. Wang et al. have studied this topic in their work[168]. They were able to collect up to 96 % of the salt in the wastewater stream. However, their study was performed without organic compounds, and it is important to explore the influence of the salts on the HTL of lignin. Indeed, it can be expected that product distribution and composition are influenced by the salts.

Although some of these salts are desired or even required in the feedstock for HTL, as already described above, this does not apply to the sulfur-containing salts. The inorganic sulfur compounds are present as anions in the BL, mainly as bisulfide (HS^-)[212], sulfite (SO_3^{2-}), sulfate (SO_4^{2-}), and thiosulfate ($S_2O_3^{2-}$). In this context, bisulfide plays an important role because it is very corrosive to metals and alloys. Furthermore, it is in chemical equilibrium with hydrogen sulfide, which is toxic, in addition to the unpleasant odor even at very low concentrations. A further aspect is the formation of organic sulfur compounds. Here, volatile molecules such as simple organic (poly)sulfides (R_1-$(S)_x$-R_2) or thiols (R-SH) play a major role. Some of these compounds, like hydrogen sulfide, are highly toxic and extremely dangerous for aquatic organisms due to their high water solubility[213]. For this reason, the emissions of these substances must be monitored and kept to low levels. From an engineering perspective, the concentrations of sulfur compounds before and after HTL must also be known for proper process design. This relates to both corrosion resistance and the use of catalysts. Because sulfur and its compounds are strong catalyst poisons[214], resistant catalysts must be used accordingly for biocrude upgrading steps. If this is not

technically possible or if fuels are the desired end product, hydrodesulfurization (HDS) must be incorporated into the process chain[215]. Finally, the formation of thiols, having a pK_a in the range 10−11, might lead to sodium losses in the context of HTL integration into a Kraft process, which is not desired. As such, the fate of sulfur during the HTL needs to be studied. A first indication of what happens to the inorganic sulfur compounds in interaction with lignin under hydrothermal conditions is provided by looking at the Kraft process itself, where hydrothermal conditions already prevail[216]. For example, Karnofski et al. have illustrated the reaction of the HS^--ion with the methoxy groups of lignin. In this process, dimethyl sulfide (H_3C-S-CH_3, DMS) is formed via the intermediate product methanethiol (H3C-SH) (see equation (4-1)(4-2)(4-3))[217]. Bordado and Gomes characterized DMS and methanethiol as two of the main sulfur-containing by-products in the flue gas of Portuguese pulp mills[218,219].

$$HS^- + Lig - OCH_3 \rightarrow CH_3SH + Lig - O^- \quad (4\text{-}1)$$

$$CH_3SH + OH^- \rightarrow CH_3S^- + H_2O \quad (4\text{-}2)$$

$$CH_3S^- + Lig - OCH_3 \rightarrow H_3CSCH_3 + Lig - O^- \quad (4\text{-}3)$$

Regarding the issues explained above, there are unsolved questions about the role of sulfur during the HTL of lignin using BL directly as a feedstock:

1) Where does sulfur end up after the process? What kind of organic or inorganic sulfur compounds are formed?
2) Do the sulfur-containing salts have any influence on the HTL process, especially the sulfide?

To tackle these questions, we analyzed all product phases produced during HTL of BL at different reaction temperatures with a special focus on the sulfur content and its chemical nature via different analytical methods. We paid special attention to the gas and liquid phases to characterize and quantify organic sulfur compounds. Another point of interest was the influence of the different sulfur anions on the HTL process. It was hypothesized that these anions, especially HS^-, could accelerate the depolymerization process because it is also used in the Kraft process for cleaving the

ether bonds. As such, batch experiments with model black liquors (MBL) containing different concentrations of HS^- anions were also performed. Another point dealt with in this work is the influence of the HS^- concentration on the yields of aromatic monomer compounds, which tend to be the main product of the HTL of lignin. Furthermore, the correlation between the HS^- concentration and specific sulfur compounds was investigated. To accomplish these goals, we performed various analytical methods focusing on sulfur and specific sulfur compounds. The influence of the sulfide concentration was investigated by measuring the changes in yields of specific aromatic product compounds and the relative molecular mass of the produced biocrude.

4.3 Materials and Methods

4.3.1 Feedstocks used for the HTL

The information about the black liquor (BL) which is used for the experiments in this study can be found in chapter 2.3.1.

Model black liquor (MBL) consisting of lignin and sulfur chemicals is prepared to adjust the HS^- concentration as accurately as possible. The composition of this model mixture is based on the characterization of the real BL. To get as close as possible to the original, the lignin extracted from the BL using the LignoBoost process[220] is used. The salts required for the liquor are sodium sulfide (Na_2S, in the form of Na_2S nonahydrate), sodium sulfite (Na_2SO_3), sodium thiosulfate ($Na_2S_2O_3$), sodium sulfate (Na_2SO_4), sodium and potassium carbonate (Na_2CO_3/K_2CO_3), and sodium and potassium hydroxide (NaOH/KOH). Four model liquors with 0, 1, 2, and 3 $g \cdot L^{-1}$ HS^- (models A – D) are prepared. Model D is the one closest to the real BL sample. The measured HS− concentration in the BL is between 3 and 3.5 $g \cdot L^{-1}$. The HS^- concentration is varied by adding Na_2S. To neglect possible effects due to higher sodium concentrations, the other salt concentrations were also adjusted. Table 8-13 in Supporting Information lists the weighed-in masses of the salts used and the volume of NaOH/KOH solution for pH adjustment for the four model liquors. The potassium carbonate is also changing because we wanted to keep the Na/K ratio similar for each MBL. The NaOH/ KOH solution used contained around 20 wt. % NaOH and 1.5 wt. % KOH and was added until a pH of approximately 12.5 was achieved

4.3.2 Batch experiments setup and product separation

The batch experiments were performed in micro autoclaves ($V_R = 25\ mL$) made of stainless steel 1.4571 (316Ti). In the first step, a certain amount of the BL was filled into the micro autoclaves. Then an inert atmosphere was created with N_2. At an initial pressure of 10 bar, the reactor was sealed. The amount of BL in the reactor varied depending on the desired reaction temperature. Because of the change in the density of water at different temperatures and the corresponding change in pressure, it was necessary to compensate for this effect by adjusting the feedstock volume. The different volumes are given with the respective reaction temperature in Table 8-2 in the Supporting Information (SI). The feedstock volumes were estimated from the density of pure water at each temperature[180]. The pressure was then set around 200 to 250 bar. The heating process was carried out in a fluidized sand bath (SBL 2, Techne, Stone, UK). A preheating time $t_{pre} = 10\ min$ was implemented, which was confirmed to be sufficient to reach the desired reaction temperatures. Reaction temperatures for HTL with real BL were set between with a holding time of $t_R = 20\ min$ (overall $t = t_R + t_{pre}$). HTL with the MBL was carried out at $T_R = 375\ °C$ and $t_R = 10\ min$. After the HTL process, the autoclaves were immediately cooled in a water bath to interrupt the ongoing reactions. After taking a gas sample with a gastight syringe, the reactor was removed from the setup, and the solid product was separated from the liquid phase by vacuum filtration. The nylon filter used has a diameter of 47 mm and a pore size of 0.45 µm (Whatman, GE Healthcare, Buckinghamshire, UK). The solid residue was dried at $T_R = 105\ °C$ for 24 h. Liquid−liquid extraction (LLE) was performed to separate the organic phase from the aqueous phase. Two milliliters of the liquid phase had to be acidified with 6 M hydrochloric acid to a pH of 2 – 4. After filtration, 0.52 mL of ethyl acetate was added to 1.3 mL of the filtrate, which served as the extractant. After shaking, the sample was allowed to rest in the vial for 1 h to allow for complete phase separation.

4.3.3 Analytical procedure and assessment

The gas sample was analyzed by gas chromatography (GC 6890N, GC 7890B, Agilent, Santa Clara, CA, USA). The detectors used were a flame ionization detector (for DMS), a temperature conductivity detector (for H_2S), and a mass spectrometer detector (5973 MSD, Agilent, Santa Clara, CA, USA). In both, a column specific to the analysis of

sulfur compounds was used (RT-U Bond 15 m, 0.25 mm, 0.25 µm, Restek, Bellefonte, PA, USA). For GC-FID/TCD, the sample was injected at 150 °C in a 1:2 split mode. The carrier gas was helium (8.69 mL·min^{-1}). The heating ramp started at 60 °C with a holding time of 1 min and heated up to 180 °C with 40 °C·min^{-1} and a holding time of 5 min. The sample at GC−MS was injected at 280 °C in splitless mode. Helium was used as carrier gas (1.5 mL·min^{-1}). The temperature ramp started at 30 °C for 5 min followed by a heating ramp of 8 °C·min^{-1} until 200 °C, which was held for 5 min. The MSD was operated in 70 eV EI (electron impact ionization) mode with a source temperature of 230 °C and a quadrupole temperature of 150 °C with scanning from 30 to 550 m/z with a frequency of 4.5 scans per second. The elemental composition of the dried solid residue was determined by elemental analysis (EA; Vario EL cube, Elementar Analysetechnik GmbH, Hanau, Germany) and inductively coupled plasma-optical emission spectrometry (ICP-OES; ICP-725, Agilent Technologies, Santa Clara, CA, USA) after microwaveassisted acid digestion in reverse aqua regia (mixture of conc. HNO_3 (65 wt. %) and conc. HCl 3:1 (37 wt. %). An aliquot of the liquid phase before LLE phase was examined by several analytical methods: to determine the inorganic as well as the organic sulfur content, 0.1 mL of the sample was mixed with 0.5 mL hydrogen peroxide, 1 mL potassium hydroxide, as well as 8.4 mL purified water. This step allows all inorganic sulfur to be converted to the highest oxidation state (+VI) in the form of sulfate ions (SO_4^{2-}), as HS^- ions strongly influence measurements and are problematic to some instruments. Sulfate can be easily quantified using ion chromatography (IC-An; IC professional detector, 930 compact IC flex, interface 830, 858 professional sample processor, column Metrosep C3−250, Metrohm, Herisau, Switzerland). The molar concentration of sulfate was calculated using the measured mass concentration $\rho_{SO_4^{2-}}$ and the molecular mass of sulfate $M_{SO_4^{2-}}$ (see eq (4-4)). The mass concentration of the inorganic sulfur $\beta\rho_{S,inorg}$ was obtained using eq (4-5)[221–223].

$$c_{SO_4^{2-}} = \frac{\rho_{SO_4^{2-}}}{M_{SO_4^{2-}}} \quad (4\text{-}4)$$

$$\rho_{S,inorg} = c_{SO_4^{2-}} * M_S \quad (4\text{-}5)$$

In parallel, a second aliquot was analyzed by using elemental analysis (EA) to determine the total sulfur content. The difference between total sulfur and inorganic sulfur was used to determine the organic sulfur content in the liquid phase. A GC with a sulfur chemiluminescence detector (SCD, GC 7890A, 355 SCD, column G3903-

63002, Agilent, Santa Clara, CA, USA) was used for the determination and quantification of organic sulfur compounds. The carrier gas was helium (3 mL min^{-1}). The sample was injected at 255 °C in a 1:10 split mode. The oven temperature ramp started at 40 °C and held this temperature for 7 min before it increased at a 7 K min^{-1} heating rate up to 220 °C for 8 min. For sample preparation, 0.5 mL of the liquid phase was dissolved in 1.5 mL of isopropanol and filtered. Together with the sulfur content in the solid phase and the detected and quantified sulfur compounds in the gas phase, a mass balance of sulfur can be prepared.

The effect of the HS^- concentration on the HTL process was determined from the yields of typical aromatic compounds and the molecular weight of the biocrude by using the extracted organic phase. For the aromatic compound quantification GC-FID and GC-MS analysis were used, the molecular weight of the extracted biocrude was determined with SEC analysis. The used analytical methods are described in chapter 2.3.4.

4.4 Results and Discussion

4.4.1 Effect of reaction temperature T_R on the sulfur mass balance

Figure 4-1 shows the sulfur mass balance for $T_R = 300 - 400\ °C$ and $t_R = 20\ min$. The mass fractions are separated into five different sections: total sulfur in the solid phase, organic and inorganic sulfur in the liquid, sulfur in the gas phase, and the sulfur deficit in the balance. In addition, the organic and inorganic sulfur in the liquid BL feed is given in the diagram as a reference. For all the investigated samples from the HTL of BL, we were able to detect around 50 wt % of all sulfur in the system. The high deficits are probably mainly due to two reasons. First, we can only quantify two gas components, hydrogen sulfide (H_2S) and DMS, whereas a quantitative determination of methanethiol, the intermediate product according to Karnofski et al. (see equations (4-1)(4-2)(4-3)), and other gaseous sulfurous components is not possible with the analysis setup used in this work. Also, we can only quantify one part of the H_2S because the pH after reaction is between 8.5 and 10 (see Figure 8-10and Figure 8-11 in SI) compared to the pK_a of H_2S, which is 7. This leads to an underestimation of the level of sulfur in the gaseous phase. Second, thiols and small sulfides are very volatile components (for example, DMS $T_{boil} = 34\ °C$, methanethiol $T_{boil} = 6\ °C$) and can lead to an underestimation of sulfur recovery in the organic sulfur mass fraction of the liquid phase, particularly after a decrease of the pH. Note that shifts in thermodynamic

equilibria are expected when decreasing the pH in the liquid phase, e.g., by dilution, which can result in loss in the gas phase. Examples are methanethiol (CH_3S^- to CH_3SH) and hydrogen sulfide (HS^- to H_2S).

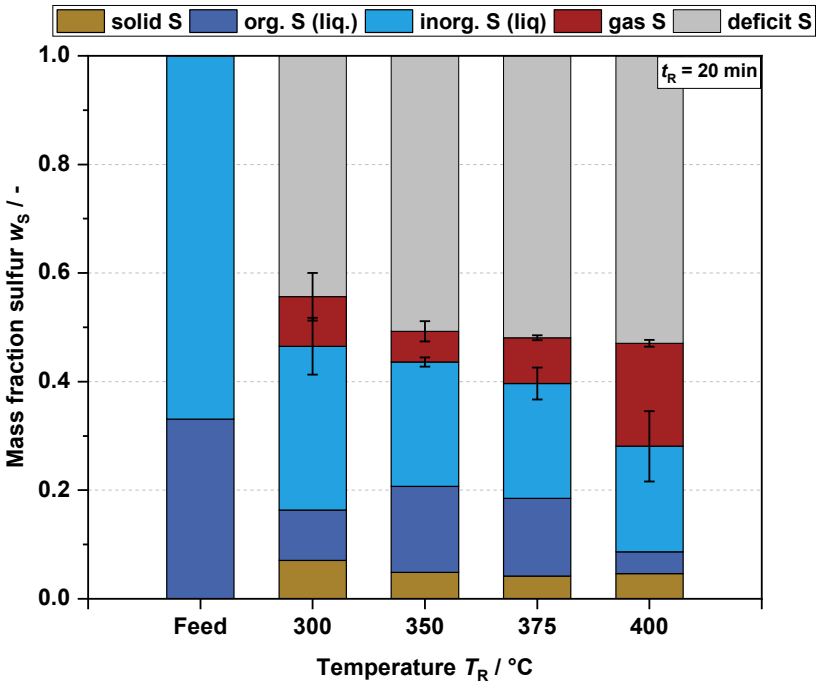

Figure 4-1: Sulfur mass balance at different reaction temperatures T_R and in the BL feedstock

Nevertheless, some important conclusions can be drawn from this sulfur balance, and to our knowledge, it is the best available sulfur balance from HTL of BL to date. The most important statement pertains to inorganic sulfur in the liquid phase, which originates from the various cooking chemicals of the pulping process. At a reaction temperature of $T_R = 300\,°C$, more than half of the inorganic sulfur has already disappeared from the liquid. This is followed by a further slight decrease until $T_R = 400\,°C$. Therefore, reactions between inorganic sulfur and organic matter are very likely, but it cannot be ruled out that the sulfidation of the walls of the reactor (e.g., to nickel sulfides) also plays a role. To validate our procedure, some tests were performed to validate the total inorganic sulfur quantification using a model BL. Figure 4-2 shows that an almost identical sulfur concentration is achieved with the proposed IC analysis compared with the theoretical sulfur concentration in the MBL. The theoretical sulfur concentration is based on the weighed-in masses of the salts and the lignin used. It can therefore be assumed that the changes in the inorganic sulfur as found in the mass balance are not seriously influenced by the significant material losses. In addition, the sulfur concentration of a MBL without lignin after the HTL process is shown in the same

graph. Here also, hardly any deviation can be observed, which validates that the method is reliable for quantification of inorganic sulfur in the product samples. It also excludes the possibility that the reaction or ab-/adsorption of inorganic sulfur with the walls of the reactor has an impact on the total sulfur balance. Plus, it shows that organic material must be present for the sulfur mass balance to change. This in turn also strengthens the assumption that direct reactions of the sulfur salts with the organic matter are occurring during the HTL.

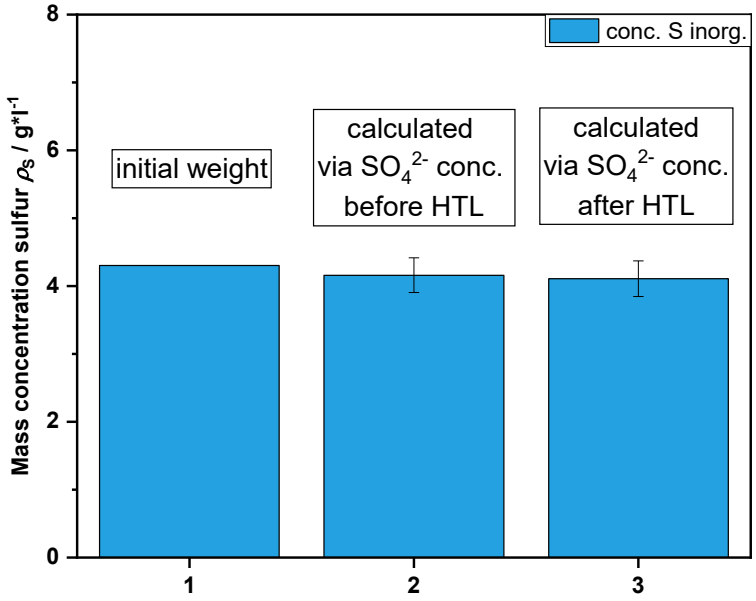

Figure 4-2: Mass concentration of sulfur for model BL calculated by the weighed masses of salts (bar 1), for model BL without lignin calculated via SO_4^{2-} concentration determined by IC-An (bar 2), and for the liquid product of HTL of model BL without lignin ($T_R = 375\ °C$, $t_R = 10\ min$) calculated via SO_4^{2-} concentration determined by IC-An (bar 3)

In contrast to the fraction of inorganic sulfur in the liquid phase, interestingly, hardly any changes were found in the fraction of sulfur bound in the solid phase. One assumption at the start of this work was that salts could precipitate. However, because sodium and potassium (see Figure 8-12 and Figure 8-13 in SI) are also found almost exclusively in the liquid phase as corresponding cations, the precipitation of salts during the performed HTL experiments plays only a minor role.

4.4.2 Effect of reaction temperature T_R on organosulfur compounds in the liquid product phase

A more detailed insight into the chemical nature of the sulfurous components of the liquid phase is possible with GC-SCD analysis, which can identify several typical

organosulfur compounds. A majority of the detected compounds are presumably the products of the reaction between the organic material from biomass and the inorganic sulfurous salts (mainly sulfide). These include various sulfides, di- and trisulfides, thiols, and thiophenes (see Figure 4-3). Quantifiable compounds include DMS, dimethyl disulfide (DMDS), and dimethyl trisulfide (DMTS). Note that DMS can be underestimated because of its low boiling point. All other components could only be detected qualitatively, mostly because their concentrations were too low. Methanethiol is an exception; its chromatogram peaks are the largest after the DMS peaks. However, quantification is not possible because of the low boiling point.

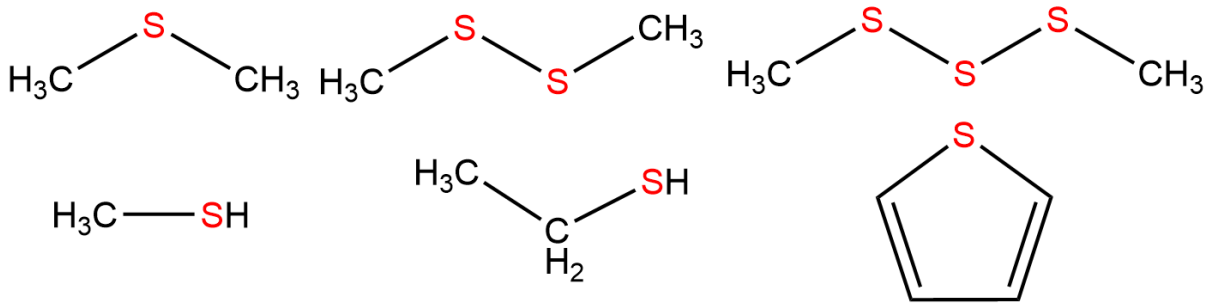

Figure 4-3: Organosulfur compounds in the liquid phase found by GC-SCD analysis

Figure 4-4 and Figure 4-5 show the concentrations of DMS, DMDS, and DMTS in the liquid phase at different temperatures. DMS reaches the highest concentration by far except at $T_R = 400\ °C$. The trend of DMS concentration correlates to the overall organic sulfur concentration in the liquid phase, showing a general decrease with increasing reaction temperature, which becomes sharp close to $T_R = 400\ °C$, after which there is a further decrease. This is an indicator that the organic-bound sulfur is mainly present in the form of DMS. The concentrations of the other two quantifiable molecules, DMDS and DMTS, follow the same behavior but at much smaller concentrations by a factor of about 10. This may be due to the (hydro)thermal instability of the S−S bond by homolytic dissociation, whereas in the case of DMS, the C−S bonds need higher temperatures to be cleaved, typically beyond the critical point of water where methyl radical formation is favored[224]. Note however that disulfides can form from the condensation of two thiols[225]. In the following course, both concentrations vary between 5 and 20 $mg \cdot L^{-1}$ with the exception of the DMTS concentration at $T_R = 350\ °C$. At the point mentioned, however, the large error bar must also be taken into account. Why this error is so large at this point for DMS and DMTS in particular cannot be determined.

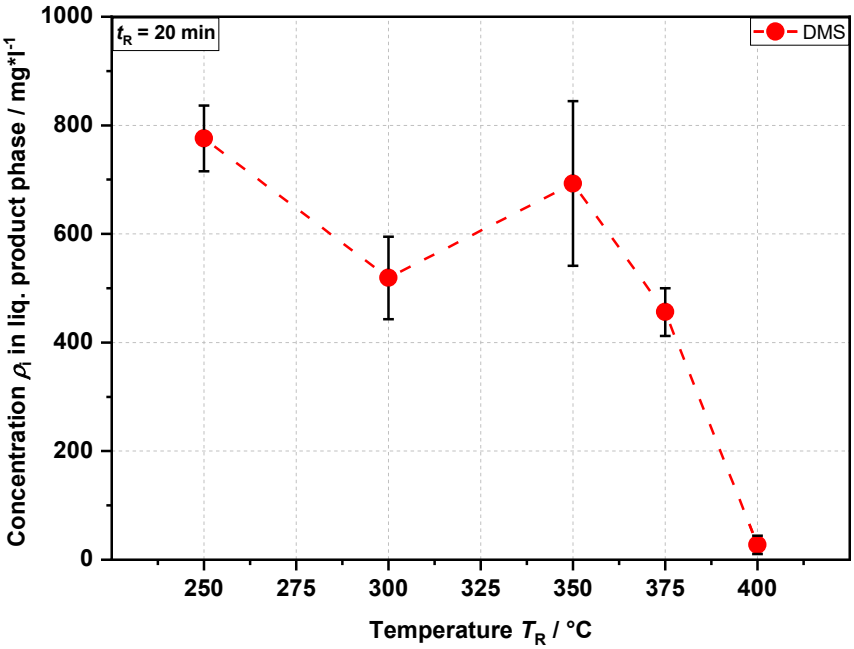

Figure 4-4: DMS concentration in the liquid product phase from HTL at different reaction temperatures T_R generated with GC-SCD

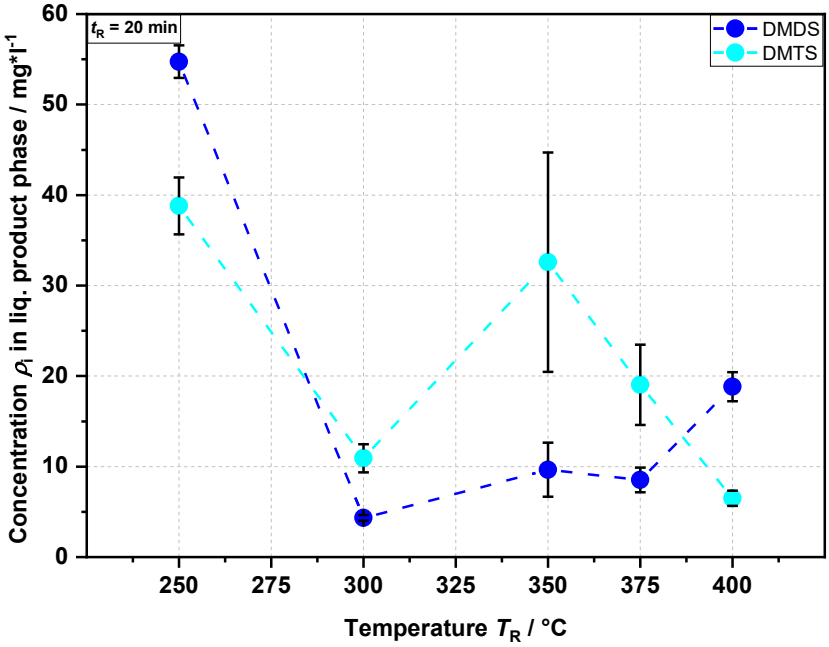

Figure 4-5: DMDS and DMTS concentration in the liquid product phase from HTL at different reaction temperatures T_R generated with GC-SCD

4.4.3 Effect of reaction temperature T_R on sulfurous compounds in the gas phase

The mass of DMS and H_2S related to biomass in the feedstock in the gas phase is shown in Figure 4-6. There is an increase in H_2S with temperature, but the mass compared to the mass of DMS is very low, as expected because of the high pH of the solution. Below $T_R = 350$ °C, no H_2S is detected, but H_2S in the gas phase appears at $T_R = 375$° C and 400 °C. This can be explained by an equilibrium shift due to a slight decrease in pH with increasing temperature. It also shows that DMS is likely one of the main organosulfur products not only in the liquid phase but also in the gas phase. The increasing masses of both compounds fit very well with the increase in the sulfur content in the gas phase.

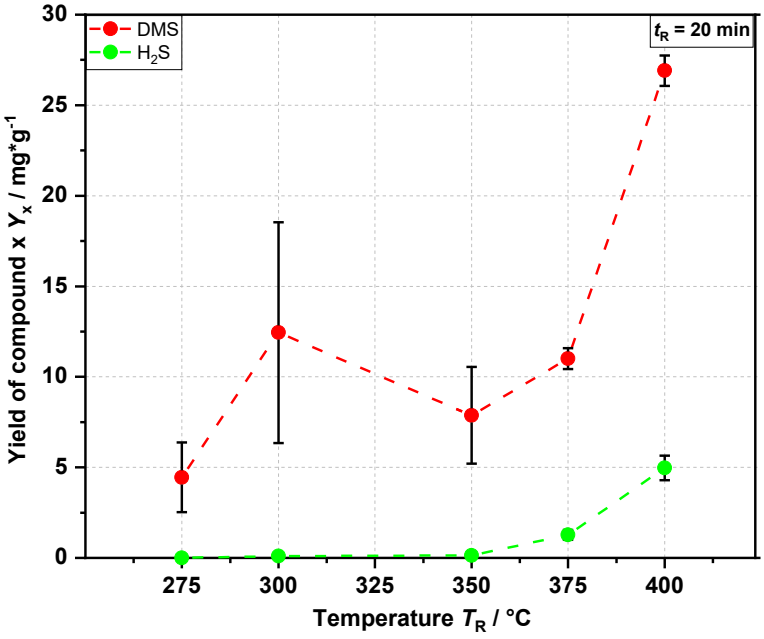

Figure 4-6: Evolution of the yields of DMS and H_2S in the analyzed product gas phase via GC-FID after HTL of real BL

After establishing the sulfur mass balance, we assumed that the largest loss of sulfur occurs via the gas phase. However, with our gas analysis via GC-FID/TCD, we were able to quantify only the two components already shown, DMS and H_2S. Nevertheless, to find out more about the gas phase, we installed the RT-U Bond column, specially designed for sulfur components, in the GC−MS. The chromatogram of the gas sample can be seen in Figure 4-7. In agreement with the results discussed above, the DMS peak is by far the largest. Interestingly, it is also possible to detect methanethiol in the

gas sample. Its peak area suggests that the sulfur content of methanethiol is of significance in relation to the total mass of sulfur. The other organosulfur compounds found are also consistent with those found in the liquid phase by GC-SCD and have a relatively high vapor pressure. The remaining peaks are hydrocarbons, mainly cyclopentenes with different numbers of methyl groups. The peak around 3.5 min retention time, before methanethiol, could not be identified. Here, the aforementioned problem of the molecular masses of the substances being too low plays a role.

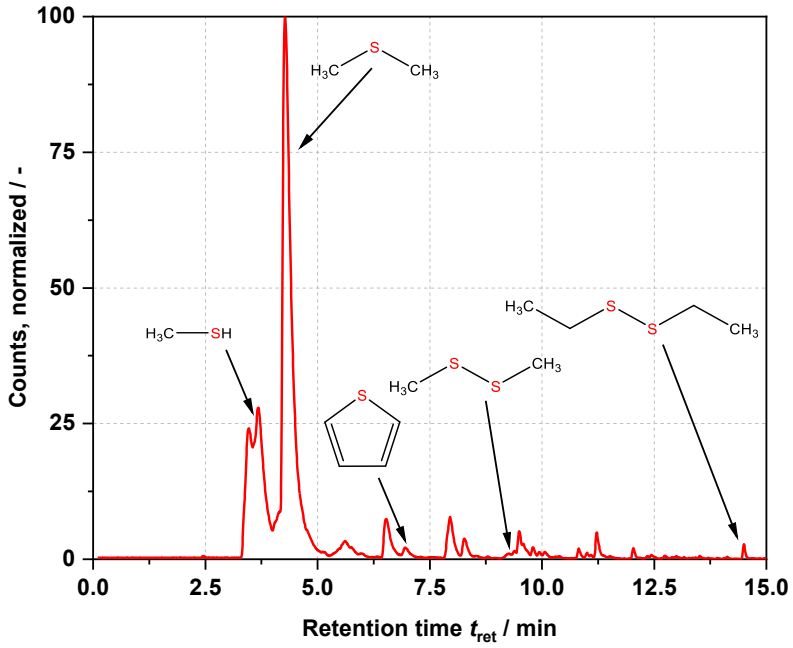

Figure 4-7: GC-MS chromatogram of a product gas sample; compounds found are methanethiol, DMS, thiophene, DMDS and diethyl disulfide

4.4.4 Comparison of the model black liquor with real black liquor

As already shown in the previous section, the HS^- ions are clearly involved in the reactions during the HTL of the BL. To draw conclusions about the effects of HS^- on the depolymerization of the lignin, we investigated product yields and the change in the relative molecular mass at different salt concentrations in the feedstock. To adjust the concentration of HS^- ions as accurately as possible, we prepared model black liquors, as described in the Materials and Methods section. Figure 4-8 shows the GC−MS spectra of the extracted organic phase after HTL of a model liquor and the real BL at $T_R = 375\ °C$ and $t_R = 10\ min$. It can be seen that the retention time of the peaks of the main components is the same for both analyzed samples. The main compounds produced are the same with the real BL and the MBL. One possible

explanation for the different peak height could be the different composition of the organic content in the feedstock, i.e., the non-lignin organic compounds. Indeed, whereas in the MBL only the extracted lignin is used, the real BL also contains many other organic components, such as hemicellulose. Because both have approximately 9 wt. % of biomass, the MBL has a higher lignin content than the BL. However, because our work is primarily concerned with the depolymerization of the lignin, this point can be neglected. In fact, the MBL even proved to be somewhat better with regard to the evaluation of the GC chromatograms: because of the absence of other organic components such as those from hemicellulose, there are fewer interfering small byproducts originating from the decomposition of the hemicellulose structures.

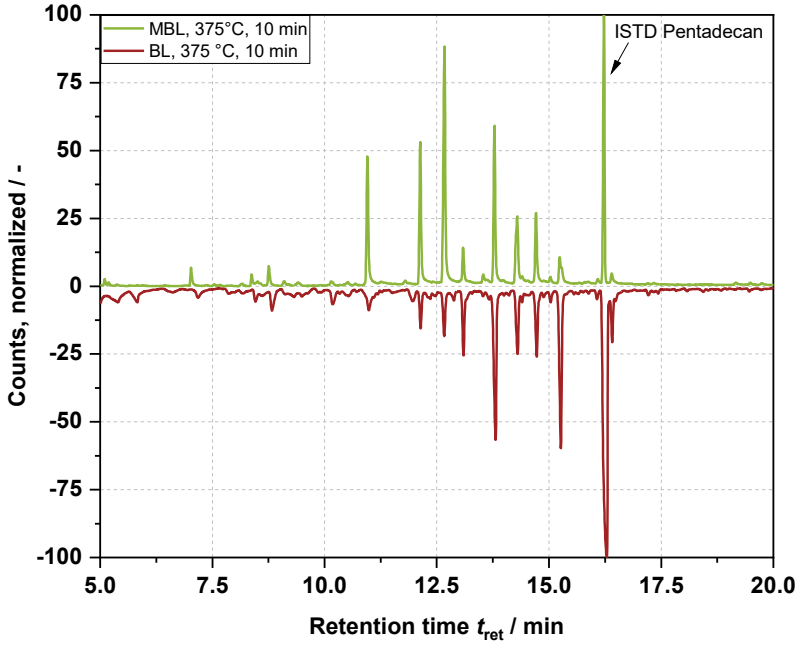

Figure 4-8: GC-MS chromatograms of MBL and real BL after HTL at $T_R = 375\,°C$ and $t_R = 10\,\mathrm{min}$. The chromatogram on the lower half is mirrored on the X axis

4.4.5 Influence of HS- ions on the gas phase

The experiments with real BL show that DMS is one of the main organosulfur products. Therefore, looking at DMS production during the HTL of the MBL is a good way to observe the possible influences of the sulfide on the HTL process. In Figure 4-9, the increase of the DMS fraction with increasing HS^- concentration in the feed can be clearly seen. Thus, there is a clear link between the DMS production and the sulfide concentration in the feedstock, indicating that the mechanism by Karnofski et al. (see equation (4-1)(4-2)(4-3)) fits for the HTL process, too. Furthermore, the results also

show that the HS^- ions remain in the liquid phase, as no significant increase in gaseous H_2S was observed with increasing NaHS concentration. The pH value of the liquid product is decreasing only a little, which leads to the minor increase in the H_2S yield with increasing sulfide concentration in the feed. Moreover, the gas analysis shows that DMS is mostly produced from lignin. Compared with the DMS yield from real BL at $T_R = 375\ °C$ and $t_R = 20\ min$ shown in Figure 4-6, the yield at 3 $g \cdot L^{-1}$ ($T_R = 375\ °C$ and $t_R = 10\ min$) is at the same level at approximately 12 $mg \cdot g^{-1}$. These results fit together because not all of the biomass in the BL is lignin, and it can be expected that the experiment with the MBL with $t_R = 20\ min$ will lead to a higher DMS yield.

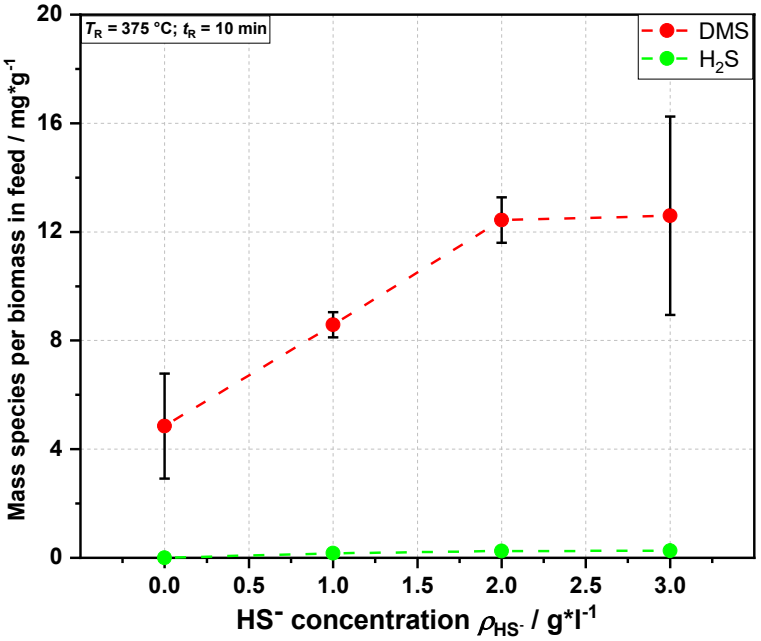

Figure 4-9: Evolution of the yields of DMS and H_2S in regard to the biomass in the feed (lignin) in the analyze product gas phase via GC-FID after HTL of MBL with different HS^- concentrations

4.4.6 Influence of HS^- ions on the depolymerization of lignin

The second step investigated the influence of the HS^- ion content on the organic phase in the liquid product with regard to molecular size. Figure 4-9 shows the recorded UV signals versus the retention volume V_{ret} detected with SEC analysis. With such a chromatogram, the lower the retention volume is, the higher is the relative molecular weight. These are relative values because absolute values are very difficult to obtain by SEC due to the lignin structure and without having appropriate standards for calibration of the method. Nevertheless, the observed trends and the evaluation of the

effect of HS^- concentration on HTL are still meaningful. The calibrated range covers 246 to 20,700 g·mol^{-1}. Four different chromatograms from extracted organic product of produced liquid phase at different temperatures are shown in Figure 4-9 (left Y axis). The hardwood lignin extracted from the feedstock is used as a reference. The calibration curve together with limits is included as well (right Y axis). The extraction of the organic phase was performed using the mixed liquid product phase obtained from three batch experiments (three repetitions). This was necessary to provide enough biocrude for the analyses. A clear trend is evident in the investigated concentration range of HS^- from 0 to 3 g·L^{-1} HS^- in the feedstock. The large peak at around 6000 g·mol^{-1} becomes smaller and shifts to a lower molecular weight. At 3 g·L^{-1} HS^-, the peak is at about 4000 g·mol^{-1}. Interestingly, the results for 1 and 2 g·L^{-1} HS^- do not fit optimally into the series. But all measurements show the formation of a molecular compound with a molecular weight of about 1500 g·mol^{-1}, which, expressed in the number of syringyl groups (see aromatic structure in Figure 4-9; syringol, $M_w = 154.16\ \mathrm{g{\cdot}mol^{-1}}$), corresponds to approximately 10 aromatic rings. Clearly, HS^- contributes significantly to the depolymerization of lignin during HTL. This is surprising because the main drivers for depolymerization of lignin according to the literature are carbonates and hydroxides[56].

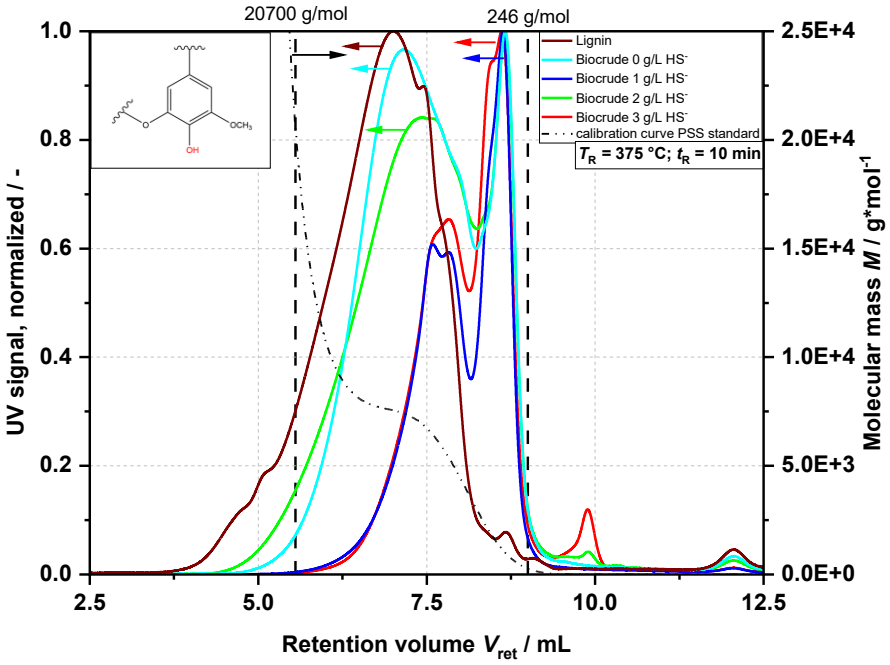

Figure 4-10: SEC chromatograms of the extracted organic product phase of the HTL of MBL together with the hardwood lignin used for the experiments. Calibrated ranges were from 246 to 20,700 g mol^{-1}. Relative molecular mass decreases with a higher retention volume V_{ret}

Because of the higher reaction temperatures during HTL and a significantly higher pressure, it is possible that the reactions based on the Karnofski mechanism are accelerated compared to the Kraft process. Gierer et al. have explained a detailed mechanism for depolymerization of lignin with sulfides in their work[216,226,227]. They describe how the HS^- ions force the cleavage of β-O-4 bonds, which are the most common type of bond in the lignin structure. With a higher HS^- concentration in the feed, it appears plausible that these cleavage reactions are favored.

Finally, the monomer yields of various aromatics present in the liquid product phase were investigated (Figure 4-11). The figure focuses on the catechol and its methylated derivatives because these form the major part of the product spectrum. The influence of HS^- concentration on the yields of the various catechol and its derivatives shows a general decreasing trend with increasing HS^- concentration, the largest decrease in yields is seen from 0 to 1 $g \cdot L^{-1}$ HS^-, and the decrease is negligible in the range of 1−3 $g \cdot L^{-1}$ HS^-. The amount of dissolved sulfide does not seem to be particularly relevant, which contradicts the SEC results showing an increased overall depolymerization.

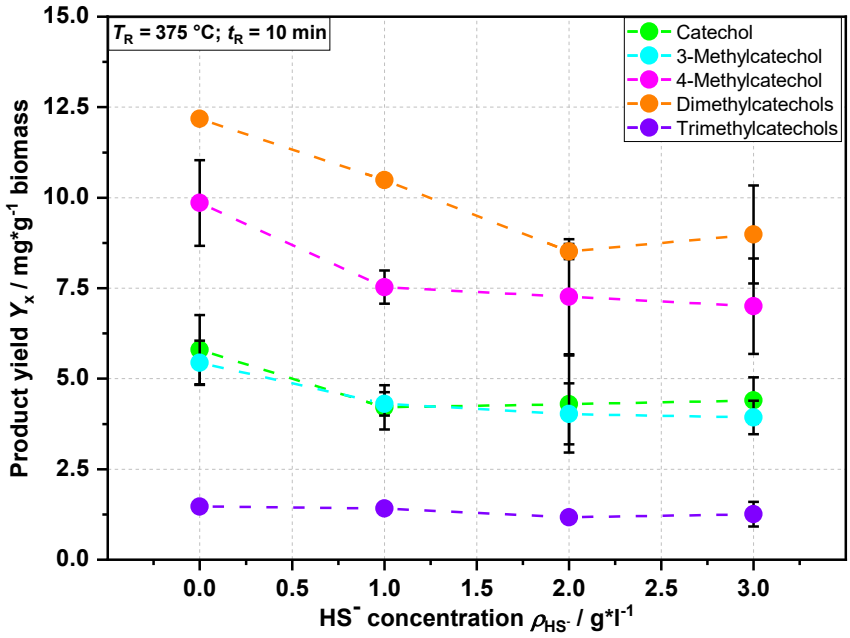

Figure 4-11: Monomer yields of different catechols in relation to the biomass in the feedstock (organic dry matter, here lignin). Dimethyl and trimethylcatechols are quantified relatively by the peak area

Based on these observations, we can hypothesize that HS^- ions, along with accelerating depolymerization, enhance the repolymerization of monomers, maybe by

favoring the formation of free functional groups or radicals, which can react further with aromatic monomers. This could lead to the decrease shown in the yield of catechol and its derivatives. Reactions between the hydroxy group of catechols and thiols or HS^- are highly unlikely because these are not thermodynamically favored. Overall, it can be concluded that the HS^- concentration has a pronounced influence on the depolymerization of the lignin, leading mainly to compounds with a molecular weight of ca. 1500 $g \cdot mol^{-1}$, corresponding to ca. 10 aromatic rings. This accelerates with an increasing HS^- concentration. However, the main aromatic monomer products, the catechols and the methylated derivatives, are barely affected. Therefore, the impact of HS^- on the HTL using BL is directly dependent on the goal of the process.

4.5 Characterization of organic sulfur compounds in the product phases

This chapter was not part of the original publication since the data was not available at the time of publication. Nonetheless, the data and the results fit well within the scope of this chapter.

With the described analysis methods, it was not possible to analyze the structure of larger molecules containing sulfur. Therefore, the fate of the sulfur within the context of organic sulfur in the liquid phase and the sulfur present in the solid phase was not clear. To overcome this issue, HPLC–high-resolution mass spectrometry (HPLC-HRMS) was performed by the group of Prof. Wisniewski Jr. at Universidade Federal de Sergipe, Brazil. The analyzed samples were collected from the continuous experiments to obtain sufficient material for the analysis (see chapter 2.3.3). This approach can be used to obtain more detailed information about complex mixtures especially containing non-volatile compounds with higher molecular weight which are not detectable with the common GC or HPLC techniques[228,229]. Therefore, it is widely used in product analysis after biomass conversion, which typically results in complex product mixtures. It can be used for all phases which are produced[230]. The main focus is the analysis of the produced biocrudes or bio-oils[231], but also other fields of application such as the analysis of saccharides in an aqueous phase[232] or the analysis of produced biochar[233] are possible. One advantage is the clear identification of heteroatoms such as nitrogen or sulfur, which are always a concern regarding the biomass or sewage sludge conversion due to the inhomogeneity of the feedstock. To investigate the fate of these atoms, HPLC-HRMS is a suitable method. Zimmermann et al. analyzed the fate of the nitrogen compounds after HTL of sewage sludge and could show a detailed analysis of fractionated biocrude[234]. The analysis of extracted and fractionated sulfur-containing compounds from vacuum gas oil with HPLC/APCI(+) Orbitrap MS was performed by de Freitas et al.[235]. Another work regarding sulfur species was conducted by Dekker et al. [236]. Their aim was to identify and characterize thiolated polysulfides in must and wine by using UHPLC-HRMS.

The phase separation was conducted in the same way as described in the material and methods section of chapter 2. The remaining ethyl acetate in the organic phase as well as in the aqueous phase (small fractions of ethyl acetate are always dissolved

in water) was evaporated under a nitrogen atmosphere before the analysis. All product phases, except for the gas phase, were analyzed. The analysis procedure is described in Martins et al. [237]. Only the characterization using H-ESI(+) (heated electrospray ionization) Orbitrap MS is relevant for the sulfur species since the APCI(-) (atmospheric pressure chemical ionization) signal did not show significant amounts of sulfur species. Approximately 10^4 ions could be detected and were assigned to a molecular formula consisting of $^{1}H_{5\text{-}150}$, $^{16}O_{0\text{-}15}$, $^{14}N_{0\text{-}5}$, $^{32}S_{0\text{-}3}$ and a +1 charge. The data was processed and analyzed using Python in a Jupyter Notebook environment.

To obtain information about the fate of the sulfur species the molecular formulas were categorized in different groups based on the heteroatoms as O_xS_x. The possible chemical structures of the molecular formulas can be suggested based on the calculated double bond equivalent (DBE, see equation (4-6)) which determines the total number of rings and π-bonds.

$$DBE = c + 1 - \frac{h}{2} + \frac{n}{2} \tag{4-6}$$

The numbers of H, C and N atoms in the molecular formula are represented by h, c and n respectively. Each group has a global relative abundance with respect to all groups found in the analyzed sample. On top of this, the scatter plots show the is-abundance of each species from one group with respect to all species found within this group. Furthermore, with the aromatic index (AI) given for one group allows conclusions about the molecular structure containing sulfur atoms is possible. The AI is weighted by the relative iso-abundance of each molecule per group with respect to the global relative abundance of the specific group (see equation (4-7)).

$$AI = \left(\frac{DBE}{c} * relative\ iso - abundance\right) * \frac{1}{relative\ abundance} \tag{4-7}$$

With this analysis method, molecular structures up to 700 g·mol^{-1} could be found. The main focus area are monomer and oligomer structures up to 3 to 4 aromatic rings.

In Figure 4-12 the relative abundance for six different groups (S1, S2, O1S1, O2S1, O3S1 and O4S1) in the biocrude, aqueous phase and solid phase at different reaction temperatures T_R is shown. These groups are the most common sulfur-containing ones found in each phase. Interestingly, molecules with two sulfur atoms are already rare, molecules with a higher number of sulfur atoms are nearly absent. These results suggest that most sulfur atoms act as sulfides. Two other options are the presence of

a thiophene inside a molecule structure or a thiol group. Since thiophenes are not as common as sulfides in the gas phase (see Figure 4-7) and thiols are highly reactive especially in the presence of methoxy groups of the lignin the probability that these sulfur species are organic sulfides is high.

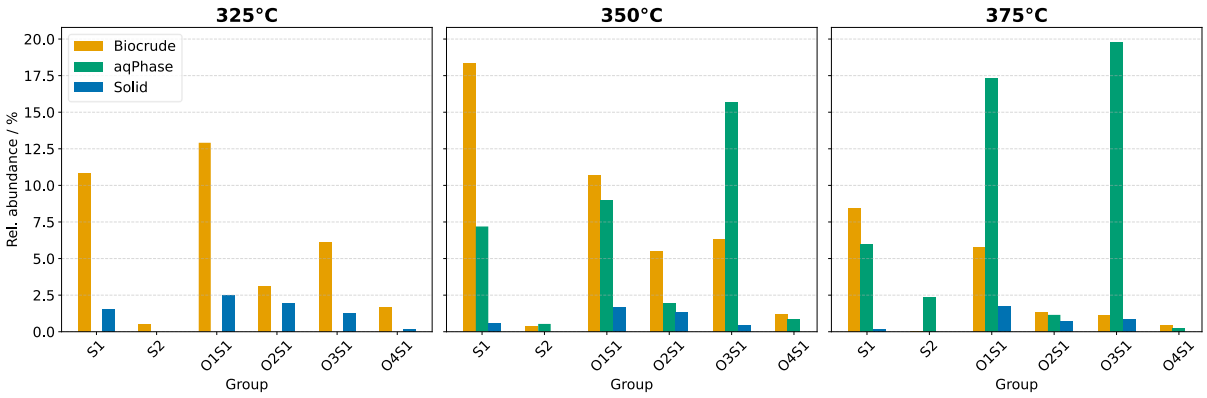

Figure 4-12: Distribution of selected sulfur-containing groups in the different product phases (biocrude, aqueous phase, solids) at different reaction temperatures T_R

Furthermore, the results confirm the findings of the sulfur mass balance shown in Figure 4-1 in which sulfur in solid phase plays only a minor role. Even the slight decline of the sulfur mass fraction in the solids with increasing reaction temperature is visible. However, the most important discovery is that at lower reaction temperatures, sulfur-containing molecules are mainly present in the biocrude and that the proportion of these decreases as the reaction temperature increases, with significantly more being found in the aqueous phase. The most dominant groups are S1 O1S1 and O3S1, some of which can have a relative abundance of well above 10 %. S1 reaches 10.9 %, 18.3 % and 8.4 % for the biocrude fraction, O3S1 even reaches 19.8 % in the aqueous phase. It is important to note that both fractions are organic sulfur, not to be mistaken with the differentiation between organic and inorganic sulfur in the sulfur mass balance. It is not clear why this phenomenon occurs, but a possible reason can at least be found in Figure 4-13, Figure 4-14 and Figure 4-15. These figures represent scatter plots of the molecules found within a group and their abundance (isolated (iso-) abundance). The darker the dot, the higher the abundance. While a more scattered abundance distribution can be seen for the groups in the biocrudes in particular, with the exception of group O3S1 (Figure 4-13 and Figure 4-14), the abundance in the aqueous phase is concentrated on a few individual molecules (Figure 4-15)

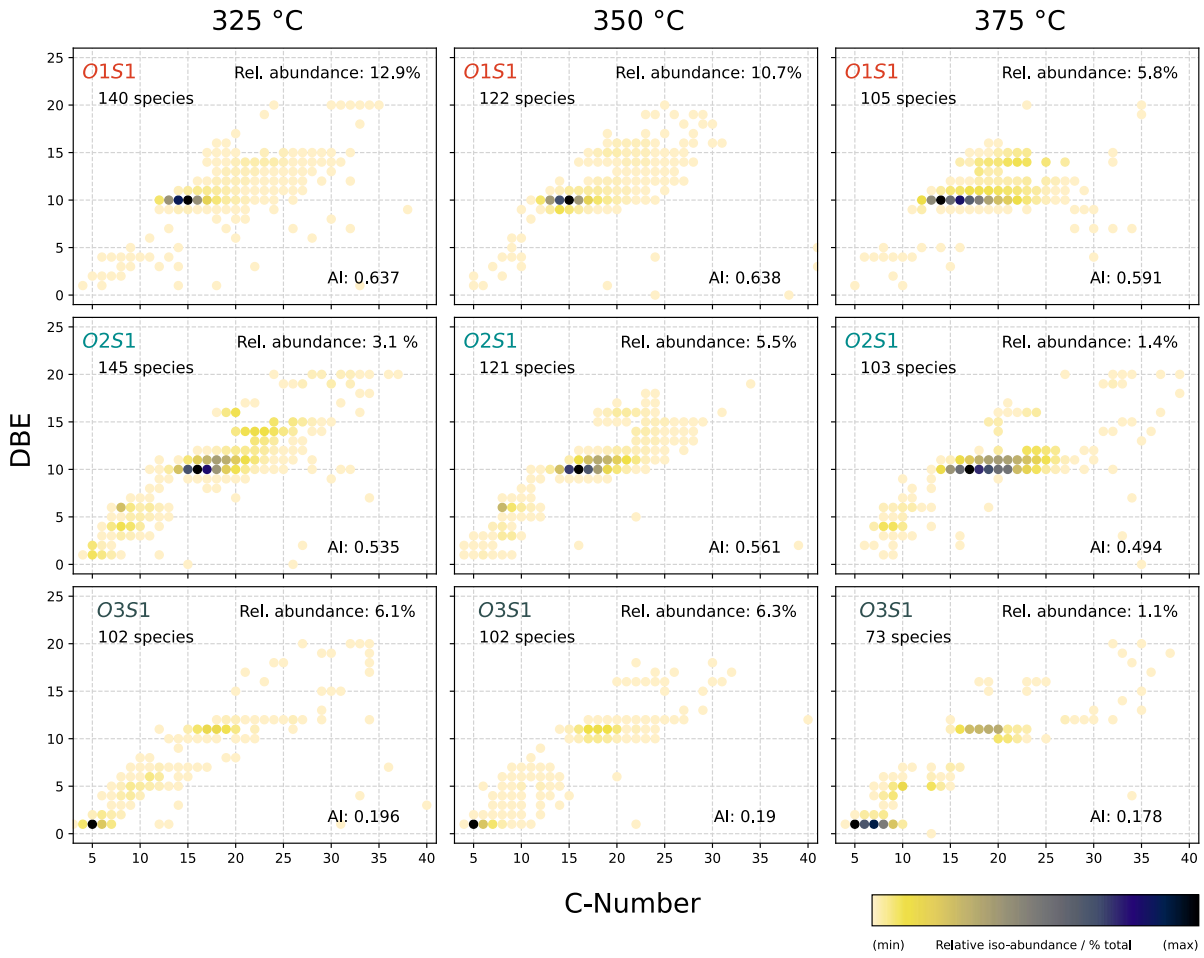

Figure 4-13: Relative intensity scatter-plots based on HPLC-HRMS data for selected O_xS_x groups in the biocrude at different reaction temperatures T_R together with the aromatic index (AI). Double-bond equivalent on y axis, carbon atom number on x axis

In fact, two molecular formulas can be clearly defined in the groups O1S1 and O3S1. One is the molecule $C_{15}H_{12}O_1S_1$ and the other is $C_5H_{10}O_3S_1$. These two molecules dominate in the respective groups of the aqueous phase. While no more precise classification is possible for the first, except that it has an aromatic structure, there are indications of a compound for the second molecular formula. It could be 2-hydroxy-4-(methylthio-)butyric acid, also known as desmeninol. One reason for this assumption is that it is also possible to qualitatively detect this compound in the GC-MS chromatogram at lower reaction temperatures, as it appears to occur in larger quantities. Although the GC-MS method used is not designed for acids, a peak with a strong tailing, which may indicate an organic acid, is clearly recognizable. The matching factor is just under 70 %. The absence of the peak at higher reaction temperatures in the organic phase is also consistent with the findings from the HPLC-

HRMS analysis, in which the relative abundance of the O3S1 group and thus of this molecule in the biocrude also decreases with increasing reaction temperature.

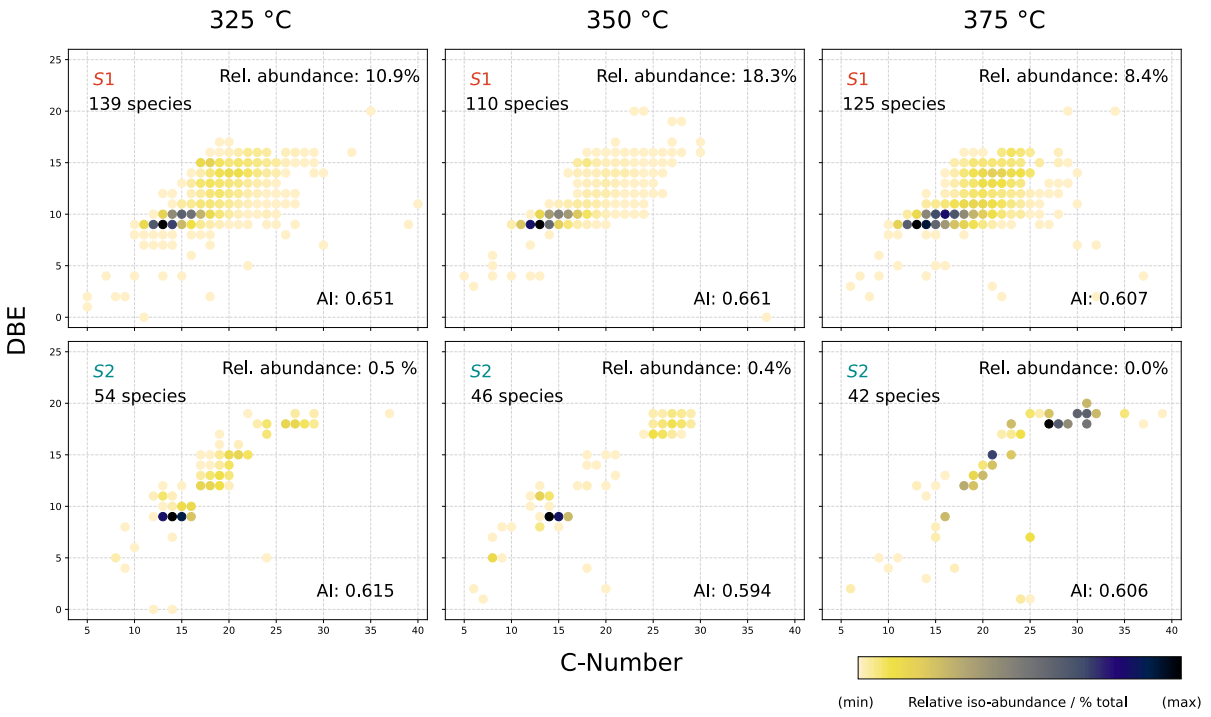

Figure 4-14: Relative intensity scatter-plots based on HPLC-HRMS data for selected S_x groups in the biocrude at different reaction temperatures T_R together with the aromatic index (AI). Double-bond equivalent on y axis, carbon atom number on x axis

In addition, the aromatic index (AI) shows a clear tendency towards aromatic compounds, even with oligomers. For AI > 0.7 it can be assumed that these are condensed aromatic ring structures with only a few short alkyl chains[229]. In the samples examined, the AI values for the biocrude were between 0.494 (O2S1, $T_R = 375$ °C) and 0.661 (S1 $T_R = 350$ °C). Since this value is influenced by the smaller, definitely non-aromatic molecules shown in the lower left corner of the scatterplots, an approximation of 0.7 for the detected compounds is plausible. Only the O3S1 group is strongly dominated by non-aromatic compounds. Here, the previously mentioned compound $C_5H_{10}O_1S_1$ plays by far the largest role. The points mentioned apply to both the investigated biocrude and the aqueous phase, with the latter tending more towards non-aromatic compounds. This is not surprising due to the non-polarity of an aromatic ring and the resulting affinity to the organic phase (biocrude) in the extraction process.

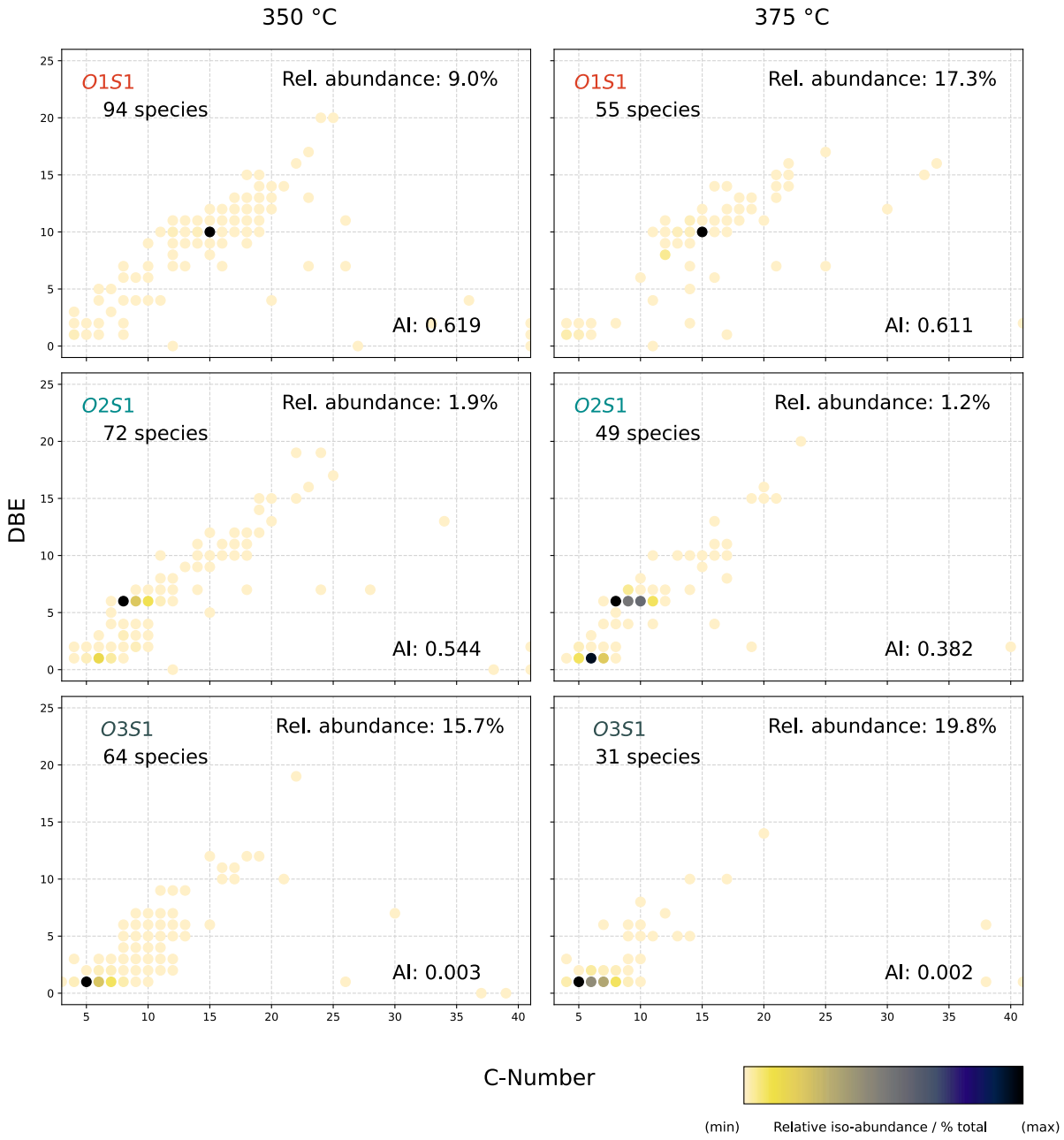

Figure 4-15: Relative intensity scatter-plots based on HPLC-HRMS data for selected O_xS_x groups in the aqueous phase at different reaction temperatures T_R together with the aromatic index (AI). Double-bond equivalent on y axis, carbon atom number on x axis

4.6 Conclusions

Our study has shown that the influence of dissolved sulfides in the BL must be taken into account for the treatment of HTL of BL and downstream processes. The sulfur bound in inorganic molecules actively participates in the reaction pathways and is partly converted to organic sulfur compounds. The clearest indication of organic-bound sulfur is the production of DMS, which is detected in both the gas phase with the

highest yield over 25 $mg \cdot g^{-1}$ biomass in feedstock and the liquid phase with a DMS concentration of up to 800 $mg \cdot L^{-1}$. Other organic sulfides as well as thiols were detected and partly quantified as well. A clear correlation between the HS^- concentration in the feedstock and the formation of DMS was found by using MBL with different HS^- concentrations as the HTL feedstock, which confirms the reaction path established by Karnofski et al. for the Kraft process. Other aspects such as the presence of methanethiol in the gas phase and the liquid phase also support this assumption. We were able to show that the HS^- concentration has an accelerating effect on lignin depolymerization reactions. Interestingly, the yields of the catechol and its derivatives are only minimally affected by the addition of HS^- to the feedstock, and the effects of increasing HS^- concentration are negligible. The HPLC-HRMS analysis of the different product phases from the continuous HTL experiments with real BL shows that sulfur is mostly present as S_1 in the organic sulfur-containing compounds. Most of it can be found in the biocrude and aqueous phase in aromatic molecule structures. Overall, this study provides new insights into the behavior of sulfur and especially the sulfide salts during the HTL of lignin by using BL directly, providing a good basis to evaluate the problems occurring from sulfur.

5 Influence of different alkali metal salts on monomer yields and carbon mass balance

5.1 Introduction

The previous chapter dealt with the influence of a specific salt, sodium sulfide, on the depolymerization of lignin during HTL. Because there has been virtually no research on this topic, this was a major focus. Nevertheless, the other dissolved salts in the black liquor also play a role in depolymerization. The various alkali metal salts based on sodium and potassium are of importance. Carbonates (CO_3^{2-}) and hydroxides (OH^-) are commonly used as anionic counterparts. The advantage of these salts is that they are easy to handle, as all of them are highly soluble in water and can therefore be used as a homogeneous catalyst. As these salts, especially NaOH and Na_2CO_3, are dissolved in the feedstock from the outset when black liquor is used directly, it is reasonable to examine the influence of these salts in more detail in addition to the sulfide. Potassium enters the system primarily via the biomass and additives[238]. The catalytic effect of alkali metal salts has not yet been precisely clarified. One important factor may be the increased concentration of hydroxide ions in solution. This type of catalyst is used both in hydrothermal processes[239,240] and in pyrolysis[241] for the conversion of biomass.

The influence of the salts mentioned has already been investigated in various scientific studies. Belkheiri et al. investigated the effect of the sodium and potassium ratio on the proportion of product phases in the HTL of lignin. Only a slight difference was found[149]. In the work by Rana et al., K_2CO_3 provided the highest biocrude yields and lower char formation compared with acidic homogeneous catalysts [211]. Singh et al. also found that a potassium-containing salt (KOH) showed the best results in terms of biocrude yield[242]. Furthermore, according to Satiada et al., hydroxides seem to achieve better bio-oil yields than carbonates[243]. In this work, however, maize straw was used, which has less lignin but more cellulose content. In the work by Hwang et al., wood was liquefied before pulping (larch and Mongolian oak). K_2CO_3 was added in various concentrations, which also increased the yield of liquid bio-oil and suppressed the hydrochar yield[244]. Interestingly, in a comparative study on the HTL of wheat stem in subcritical water, sodium salts (NaOH, Na_2CO_3) performed slightly better than

potassium salts (KOH, K_2CO_3) in terms of biocrude yields[245]. As can be seen, there are a number of studies that have investigated the effects of alkali metal salts on the HTL of biomass. However, it should be noted that there is no clear tendency, as the feedstocks always differ from each other. It is therefore important to carry out a separate investigation of the influence on HTL for each type of feedstock in order to achieve the best possible conditions for conversion of the respective feedstock. In addition, most studies on this topic barely address the individual yields of individual substances. These are usually grouped together and compared, such as in the publication by Ye et al., which, although it identifies a tendency towards phenolic compounds with increasing Na_2CO_3 concentration in the feed, does not differentiate more precisely[246]. Therefore, in addition to the influence of the HS^- ion on the depolymerization of lignin, this work also deals with the influence of NaOH, Na_2CO_3, KOH and K_2CO_3. The carbon mass balances of the individual experiments, as well as the yields of the typical catechols, were compared.

5.2 Materials and Methods

In order to achieve the best possible comparability, suitable model black liquors (MBL) were produced for the feedstock, as in the investigation of the influence of HS^- ions. Four different MBL were produced. For all four, the sulfur-containing salts (Na_2S, Na_2SO_4, Na_2SO_3, $Na_2S_2O_3$) were used in the same concentration. One of the four salts to be tested was added to each of the four MBL. It was ensured that the concentration of alkali metal ions was approximately 14.5 $g \cdot L^{-1}$, which corresponds approximately to the amount of alkali metals in the real black liquor. Due to the sodium-containing sulfur salts, approx. 6 $g \cdot L^{-1}$ of sodium was also present in the MBL with potassium salts. The salt concentrations per liter are listed in Table 5-1. The lignin concentration in the solution was likewise 90 $g \cdot L^{-1}$ as in the HS^- MBL.

Table 5-1: Concentrations of the salts in the prepared MBL

Salts	MBL NaOH	MBL Na_2CO_3	MBL KOH	MBL K_2CO_3
	Concentration of salts in MBL / $g \cdot L^{-1}$			
Na_2CO_3	0	21.28	0	0
K_2CO_3	0	0	0	24.74
Na_2SO_3	1.32	1.32	1.32	1.32
Na_2SO_4	1.09	1.09	1.09	1.09
$Na_2S_2O_3$	1.94	1.94	1.94	1.94
$Na_2S \cdot 9\ H_2O$	22.50	22.50	22.50	22.50
NaOH	14.32	0	0	0
KOH	0	0	20.09	0

The experiments in the micro autoclaves were carried out as described in chapter 2.3.2. The phase separation and the subsequent analysis procedures for determining the values for the carbon mass balance and the yields of the monomers are identical to those in chapter 2.3.4. Therefore, these are not described in more detail in this chapter. The experiments were carried out at a reaction temperature $T_R = 375\ °C$ and a holding time of $t_R = 1\ min$ in order to come close to the desired conditions in the BL2F project.

5.3 Results and Discussion

5.3.1 Comparison of carbon mass balances

As Figure 5-1 shows, the differences in the carbon content in the individual product phases are only minor. Nevertheless, there are clear trends that can be described. The proportion of solids in the carbon mass balance is slightly higher in the MBL with potassium salts compared to those with sodium salts. This observation is contrary to some results in the literature[211,247–249]. It is possible that the method of mixing the three solid samples from the triplet experiments to obtain sufficient mass for analysis leads to uncertainties. However, the slight increase in organic carbon in the liquid phase is consistent with these results. This can also be observed in the cited sources. The significantly higher reaction temperature $T_R = 375\ °C$ may play a role here. In the work by Karagöz et al., for example, work was carried out at a reaction temperature of only

$T_R = 280$ °C[249]. It is possible that better depolymerization of the lignin by potassium salts leads to increased repolymerization due to the high reaction temperature. Both contributions would therefore increase. Another point that does not fit with the studies cited is the comparison between the influence of OH^- and CO_3^{2-} ions. It was observed that OH^- ions help to produce more organic carbon and less solid matter, independent of the cation. This is consistent with the assumption that a higher basicity, which is associated with OH^- ions, leads to better results in the biocrude yield. The literature research of Satiada et al. comes to a similar conclusion[243]. A further expected difference is the minimally higher proportion of inorganic carbon in the liquid phase and in the gas phase in the carbonates. Both can be explained on account of the dissolved carbonate ions and the shifting balance of dissolved CO_2, which is also transferred to the gas phase. The MBL K_2CO_3 shows no increase in the gas. This is either due to a measurement error or to the generally very low gas concentrations, which means that hardly any differences are visible. The high losses have already been explained in chapter 2.4.4. This is particularly the case at $T_R = 375$ °C.

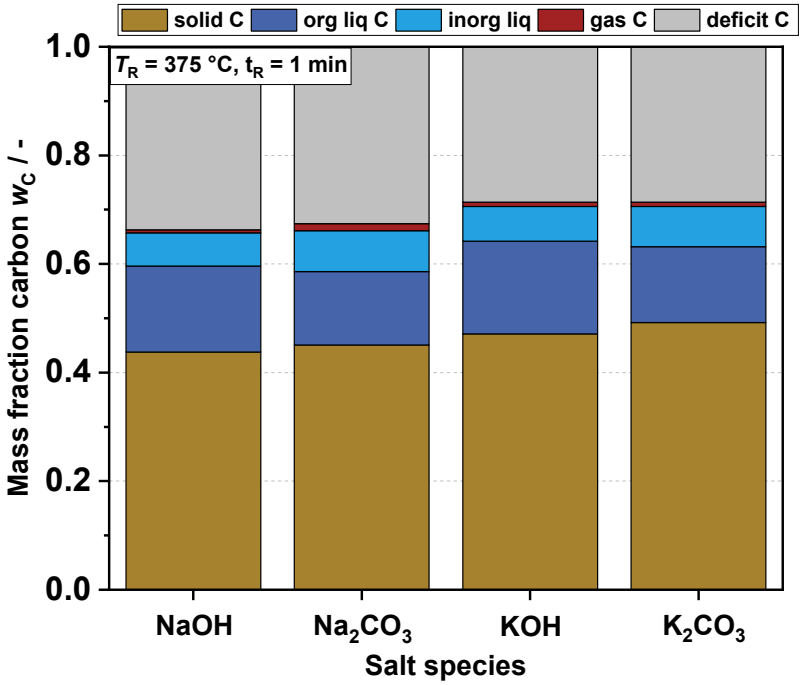

Figure 5-1: Carbon mass balance of the product phases from the four different MBL at reaction temperature $T_R = 375$ °C and holding time $t_R = 1$ min

In conclusion, it can be stated that the results are similar to those of Belkheiri et al. and that the influence can be regarded as rather small[149]. In the cited work, the reaction temperature $T_R = 350$ °C was used, which is closer to the reaction conditions described

here than most of the other cited works. It is possible that the significantly stronger influence of the reaction temperature (see chapter 2) is one reason why no substantial differences can be observed between the results from the HTL experiments with different MBL at higher temperatures.

5.3.2 Differences in aromatic monomer yields

The same was observed for the yields of various aromatic monomers as for the carbon mass balance. The yields shown in Figure 5-2 for each of the four MBL again show only marginal differences. The different catechol derivatives are shown as these are the most relevant compounds. In general, the amount of yield corresponds to the amount of organic carbon in the liquid phase. The higher the amount of organic carbon detected in the liquid phase, the higher the catechol yield. Therefore, KOH was able to achieve the highest yields, while lower yields by 0.2 to 2 $mg \cdot L^{-1}$ were achieved with the MBL with Na_2CO_3. The values determined for NaOH and K_2CO_3 are very close to each other. A specific catalytic effect of an individual salt or ion on reactions such as catechol methylation could not be identified, as the differences are small and systematic and do not stand out specifically for one or more compounds.

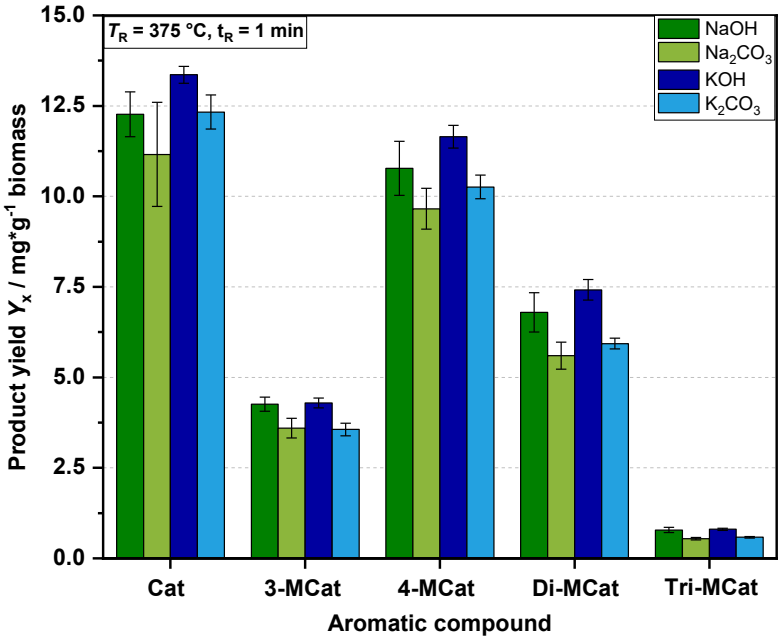

Figure 5-2: Comparison of the aromatic monomer product yields extracted from the liquid product phase after HTL of the MBL at reaction temperature $T_R = 375\,°C$ and holding time $t_R = 1\,min$

5.4 Conclusions

It can be concluded from the results produced that KOH delivers the best results overall. The highest aromatic yields were achieved with it. Only the accumulation of carbon in the solid phase could be reduced with the sodium salts. Ultimately, however, the differences in the catalyst effect between the alkali metal salts are only slight. While most studies have shown significant differences in some cases, this is not the case for this work. Only the study by Belkheiri et al., which was also carried out at a higher reaction temperature, shows similar results[149]. Thus, the influence of temperature seems to be significantly more important than that of the salts, especially in the higher temperature regime. This ultimately leads to the question of whether it is really necessary and above all economically feasible to adapt the Kraft process to improve aromatic yields in a potential downstream HTL process, or to change the black liquor composition before the HTL by removing or adding specific salts.

6 Final conclusions and outlook

This thesis presents and discusses various aspects of the hydrothermal liquefaction of black liquor in detail. The results of this work address the identified research gaps and provide answers to the research questions regarding the direct HTL of black liquor, the underlying reaction pathways, and the influence of salts. The main focus was on the depolymerization of lignin dissolved in black liquor into monocyclic aromatics. Several steps were taken to investigate which main products are formed, what the characteristic reaction pathways are under the given conditions, and how the salts dissolved in black liquor influence the process and the target products.

Direct use of black liquor for lignin depolymerization under HTL conditions with a focus on aromatic monomers:

The results of the first part address the research question regarding the direct use of black liquor and show that the direct use of black liquor in hydrothermal liquefaction is feasible for lignin valorization and leads to aromatic monomer compounds. Using a variety of different analytical methods, it was found that catechols are the main products. This differs from some other work in the field of lignin recycling, where phenol is often the main product. In the work presented here, phenol could only be detected in small quantities. Overall, aromatic yields are low but comparable to those reported in other studies, with a total yield for monomers of less than 5 wt. % based on the biomass used. The influence of temperature was clearly observable and was far greater than that of the holding time. The highest yields of aromatics were obtained at a temperature of $T_R = 300 - 325\ °C$ and holding times of $t_R = 0 - 10\ \mathrm{min}$. In addition to the main products, various intermediate products, in particular 3-methoxycatechol, were also identified. These findings demonstrate that the direct use of black liquor is a viable approach for lignin valorization and thus help close the identified research gap.

Reaction pathways of lignin depolymerization in the BL environment and development of a kinetic model

Based on the results of the detailed parameter study and experiments with model substances, the research question regarding the reaction pathways of lignin depolymerization was addressed by developing a reaction network for the depolymerization of lignin under the given hydrothermal conditions and under the

influence of the various salts dissolved in the black liquor. Since this reaction network primarily focuses on monomers, oligomers were also investigated using ^{31}P and ^{13}C NMR as well as SEC analysis to determine the relative molecular weight of the organic phase. NMR analysis in particular revealed that the reactions we observed in the monomers also occur in the functional groups of the oligomers. The comparison between the quantified specific OH groups of syringyl and guaiacyl units with the yields of the monomers showed good agreement with increasing reaction temperature. The reaction scheme was used in the next part of the work to develop a kinetic model that describes the depolymerization of lignin to aromatics. For the model, the temperature range was limited to $T_R = 300 - 350\,°C$ and the holding time was examined in more detail. The kinetic model provides very good results, especially for the intermediate product 3-methoxycatechol and the stepwise methylation of catechol to trimethylcatechols. Overall, the simulated values for the monomers are all within an acceptable range. In addition, the calculated values also clearly show that a large portion of the biomass ends up in solids or in unspecified organic compounds such as oligomers or alcohols and acids. This was already evident from the carbon mass balance and was further emphasized by the model. Possible reasons include the high salt load and the adsorption of organic material on the solid surface of the char. Aromatic compounds in particular are known to contribute to rapid char formation.

In addition to the primary use of black liquor based on hardwood, it was successfully demonstrated that black liquor based on softwood behaves only slightly differently. In the experimental tests in Chapter 2, hardly any differences were found when comparing the carbon mass balances and the yields of aromatic monomers. Only the expected differences in the intermediate products, more guaiacol and no 3-methoxycatechol in the case of softwood, were visible. However, these had little influence on the yields of catechols. Subsequently, the idea of incorporating this into the kinetic model was pursued, for which the simulated values based on the hardwood BL parameter study were compared with the experimentally determined values for softwood BL HTL. The results show that, with minor adjustments, the kinetic model can also be used for experiments with softwood BL, which underscores its flexibility. Overall, these results significantly improve the understanding of lignin depolymerization under HTL conditions.

The influence of sulfide and other salts on lignin depolymerization and the fate of sulfur:

The final part of the work addresses the research questions concerning the influence of salts, particularly sulfide, on lignin depolymerization and the fate of sulfur. As the least investigated salt, the focus was on sulfide, which is used as Na_2S in the Kraft process. In addition to its influence on the yields of aromatics and depolymerization, the question of the fate of sulfur was also important, especially with regard to subsequent processes or a possible larger technical design of the HTL process. It was shown that sulfide in the form of HS^- ions is directly involved in reactions with organic matter and does not act solely through catalytic or inhibiting effects. The sulfur mass balance shows an increase in organic sulfur in the liquid product due to an increase in temperature. Furthermore, using model black liquors with different HS^- concentrations, it was possible to establish a direct correlation between the dimethyl sulfide (DMS) yield in the gas phase and the HS^- concentration in the feed. At the same time, the mechanism for DMS production in the Kraft process postulated by Karnofski et al. was also confirmed for the direct use of black liquor in HTL[217]. These findings provide a clear answer to the question of how inorganic sulfur is transformed under HTL conditions. Apart from DMS, other sulfides and thiols were identified in the different product phases. This trend is confirmed in the oligomers, as shown by the evaluation of HPLC-HRMS data from biocrude and solids. In most cases, there is only one sulfur atom in the molecular formula. Since organic sulfides are more stable than thiol groups, it can be assumed that the sulfur is primarily present as sulfide bridges. In addition to the incorporation of inorganic sulfur into the organic matter, a catalytic effect was also evident. The results of the HTL of the model black liquors with higher HS^- concentrations show a faster depolymerization of the lignin, which is evident from the molecular weight. Thus, both the chemical and catalytic roles of sulfide could be clarified.

The influence of other salts contained in black liquor, KOH, NaOH, K_2CO_3 and Na_2CO_3, was also investigated. This addresses the question of how other alkali metal salts influence product yields and carbon distribution. It was found that hydroxide has a more favorable effect than carbonate in as it slightly suppresses char formation while increasing aromatic yields. The comparison of sodium and potassium ions comes to

the same conclusion, with potassium performing better. Overall, the influence of these salts is secondary compared to temperature and sulfide effects.

Evaluation of the direct use of black liquor in an HTL process

In summary, the results of this work show that the direct use of black liquor leads to comparable outcomes to extracted lignin, such as those by Forchheim et al. or Schuler et al.[171,183], thereby validating the central hypothesis of this thesis. Similar product groups are produced and mainly differ due to the wood type used. On the one hand, depolymerization reactions seem to be faster due to the catalytic effects of the HS-ions, but on the other hand repolymerization and solid formation are also enhanced. The avoidance of additional intermediate steps should be highlighted as a positive aspect. This is particularly relevant in the context of biorefinery concepts, where process simplicity and integration are crucial.

What are the next steps?

This work provides a comprehensive picture of the depolymerization of lignin under hydrothermal conditions with the direct use of black liquor. While the main research questions have been answered, several aspects remain open and require further investigation.

1) Further experimental investigations:

The already detailed experimental work can be expanded further. With regard to oligomers in particular, more in-depth analyses are conceivable in order to better capture them in a kinetic model. This is particularly important, as oligomers represent a significant fraction that is not yet fully described in the current model. According to the simulation, approximately 50 % of the carbon is present in this fraction. Possibilities include more extensive NMR analysis, e.g., the recording and interpretation of HSQC (heteronuclear single quantum coherence) spectra. Improvements to the SEC analysis are also possible, as a relatively simple setup was used for this work. This setup has since been revised by adjusting the eluent. This allowed values for molecular weights to be determined that also appear reasonable in absolute terms. An example of this is an analysis of a biocrude sample including calibration in Figure 6-1. There is potential here to distinguish between different sizes of oligomers, which may enable a more detailed description of depolymerization and repolymerization during the HTL process.

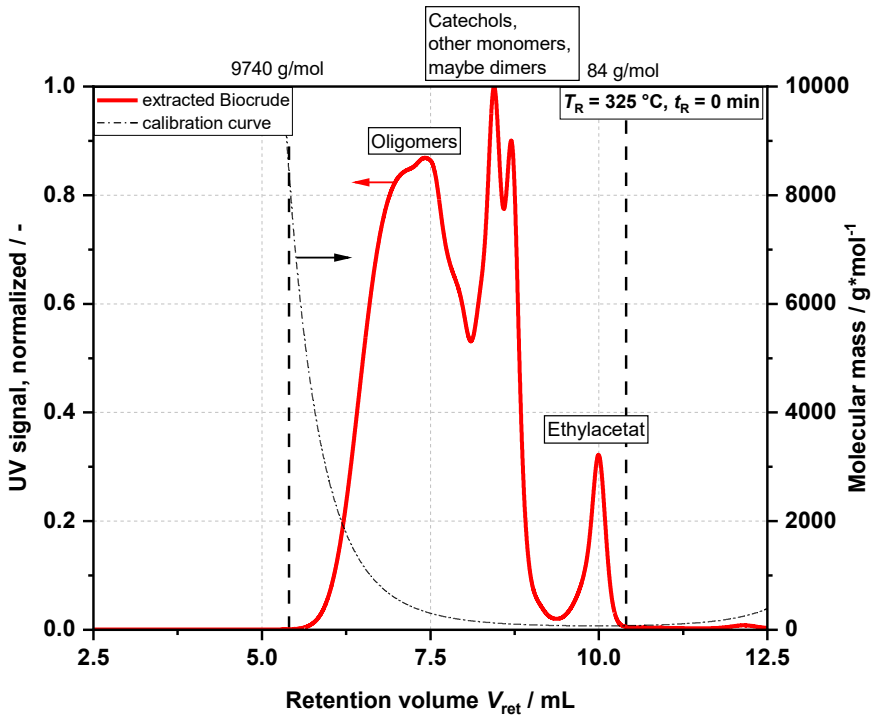

Figure 6-1: SEC Analysis of a biocrude sample from an HTL process with BL as feedstock; new method and eluent used; calibration curve is included

Moreover, further experiments with model substances are useful. 3-Methoxycatechol is particularly suitable for this purpose, as it allows for better differentiation between the individual reaction pathways leading to catechol.

2) Treatment of product phases and product separation

During the experimental work, it emerged that both the treatment and the subsequent separation of the product phases are critical points. It may be possible to increase the yields of the monomers with an even better adjusted process. The salts in particular seem to play a major role in the separation processes. The extraction of organic material from the solid phase is also possible and should be considered in future work, as a large amount of carbon is lost here. In addition to phase separation, product separation is also crucial for the meaningful use of lignin depolymerization. Separating the aromatics from each other is a complex topic, as some of them hardly differ in their properties. Deep eutectic solvents are currently being investigated as potential candidates for the separation of guaiacol, catechol, etc.[194,250]. Improving product separation is essential to translate the experimental findings into practical applications.

3) Economic analysis of the process

Alongside further experimental studies that contribute to the successful implementation of HTL of black liquor for aromatic production, it is essential to examine the economic aspects of the process. For this purpose, an overall concept for integrating the process into an existing system must be developed, taking into account feedstock supply and the integration of products into subsequent process chains. On the other hand, it is also important to consider the process itself from an economic perspective. In a rough assessment based on the data generated in this study, HTL of black liquor was still far from being economically viable. A key point that was highlighted is that not only the target products must be used, but also all other process streams. These include, for example, the solid waste produced and organic products soluble in water. Therefore, further studies must be carried out to analyze these product phases in more detail and investigate their potential. Only in this way can a viable process be developed that can ultimately be integrated into the chemical industry.

7 References

(1) Abbass, K.; Qasim, M. Z.; Song, H.; Murshed, M.; Mahmood, H.; Younis, I. A Review of the Global Climate Change Impacts, Adaptation, and Sustainable Mitigation Measures. *Environ. Sci. Pollut. Res.* **2022**, *29* (28), 42539–42559. https://doi.org/10.1007/s11356-022-19718-6.

(2) Meinshausen, M.; Lewis, J.; McGlade, C.; Gütschow, J.; Nicholls, Z.; Burdon, R.; Cozzi, L.; Hackmann, B. Realization of Paris Agreement Pledges May Limit Warming Just below 2 °C. *Nature* **2022**, *604* (7905), 304–309. https://doi.org/10.1038/s41586-022-04553-z.

(3) Alšauskas, O. World Energy Outlook 2024.

(4) Energy Institute. *Statistical Review of World Energy 2024 - 73th Edition*; 2024. https://www.energyinst.org/statistical-review/resources-and-data-downloads.

(5) Franck, H.-G.; Stadelhofer, J. W. *Industrial Aromatic Chemistry: Raw Materials · Processes · Products*; Springer Berlin Heidelberg: Berlin, Heidelberg, 1988. https://doi.org/10.1007/978-3-642-73432-8.

(6) straits research. *Benzene-Toluene-Xylene (BTX) Market Size, Share & Trends, Forecasts, 2021-2030*. https://straitsresearch.com/report/benzene-toluene-xylene-market.

(7) Naik, S. N.; Goud, V. V.; Rout, P. K.; Dalai, A. K. Production of First and Second Generation Biofuels: A Comprehensive Review. *Renew. Sustain. Energy Rev.* **2010**, *14* (2), 578–597. https://doi.org/10.1016/j.rser.2009.10.003.

(8) Liu, Y.; Li, G.; Chen, Z.; Shen, Y.; Zhang, H.; Wang, S.; Qi, J.; Zhu, Z.; Wang, Y.; Gao, J. Comprehensive Analysis of Environmental Impacts and Energy Consumption of Biomass-to-Methanol and Coal-to-Methanol via Life Cycle Assessment. *Energy* **2020**, *204*, 117961. https://doi.org/10.1016/j.energy.2020.117961.

(9) Gautam, P.; Neha; Upadhyay, S. N.; Dubey, S. K. Bio-Methanol as a Renewable Fuel from Waste Biomass: Current Trends and Future Perspective. *Fuel* **2020**, *273*, 117783. https://doi.org/10.1016/j.fuel.2020.117783.

(10) de Klerk, A. Chapter 12 - Transport Fuel: Biomass-, Coal-, Gas- and Waste-to-Liquids Processes. In *Future Energy (Second Edition)*; Letcher, T. M., Ed.; Elsevier: Boston, 2014; pp 245–270. https://doi.org/10.1016/B978-0-08-099424-6.00012-0.

(11) Heidenreich, S.; Foscolo, P. U. New Concepts in Biomass Gasification. *Prog. Energy Combust. Sci.* **2015**, *46*, 72–95. https://doi.org/10.1016/j.pecs.2014.06.002.

(12) Molino, A.; Chianese, S.; Musmarra, D. Biomass Gasification Technology: The State of the Art Overview. *J. Energy Chem.* **2016**, *25* (1), 10–25. https://doi.org/10.1016/j.jechem.2015.11.005.

(13) Singh Sikarwar, V.; Zhao, M.; Clough, P.; Yao, J.; Zhong, X.; Zaki Memon, M.; Shah, N.; J. Anthony, E.; S. Fennell, P. An Overview of Advances in Biomass Gasification. *Energy Environ. Sci.* **2016**, *9* (10), 2939–2977. https://doi.org/10.1039/C6EE00935B.

(14) Campos, B. L. de O.; Costa, A. O. S. da; Delgado, K. H.; Pitter, S.; Sauer, J.; Junior, E. F. da C. Development of a Surrogate Artificial Neural Network for Microkinetic Modeling: Case Study with Methanol Synthesis. *React. Chem. Eng.* **2024**, *9* (5), 1047–1060. https://doi.org/10.1039/D3RE00409K.

(15) Campos, B. L. de O.; Delgado, K. H.; Wild, S.; Studt, F.; Pitter, S.; Sauer, J. Surface Reaction Kinetics of the Methanol Synthesis and the Water Gas Shift Reaction on Cu/ZnO/Al 2 O 3. *React. Chem. Eng.* **2021**, *6* (5), 868–887. https://doi.org/10.1039/D1RE00040C.

(16) Lacerda de Oliveira Campos, B.; John, K.; Beeskow, P.; Herrera Delgado, K.; Pitter, S.; Dahmen, N.; Sauer, J. A Detailed Process and Techno-Economic Analysis of Methanol Synthesis from H2 and CO2 with Intermediate Condensation Steps. *Processes* **2022**, *10* (8), 1535. https://doi.org/10.3390/pr10081535.

(17) Wang, S.; Song, G. A Pathway to Bio-Based Aromatics. *Nat. Sustain.* **2023**, *6* (11), 1295–1296. https://doi.org/10.1038/s41893-023-01191-9.

(18) Wegelin, S.; Meier, M. A. R. Bio-Based Aromatics for Chemicals and Materials: Advances in Renewable Drop-in and Functional Alternatives. *Curr. Opin. Green Sustain. Chem.* **2024**, *47*, 100931. https://doi.org/10.1016/j.cogsc.2024.100931.

(19) Li, Z.; Jiang, Y.; Li, Y.; Zhang, H.; Li, H.; Yang, S. Advances in Diels–Alder/Aromatization of Biomass Furan Derivatives towards Renewable Aromatic

Hydrocarbons. *Catal. Sci. Technol.* **2022**, *12* (6), 1902–1921. https://doi.org/10.1039/D1CY02122B.

(20) Kammoun, M.; Margellou, A.; Toteva, V. B.; Aladjadjiyan, A.; Sousa, A. F.; Luis, S. V.; Garcia-Verdugo, E.; Triantafyllidis, K. S.; Richel, A. The Key Role of Pretreatment for the One-Step and Multi-Step Conversions of European Lignocellulosic Materials into Furan Compounds. *RSC Adv.* **2023**, *13* (31), 21587–21612. https://doi.org/10.1039/D3RA01533E.

(21) Schade, O. R.; Dannecker, P.-K.; Kalz, K. F.; Steinbach, D.; Meier, M. A. R.; Grunwaldt, J.-D. Direct Catalytic Route to Biomass-Derived 2,5-Furandicarboxylic Acid and Its Use as Monomer in a Multicomponent Polymerization. *ACS Omega* **2019**, *4* (16), 16972–16979. https://doi.org/10.1021/acsomega.9b02373.

(22) Pfersich, J.; Arauzo, P. J.; Lucian, M.; Modugno, P.; Titirici, M.-M.; Fiori, L.; Kruse, A. Hydrothermal Conversion of Spent Sugar Beets into High-Value Platform Molecules. *Molecules* **2020**, *25* (17), 3914. https://doi.org/10.3390/molecules25173914.

(23) Neukum, D.; Baumgarten, L.; Wüst, D.; Sarma, B. B.; Saraçi, E.; Kruse, A.; Grunwaldt, J.-D. Challenges of Green Production of 2,5-Furandicarboxylic Acid from Bio-Derived 5-Hydroxymethylfurfural: Overcoming Deactivation by Concomitant Amino Acids. *ChemSusChem* **2022**, *15* (13), e202200418. https://doi.org/10.1002/cssc.202200418.

(24) Tachibana, Y.; Kasuya, K. Chapter 10 - Bio-Based Polymers Synthesized from Furan Derivatives. In *Biopolymers*; Sessini, V., Ghosh, S., Mosquera, M. E. G., Eds.; Elsevier, 2023; pp 295–345. https://doi.org/10.1016/B978-0-323-90939-6.00011-X.

(25) Gandini, A.; M. Lacerda, T. Furan Polymers: State of the Art and Perspectives. *Macromol. Mater. Eng.* **2022**, *307* (6), 2100902. https://doi.org/10.1002/mame.202100902.

(26) Clark, J.; Deswarte, F. The Biorefinery Concept. In *Introduction to chemicals from biomass*; Clark, J. H., Deswarte, F. E. I., Eds.; Wiley series in renewable resources; Wiley: Chichester, West Sussex, 2015; pp 1–29. https://doi.org/10.1002/9781118714478.ch1.

(27) Ferreira, A. F. Biorefinery Concept. In *Bio-refineries: Targeting energy, high value products and waste valorisation*; Rabaçal, M., Ferreira, A. F., Silva, C. A. M., Costa, M., Eds.; Lecture Notes in Energy; Springer: Cham, 2017; Vol. Volume 57, pp 1–20. https://doi.org/10.1007/978-3-319-48288-0_1.

(28) Ragauskas, A. J.; Williams, C. K.; Davison, B. H.; Britovsek, G.; Cairney, J.; Eckert, C. A.; Frederick, W. J.; Hallett, J. P.; Leak, D. J.; Liotta, C. L.; et al. The Path Forward for Biofuels and Biomaterials. *Science* **2006**, *311* (5760), 484–489. https://doi.org/10.1126/science.1114736.

(29) Ragauskas, A. J.; Beckham, G. T.; Biddy, M. J.; Chandra, R.; Chen, F.; Davis, M. F.; Davison, B. H.; Dixon, R. A.; Gilna, P.; Keller, M.; et al. Lignin Valorization: Improving Lignin Processing in the Biorefinery. *Science* **2014**, *344* (6185), 1246843. https://doi.org/10.1126/science.1246843.

(30) Cherubini, F. The Biorefinery Concept: Using Biomass Instead of Oil for Producing Energy and Chemicals. *Energy Convers. Manag.* **2010**, *51* (7), 1412–1421. https://doi.org/10.1016/j.enconman.2010.01.015.

(31) *Free icons designed by Freepik*. Flaticon. https://www.flaticon.com/authors/freepik (accessed 2025-01-04).

(32) *Bioproduct mill concept*. Metsä Fibre. https://www.metsagroup.com/metsafibre/about-metsafibre/bioproduct-mill-concept/ (accessed 2025-01-04).

(33) *Lenzing – von Natur innovativ*. https://www.lenzing.com/de/ (accessed 2025-11-09).

(34) *Bioraffinerie Leuna*. Bioraffinerie Leuna | UPM Biochemicals. https://www.upmbiochemicals.com/de/uber-upm-biochemicals/bioraffinerie-leuna/ (accessed 2025-11-09).

(35) Singh, N.; Singhania, R. R.; Nigam, P. S.; Dong, C.-D.; Patel, A. K.; Puri, M. Global Status of Lignocellulosic Biorefinery: Challenges and Perspectives. *Bioresour. Technol.* **2022**, *344*, 126415. https://doi.org/10.1016/j.biortech.2021.126415.

(36) Dahmen, N.; Lewandowski, I.; Zibek, S.; Weidtmann, A. Integrated Lignocellulosic Value Chains in a Growing Bioeconomy: Status Quo and Perspectives. *GCB Bioenergy* **2019**, *11* (1), 107–117. https://doi.org/10.1111/gcbb.12586.

(37) Chen, H. Chemical Composition and Structure of Natural Lignocellulose. In *Biotechnology of Lignocellulose: Theory and Practice*; Chen, H., Ed.; Springer Netherlands: Dordrecht, 2014; pp 25–71. https://doi.org/10.1007/978-94-007-6898-7_2.

(38) Lourenço, A.; Pereira, H. Compositional Variability of Lignin in Biomass. In *Lignin - Trends and Applications*; Poletto, M., Ed.; IntechOpen: Erscheinungsort nicht ermittelbar, 2018. https://doi.org/10.5772/intechopen.71208.

(39) Bresinsky, A.; Körner, C.; Kadereit, J. W.; Neuhaus, G.; Sonnewald, U. *Lehrbuch Der Botanik*, 36. Aufl.; Strasburger, E., Bresinsky, A., Körner, C., Kadereit, J. W., Neuhaus, G., Sonnewald, U., Eds.; Spektrum Akad. Verl.: Heidelberg, 2008. https://doi.org/Eduard.

(40) Lange, H.; Decina, S.; Crestini, C. Oxidative Upgrade of Lignin – Recent Routes Reviewed. *Eur. Polym. J.* **2013**, *49* (6), 1151–1173. https://doi.org/10.1016/j.eurpolymj.2013.03.002.

(41) Ralph, J.; Lapierre, C.; Boerjan, W. Lignin Structure and Its Engineering. *Curr. Opin. Biotechnol.* **2019**, *56*, 240–249. https://doi.org/10.1016/j.copbio.2019.02.019.

(42) Sun, R.-C. Lignin Source and Structural Characterization. *ChemSusChem* **2020**, *13* (17), 4385–4393. https://doi.org/10.1002/cssc.202001324.

(43) Xie, M.; Zhang, J.; Tschaplinski, T. J.; Tuskan, G. A.; Chen, J.-G.; Muchero, W. Regulation of Lignin Biosynthesis and Its Role in Growth-Defense Tradeoffs. *Front. Plant Sci.* **2018**, *9*, 1427. https://doi.org/10.3389/fpls.2018.01427.

(44) Zhou, S.; Xue, Y.; Sharma, A.; Bai, X. Lignin Valorization through Thermochemical Conversion: Comparison of Hardwood, Softwood and Herbaceous Lignin. *ACS Sustain. Chem. Eng.* **2016**, *4* (12), 6608–6617. https://doi.org/10.1021/acssuschemeng.6b01488.

(45) Suota, M. J.; da Silva, T. A.; Zawadzki, S. F.; Sassaki, G. L.; Hansel, F. A.; Paleologou, M.; Ramos, L. P. Chemical and Structural Characterization of Hardwood and Softwood LignoForce™ Lignins. *Ind. Crops Prod.* **2021**, *173*, 114138. https://doi.org/10.1016/j.indcrop.2021.114138.

(46) Tolbert, A.; Akinosho, H.; Khunsupat, R.; Naskar, A. K.; Ragauskas, A. J. Characterization and Analysis of the Molecular Weight of Lignin for Biorefining Studies. *Biofuels Bioprod. Biorefining* **2014**, *8* (6), 836–856. https://doi.org/10.1002/bbb.1500.

(47) Poveda-Giraldo, J. A.; Solarte-Toro, J. C.; Cardona Alzate, C. A. The Potential Use of Lignin as a Platform Product in Biorefineries: A Review. *Renew. Sustain. Energy Rev.* **2021**, *138*, 110688. https://doi.org/10.1016/j.rser.2020.110688.

(48) Fache, M.; Boutevin, B.; Caillol, S. Vanillin Production from Lignin and Its Use as a Renewable Chemical. *ACS Sustain. Chem. Eng.* **2016**, *4* (1), 35–46. https://doi.org/10.1021/acssuschemeng.5b01344.

(49) José Borges Gomes, F.; Souza, R. E.; Brito, E. O.; Costa Lelis, R. C. A Review on Lignin Sources and Uses. *J. Appl. Biotechnol. Bioeng.* **2020**, 100–105. https://doi.org/10.15406/jabb.2020.07.00222.

(50) de la Torre, M. J.; Moral, A.; Hernández, M. D.; Cabeza, E.; Tijero, A. Organosolv Lignin for Biofuel. *Ind. Crops Prod.* **2013**, *45*, 58–63. https://doi.org/10.1016/j.indcrop.2012.12.002.

(51) Xu, F.; Sun, J.-X.; Sun, R.; Fowler, P.; Baird, M. S. Comparative Study of Organosolv Lignins from Wheat Straw. *Ind. Crops Prod.* **2006**, *23* (2), 180–193. https://doi.org/10.1016/j.indcrop.2005.05.008.

(52) Watkins, D.; Nuruddin, Md.; Hosur, M.; Tcherbi-Narteh, A.; Jeelani, S. Extraction and Characterization of Lignin from Different Biomass Resources. *J. Mater. Res. Technol.* **2015**, *4* (1), 26–32. https://doi.org/10.1016/j.jmrt.2014.10.009.

(53) Schutyser, W.; Renders, T.; van den Bosch, S.; Koelewijn, S.-F.; Beckham, G. T.; Sels, B. F. Chemicals from Lignin: An Interplay of Lignocellulose Fractionation, Depolymerisation, and Upgrading. *Chem. Soc. Rev.* **2018**, *47* (3), 852–908. https://doi.org/10.1039/C7CS00566K.

(54) Tricker, A. W.; Stellato, M. J.; Kwok, T. T.; Kruyer, N. S.; Wang, Z.; Nair, S.; Thomas, V. M.; Realff, M. J.; Bommarius, A. S.; Sievers, C. Similarities in Recalcitrant Structures of Industrial Non-Kraft and Kraft Lignin. *ChemSusChem* **2020**, *13* (17), 4624–4632. https://doi.org/10.1002/cssc.202001219.

(55) Metsä Group. *Metsä Group. Sustainability Report 2018*; 2019.

(56) Lappalainen, J.; Baudouin, D.; Hornung, U.; Schuler, J.; Melin, K.; Bjelić, S.; Vogel, F.; Konttinen, J.; Joronen, T. Sub- and Supercritical Water Liquefaction of Kraft Lignin and Black Liquor Derived Lignin. *Energies* **2020**, *13* (13), 3309. https://doi.org/10.3390/en13133309.

(57) Alén, R. Pulp Mills and Wood-Based Biorefineries. In *Industrial Biorefineries & White Biotechnology*; Elsevier, 2015; pp 91–126. https://doi.org/10.1016/B978-0-444-63453-5.00003-3.

(58) Weng, C.; Peng, X.; Han, Y. Depolymerization and Conversion of Lignin to Value-Added Bioproducts by Microbial and Enzymatic Catalysis. *Biotechnol. Biofuels* **2021**, *14* (1), 84. https://doi.org/10.1186/s13068-021-01934-w.

(59) Leonowicz, A.; Cho, N.; Luterek, J.; Wilkolazka, A.; Wojtas-Wasilewska, M.; Matuszewska, A.; Hofrichter, M.; Wesenberg, D.; Rogalski, J. Fungal Laccase: Properties and Activity on Lignin. *J. Basic Microbiol.* **2001**, *41* (3–4), 185–227. https://doi.org/10.1002/1521-4028(200107)41:3/4%253C185::AID-JOBM185%253E3.0.CO;2-T.

(60) Ayuso-Fernández, I.; Ruiz-Dueñas, F. J.; Martínez, A. T. Evolutionary Convergence in Lignin-Degrading Enzymes. *Proc. Natl. Acad. Sci.* **2018**, *115* (25), 6428–6433. https://doi.org/10.1073/pnas.1802555115.

(61) Jahn, A.; Hoffmann, A.; Blaesing, L.; Kunde, F.; Bertau, M.; Bremer, M.; Fischer, S. Lignin from Annual Plants as Raw Material Source for Flavors and Basic Chemicals. *Chem. Ing. Tech.* **2020**, *92* (11), 1733–1740. https://doi.org/10.1002/cite.202000097.

(62) Rodríguez-Escribano, D.; de Salas, F.; Pliego, R.; Marques, G.; Levée, T.; Suonpää, A.; Gutiérrez, A.; Martínez, Á. T.; Ihalainen, P.; Rencoret, J.; Camarero, S. Depolymerisation of Kraft Lignin by Tailor-Made Alkaliphilic Fungal Laccases. *Polymers* **2023**, *15* (22), 4433. https://doi.org/10.3390/polym15224433.

(63) Du, X.; Zhang, H.; Sullivan, K. P.; Gogoi, P.; Deng, Y. Electrochemical Lignin Conversion. *ChemSusChem* **2020**, *13* (17), 4318–4343. https://doi.org/10.1002/cssc.202001187.

(64) Movil-Cabrera, O.; Rodriguez-Silva, A.; Arroyo-Torres, C.; Staser, J. A. Electrochemical Conversion of Lignin to Useful Chemicals. *Biomass Bioenergy* **2016**, *88*, 89–96. https://doi.org/10.1016/j.biombioe.2016.03.014.

(65) Xie, B.; Tobimatsu, Y.; Narita, K.; Yokohata, S.; Kamitakahara, H.; Takano, T. Electro-Oxidation of Lignin Model Compounds and Synthetic Lignin with Transition-Metal Complexes (Manganese and Iron Complexes). *ACS Sustain. Chem. Eng.* **2022**, *10* (50), 16701–16708. https://doi.org/10.1021/acssuschemeng.2c04811.

(66) Marino, D. D.; Stöckmann, D.; Kriescher, S.; Stiefel, S.; Wessling, M. Electrochemical Depolymerisation of Lignin in a Deep Eutectic Solvent. *Green Chem.* **2016**, *18* (22), 6021–6028. https://doi.org/10.1039/C6GC01353H.

(67) Marino, D. D.; Aniko, V.; Stocco, A.; Kriescher, S.; Wessling, M. Emulsion Electro-Oxidation of Kraft Lignin. *Green Chem.* **2017**, *19* (20), 4778–4784. https://doi.org/10.1039/C7GC02115A.

(68) Wan, Z.; Zhang, H.; Guo, Y.; Li, H. Advances in Catalytic Depolymerization of Lignin. *ChemistrySelect* **2022**, *7* (40), e202202582. https://doi.org/10.1002/slct.202202582.

(69) Liu, X.; Bouxin, F. P.; Fan, J.; Budarin, V. L.; Hu, C.; Clark, J. H. Recent Advances in the Catalytic Depolymerization of Lignin towards Phenolic Chemicals: A Review. *ChemSusChem* **2020**, *13* (17), 4296–4317. https://doi.org/10.1002/cssc.202001213.

(70) Jing, Y.; Dong, L.; Guo, Y.; Liu, X.; Wang, Y. Chemicals from Lignin: A Review of Catalytic Conversion Involving Hydrogen. *ChemSusChem* **2020**, *13* (17), 4181–4198. https://doi.org/10.1002/cssc.201903174.

(71) Cheng, C.; Shen, D.; Gu, S.; Hong Luo, K. State-of-the-Art Catalytic Hydrogenolysis of Lignin for the Production of Aromatic Chemicals. *Catal. Sci. Technol.* **2018**, *8* (24), 6275–6296. https://doi.org/10.1039/C8CY00845K.

(72) Ye, K.; Liu, Y.; Wu, S.; Zhuang, J. A Review for Lignin Valorization: Challenges and Perspectives in Catalytic Hydrogenolysis. *Ind. Crops Prod.* **2021**, *172*, 114008. https://doi.org/10.1016/j.indcrop.2021.114008.

(73) Kumaravel, S.; Thiruvengetam, P.; Karthick, K.; Sankar, S. S.; Karmakar, A.; Kundu, S. Green and Sustainable Route for Oxidative Depolymerization of Lignin: New Platform for Fine Chemicals and Fuels. *Biotechnol. Prog.* **2021**, *37* (2), e3111. https://doi.org/10.1002/btpr.3111.

(74) Bourbiaux, D.; Pu, J.; Rataboul, F.; Djakovitch, L.; Geantet, C.; Laurenti, D. Reductive or Oxidative Catalytic Lignin Depolymerization: An Overview of Recent Advances. *Catal. Today* **2021**, *373*, 24–37. https://doi.org/10.1016/j.cattod.2021.03.027.

(75) Wu, Z.; Hu, L.; Jiang, Y.; Wang, X.; Xu, J.; Wang, Q.; Jiang, S. Recent Advances in the Acid-Catalyzed Conversion of Lignin. *Biomass Convers. Biorefinery* **2023**, *13* (1), 519–539. https://doi.org/10.1007/s13399-020-00976-8.

(76) Roberts, Virginia. M.; Stein, V.; Reiner, T.; Lemonidou, A.; Li, X.; Lercher, J. A. Towards Quantitative Catalytic Lignin Depolymerization. *Chem. – Eur. J.* **2011**, *17* (21), 5939–5948. https://doi.org/10.1002/chem.201002438.

(77) Sedai, B.; Díaz-Urrutia, C.; Baker, R. T.; Wu, R.; Silks, L. A. "Pete"; Hanson, S. K. Comparison of Copper and Vanadium Homogeneous Catalysts for Aerobic Oxidation of Lignin Models. *ACS Catal.* **2011**, *1* (7), 794–804. https://doi.org/10.1021/cs200149v.

(78) Biannic, B.; Bozell, J. J. Efficient Cobalt-Catalyzed Oxidative Conversion of Lignin Models to Benzoquinones. *Org. Lett.* **2013**, *15* (11), 2730–2733. https://doi.org/10.1021/ol401065r.

(79) Ahmad, Z.; Paleologou, M.; Xu, C. C. Oxidative Depolymerization of Lignin Using Nitric Acid under Ambient Conditions. *Ind. Crops Prod.* **2021**, *170*, 113757. https://doi.org/10.1016/j.indcrop.2021.113757.

(80) Lin, F.; Liu, C.; Wang, X.; Hu, C.; Wu, S.; Xiao, R. Catalytic Oxidation of Biorefinery Corncob Lignin via Zirconium(IV) Chloride and Sodium Hydroxide in Acetonitrile/Water: A Functionality Study. *Sci. Total Environ.* **2019**, *675*, 203–212. https://doi.org/10.1016/j.scitotenv.2019.04.224.

(81) Luo, H.; Wang, L.; Li, G.; Shang, S.; Lv, Y.; Niu, J.; Gao, S. Nitrogen-Doped Carbon-Modified Cobalt-Nanoparticle-Catalyzed Oxidative Cleavage of Lignin β-O-4 Model Compounds under Mild Conditions. *ACS Sustain. Chem. Eng.* **2018**, *6* (11), 14188–14196. https://doi.org/10.1021/acssuschemeng.8b02802.

(82) Backa, S.; Rojahn, M. A. & T. Biorefineries Using Wood for Production of Speciality Cellulose Fibers, Lignosulfonates, Vanillin, Bioethanol and Biogas – the Borregaard Sarpsborg Example. In *Biomass as Energy Source*; CRC Press, 2012.

(83) Peng, M.; Muraishi, T.; Hou, X.; Zhao, M.; Kamiya, K.; Qian, E. W. Oxidative Depolymerization of Lignin to Vanillin and Lactic Acid in an Aqueous Solution. *Fuel* **2023**, *348*, 128486. https://doi.org/10.1016/j.fuel.2023.128486.

(84) Mottweiler, J.; Rinesch, T.; Besson, C.; Buendia, J.; Bolm, C. Iron-Catalysed Oxidative Cleavage of Lignin and β-O-4 Lignin Model Compounds with Peroxides in DMSO. *Green Chem.* **2015**, *17* (11), 5001–5008. https://doi.org/10.1039/C5GC01306B.

(85) Villar, J. C.; Caperos, A.; García-Ochoa, F. Oxidation of Hardwood Kraft-Lignin to Phenolic Derivatives with Oxygen as Oxidant. *Wood Sci. Technol.* **2001**, *35* (3), 245–255. https://doi.org/10.1007/s002260100089.

(86) Hdidou, L.; Kouisni, L.; Manoun, B.; Hannache, H.; Solhy, A.; Barakat, A. Oxidative Conversion of Lignin over Cobalt-Iron Mixed Oxides Prepared via the Alginate Gelation. *Catal. Commun.* **2018**, *117*, 99–104. https://doi.org/10.1016/j.catcom.2018.08.027.

(87) Hdidou, L.; Khallouk, K.; Solhy, A.; Manoun, B.; Oukarroum, A.; Barakat, A. Synthesis of CoFeO Mixed Oxides via an Alginate Gelation Process as Efficient Heterogeneous Catalysts for Lignin Depolymerization in Water. *Catal. Sci. Technol.* **2018**, *8* (21), 5445–5453. https://doi.org/10.1039/C8CY00576A.

(88) Voitl, T.; Rohr, P. R. von. Demonstration of a Process for the Conversion of Kraft Lignin into Vanillin and Methyl Vanillate by Acidic Oxidation in Aqueous Methanol. *Ind. Eng. Chem. Res.* **2010**, *49* (2), 520–525. https://doi.org/10.1021/ie901293p.

(89) Zhao, Y.; Xu, Q.; Pan, T.; Zuo, Y.; Fu, Y.; Guo, Q.-X. Depolymerization of Lignin by Catalytic Oxidation with Aqueous Polyoxometalates. *Appl. Catal. Gen.* **2013**, *467*, 504–508. https://doi.org/10.1016/j.apcata.2013.07.044.

(90) Yang, M.; Xu, A.; Du, H.; Sun, C.; Li, C. Removal of Salicylic Acid on Perovskite-Type Oxide LaFeO3 Catalyst in Catalytic Wet Air Oxidation Process. *J. Hazard. Mater.* **2007**, *139* (1), 86–92. https://doi.org/10.1016/j.jhazmat.2006.06.001.

(91) Deng, H.; Lin, L.; Sun, Y.; Pang, C.; Zhuang, J.; Ouyang, P.; Li, Z.; Liu, S. Perovskite-Type Oxide LaMnO3: An Efficient and Recyclable Heterogeneous Catalyst for the Wet Aerobic Oxidation of Lignin to Aromatic Aldehydes. *Catal. Lett.* **2008**, *126* (1), 106–111. https://doi.org/10.1007/s10562-008-9588-0.

(92) Zhang, J.; Deng, H.; Lin, L. Wet Aerobic Oxidation of Lignin into Aromatic Aldehydes Catalysed by a Perovskite-Type Oxide: LaFe1-xCuxO3 (X=0, 0.1, 0.2). *Molecules* **2009**, *14* (8), 2747–2757. https://doi.org/10.3390/molecules14082747.

(93) Deng, H.; Lin, L.; Sun, Y.; Pang, C.; Zhuang, J.; Ouyang, P.; Li, J.; Liu, S. Activity and Stability of Perovskite-Type Oxide LaCoO3 Catalyst in Lignin Catalytic Wet Oxidation to Aromatic Aldehydes Process. *Energy Fuels* **2009**, *23* (1), 19–24. https://doi.org/10.1021/ef8005349.

(94) Wang, Y.; Wei, L.; Hou, Q.; Mo, Z.; Liu, X.; Li, W. A Review on Catalytic Depolymerization of Lignin towards High-Value Chemicals: Solvent and Catalyst. *Fermentation* **2023**, *9* (4), 386. https://doi.org/10.3390/fermentation9040386.

(95) Shu, R.; Long, J.; Xu, Y.; Ma, L.; Zhang, Q.; Wang, T.; Wang, C.; Yuan, Z.; Wu, Q. Investigation on the Structural Effect of Lignin during the Hydrogenolysis Process. *Bioresour. Technol.* **2016**, *200*, 14–22. https://doi.org/10.1016/j.biortech.2015.09.112.

(96) Chen, M.; Li, Y.; Lu, F.; Luterbacher, J. S.; Ralph, J. Lignin Hydrogenolysis: Phenolic Monomers from Lignin and Associated Phenolates across Plant Clades. *ACS Sustain. Chem. Eng.* **2023**, *11* (27), 10001–10017. https://doi.org/10.1021/acssuschemeng.3c01320.

(97) Shen, Z.; Shi, C.; Liu, F.; Wang, W.; Ai, M.; Huang, Z.; Zhang, X.; Pan, L.; Zou, J.-J. Advances in Heterogeneous Catalysts for Lignin Hydrogenolysis. *Adv. Sci.* **2024**, *11* (1), 2306693. https://doi.org/10.1002/advs.202306693.

(98) Rensel, D. J.; Rouvimov, S.; Gin, M. E.; Hicks, J. C. Highly Selective Bimetallic FeMoP Catalyst for C–O Bond Cleavage of Aryl Ethers. *J. Catal.* **2013**, *305*, 256–263. https://doi.org/10.1016/j.jcat.2013.05.026.

(99) Chen, J.; Lu, F.; Si, X.; Nie, X.; Chen, J.; Lu, R.; Xu, J. High Yield Production of Natural Phenolic Alcohols from Woody Biomass Using a Nickel-Based Catalyst. *ChemSusChem* **2016**, *9* (23), 3353–3360. https://doi.org/10.1002/cssc.201601273.

(100) Paone, E.; Beneduci, A.; Corrente, G. A.; Malara, A.; Mauriello, F. Hydrogenolysis of Aromatic Ethers under Lignin-First Conditions. *Mol. Catal.* **2020**, *497*, 111228. https://doi.org/10.1016/j.mcat.2020.111228.

(101) Jeong, H.; Park, J. B.; Oh, D. H.; Yoo, C. G.; Jeong, K.; Kim, K. H. Comparative Analysis of Catalytic Hydrogenolysis of Technical Lignins and Lignin Model

Compounds. *Energy Fuels* **2024**, *38* (18), 17717–17725. https://doi.org/10.1021/acs.energyfuels.4c03293.

(102) Huang, X.; Atay, C.; Zhu, J.; Palstra, S. W. L.; Korányi, T. I.; Boot, M. D.; Hensen, E. J. M. Catalytic Depolymerization of Lignin and Woody Biomass in Supercritical Ethanol: Influence of Reaction Temperature and Feedstock. *ACS Sustain. Chem. Eng.* **2017**, *5* (11), 10864–10874. https://doi.org/10.1021/acssuschemeng.7b02790.

(103) Huang, X.; Korányi, T. I.; Boot, M. D.; Hensen, E. J. M. Catalytic Depolymerization of Lignin in Supercritical Ethanol. *ChemSusChem* **2014**, *7* (8), 2276–2288. https://doi.org/10.1002/cssc.201402094.

(104) Xie, J.; Wu, X.; Zhang, J.; Dai, X.; Li, Z.; Li, C. The Highly Selective Conversion of Lignin Models and Organosolv Lignin to Amines over a Ru/C Catalyst. *RSC Sustain.* **2023**, *1* (8), 2066–2071. https://doi.org/10.1039/D3SU00250K.

(105) Dutta, T.; Isern, N. G.; Sun, J.; Wang, E.; Hull, S.; Cort, J. R.; Simmons, B. A.; Singh, S. Survey of Lignin-Structure Changes and Depolymerization during Ionic Liquid Pretreatment. *ACS Sustain. Chem. Eng.* **2017**, *5* (11), 10116–10127. https://doi.org/10.1021/acssuschemeng.7b02123.

(106) Deuss, P. J.; Scott, M.; Tran, F.; Westwood, N. J.; de Vries, J. G.; Barta, K. Aromatic Monomers by in Situ Conversion of Reactive Intermediates in the Acid-Catalyzed Depolymerization of Lignin. *J. Am. Chem. Soc.* **2015**, *137* (23), 7456–7467. https://doi.org/10.1021/jacs.5b03693.

(107) Holmelid, B.; Barth, T.; Brusletto, R.; Kleinert, M. Production of Monomeric Phenols by Formic Acid Assisted Hydrous Liquefaction of Lignin. *Biomass Bioenergy* **2017**, *105*, 298–309. https://doi.org/10.1016/j.biombioe.2017.07.017.

(108) Jiang, Y.; Li, Z.; Tang, X.; Sun, Y.; Zeng, X.; Liu, S.; Lin, L. Depolymerization of Cellulolytic Enzyme Lignin for the Production of Monomeric Phenols over Raney Ni and Acidic Zeolite Catalysts. *Energy Fuels* **2015**, *29* (3), 1662–1668. https://doi.org/10.1021/ef5022297.

(109) Stärk, K.; Taccardi, N.; Bösmann, A.; Wasserscheid, P. Oxidative Depolymerization of Lignin in Ionic Liquids. *ChemSusChem* **2010**, *3* (6), 719–723. https://doi.org/10.1002/cssc.200900242.

(110) Sturgeon, M. R.; Kim, S.; Lawrence, K.; Paton, R. S.; Chmely, S. C.; Nimlos, M.; Foust, T. D.; Beckham, G. T. A Mechanistic Investigation of Acid-Catalyzed Cleavage of Aryl-Ether Linkages: Implications for Lignin Depolymerization in Acidic Environments. *ACS Sustain. Chem. Eng.* **2014**, *2* (3), 472–485. https://doi.org/10.1021/sc400384w.

(111) Deepa, A. K.; Dhepe, P. L. Lignin Depolymerization into Aromatic Monomers over Solid Acid Catalysts. *ACS Catal.* **2015**, *5* (1), 365–379. https://doi.org/10.1021/cs501371q.

(112) Nandiwale, K. Y.; Danby, A. M.; Ramanathan, A.; Chaudhari, R. V.; Motagamwala, A. H.; Dumesic, J. A.; Subramaniam, B. Enhanced Acid-Catalyzed Lignin Depolymerization in a Continuous Reactor with Stable Activity. *ACS Sustain. Chem. Eng.* **2020**, *8* (10), 4096–4106. https://doi.org/10.1021/acssuschemeng.9b06556.

(113) Paananen, H.; Eronen, E.; Mäkinen, M.; Jänis, J.; Suvanto, M.; Pakkanen, T. T. Base-Catalyzed Oxidative Depolymerization of Softwood Kraft Lignin. *Ind. Crops Prod.* **2020**, *152*, 112473. https://doi.org/10.1016/j.indcrop.2020.112473.

(114) Roy, R.; Rahman, M. S.; Amit, T. A.; Jadhav, B. Recent Advances in Lignin Depolymerization Techniques: A Comparative Overview of Traditional and Greener Approaches. *Biomass* **2022**, *2* (3), 130–154. https://doi.org/10.3390/biomass2030009.

(115) Castro Garcia, A.; Cheng, S.; McGlynn, S. E.; Cross, J. S. Machine Learning Model Insights into Base-Catalyzed Hydrothermal Lignin Depolymerization. *ACS Omega* **2023**, *8* (35), 32078–32089. https://doi.org/10.1021/acsomega.3c04168.

(116) Schmiedl, D.; Böringer, S.; Tübke, B.; Liitiä, T.; Rovio, S.; Tamminen, T.; Rencoret, J.; Gutiérrez, A.; del Rio, J. C. Kraft Lignin Depolymerisation by Base Catalysed Degradation–Effect of Process Parameters on Conversion Degree, Structural Features of BCD Fractions and Their …. In *NWBC 2015: The 6th Nordig Wood Biorefinery Conference : Helsinki, Finland, 20-22 October, 2015*; Hytönen, E., Ed.; VTT technology; VTT Technical Research Centre of Finland Ltd: Espoo, 2015; Vol. 233.

(117) Hidajat, M. J.; Riaz, A.; Park, J.; Insyani, R.; Verma, D.; Kim, J. Depolymerization of Concentrated Sulfuric Acid Hydrolysis Lignin to High-Yield

Aromatic Monomers in Basic Sub- and Supercritical Fluids. *Chem. Eng. J.* **2017**, *317*, 9–19. https://doi.org/10.1016/j.cej.2017.02.045.

(118) Katahira, R.; Mittal, A.; McKinney, K.; Chen, X.; Tucker, M. P.; Johnson, D. K.; Beckham, G. T. Base-Catalyzed Depolymerization of Biorefinery Lignins. *ACS Sustain. Chem. Eng.* **2016**, *4* (3), 1474–1486. https://doi.org/10.1021/acssuschemeng.5b01451.

(119) Erdocia, X.; Prado, R.; Corcuera, M. Á.; Labidi, J. Base Catalyzed Depolymerization of Lignin: Influence of Organosolv Lignin Nature. *Biomass Bioenergy* **2014**, *66*, 379–386. https://doi.org/10.1016/j.biombioe.2014.03.021.

(120) Kim, G. H.; Kim, Y. I.; Um, B. H. Base-Catalyzed Depolymerization of Organosolv Lignin into Monoaromatic Phenolic Compounds. *Waste Biomass Valorization* **2024**. https://doi.org/10.1007/s12649-024-02655-5.

(121) Chaudhary, R.; L. Dhepe, P. Solid Base Catalyzed Depolymerization of Lignin into Low Molecular Weight Products. *Green Chem.* **2017**, *19* (3), 778–788. https://doi.org/10.1039/C6GC02701F.

(122) Biswas, B.; Kumar, A.; Krishna, B. B.; Bhaskar, T. Effects of Solid Base Catalysts on Depolymerization of Alkali Lignin for the Production of Phenolic Monomer Compounds. *Renew. Energy* **2021**, *175*, 270–280. https://doi.org/10.1016/j.renene.2021.04.039.

(123) Kawamoto, H. Lignin Pyrolysis Reactions. *J. Wood Sci.* **2017**, *63* (2), 117–132. https://doi.org/10.1007/s10086-016-1606-z.

(124) Al Arni, S. Comparison of Slow and Fast Pyrolysis for Converting Biomass into Fuel. *Renew. Energy* **2018**, *124*, 197–201. https://doi.org/10.1016/j.renene.2017.04.060.

(125) Shen, D.; Liu, G.; Zhao, J.; Xue, J.; Guan, S.; Xiao, R. Thermo-Chemical Conversion of Lignin to Aromatic Compounds: Effect of Lignin Source and Reaction Temperature. *J. Anal. Appl. Pyrolysis* **2015**, *112*, 56–65. https://doi.org/10.1016/j.jaap.2015.02.022.

(126) Kibet, J.; Khachatryan, L.; Dellinger, B. Molecular Products and Radicals from Pyrolysis of Lignin. *Environ. Sci. Technol.* **2012**, *46* (23), 12994–13001. https://doi.org/10.1021/es302942c.

(127) Patwardhan, P. R.; Brown, R. C.; Shanks, B. H. Understanding the Fast Pyrolysis of Lignin. *ChemSusChem* **2011**, *4* (11), 1629–1636. https://doi.org/10.1002/cssc.201100133.

(128) Fan, L.; Ruan, R.; Li, J.; Ma, L.; Wang, C.; Zhou, W. Aromatics Production from Fast Co-Pyrolysis of Lignin and Waste Cooking Oil Catalyzed by HZSM-5 Zeolite. *Appl. Energy* **2020**, *263*, 114629. https://doi.org/10.1016/j.apenergy.2020.114629.

(129) Ke, L.; Wu, Q.; Zhou, N.; Xiong, J.; Yang, Q.; Zhang, L.; Wang, Y.; Dai, L.; Zou, R.; Liu, Y.; Ruan, R.; Wang, Y. Lignocellulosic Biomass Pyrolysis for Aromatic Hydrocarbons Production: Pre and in-Process Enhancement Methods. *Renew. Sustain. Energy Rev.* **2022**, *165*, 112607. https://doi.org/10.1016/j.rser.2022.112607.

(130) Wu, L.; Liu, J.; Chen, L.; Wang, X.; Zhou, Q.; Yu, F.; Liang, J. Hierarchical Beta Zeolites Assisted Aromatics Production from Lignin via Catalytic Fast Pyrolysis. *Chem. Eng. J.* **2024**, *484*, 149618. https://doi.org/10.1016/j.cej.2024.149618.

(131) Shen, D.; Zhao, J.; Xiao, R.; Gu, S. Production of Aromatic Monomers from Catalytic Pyrolysis of Black-Liquor Lignin. *J. Anal. Appl. Pyrolysis* **2015**, *111*, 47–54. https://doi.org/10.1016/j.jaap.2014.12.013.

(132) Motta, I. L.; Miranda, N. T.; Maciel Filho, R.; Wolf Maciel, M. R. Biomass Gasification in Fluidized Beds: A Review of Biomass Moisture Content and Operating Pressure Effects. *Renew. Sustain. Energy Rev.* **2018**, *94*, 998–1023. https://doi.org/10.1016/j.rser.2018.06.042.

(133) Doassans-Carrère, N.; Ferrasse, J.-H.; Boutin, O.; Mauviel, G.; Lédé, J. Comparative Study of Biomass Fast Pyrolysis and Direct Liquefaction for Bio-Oils Production: Products Yield and Characterizations. *Energy Fuels* **2014**, *28* (8), 5103–5111. https://doi.org/10.1021/ef500641c.

(134) Kruse, A.; Funke, A.; Titirici, M.-M. Hydrothermal Conversion of Biomass to Fuels and Energetic Materials. *Curr. Opin. Chem. Biol.* **2013**, *17* (3), 515–521. https://doi.org/10.1016/j.cbpa.2013.05.004.

(135) Kruse, A. Hydrothermal Biomass Gasification. *J. Supercrit. Fluids* **2009**, *47* (3), 391–399. https://doi.org/10.1016/j.supflu.2008.10.009.

(136) Toor, S. S.; Rosendahl, L.; Rudolf, A. Hydrothermal Liquefaction of Biomass: A Review of Subcritical Water Technologies. *Energy* **2011**, *36* (5), 2328–2342. https://doi.org/10.1016/j.energy.2011.03.013.

(137) Gollakota, A. R. K.; Kishore, N.; Gu, S. A Review on Hydrothermal Liquefaction of Biomass. *Renew. Sustain. Energy Rev.* **2018**, *81*, 1378–1392. https://doi.org/10.1016/j.rser.2017.05.178.

(138) González-Arias, J.; Sánchez, M. E.; Cara-Jiménez, J.; Baena-Moreno, F. M.; Zhang, Z. Hydrothermal Carbonization of Biomass and Waste: A Review. *Environ. Chem. Lett.* **2022**, *20* (1), 211–221. https://doi.org/10.1007/s10311-021-01311-x.

(139) Reza, M. T.; Lynam, J. G.; Uddin, M. H.; Coronella, C. J. Hydrothermal Carbonization: Fate of Inorganics. *Biomass Bioenergy* **2013**, *49*, 86–94. https://doi.org/10.1016/j.biombioe.2012.12.004.

(140) Kruse, A. Supercritical Water Gasification. *Biofuels Bioprod. Biorefining* **2008**, *2* (5), 415–437. https://doi.org/10.1002/bbb.93.

(141) Elliott, D. C. Catalytic Hydrothermal Gasification of Biomass. *Biofuels Bioprod. Biorefining* **2008**, *2* (3), 254–265. https://doi.org/10.1002/bbb.74.

(142) Wagner, W.; Pruß, A. The IAPWS Formulation 1995 for the Thermodynamic Properties of Ordinary Water Substance for General and Scientific Use. *J. Phys. Chem. Ref. Data* **2002**, *31* (2), 387–535. https://doi.org/10.1063/1.1461829.

(143) *Release on the Ionization Constant of H2O*; IAPWS: Banff, Canada, 2019.

(144) Uematsu, M.; Franck, E. U. Static Dielectric Constant of Water and Steam. *J. Phys. Chem. Ref. Data* **1980**, *9* (4), 1291–1306. https://doi.org/10.1063/1.555632.

(145) Kruse, A.; Dahmen, N. Water – A Magic Solvent for Biomass Conversion. *J. Supercrit. Fluids* **2015**, *96*, 36–45. https://doi.org/10.1016/j.supflu.2014.09.038.

(146) Akiya, N.; Savage, P. E. Roles of Water for Chemical Reactions in High-Temperature Water. *Chem. Rev.* **2002**, *102* (8), 2725–2750. https://doi.org/10.1021/cr000668w.

(147) Hunter, S. E.; Savage, P. E. Recent Advances in Acid- and Base-Catalyzed Organic Synthesis in High-Temperature Liquid Water. *Chem. Eng. Sci.* **2004**, *59* (22–23), 4903–4909. https://doi.org/10.1016/j.ces.2004.09.009.

(148) Belkheiri, T.; Andersson, S.-I.; Mattsson, C.; Olausson, L.; Theliander, H.; Vamling, L. Hydrothermal Liquefaction of Kraft Lignin in Subcritical Water: Influence of Phenol as Capping Agent. *Energy Fuels* **2018**, *32* (5), 5923–5932. https://doi.org/10.1021/acs.energyfuels.8b00068.

(149) Belkheiri, T.; Andersson, S.-I.; Mattsson, C.; Olausson, L.; Theliander, H.; Vamling, L. Hydrothermal Liquefaction of Kraft Lignin in Sub-Critical Water: The Influence of the Sodium and Potassium Fraction. *Biomass Convers. Biorefinery* **2018**, *8* (3), 585–595. https://doi.org/10.1007/s13399-018-0307-9.

(150) Cao, Y.; Zhang, C.; Tsang, D. C. W.; Fan, J.; Clark, J. H.; Zhang, S. Hydrothermal Liquefaction of Lignin to Aromatic Chemicals: Impact of Lignin Structure. *Ind. Eng. Chem. Res.* **2020**, *59* (39), 16957–16969. https://doi.org/10.1021/acs.iecr.0c01617.

(151) Breunig, M.; Gebhart, P.; Hornung, U.; Kruse, A.; Dinjus, E. Direct Liquefaction of Lignin and Lignin Rich Biomasses by Heterogenic Catalytic Hydrogenolysis. *Biomass Bioenergy* **2018**, *111*, 352–360. https://doi.org/10.1016/j.biombioe.2017.06.001.

(152) Forchheim, D.; Hornung, U.; Kempe, P.; Kruse, A.; Steinbach, D. Influence of RANEY Nickel on the Formation of Intermediates in the Degradation of Lignin. *Int. J. Chem. Eng.* **2012**, *2012* (4), 1–8. https://doi.org/10.1155/2012/589749.

(153) Cheng, S.; Wilks, C.; Yuan, Z.; Leitch, M.; Xu, C. Hydrothermal Degradation of Alkali Lignin to Bio-Phenolic Compounds in Sub/Supercritical Ethanol and Water–Ethanol Co-Solvent. *Polym. Degrad. Stab.* **2012**, *97* (6), 839–848. https://doi.org/10.1016/j.polymdegradstab.2012.03.044.

(154) Toledano, A.; Serrano, L.; Labidi, J. Improving Base Catalyzed Lignin Depolymerization by Avoiding Lignin Repolymerization. *Fuel* **2014**, *116*, 617–624. https://doi.org/10.1016/j.fuel.2013.08.071.

(155) Wahyudiono; Sasaki, M.; Goto, M. Recovery of Phenolic Compounds through the Decomposition of Lignin in near and Supercritical Water. *Chem. Eng. Process. Process Intensif.* **2008**, *47* (9–10), 1609–1619. https://doi.org/10.1016/j.cep.2007.09.001.

(156) Wahyudiono; Sasaki, M.; Goto, M. Thermal Decomposition of Guaiacol in Sub- and Supercritical Water and Its Kinetic Analysis. *J. Mater. Cycles Waste Manag.* **2011**, *13* (1), 68–79. https://doi.org/10.1007/s10163-010-0309-6.

(157) Wahyudiono; Sasaki, M.; Goto, M. Conversion of Biomass Model Compound under Hydrothermal Conditions Using Batch Reactor. *Fuel* **2009**, *88* (9), 1656–1664. https://doi.org/10.1016/j.fuel.2009.02.028.

(158) Yong, T. L.-K.; Matsumura, Y. Reaction Kinetics of the Lignin Conversion in Supercritical Water. *Ind. Eng. Chem. Res.* **2012**, *51* (37), 11975–11988. https://doi.org/10.1021/ie300921d.

(159) Yong, T. L.-K.; Matsumura, Y. Kinetic Analysis of Lignin Hydrothermal Conversion in Sub- and Supercritical Water. *Ind. Eng. Chem. Res.* **2013**, *52* (16), 5626–5639. https://doi.org/10.1021/ie400600x.

(160) Niemelä, K.; Alén, R. Characterization of Pulping Liquors. In *Analytical methods in wood chemistry, pulping, and papermaking*; Alén, R., Sjöström, E., Eds.; Springer Series in Wood Science; Springer: Berlin, Germany; New York, New York, 1999; pp 193–231. https://doi.org/10.1007/978-3-662-03898-7_7.

(161) Morya, R.; Kumar, M.; Tyagi, I.; Kumar Pandey, A.; Park, J.; Raj, T.; Sirohi, R.; Kumar, V.; Kim, S.-H. Recent Advances in Black Liquor Valorization. *Bioresour. Technol.* **2022**, *350*, 126916. https://doi.org/10.1016/j.biortech.2022.126916.

(162) Jia, Y.; Wang, Y.; Wang, M.; Li, B.; Song, X.; Wu, M.; Nong, G.; Yin, Y. Efficient Separation of Biofuel, Lignin and Alkali from Black Liquor by Acid Precipitation and Ethanol Extraction for Valorization. *Ind. Crops Prod.* **2024**, *209*, 117987. https://doi.org/10.1016/j.indcrop.2023.117987.

(163) Ribeiro Domingos, M. E. G.; Flórez-Orrego, D.; dos Santos, M. T.; de Oliveira Junior, S.; Maréchal, F. Process Modeling and Integration of Hydrogen and Synthetic Natural Gas Production in a Kraft Pulp Mill via Black Liquor Gasification. *Renew. Energy* **2023**, *219*, 119396. https://doi.org/10.1016/j.renene.2023.119396.

(164) Harisankar, S.; Vinu, R. Platform Chemicals from Hardwood Black Liquor via Hydrothermal Liquefaction: Influence of Process Conditions on Product Yields and Quality. *Sustain. Energy Fuels* **2023**, *7* (18), 4423–4441. https://doi.org/10.1039/D3SE00308F.

(165) Orebom, A.; Verendel, J. J.; Samec, J. S. M. High Yields of Bio Oils from Hydrothermal Processing of Thin Black Liquor without the Use of Catalysts or Capping Agents. *ACS Omega* **2018**, *3* (6), 6757–6763. https://doi.org/10.1021/acsomega.8b00854.

(166) Huet, M.; Roubaud, A.; Chirat, C.; Lachenal, D. Hydrothermal Treatment of Black Liquor for Energy and Phenolic Platform Molecules Recovery in a Pulp Mill. *Biomass Bioenergy* **2016**, *89*, 105–112. https://doi.org/10.1016/j.biombioe.2016.03.023.

(167) *Black Liquor to fuels - project website*. BL2F. https://www.bl2f.eu/about-the-project/ (accessed 2025-01-07).

(168) Wang, R.; Deplazes, R.; Vogel, F.; Baudouin, D. Continuous Extraction of Black Liquor Salts under Hydrothermal Conditions. *Ind. Eng. Chem. Res.* **2021**, *60* (10), 4072–4085. https://doi.org/10.1021/acs.iecr.0c05203.

(169) Canabarro, N. I.; Yeadon, D. J.; Wörner, M.; Hornung, U.; Vogel, F.; Baudouin, D. Development of Strategies for Continuous Desalination of Weak Black Liquor Based on Phase-Behaviour Analysis. *J. Supercrit. Fluids* **2024**, *209*, 106230. https://doi.org/10.1016/j.supflu.2024.106230.

(170) Cardoso, M.; Oliveira, É. D.; Passos, M. L. Chemical Composition and Physical Properties of Black Liquors and Their Effects on Liquor Recovery Operation in Brazilian Pulp Mills. *Fuel* **2009**, *88* (4), 756–763. https://doi.org/10.1016/j.fuel.2008.10.016.

(171) Forchheim, D.; Hornung, U.; Kruse, A.; Sutter, T. Kinetic Modelling of Hydrothermal Lignin Depolymerisation. *Waste Biomass Valorization* **2014**, *5* (6), 985–994. https://doi.org/10.1007/s12649-014-9307-6.

(172) Argyropoulos, D. S. 31P NMR in Wood Chemistry: A Review of Recent Progress. *Res. Chem. Intermed.* **1995**, *21* (3–5), 373–395. https://doi.org/10.1007/BF03052265.

(173) Kim, H.; Ralph, J.; Lu, F.; Ralph, S. A.; Boudet, A. M.; MacKay, J. J.; Sederoff, R. R.; Ito, T.; Kawai, S.; Ohashi, H.; Higuchi, T. NMR Analysis of Lignins in CAD-Deficient Plants. Part 1. Incorporation of Hydroxycinnamaldehydes and Hydroxybenzaldehydes into Lignins. *Org. Biomol. Chem.* **2003**, *1* (2), 268–281. https://doi.org/10.1039/B209686B.

(174) Terashima, N.; Atalla, R. H.; Vanderhart, D. L. Solid State NMR Spectroscopy of Specifically 13C-Enriched Lignin in Wheat Straw from Coniferin. *Phytochemistry* **1997**, *46* (5), 863–870. https://doi.org/10.1016/S0031-9422(97)00359-2.

(175) Pu, Y.; Cao, S.; Ragauskas, A. J. Application of Quantitative 31P NMR in Biomass Lignin and Biofuel Precursors Characterization. *Energy Environ. Sci.* **2011**, *4* (9), 3154. https://doi.org/10.1039/c1ee01201k.

(176) Bartolomei, E.; Le Brech, Y.; Gadiou, R.; Bertaud, F.; Leclerc, S.; Vidal, L.; Le Meins, J.-M.; Dufour, A. Depolymerization of Technical Lignins in Supercritical Ethanol: Effects of Lignin Structure and Catalyst. *Energy Fuels* **2021**, *35* (21), 17769–17783. https://doi.org/10.1021/acs.energyfuels.1c02704.

(177) Le Brech, Y.; Raya, J.; Delmotte, L.; Brosse, N.; Gadiou, R.; Dufour, A. Characterization of Biomass Char Formation Investigated by Advanced Solid State NMR. *Carbon* **2016**, *108*, 165–177. https://doi.org/10.1016/j.carbon.2016.06.033.

(178) Crestini, C.; Lange, H.; Sette, M.; Argyropoulos, D. S. On the Structure of Softwood Kraft Lignin. *Green Chem.* **2017**, *19* (17), 4104–4121. https://doi.org/10.1039/C7GC01812F.

(179) Karlsson, M.; Romson, J.; Elder, T.; Emmer, Å.; Lawoko, M. Lignin Structure and Reactivity in the Organosolv Process Studied by NMR Spectroscopy, Mass Spectrometry, and Density Functional Theory. *Biomacromolecules* **2023**, *24* (5), 2314–2326. https://doi.org/10.1021/acs.biomac.3c00186.

(180) *VDI-Wärmeatlas*; Springer Berlin Heidelberg: Berlin, Heidelberg, 2013. https://doi.org/10.1007/978-3-642-19981-3.

(181) Korntner, P.; Sumerskii, I.; Bacher, M.; Rosenau, T.; Potthast, A. Characterization of Technical Lignins by NMR Spectroscopy: Optimization of Functional Group Analysis by 31 P NMR Spectroscopy. *Holzforschung* **2015**, *69* (6), 807–814. https://doi.org/10.1515/hf-2014-0281.

(182) Belkheiri, T.; Mattsson, C.; Andersson, S.-I.; Olausson, L.; Åmand, L.-E.; Theliander, H.; Vamling, L. Effect of pH on Kraft Lignin Depolymerisation in Subcritical Water. *Energy Fuels* **2016**, *30* (6), 4916–4924. https://doi.org/10.1021/acs.energyfuels.6b00462.

(183) Schuler, J.; Hornung, U.; Dahmen, N.; Sauer, J. Lignin from Bark as a Resource for Aromatics Production by Hydrothermal Liquefaction. *GCB Bioenergy* **2019**, *11* (1), 218–229. https://doi.org/10.1111/gcbb.12562.

(184) Nimmanwudipong, T.; Runnebaum, R. C.; Block, D. E.; Gates, B. C. Catalytic Conversion of Guaiacol Catalyzed by Platinum Supported on Alumina: Reaction Network Including Hydrodeoxygenation Reactions. *Energy Fuels* **2011**, *25* (8), 3417–3427. https://doi.org/10.1021/ef200803d.

(185) Ishikawa, M.; Tamura, M.; Nakagawa, Y.; Tomishige, K. Demethoxylation of Guaiacol and Methoxybenzenes over Carbon-Supported Ru–Mn Catalyst. *Appl. Catal. B Environ.* **2016**, *182*, 193–203. https://doi.org/10.1016/j.apcatb.2015.09.021.

(186) Zhu, X.; Lobban, L. L.; Mallinson, R. G.; Resasco, D. E. Bifunctional Transalkylation and Hydrodeoxygenation of Anisole over a Pt/HBeta Catalyst. *J. Catal.* **2011**, *281* (1), 21–29. https://doi.org/10.1016/j.jcat.2011.03.030.

(187) Ma, H.; Li, T.; Wu, S.; Zhang, X. Demethylation of a Methoxy Group to Inhibit Repolymerization during Alkaline Lignin Pyrolysis. *Fuel* **2021**, *286*, 119394. https://doi.org/10.1016/j.fuel.2020.119394.

(188) Wang, C.; Fan, Y.; Hornung, U.; Zhu, W.; Dahmen, N. Char and Tar Formation during Hydrothermal Treatment of Sewage Sludge in Subcritical and Supercritical Water: Effect of Organic Matter Composition and Experiments with Model Compounds. *J. Clean. Prod.* **2020**, *242*, 118586. https://doi.org/10.1016/j.jclepro.2019.118586.

(189) Towfighi, J.; Sadrameli, M.; Niaei, A. Coke Formation Mechanisms and Coke Inhibiting Methods in Pyrolysis Furnaces. *J. Chem. Eng. Jpn.* **2002**, *35* (10), 923–937. https://doi.org/10.1252/jcej.35.923.

(190) Asafu-Adjaye, O. A.; Street, J.; Bansode, A.; Auad, M. L.; Peresin, M. S.; Adhikari, S.; Liles, T.; Via, B. K. Fast Pyrolysis Bio-Oil-Based Epoxy as an Adhesive in Oriented Strand Board Production. *Polymers* **2022**, *14* (6). https://doi.org/10.3390/polym14061244.

(191) Li, M.; Yoo, C. G.; Pu, Y.; Ragauskas, A. J. 31 P NMR Chemical Shifts of Solvents and Products Impurities in Biomass Pretreatments. *ACS Sustain. Chem. Eng.* **2018**, *6* (1), 1265–1270. https://doi.org/10.1021/acssuschemeng.7b03602.

(192) Zhao, J.; Xiuwen, W.; Hu, J.; Liu, Q.; Shen, D.; Xiao, R. Thermal Degradation of Softwood Lignin and Hardwood Lignin by TG-FTIR and Py-GC/MS. *Polym. Degrad. Stab.* **2014**, *108*, 133–138. https://doi.org/10.1016/j.polymdegradstab.2014.06.006.

(193) Pipitone, G.; Zoppi, G.; Bocchini, S.; Rizzo, A. M.; Chiaramonti, D.; Pirone, R.; Bensaid, S. Aqueous Phase Reforming of the Residual Waters Derived from Lignin-Rich Hydrothermal Liquefaction: Investigation of Representative Organic Compounds and Actual Biorefinery Streams. *Catal. Today* **2020**, *345*, 237–250. https://doi.org/10.1016/j.cattod.2019.09.040.

(194) Pola, L.; Collado, S.; Wörner, M.; Hornung, U.; Díaz, M. Eutectic Solvents for the Valorisation of the Aqueous Phase from Hydrothermally Liquefied Black Liquor. *J. Environ. Chem. Eng.* **2023**, *11* (5), 111040. https://doi.org/10.1016/j.jece.2023.111040.

(195) Gasson, J. R.; Forchheim, D.; Sutter, T.; Hornung, U.; Kruse, A.; Barth, T. Modeling the Lignin Degradation Kinetics in an Ethanol/Formic Acid Solvolysis Approach. Part 1. Kinetic Model Development. *Ind. Eng. Chem. Res.* **2012**, *51* (32), 10595–10606. https://doi.org/10.1021/ie301487v.

(196) Jayathilake, M.; Rudra, S.; Rosendahl, L. A. Hydrothermal Liquefaction of Wood Using a Modified Multistage Shrinking-Core Model. *Fuel* **2020**, *280*, 118616. https://doi.org/10.1016/j.fuel.2020.118616.

(197) Hashmi, S. F.; Meriö-Talvio, H.; Hakonen, K. J.; Ruuttunen, K.; Sixta, H. Hydrothermolysis of Organosolv Lignin for the Production of Bio-Oil Rich in Monoaromatic Phenolic Compounds. *Fuel Process. Technol.* **2017**, *168*, 74–83. https://doi.org/10.1016/j.fuproc.2017.09.005.

(198) Pan, Z.; Wu, X.; Bodi, A.; Bokhoven, J. A. van; Hemberger, P. Catalytic Pyrolysis Mechanism of Lignin Moieties Driven by Aldehyde, Hydroxyl, Methoxy, and Allyl Functionalization: The Role of Reactive Quinone Methide and Ketene Intermediates. *Green Chem.* **2024**, *26* (18), 9899–9910. https://doi.org/10.1039/D4GC03143A.

(199) Boukis, N.; Diem, V.; Habicht, W.; Dinjus, E. Methanol Reforming in Supercritical Water. *Ind. Eng. Chem. Res.* **2003**, *42* (4), 728–735. https://doi.org/10.1021/ie020557i.

(200) Yaws, C. L. *The Yaws Handbook of Vapor Pressure: Antoine Coefficients*, 2nd edition.; Elsevier/GPP, Gulf Professional Publishing is an imprint of Elsevier: Amsterdam Boston, 2015.

(201) James, G.; Witten, D.; Hastie, T.; Tibshirani, R. *An Introduction to Statistical Learning: With Applications in R*, Zweite Ausgabe 2021 Edition.; Springer: New York, 2021.

(202) Slotboom, Y.; Bos, M. J.; Pieper, J.; Vrieswijk, V.; Likozar, B.; Kersten, S. R. A.; Brilman, D. W. F. Critical Assessment of Steady-State Kinetic Models for the Synthesis of Methanol over an Industrial Cu/ZnO/Al2O3 Catalyst. *Chem. Eng. J.* **2020**, *389*, 124181. https://doi.org/10.1016/j.cej.2020.124181.

(203) Rodrigues Niquini, G.; Lacerda de Oliveira Campos, B.; Herrera Delgado, K.; Pitter, S.; Sauer, J. Experimental Study and Comprehensive Kinetic Modeling of the Direct Dimethyl Ether Synthesis on Cu/ZnO/ZrO2 and H-FER-20. *Chem. Eng. J.* **2024**, *480*, 147968. https://doi.org/10.1016/j.cej.2023.147968.

(204) Kruse, A.; Meier, D.; Rimbrecht, P.; Schacht, M. Gasification of Pyrocatechol in Supercritical Water in the Presence of Potassium Hydroxide. *Ind. Eng. Chem. Res.* **2000**, *39* (12), 4842–4848. https://doi.org/10.1021/ie0001570.

(205) Yang, H.; Yin, W.; Zhu, X.; Deuss, P. J.; Heeres, H. J. Selective Demethoxylation of Guaiacols to Phenols Using Supported MoO3 Catalysts. *ChemCatChem* **2022**, *14* (16), e202200297. https://doi.org/10.1002/cctc.202200297.

(206) Ren, X.; Qiang, Q.; Sun, Z.; Wei, T.; Yu, X.; Rong, Z.; Li, C. Water Splitting Integrated with Self-Transfer Hydrogenolysis for Efficient Demethoxylation of Guaiacols to Phenols over the Ni/MgO Catalyst. *ACS Catal.* **2024**, *14* (7), 5247–5259. https://doi.org/10.1021/acscatal.4c00038.

(207) Schuler, J.; Hornung, U.; Kruse, A.; Dahmen, N.; Sauer, J. Hydrothermal Liquefaction of Lignin. *J. Biomater. Nanobiotechnology* **2017**, *08* (01), 96–108. https://doi.org/10.4236/jbnb.2017.81007.

(208) Schuler, J. *Hydrothermal Liquefaction of Lignin*; Karlsruhe, 2020. https://doi.org/10.5445/IR/1000117444.

(209) Abad-Fernández, N.; Pérez, E.; Cocero, M. J. Aromatics from Lignin through Ultrafast Reactions in Water. *Green Chem.* **2019**, *21* (6), 1351–1360. https://doi.org/10.1039/C8GC03989E.

(210) Abad-Fernández, N.; Pérez, E.; Martín, Á.; Cocero, M. J. Kraft Lignin Depolymerisation in Sub- and Supercritical Water Using Ultrafast Continuous Reactors. Optimization and Reaction Kinetics. *J. Supercrit. Fluids* **2020**, *165*, 104940. https://doi.org/10.1016/j.supflu.2020.104940.

(211) Rana, M.; Taki, G.; Islam, M. N.; Agarwal, A.; Jo, Y.-T.; Park, J.-H. Effects of Temperature and Salt Catalysts on Depolymerization of Kraft Lignin to Aromatic Phenolic Compounds. *Energy Fuels* **2019**, *33* (7), 6390–6404. https://doi.org/10.1021/acs.energyfuels.9b00808.

(212) May, P. M.; Batka, D.; Hefter, G.; Königsberger, E.; Rowland, D. Goodbye to S2- in Aqueous Solution. *Chem. Commun. Camb. Engl.* **2018**, *54* (16), 1980–1983. https://doi.org/10.1039/c8cc00187a.

(213) Cheremisinoff, N. P. *Best Practices in the Wood and Paper Industries*, 1. ed.; Handbook of pollution prevention and cleaner production / Nicholas P. Cheremisinoff; Elsevier: Amsterdam, 2010; Vol. Vol. 2.

(214) Rostrup-Nielsen, J. R. Sulfur Poisoning. In *Progress in Catalyst Deactivation: Proceedings of the NATO Advanced Study Institute on Catalyst Deactivation, Algarve, Portugal, May 18-29, 1981*; Figueiredo, J. L., Ed.; NATO Advanced Study Institutes Series, Series E; Springer: Dordrecht, 1982; Vol. 54, pp 209–227. https://doi.org/10.1007/978-94-009-7597-2_11.

(215) Kabe, T.; Ishihara, A.; Qian, W. *Hydrodesulfurization and Hydrodenitrogenation: Chemistry and Engineering*; Wiley-VCH; Kodansha: Weinheim; Berlin; Tokyo, 1999.

(216) Gierer, J. Chemical Aspects of Kraft Pulping. *Wood Sci. Technol.* **1980**, *14* (4), 241–266. https://doi.org/10.1007/BF00383453.

(217) Karnofski, M. A. Odor Generation in the Kraft Process. *J. Chem. Educ.* **1975**, *52* (8), 490. https://doi.org/10.1021/ed052p490.

(218) Bordado, J. C.; Gomes, J. F. Characterisation of Non-Condensable Sulphur Containing Gases from Kraft Pulp Mills. *Chemosphere* **2001**, *44* (5), 1011–1016. https://doi.org/10.1016/S0045-6535(00)00483-5.

(219) Bordado, J. C. M.; Gomes, J. F. P. Emission and Odour Control in Kraft Pulp Mills. *J. Clean. Prod.* **2003**, *11* (7), 797–801. https://doi.org/10.1016/S0959-6526(02)00101-4.

(220) Tomani, P. The Lignoboost Process. *Cellul. Chem. Technol.* **2010**, No. 44, 53–58.

(221) Jeyakumar, S.; Rastogi, R. K.; Chaudhuri, N. K.; Ramakumar, K. L. Determination of Sulphur Species in the Presence of Common Anions with Indirect Measurement of Sulphide by Ion Chromatography (IC). *Anal. Lett.* **2002**, *35* (2), 383–395. https://doi.org/10.1081/AL-120002537.

(222) Millero, F. J.; LeFerriere, A.; Fernandez, M.; Hubinger, S.; Hershey, J. P. Oxidation of Hydrogen Sulfide with Hydrogen Peroxide in Natural Waters. *Environ. Sci. Technol.* **1989**, *23* (2), 209–213. https://doi.org/10.1021/es00179a012.

(223) Takenaka, N.; Furuya, S.; Sato, K.; Bandow, H.; Maeda, Y.; Furukawa, Y. Rapid Reaction of Sulfide with Hydrogen Peroxide and Formation of Different Final Products by Freezing Compared to Those in Solution. *Int. J. Chem. Kinet.* **2003**, *35* (5), 198–205. https://doi.org/10.1002/kin.10118.

(224) Braye, E. H.; Sehon, A. H.; Darwent, B. deB. Thermal Decomposition of Sulfides. *J. Am. Chem. Soc.* **1955**, *77* (20), 5282–5285. https://doi.org/10.1021/ja01625a019.

(225) Baudouin, D.; Xiang, H.; Vogel, F. On the Selective Desulphurization of Biomass Derivatives in Supercritical Water. *Biomass Bioenergy* **2022**, *164*, 106529. https://doi.org/10.1016/j.biombioe.2022.106529.

(226) Gierer, J.; Smedman, L.-Å.; Falkehag, I.; Halvarson, H.; Nilsson, L. The Cleavage of Beta-Mercaptoalkyl-Arylethers with Alkali. *Acta Chem. Scand.* **1964**, *18*, 1244–1248. https://doi.org/10.3891/acta.chem.scand.18-1244.

(227) Gierer, J.; Smedman, L.-Å.; Cederberg, G.; Jensen, R. B.; Pederson, C. T.; Larsen, E. The Reactions of Lignin during Sulphate Cooking. Part VIII. The Mechanism of Splitting of Beta-Arylether Bonds in Phenolic Units by White Liquor. *Acta Chem. Scand.* **1965**, *19*, 1103–1112. https://doi.org/10.3891/acta.chem.scand.19-1103.

(228) Gaspar, A.; Zellermann, E.; Lababidi, S.; Reece, J.; Schrader, W. Characterization of Saturates, Aromatics, Resins, and Asphaltenes Heavy Crude Oil

Fractions by Atmospheric Pressure Laser Ionization Fourier Transform Ion Cyclotron Resonance Mass Spectrometry. *Energy Fuels* **2012**, *26* (6), 3481–3487. https://doi.org/10.1021/ef3001407.

(229) Santos, J. M.; Vetere, A.; Wisniewski, A.; Eberlin, M. N.; Schrader, W. Modified SARA Method to Unravel the Complexity of Resin Fraction(s) in Crude Oil. *Energy Fuels* **2020**, *34* (12), 16006–16013. https://doi.org/10.1021/acs.energyfuels.0c02833.

(230) Xu, Y.; Schrader, W. Studying the Complexity of Biomass Derived Biofuels. *Energies* **2021**, *14* (8), 2032. https://doi.org/10.3390/en14082032.

(231) Hertzog, J.; Carré, V.; Le Brech, Y.; Mackay, C. L.; Dufour, A.; Mašek, O.; Aubriet, F. Combination of Electrospray Ionization, Atmospheric Pressure Photoionization and Laser Desorption Ionization Fourier Transform Ion Cyclotronic Resonance Mass Spectrometry for the Investigation of Complex Mixtures – Application to the Petroleomic Analysis of Bio-Oils. *Anal. Chim. Acta* **2017**, *969*, 26–34. https://doi.org/10.1016/j.aca.2017.03.022.

(232) Ricochon, G.; Paris, C.; Girardin, M.; Muniglia, L. Highly Sensitive, Quick and Simple Quantification Method for Mono and Disaccharides in Aqueous Media Using Liquid Chromatography–Atmospheric Pressure Chemical Ionization–Mass Spectrometry (LC–APCI–MS). *J. Chromatogr. B* **2011**, *879* (19), 1529–1536. https://doi.org/10.1016/j.jchromb.2011.03.044.

(233) Stefaniuk, M.; Oleszczuk, P. Characterization of Biochars Produced from Residues from Biogas Production. *J. Anal. Appl. Pyrolysis* **2015**, *115*, 157–165. https://doi.org/10.1016/j.jaap.2015.07.011.

(234) Zimmermann, J.; Chiaberge, S.; Iversen, S. B.; Raffelt, K.; Dahmen, N. Sequential Extraction and Characterization of Nitrogen Compounds after Hydrothermal Liquefaction of Sewage Sludge. *Energy Fuels* **2022**, *36* (23), 14292–14303. https://doi.org/10.1021/acs.energyfuels.2c02622.

(235) Santos de Freitas, C.; Valencia-Dávila, J. A.; Lopes Pereira, R. C.; Torres Abrantes, L.; Kato, L.; Gontijo Vaz, B. Isolation and Characterization of Sulfur-Containing Compounds by Positive-Ion Electrospray Ionization and Online HPLC/Atmospheric Pressure Chemical Ionization Coupled to Orbitrap Mass Spectrometry. *Fuel* **2021**, *289*, 119783. https://doi.org/10.1016/j.fuel.2020.119783.

(236) Dekker, S.; Nardin, T.; Mattana, M.; Fochi, I.; Larcher, R. Identification and Characterisation of Thiolated Polysulfides in Must and Wine Using Online SPE UHPLC-HRMS. *Anal. Bioanal. Chem.* **2020**, *412* (22), 5229–5245. https://doi.org/10.1007/s00216-020-02734-1.

(237) Martins, T.; Sá, M. S. de; Silva, W. R.; Schmitt, C. C.; Moreira, R.; Raffelt, K.; Dahmen, N.; Wisniewski, A. Sugarcane Biorefinery: Unlocking the Potential of the Pyrolytic Process to Convert Waste Biomasses into Value-Added Products. *Energy Convers. Manag.* **2024**, *318*, 118913. https://doi.org/10.1016/j.enconman.2024.118913.

(238) Tran, H.; Earl, P. F. Chloride and Potassium Removal Processes for Kraft Pulp Mills: A Technical Review. **2004**, *1*, 381–392.

(239) Sarker, T. R.; Meda, V.; Dalai, A. K. Catalytic Hydrothermal Gasification of Aqueous Effluents Obtained from Microwave Torrefaction of Agricultural Residue. *J. Environ. Chem. Eng.* **2022**, *10* (6), 108835. https://doi.org/10.1016/j.jece.2022.108835.

(240) Le, T.-H.; Wang, S.; Kim, B.-S.; Nam, H.; Lee, D. Advancements and Challenges in Catalytic Hydrothermal Liquefaction of Lignocellulosic Biomass: A Comprehensive Review. *Chem. Eng. J.* **2024**, *498*, 155559. https://doi.org/10.1016/j.cej.2024.155559.

(241) Wang, W.; Lemaire, R.; Bensakhria, A.; Luart, D. Review on the Catalytic Effects of Alkali and Alkaline Earth Metals (AAEMs) Including Sodium, Potassium, Calcium and Magnesium on the Pyrolysis of Lignocellulosic Biomass and on the Co-Pyrolysis of Coal with Biomass. *J. Anal. Appl. Pyrolysis* **2022**, *163*, 105479. https://doi.org/10.1016/j.jaap.2022.105479.

(242) Singh, R.; Krishna, B.; Bhaskar, T. Hydrothermal Liquefaction of Lignocellulosic Biomass Components: Effect of Alkaline Catalyst. In *Green Energy and Technology*; 2017; pp 69–84. https://doi.org/10.1007/978-981-10-3791-7_5.

(243) Satiada, G. B. D. A.; Carpio, R. B.; Guerrero, G. A. M.; Detras, M. C. M.; Bambase, M. E. Influence of Alkali Catalysts on Product Yield and Si-Containing Products from Hydrothermal Liquefaction of Corn Stover. *Heliyon* **2024**, *10* (17), e37520. https://doi.org/10.1016/j.heliyon.2024.e37520.

(244) Hwang, H.; Lee, J. H.; Choi, I.-G.; Choi, J. W. Comprehensive Characterization of Hydrothermal Liquefaction Products Obtained from Woody Biomass under Various Alkali Catalyst Concentrations. *Environ. Technol.* **2019**, *40* (13), 1657–1667. https://doi.org/10.1080/09593330.2018.1427799.

(245) Marrakchi, F.; Sohail Toor, S.; Haaning Nielsen, A.; Helmer Pedersen, T.; Aistrup Rosendahl, L. Bio-Crude Oils Production from Wheat Stem under Subcritical Water Conditions and Batch Adsorption of Post-Hydrothermal Liquefaction Aqueous Phase onto Activated Hydrochars. *Chem. Eng. J.* **2023**, *452*, 139293. https://doi.org/10.1016/j.cej.2022.139293.

(246) Ye, W.; Lin, X.; Zhong, X.; Lan, Q.; Yang, G.; Huang, J.; Wu, Y.; Zhao, Z.; (Sophia) He, Q.; Wu, Y.; Xu, X.; Yang, J. Unraveling the Effects of Sodium Carbonate on Hydrothermal Liquefaction through Individual Biomass Model Component and Machine Learning-Enabled Prediction. *Fuel* **2024**, *358*, 130330. https://doi.org/10.1016/j.fuel.2023.130330.

(247) Carpio, R. B.; Avendaño, C. I. L.; Basbas, C. A.; Habulan, A. A.; Guerrero, G. A. M.; Maguyon-Detras, M. C.; Bambase, M. E. Assessing the Effect of K2CO3 and Aqueous Phase Recycling on Hydrothermal Liquefaction of Corn Stover. *Bioresour. Technol. Rep.* **2022**, *18*, 101093. https://doi.org/10.1016/j.biteb.2022.101093.

(248) Akhtar, J.; Kuang, S. K.; Amin, N. S. Liquefaction of Empty Palm Fruit Bunch (EPFB) in Alkaline Hot Compressed Water. *Renew. Energy* **2010**, *35* (6), 1220–1227. https://doi.org/10.1016/j.renene.2009.10.003.

(249) Karagöz, S.; Bhaskar, T.; Muto, A.; Sakata, Y.; Oshiki, T.; Kishimoto, T. Low-Temperature Catalytic Hydrothermal Treatment of Wood Biomass: Analysis of Liquid Products. *Chem. Eng. J.* **2005**, *108* (1), 127–137. https://doi.org/10.1016/j.cej.2005.01.007.

(250) Bala, E.; Hornung, U.; Dahmen, N. Hydrothermal Liquefaction (HTL) of Lignin: The Adsorption Separation of Catechol Guaiacol and Phenol. *Energies* **2025**, *18* (9), 2181. https://doi.org/10.3390/en18092181.

8 Supplementary Material

8.1 Supplementary Material – Chapter 1

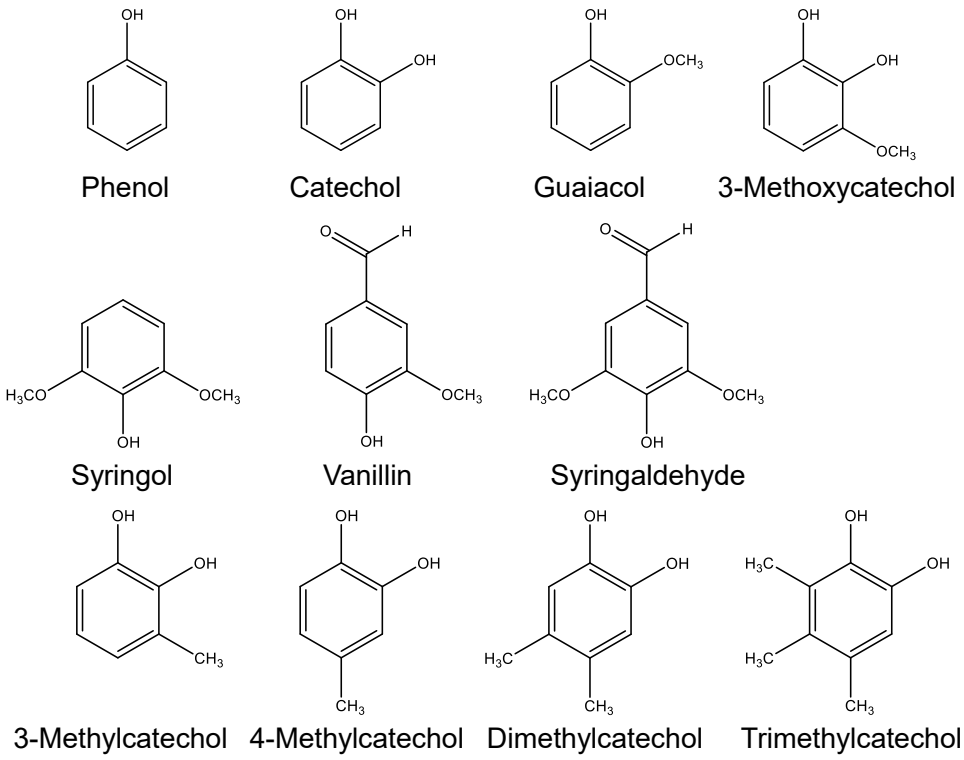

Figure 8-1: Overview of the most discussed aromatics in the thesis with molecular structure and name; The methyl groups of dimethylcatechol and trimethylcatechol could be in different positions; only two were chosen as representants in the figure.

8.2 Supplementary Material – Chapter 2

8.2.1 Weighed-in masses of salts for model salt solution preparation

The following Table 8-1 lists the salts used for the preparation of the model salt solution. The salt solution was used for HTL experiments with model substances and should mimic the salt concentrations in the real black liquor. The masses are based on the preparation of 100 mL of solution. Due to easier handling sodium sulfide was used in form of a nonahydrate. To set up a pH > 12.5 we used a mixture of concentrated NaOH/KOH (ratio based on the ratio of Na and K in the used salts).

Table 8-1: Weighed-in masses of salts used for preparation of 100 mL of salt solution

Salts	Weighed-in mass / g
Na_2CO_3	1.781
K_2CO_3	0.275
Na_2SO_3	0.132
Na_2SO_4	0.109
$Na_2S_2O_3$	0.194
$Na_2S * 9 H_2O$	2.363

8.2.2 Batch micro autoclave experiments and micro autoclave station

In Figure 8-2 the flow scheme of the micro autoclave station is shown. The station was used for all batch autoclave experiments in this work. The autoclave was filled with the feedstock. The volume of feedstock used depends on the reaction temperature TR later in the sand bath (see Table 8-2). The different volumes should negate the changes in density of water under the reaction conditions, especially entering the supercritical area, which would lead to drastic pressure changes.

After the filling the autoclave is placed in the container (a). The container and the autoclave are purged with nitrogen from the bottle (dashed line). After purging for 1 minute, the autoclave is sealed with a torque wrench. The reactor is taken out and placed in the sand bath for the HTL. After the heating and reaction time the autoclave is cooled down in a water bath and put back in the container (a). Now, nitrogen is used to purge the system before opening the autoclave and releasing the produced gas into

the tubes ((d) is an outlet to a beaker filled with water to confirm nitrogen flow). When opened, we are able to close the valves and trap the gas inside the autoclave station. A septum at point (b) allows us to take a gas sample with the syringe and the manometer and point (c) shows us the pressure inside the system. After taking a gas sample the remaining gas is released.

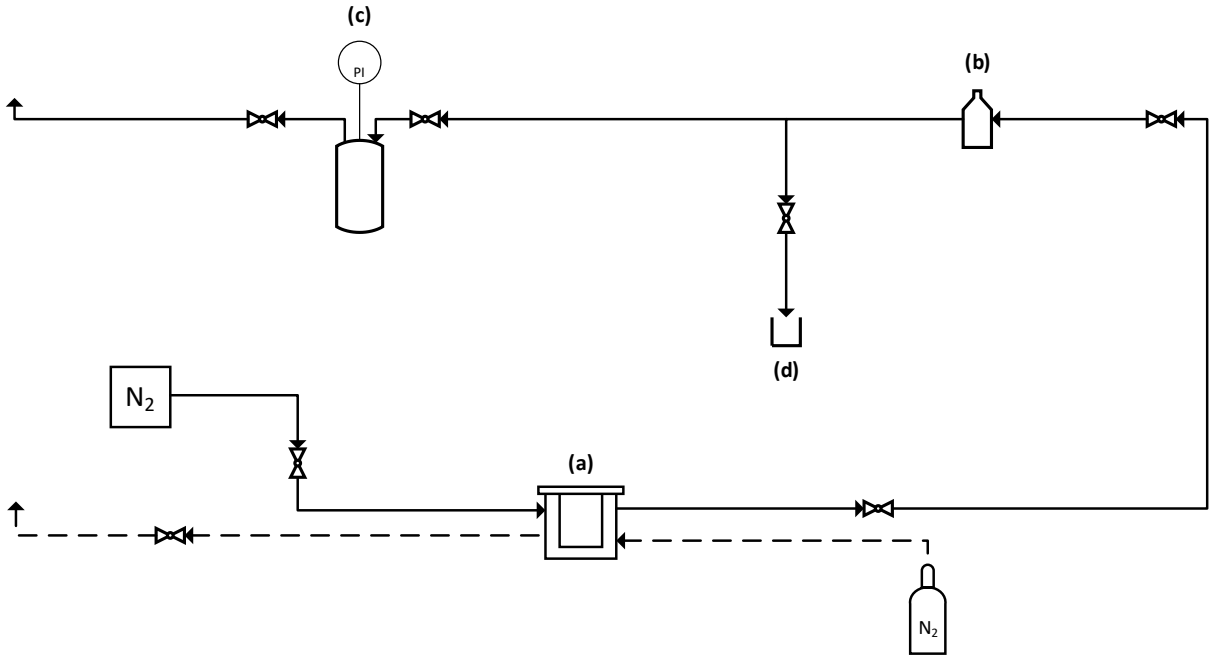

Figure 8-2: micro autoclave station for closing and opening the reactors and gas sample

Table 8-2: Volumes of black liquor used at different reaction temperatures T_R

Reaction temperature T_R / °C	**V_{Feed} / mL**
250 – 275	17.5
300 – 350	15.0
375	12.5
400	5.0

8.2.3 Calculation of the carbon mass in the gas phase

With the help of a manometer (PI in Figure 8-2), the pressure p could be determined. Since this pressure describes the entire system instead of only the micro autoclave, a correction is necessary for later calculations of the resulting gas phase. The correlation to the pressure in the reactor p_{corr} was determined before by filling the autoclaves with

nitrogen up to different pressures and releasing the gas afterwards into the micro autoclave station (see following table).

$$p_{\mathrm{corr}} = \frac{p}{0.083} \tag{8-1}$$

Table 8-3: Data for calculation of the used coefficient in equation (8-1) to calculate p_{corr}. Autoclaves are filled with N_2 up to the pressure $p_{\mathrm{Autoclave}}$. After opening the autoclave in the autoclave station (see Figure 8-2) p_{System} is shown on the manometer. $p_{\mathrm{Autoclave}}$ was in the range from 0 to 2 bar for all the experiments done for this study.

	$p_{\mathrm{Autoclave}}$ / bar	p_{System} / bar	Calculated coefficient
	5	0.4	0.08
	10	0.8	0.08
	15	1.3	0.087
	20	1.7	0.085
Mean coefficient			0.083

Equation (8-2) is used to determine the amount of substance in each gas component n_i. V_G is the free volume in the micro autoclave. The room temperature $T_{room} = 296.15\ \mathrm{K}$ is used as the temperature and R is the universal gas constant. The measured volume percentage of the gas compound via GC-FID/TCD is inserted as φ_i. From this, the total mass of carbon $m_{c,g}$, which is relevant for the carbon mass balance, can be calculated in the next step (equation (8-3)) For this, the number of carbon atoms per molecule v_i and the molecular weight of carbon M_C are required. Table 8-4 lists all the detectable gas compounds with our setup.

$$n_i = \frac{p_{corr} * V_G * \frac{\varphi_i}{100}}{R * T_{room}} \tag{8-2}$$

$$m_{c,g} = \left(\sum n_i * v_i\right) * M_C \tag{8-3}$$

Table 8-4: Gas compounds which are detectable with the used GC setup (TCD and FID)

Permanent gases (TCD)	Hydrocarbons (FID)
H_2	CH_4
CO	C_2H_4
CO_2	C_2H_6
O_2	C_3H_6
N_2	C_3H_8
	n-C_4H_{10}
	iso-CH_4H_{10}

8.2.4 Distribution coefficients for quantification of aromatic compounds

In Table 8-5 the experimentally determined distribution coefficients K_i for the quantified aromatic compounds via GC-FID are listed. The coefficients were determined by preparing an aqueous solution with a known concentration of component i and carrying out the extraction procedure which is described in this work. A following GC-FID analysis of the separated phase gives the information how much of component I ends up in the organic phase.

Table 8-5: Experimentally determined distribution coefficients for different monocyclic phenolic compounds when using the described extraction procedure

Component i	Distribution coefficient K_i
Phenol	0.95
Guaiacol	0.92
Catechol	0.82
3-Methoxycatechol	0.7
3-Methylcatechol	0.83
4-Methylcatechol	0.7
Syringol	0.75

8.2.5 Detailed information about the ^{13}C NMR analysis

The calibration and optimization of the recording parameters for ^{13}C (among others, contact time for the CP/MAS) have been optimized using adamantane and glycine. All the samples were beforehand grinded to give homogeneous, finely powdered materials. The samples were filed in proprietary 3,2 mm Rotors (zirconia with Vespel/PEEK caps). The spectra were recorded at a spinning rate of 15 KHz.

The ^{13}C single pulse spectra were recorded using the standard pulses sequences single_pulse_dec_solid.jxp cpmas_dipolar.jxp and cpmas_dipolar_dephase.jxp with a ^{1}H 90°pulse length of 2.7 μs, an optimized contact time of 1 ms for CP/MAS (checked using a CT array from 0.5 to 2 ms), a relaxation delay of 5 s, a spectral width of 500 ppm (x_sweep); 4096 scans. Chemical shifts, δ, were calibrated relatively to the adamantane signals ($C_{10}H_{16}$: δ =xx and yy ppm) as external standard.

The measurements are conducted using the proprietary software of Jeol Delta 5.3.3., the pulse sequences used belong to the standard Delta library and were optimized when necessary. The evaluation and plotting of the spectra were performed using Delta 5.3.3 and the MNova 10 NMR software package (https://mestrelab.com/software/mnova/nmr/).

8.2.6 Batch HTL experiments with model substances - Additions

In chapter 2.4.2 the HTL experiments with model substances were discussed. Additionally, experiments with vanillin and syringaldehyde were performed. The results for the monomer yields are shown in Figure 8-3 and Figure 8-4. The yields are decreased compared to guaiacol and syringol as feedstock. Furthermore, more different aromatic compounds are produced in quantifiable amounts. In case of syringaldehyde even isomers play a role. However, it was not possible to clarify whether the isomer came from a contaminated feedstock or was formed during the process. The main difference relevant for the reaction pathway model is visible. Vanillin, which is related to guaiacol does not produce 3 – methoxycatechol. On the other hand, syringaldehyde as feedstock produces the specific compound. Overall, it can be stated, that more functional groups attached to the aromatic ring the more different species are produced and the lower are the yields of these compounds. In addition to this finding, the production of solids is also increased as the carbon mass balance for the for the four different feedstocks shows (see Figure 8-5), which is a clear

sign of increased and faster repolyemerization. An expected difference between solids production when using softwood or hardwood based on the results of guaiacol and syringol could not be found as Figure 2-14 shows. It is very likely that the abundance of functional groups on the individual aromatic compounds only plays a subordinate role due to the extensive branching of the lignin. The carbon content for vanillin and syringaldehyde is already very close to each other at higher reaction temperatures T_R.

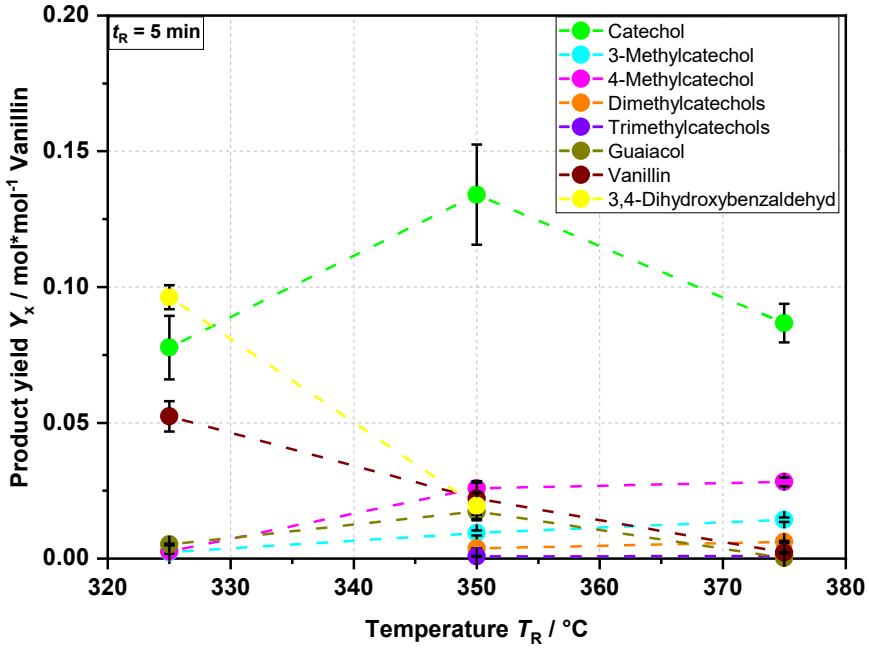

Figure 8-3: Product yields in mol per mol vanillin of the main aromatic monomer compounds at different reaction temperatures T_R

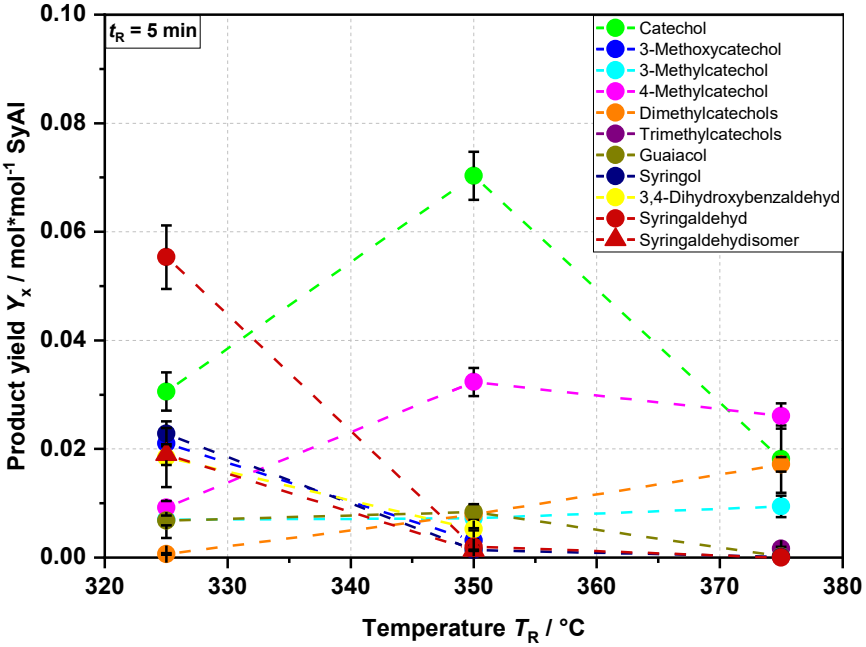

Figure 8-4: Product yields in mol per mol syringaldehyde (SyAl) of the main aromatic monomer compounds at different reaction temperatures T_R

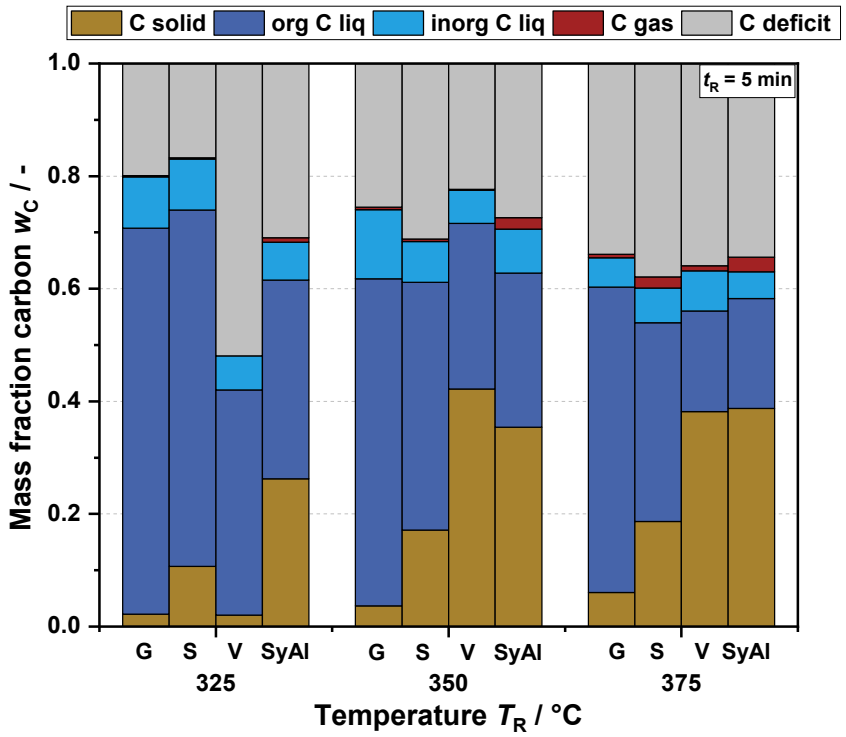

Figure 8-5: Carbon mass fractions at different reaction temperatures T_R for each used model compound (G = guaiacol; S = syringol; V = vanillin; SyAl = syringaldehyde); brown: C mass fraction solid; green: organic C mass fraction liquid phase; blue: inorganic C mass fraction liquid phase; red: C mass fraction gas phase (calculated from the detected gas compounds); and gray: deficit of carbon

8.3 Supplementary Material – Chapter 3

8.3.1 Estimation of heating curves in the sand bath

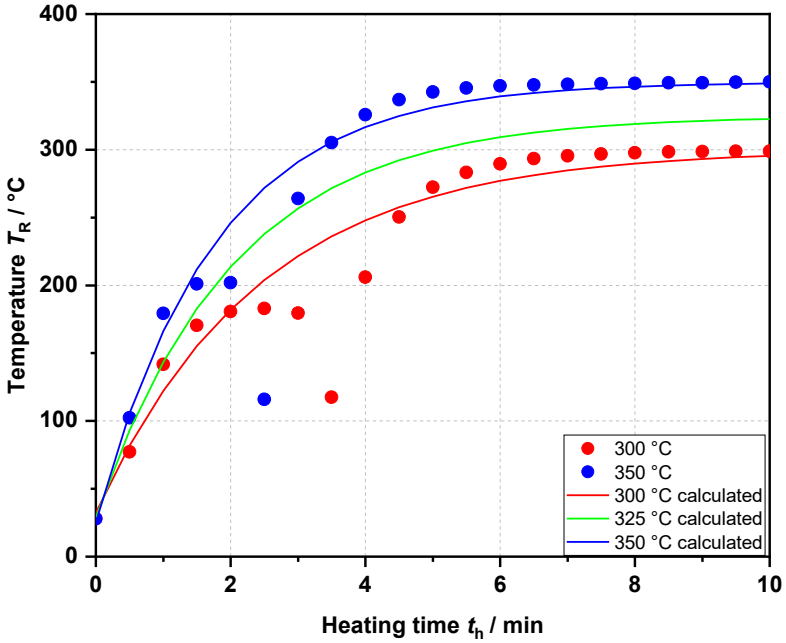

Figure 8-6: Heating curves for a set temperature of $T_R = 300$ °C and 350 °C for the heating process of the micro autoclaves in the fluidized sand bath (SBL 2, Techne, Stone, UK). The autoclaves were filled with water and with a temperature sensor to investigate the heating phase. The heating phase with pure water is comparable with black liquor containing approx. 85. wt. % of water. The temperature drop between 2 and 4 minutes is based probably on vapor bubbles forming around the temperature sensor. This is neglected fast due to the sharp rise of the pressure with increasing temperature. The calculated exponential fits for $T_R = 300$ °C, 325 °C and 350 °C are included as well.

Based on Figure 8-6 equations for the heating phase to describe the temperature were developed by using the solver function in Microsoft Excel. An exponential formula was chosen (see equation (8-4)). The parameters A and B were later used in the kinetic model. The parameters as well as the temperature curve for $T_R = 325$ °C were estimated via interpolation. In Table 8-6 the setpoints and the parameters A and B are listed. The calculations were made with temperature in Kelvin. The exponential fits are also included in Figure 8-6. The equation is used to describe the temperature during heating time in the kinetic model.

$$T(t) = SP - A \cdot \exp(-Bt) \qquad (8\text{-}4)$$

Table 8-6: Setpoints and their estimated parameters A and B.

Setpoint	A	B
300 °C (573 K)	267.49	0.41
325 °C (598 K)	295.95	0.49
350 °C (623 K)	324.41	0.57

8.3.2 Weight factors for each compound

Table 8-7: Weight factors for each compound in each experiment. MCat = 3-Methoxycatechol; Cat = Catechol; MeCat = Methylcatechol; DiMeCat = Dimethylcatechol; TriMeCat = Trimethylcatechol

Exp	Lignin	OL_int	MCat	Cat	MeCat	DiMeCat	TriMeCat	Solids	OL_fixed	H_2O	H_2	CH_4	CO_2
1	0	0	200	50	100	10	5	0.1	0.1	0	0.01	0.01	0.01
2	0	0	200	50	100	10	5	0.1	0.1	0	0.01	0.01	0.01
3	0	0	200	50	100	10	5	0.1	0.1	0	0.01	0.01	0.01
4	0	0	200	50	100	10	5	0.1	0.1	0	0.01	0.01	0.01
5	0	0	200	50	100	10	5	0.1	0.1	0	0.01	0.01	0.01
6	0	0	200	50	100	10	5	0.1	0.1	0	0.01	0.01	0.01
7	0	0	200	50	100	10	5	0.1	0.1	0	0.01	0.01	0.01
8	0	0	200	50	100	10	5	0.1	0.1	0	0.01	0.01	0.01
9	0	0	200	50	100	10	5	0.1	0.1	0	0.01	0.01	0.01
10	0	0	20	50	100	10	5	0.1	0.1	0	0.01	0.01	0.01
11	0	0	20	50	100	10	5	0.1	0.1	0	0.01	0.01	0.01
12	0	0	20	50	100	10	5	0.1	0.1	0	0.01	0.01	0.01
13	0	0	20	50	100	10	5	0.1	0.1	0	0.01	0.01	0.01
14	0	0	20	50	100	10	5	0.1	0.1	0	0.01	0.01	0.01
15	0	0	20	50	100	10	5	0.1	0.1	0	0.01	0.01	0.01
16	0	0	20	50	100	10	5	0.1	0.1	0	0.01	0.01	0.01
17	0	0	20	50	100	10	5	0.1	0.1	0	0.01	0.01	0.01

8.3.3 Experiments used in the model

Table 8-8: Experimental values of each experiment used for the kinetic model; temperature in °C; reaction time in min; initial masses of aromatic monomers from GC-FID analysis of pristine BL; masses are all converted into yields g*g^{-1} biomass; initial mass of lignin = 1 – all other initial masses; total mass in g; MCat = 3-Methoxycatechol; Cat = Catechol; MeCat = Methylcatechol; DiMeCat = Dimethylcatechol; TriMeCat = Trimethylcatechol

exp_number	Temperature	Reaction time	initial_lignin_mass	initial_Guaiacol_mass	initial_Syringol_mass	initial_MCat_mass
1	300	10	0.997	0.0004	0.002	0.0002
2	300	15	0.997	0.0004	0.002	0.0002
3	300	20	0.997	0.0004	0.002	0.0002
4	300	30	0.997	0.0004	0.002	0.0002
5	300	40	0.997	0.0004	0.002	0.0002
6	325	10	0.997	0.0004	0.002	0.0002
7	325	11	0.997	0.0004	0.002	0.0002
8	325	15	0.997	0.0004	0.002	0.0002
9	325	20	0.997	0.0004	0.002	0.0002
10	325	25	0.997	0.0004	0.002	0.0002
11	325	30	0.997	0.0004	0.002	0.0002
12	325	40	0.997	0.0004	0.002	0.0002
13	350	10	0.997	0.0004	0.002	0.0002
14	350	15	0.997	0.0004	0.002	0.0002
15	350	20	0.997	0.0004	0.002	0.0002
16	350	30	0.997	0.0004	0.002	0.0002
17	350	40	0.997	0.0004	0.002	0.0002

Table 8-9: Experimental values of each experiment used for the kinetic model (prolongation)

exp_number	Temperature	Reaction time	initial_Cat_mass	initial_MeCat_mass	Lignin	OL_int	Mcat	Cat	MeCat
1	300	10	0.0002	0.0002	0	0	0.017	0.0122	0.0066
2	300	15	0.0002	0.0002	0	0	0.0074	0.0139	0.0088
3	300	20	0.0002	0.0002	0	0	0.0012	0.0122	0.01
4	300	30	0.0002	0.0002	0	0	0.0003	0.0104	0.0097
5	300	40	0.0002	0.0002	0	0	0	0.0094	0.0095
6	325	10	0.0002	0.0002	0	0	0.0024	0.0156	0.0122
7	325	11	0.0002	0.0002	0	0	0.0019	0.022	0.0163
8	325	15	0.0002	0.0002	0	0	0	0.0154	0.0143
9	325	20	0.0002	0.0002	0	0	0	0.0134	0.0153
10	325	25	0.0002	0.0002	0	0	0	0.0099	0.0135
11	325	30	0.0002	0.0002	0	0	0	0.0087	0.0135
12	325	40	0.0002	0.0002	0	0	0	0.008	0.0119
13	350	10	0.0002	0.0002	0	0	0	0.0096	0.0142
14	350	15	0.0002	0.0002	0	0	0	0.0056	0.0106
15	350	20	0.0002	0.0002	0	0	0	0.0027	0.0061
16	350	30	0.0002	0.0002	0	0	0	0.0012	0.0025
17	350	40	0.0002	0.0002	0	0	0	0.0009	0.0015

Table 8-10: Experimental values of each experiment used for the kinetic model (prolongation)

exp_number	Temperature	Reaction time	DiMeCat	TriMeCat	Solids	OL_fixed	H_2O	H_2	CH_4	CO_2	Total mass
1	300	10	0.002	0	0.3858	0.57775	0	0.0000	0.0005	0.0001	16.4
2	300	15	0.0027	0	0.4096	0.55872	0	0.0000	0.0007	0.0009	16.6
3	300	20	0.0032	0	0.5673	0.40728	0	0.0000	0.0007	0.0013	15.7
4	300	30	0.0037	0	0.5597	0.41739	0	0.0002	0.0008	0.0016	16.2
5	300	40	0.0035	0	0.6316	0.34627	0	0.0001	0.0005	0.0027	16.3
6	325	10	0.0037	0	0.4188	0.54584	0	0.0000	0.0012	0.0040	16
7	325	11	0.0035	0	0.4313	0.52515	0	0.0003	0.0013	0.0018	16
8	325	15	0.0034	0	0.5093	0.45077	0	0.0005	0.0014	0.0084	16.1
9	325	20	0.0043	0	0.4371	0.52672	0	0.0005	0.0013	0.0057	16.7
10	325	25	0.0047	0	0.4233	0.54415	0	0.0007	0.0014	0.0071	16.3
11	325	30	0.005	0.0003	0.4074	0.55873	0	0.0008	0.0015	0.0093	16.2
12	325	40	0.0057	0.0004	0.4620	0.5083	0	0.0009	0.0016	0.0072	15.8
13	350	10	0.0065	0	0.5009	0.45833	0	0.0008	0.0014	0.0148	16.1
14	350	15	0.0079	0.0008	0.4809	0.48332	0	0.0008	0.0010	0.0178	16.2
15	350	20	0.0079	0.0013	0.4397	0.51129	0	0.0015	0.0018	0.0369	16
16	350	30	0.0053	0.0012	0.4249	0.55283	0	0.0016	0.0022	0.0147	15.9
17	350	40	0.0048	0.0014	0.4094	0.55773	0	0.0011	0.0017	0.0276	16.5

8.3.4 Simulated yield plots after cross validation

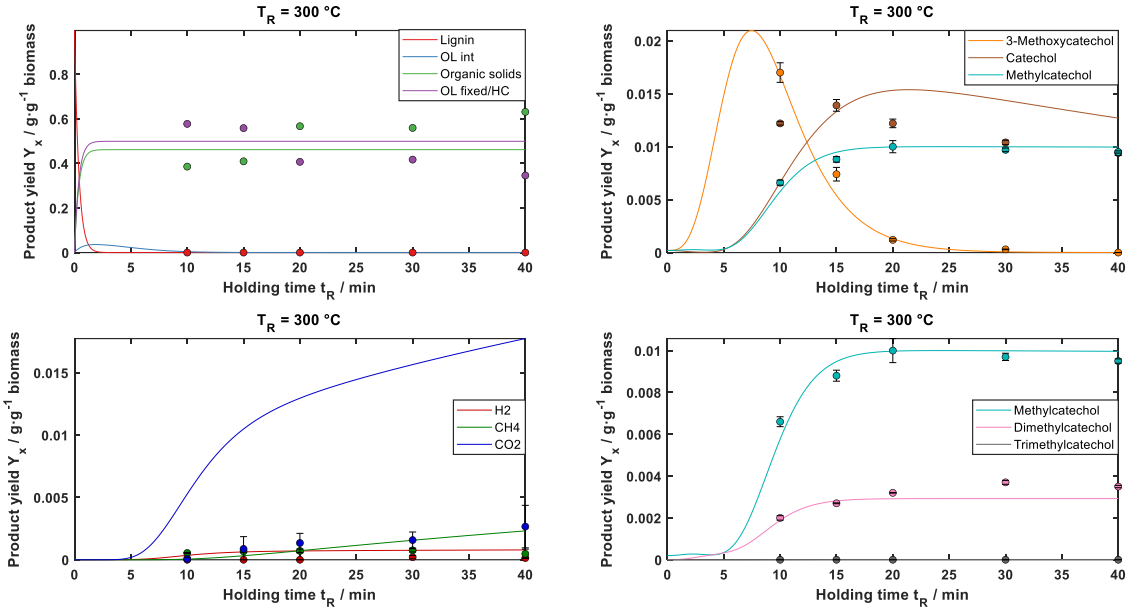

Figure 8-7: Comparison between calculated kinetic model fits (lines) and the experimental results (dots) for the batch experiments at reaction temperature $T_R = 300$ °C and holding times $t_R = 0 - 30$ min. No experimental values for OL_int. The heating phase from 0 – 10 min is included; top left: oligomeric structures; top right: main aromatic monomers; bottom left: gaseous compounds; bottom right: methylated catechols; after cross validation

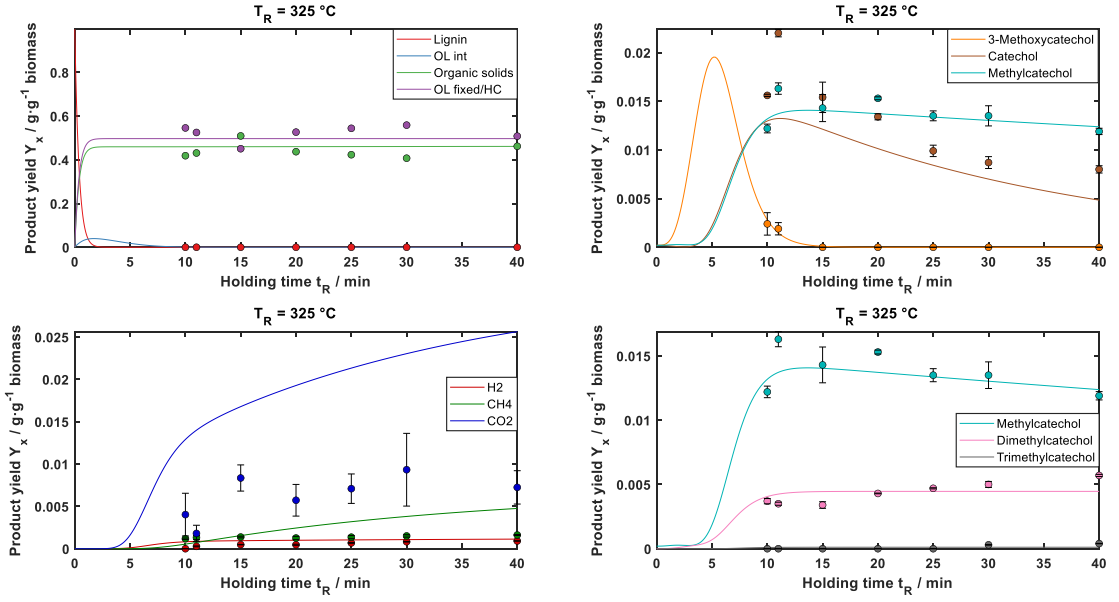

Figure 8-8: Comparison between calculated kinetic model fits (lines) and the experimental results (dots) for the batch experiments at reaction temperature $T_R = 325$ °C and holding times $t_R = 0 - 30$ min. No experimental values for OL_int. The heating phase from 0 – 10 min is

included; top left: oligomeric structures; top right: main aromatic monomers; bottom left: gaseous compounds; bottom right: methylated catechols; after cross validation

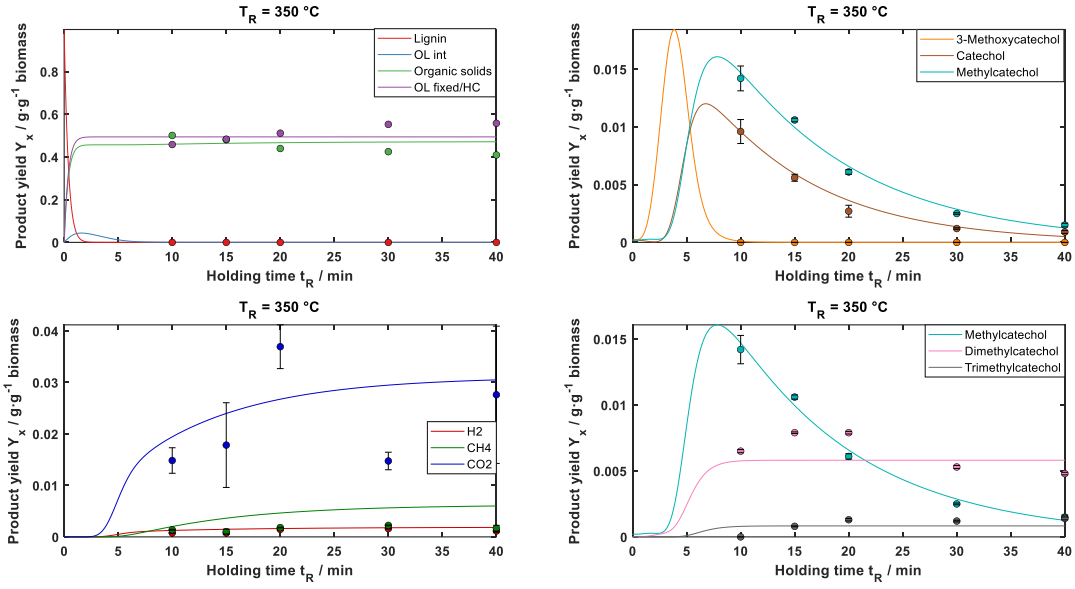

Figure 8-9: Comparison between calculated kinetic model fits (lines) and the experimental results (dots) for the batch experiments at reaction temperature $T_R = 350\ °C$ and holding times $t_R = 0 - 30\ min$. No experimental values for OL_int. The heating phase from 0 – 10 min is included; top left: oligomeric structures; top right: main aromatic monomers; bottom left: gaseous compounds; bottom right: methylated catechols; after cross validation

8.3.5 Kinetic parameters for all 13 reactions of the kinetic model

Table 8-11: Activation energies $E_{A,j}$, Arrhenius factor A_j and the respective rate coefficients k_j for each reaction temperature for all 13 reactions of the developed model

Reaction Number	$E_{A,j}$ / kJ*mol^{-1}	A_j / -	k (300 °C) / min^{-1}	k (325 °C) / min^{-1}	k (350 °C) / min^{-1}
1	0	1.24	$2.88 \cdot 10^{-1}$	$2.88 \cdot 10^{-1}$	$2.88 \cdot 10^{-1}$
2	0	1.21	$2.69 \cdot 10^{-1}$	$2.69 \cdot 10^{-1}$	$2.69 \cdot 10^{-1}$
3	10.87	0.48	$4.60 \cdot 10^{-2}$	$5.06 \cdot 10^{-2}$	$5.52 \cdot 10^{-2}$
4	54.37	1.62	$4.34 \cdot 10^{-1}$	$7.00 \cdot 10^{-1}$	$1.09 \cdot 10^{0}$
5	0.01	0.17	$2.49 \cdot 10^{-2}$	$2.49 \cdot 10^{-2}$	$2.49 \cdot 10^{-2}$
6	133.48	1.81	$3.34 \cdot 10^{-1}$	$1.08 \cdot 10^{0}$	$3.16 \cdot 10^{0}$
7	56.24	1.72	$5.34 \cdot 10^{-1}$	$8.75 \cdot 10^{-1}$	$1.38 \cdot 10^{0}$
8	57.89	1.14	$1.37 \cdot 10^{-1}$	$2.28 \cdot 10^{-1}$	$3.64 \cdot 10^{-1}$
9	240.99	0.35	$4.46 \cdot 10^{-3}$	$3.69 \cdot 10^{-2}$	$2.58 \cdot 10^{-1}$
10	112.67	0.59	$2.42 \cdot 10^{-2}$	$6.50 \cdot 10^{-2}$	$1.61 \cdot 10^{-1}$
11	229.84	-2.63	$5.22 \cdot 10^{-6}$	$3.92 \cdot 10^{-5}$	$2.50 \cdot 10^{-4}$
12	344.39	-0.51	$2.54 \cdot 10^{-4}$	$5.21 \cdot 10^{-3}$	$8.37 \cdot 10^{-2}$
13	452.28	-1.90	$4.01 \cdot 10^{-6}$	$2.12 \cdot 10^{-4}$	$8.13 \cdot 10^{-3}$

8.3.6 Error calculation changes after CV

Table 8-12: Error estimations for the simulated aromatic monomer compounds at different reaction temperatures T_R after CV. green numbers show improvement. red numbers show deterioration compared to the original values

	300 °C			325 °C			350 °C		
	R^2	MAE / g*g^{-1}	RMSE/ g*g^{-1}	R^2	MAE/ g*g^{-1}	RMSE/ g*g^{-1}	R^2	MAE/ g*g^{-1}	RMSE/ g*g^{-1}
3-Methoxycatechol	0.98	0.0005	0.0009	0.95	0.0001	0.0002	n.a.	n.a.	n.a.
Catechol	-4.52	0.0033	0.0037	0.18	0.0035	0.0041	0.98	0.0004	0.0005
Methylcatechol	0.81	0.0003	0.0003	0.29	0.0009	0.0012	0.99	0.0004	0.0005
Dimethylcatechol	0.44	0.0004	0.0005	0.16	0.0006	0.0007	-0.28	0.0013	0.0015
Trimethylcatechol	n.a.	n.a.	n.a.	0.03	0.0001	0.0002	0	0.0004	0.0005

8.4 Supplementary Material – Chapter 4

8.4.1 Model black liquor preparation

The following table lists the weighed-in masses of the salts, the lignin, the volume of NaOH/KOH solution for setting the pH > 12.5 and the HS^- concentration for each model black liquor (MBL) used in the study.

Table 8-13: Weighed-in masses of the compounds and volume of the NaOH/KOH solution for each model black liquor (based on 100 mL)

Compound	MBL-A	MBL-B	MBL-C	MBL-D
Na_2CO_3 / g	1.777	1.778	1.778	1.781
K_2CO_3 / g	0.183	0.215	0.244	0.275
Na_2SO_3 / g	0.132	0.133	0.131	0.132
Na_2SO_4 / g	0.110	0.109	0.106	0.109
$Na_2S_2O_3$ / g	0.195	0.196	0.195	0.194
$Na_2S * 9\ H_2O$ / g	0	0.785	1.573	2.363
Lignin /g	9.001	8.998	8.998	9.002
NaOH/KOH solution / mL	8.75	7.5	6.25	5
$HS^- / g \cdot L^{-1}$	0	approx. 1	approx. 2	approx. 3

8.4.2 pH values for the liquid products

The following two figures show the pH value of the produced liquid phase after filtration of the solids at different reaction temperatures T_R and HS^- concentrations ρ_{HS^-}. Both a corresponding to the production of H_2S in the gas phase due to the shift in equilibrium with decreasing pH. The pH value was measured with a Metrohm 691 pH Meter (Metrohm, Herisau, Switzerland).

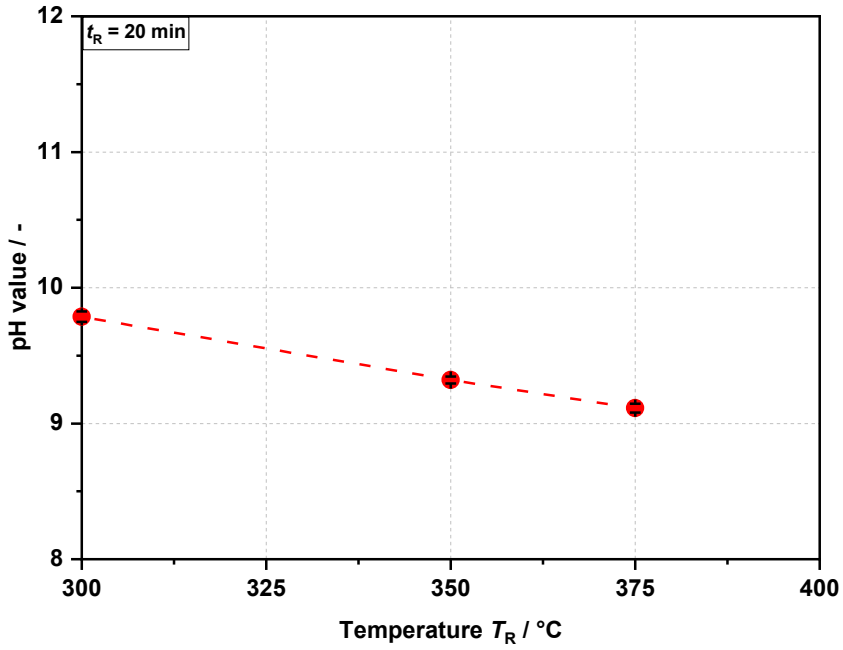

Figure 8-10: pH values for the liquid product after HTL of BL at three different reaction temperatures $T_R = 300\ °C, 350\ °C, 375\ °C$) and holding time $t_R = 20\ min$

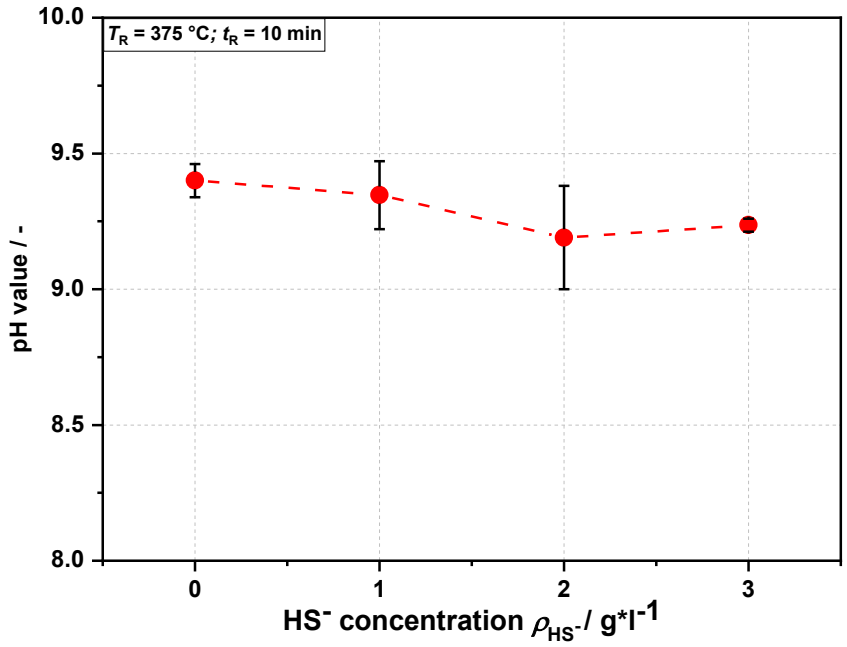

Figure 8-11: pH values for the liquid product after HTL of MBL at $T_R = 375\ °C$ and $t_R = 10\ min$ with different HS^- feedstock concentrations

8.4.3 Sodium and potassium mass balance at different reaction temperatures

Figure 8-12 shows the sodium mass balance and Figure 8-13 shows the potassium mass balance at different reaction temperatures. The ICP-OES for liquid samples and the EA for solid samples were used. Both analytical methods are described chapter

2.3.4. The alkali metals show similar behavior. They are dominant in the liquid phase in form of dissolved salts over all temperatures. The solid ratio is slightly under 10 wt. % at $T_R = 300\ °C$ and decreases afterwards to 1 – 2 wt. %.

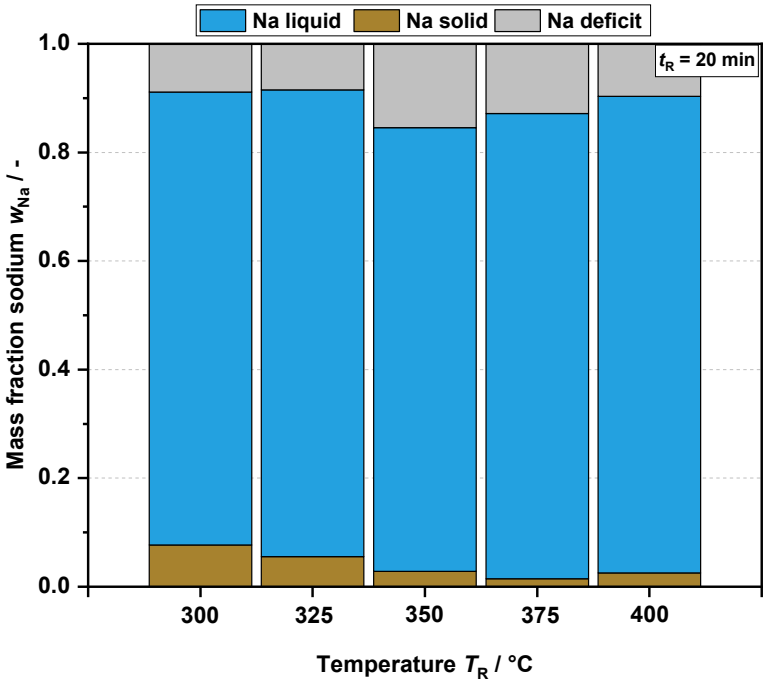

Figure 8-12: Sodium mass balance at different reaction temperatures T_R

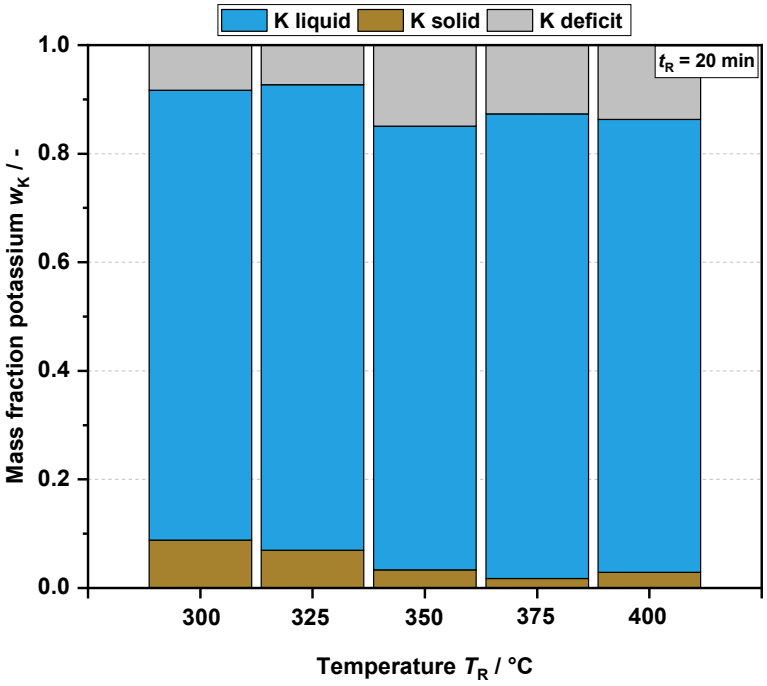

Figure 8-13: Potassium mass balance at different reaction temperatures T_R

List of Figures

List of Tables

Nomenclature

$E_{A,j}$	Activation energy
n_i	Amount of substance of species i
A_j	Arrhenius factor
$w_{\text{ash, 815 °C}}$	Ash content
T_{boil}	Boiling point temperature
$t_{\alpha/2,k-1}$	Critical value from Student's t-distribution
ρ	Density
ε_{r}	Dielectric constant
K_{i}	Distribution coefficient
w_{tr}	Dry matter content
t_{pre}	Heating time
t_{R}	Holding time
pK_{w}	Ion product of water
c	ISTD factor
θ_j	Kinetic parameter $\in \{\text{A}_\text{j}, \text{E}_{\text{A,j}}\}$
ρ_{i}	Mass concentration of species i
m_{feed}	Mass of feedstock
$m_{\text{liq,prod}}$	Mass of liquid product
m_{i}	Mass of species i
$m_{i,liq}$	Mass of species i in liquid phase
$m_{\text{i,calc}}$	Mass of species I, calculated
$m_{\text{i,exp}}$	Mass of species i, experimental determined
m/z	Mass-to-charge ratio
$\bar{\theta}_j$	Mean parameter value
$\rho_{\text{i,raw}}$	Measured concentration with GC
$c_{\text{SO}_4^{2-}}$	Molar concentration of SO_4^{2-}
M_{w}	Molecular weight
M_{i}	Molecular weight of species i

k	Number of groups
j	Number of reactions steps
P	Pressure
$w_{\mathrm{BL,\ burnable}}$	Raw BL-based burnable matter
k_j	Reaction constant of reaction j
r_j	Reaction rate of reaction j
T_{R}	Reaction temperature
M_{rel}	Relative molecular weight
n	Sample size
b	Sample volume / EtAc ratio factor
$SC_{i,j}$	Stoichiometric factor
T	Temperature
$n_{gas,tot}$	Total amount of substance in gas phase
a	Total dilution factor
R	Universal gas constant
p_{v,H_2O}	Vapor pressure of water
V	volume
V_G	Volume of gas phase in reactor
V_L	Volume of liquid phase in reactor
V_{R}	Volume of reactor
$w_{i,l}$	Weighting factor
Y_{x}	Yield of compound x
$Y_{\mathrm{x,calc}}$	Yield of compound x, calculated
$Y_{\mathrm{x,exp}}$	Yield of compound x, experimental determined

List of abbreviations

APR	Aqueous phase reforming
AI	Aromatic index
APCI(-)	Atmospheric pressure chemical ionization
BTX	Benzene, Toluene, Xylene
HS^-	Bisulfide ions
BL	Black liquor
BL2F	Black liquor to Fuels (project)
CO_2	Carbon dioxide
CI	Confidence interval
CP/MAS	Cross-polarization magic angle spinning
CV	Cross-validation
DMDS	Dimethyl disulfide
DMS	Dimethyl sulfide
DMTS	Dimethyl trisulfide
DMF	Dimethylfuran
DBE	Double bond equivalent
EA	Elemental analysis
EtAc	Ethyl acetate
OL_fixed	Fixed oligomers
FID	Flame ionization detector
FF	Furfural
GC	Gas chromatography
H-ESI(+)	Heated electrospray ionization
HSQC	Heteronuclear single quantum correlation
HPLC	High-perfomance liquid chromatography
HRMS	High-resolution mass spectroscopy
HDO	Hydrodeoxygenation
H_2	Hydrogen
HTC	Hydrothermal carbonization
HTG	Hydrothermal gasification

HTL	Hydrothermal Liquefaction
ICP-OES	Inductively coupled plasma – optical emission spectroscopy
OL_int	Intermediate oligomers
ISTD	Internal standard
IC-An	Ion chromatography for anions
LLE	Liquid-liquid extraction
MS	Mass spectroscopy
MAE	Mean absolute error
MT	Megaton
CH_4	Methane
MtA	Methanol to aromatics
MF	Methylfuran
MBL	Model black liquor
MSW	Municipal solid waste
NIST	National Institute of Standards and Technology
NMR	Nuclear magnetic resonance
K_2CO_3	Potassium carbonate
KOH	Potassium hydroxide
RMSE	Root mean square error
SEC	Size exclusion chromatography
Na_2CO_3	Sodium carbonate
NaOH	Sodium hydroxide
Na_2SO_4	Sodium sulfate
Na_2S	Sodium sulfide
Na_2SO_3	Sodium sulfite
$Na_2S_2O_3$	Sodium thiosulfate
SCD	Sulfur chemiluminescence detector
TCD	Temperature conductivity detector
TIC	Total inorganic carbon
TOC	Total organic carbon
UHPLC	Ultra-high-performance liquid chromatography